# International Journal of Interactive Multimedia and Artificial Intelligence

June 2016, Vol III, Number 7, ISSN: 1989-1660

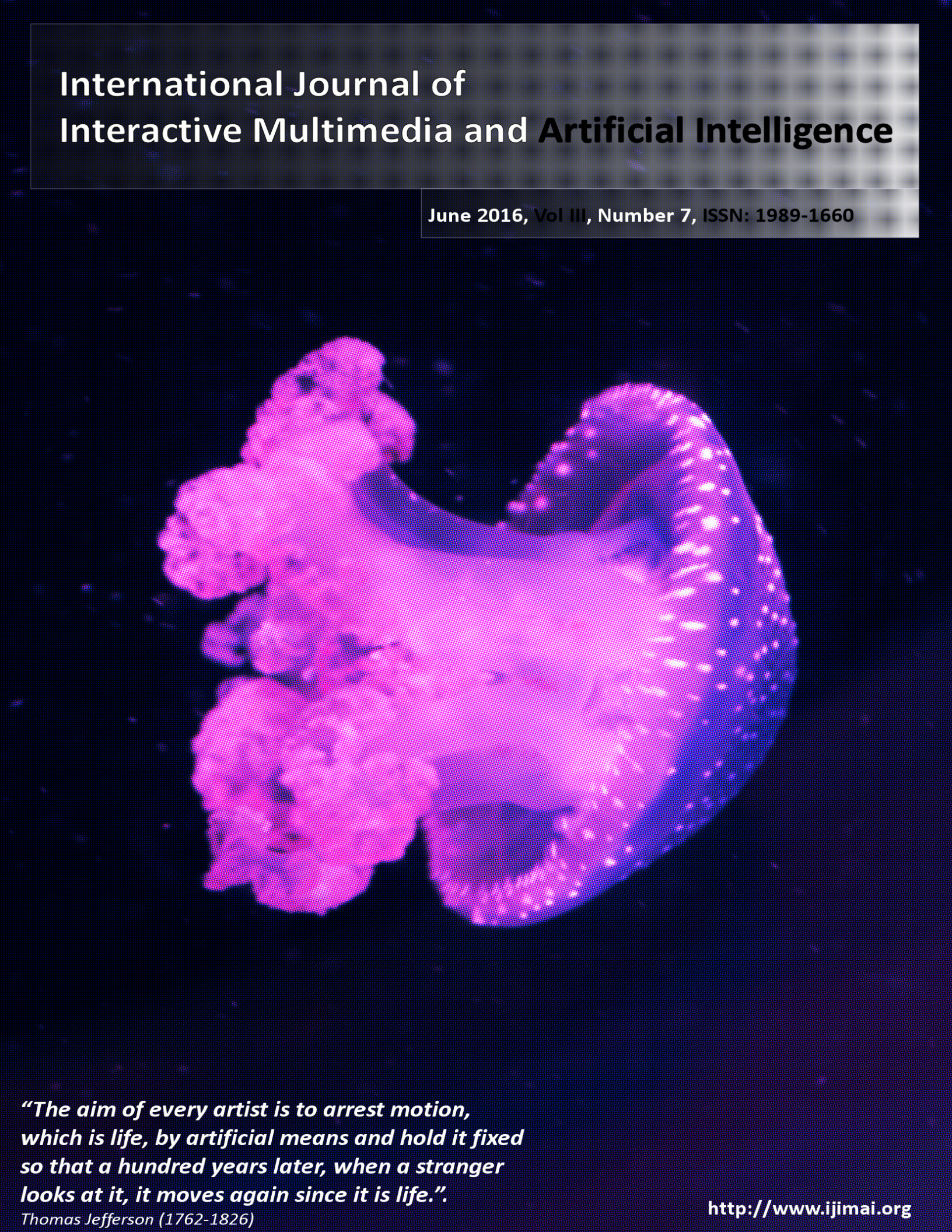

*"The aim of every artist is to arrest motion, which is life, by artificial means and hold it fixed so that a hundred years later, when a stranger looks at it, it moves again since it is life.".*

*Thomas Jefferson (1762-1826)*

http://www.ijimai.org

INTERNATIONAL JOURNAL OF INTERACTIVE MULTIMEDIA AND ARTIFICIAL INTELLIGENCE
ISSN: 1989-1660–VOL. III, NUMBER 7

# Editor's Note

The International Journal of Interactive Multimedia and Artificial Intelligence provides an interdisciplinary forum in which scientists and professionals can share their research results and report new advances on Artificial Intelligence and Interactive Multimedia techniques. The research works presented in this issue are based on various topics of interest, among which are included:

SVM and ANN Based Classification, Security in Android, Semantic Data, Planning and Software Agents, Mission Planning, Clustering in Text Mining, Mobile Networks, Weather Radars, Human Activity Recognition, LIF Neurons and DDF, Theft Prevention, Constraint Programming, Measuring Meditations Effects, Neural Networks and Deep Learning.

Pujari, J. Et al. [1] Talks about a study that presented a reduced feature set based approach for recognition and classification of images of plant diseases. The results reveal that SVM classifier is more suitable for identification and classification of plant diseases affecting agriculture/horticulture crops.

Latifa, E. Et al. [2] Presents a new tool called PermisSecure that is able to perform both static and dynamic analysis on Android programs to automatically detect suspicious applications that request unnecessary or dangerous permissions.

Soussi, M. Et al. [3] tries to bridge an important gap between these two heterogeneous worlds (object oriented and semantic web world) by proposing the first provably semantics preserving OQLto-SPARQL translation algorithm for each element of OQL Query(SELECT clause, FROM clause, FILTER constraint, implicit/explicit join and union/ intersection SELECT queries).

Castillo, J. [4] talks about the use of the agents technology within a new methodological approach to envision future possible scenarios more quickly and more accurately than the classical methods we currently use.

Kumar, A. Et al. [5] describes the Linear Temporal Logic-based reactive motion planning. They address the problem of motion planning for mobile robots, wherein the goal specification of planning is given in complex environments.

Jalil, A. Et al. [6] presents a classical process of knowledge discovery databases, in order to treat textual data. This process is divided into three parts: preprocessing, processing and post-processing.

Petearson, J. Et al. [7] proposes a methodology that enables a systematic design of routing algorithms based on schemes of biclustering, which allows you to respond with timely techniques, clustering heuristics proposed by a researcher, and a focused approach to routing in the choice of clusterhead nodes.

Gomez, A. Et al. [8] introduces an uncertainty model for the quantitatively estimate precipitation using weather radars. The model considers various key aspects associated to radar calibration, attenuation, and the tradeoff between accuracy and radar coverage.

Kumar, A. Et al. [9] proposes a most effective noble approach for Human activity recognition in real-time environments. We recognize several distinct dynamic human activity actions using kinect.

Kumar, S. Et al. [10] talks about the evolution of membrane potential and spiking activity for a single leaky integrate-and-fire (LIF) neuron in distributed delay framework (DDF).

Mehta, V. Et al. [11] discusses a theft prevention system, which can prevent the theft and also can track the object.

Amadini, R. Et al. [12] describes in the context of Constraint Programming, a portfolio approach that exploits the complementary strengths of a portfolio of different constraint solvers. The goal is to predict and run the best solver(s) of the portfolio for solving a new, unseen problem.

Dey, A. Et al. [13] explains that cardiac disease is one of the major causes for death all over the world. Heart rate variability (HRV) is a significant parameter that used in assessing Autonomous Nervous System (ANS) activity, they show how metitation affect all this parameters.

Machado, J. Et al. [14] talks about how the discrimination of the clutter interfering signal isa current problem in modern radars' design, especially in coastal or offshore environments where the histogram of the backgroundsignal often displays heavy tails. The statistical characterization of this signal is very important for the cancellation of sea clutter, whose behavior obey.

Dr.Óscar Sanjuán Martínez

## References


[1] Pujari. J. D. et al. "SVM and ANN Based Classi cation of Plant Diseases Using Feature Reduction Technique", International Journal of Interactive Multimedia and Artificial Intelligence, vol. 3, no. 7, pp. 6-14, 2016.

[2] Lafita, E.R. et al. "A New Protection for Android Applications", International Journal of Interactive Multimedia and Artificial Intelligence, vol. 3, no. 7, pp. 15-19, 2016.

[3] Nassima, S. et al. "Query Migration from Object Oriented World to Semantic World", International Journal of Interactive Multimedia and Artificial Intelligence, vol. 3, no. 7, pp. 20-25, 2016.

[4] Castillo, J. M. et al. "The Silver Lining Methodology", International Journal of Interactive Multimedia and Artificial Intelligence, vol. 3, no. 7, pp. 26-31, 2016.

[5] Kumar, A. et al. "Linear Temporal Logic-based Mission Planning", International Journal of Interactive Multimedia and Artificial Intelligence, vol. 3, no. 7, pp. 32-41, 2016.

[6] Jalil, A. M. et al. "Comparative study of clustering algorithms in text mining context", International Journal of Interactive Multimedia and Artificial Intelligence, vol. 3, no. 7, pp. 42-45, 2016.

[7] Petearson, J. et al. "Design Methodology for Self-organized Mobile Networks Based", International Journal of Interactive Multimedia and Artificial Intelligence, vol. 3, no. 7, pp. 46-53, 2016.

[8] Gomez-Vargas, A. E. et al. "Uncertainty Model for Quantitative Precipitation Estimation Using Weather Radars", International Journal of Interactive Multimedia and Artificial Intelligence, vol. 3, no. 7, pp. 54-60, 2016.

[9] Kumar, A. et al. "Human Activity Recognition in Real-Times Environments using Skeleton Joints", International Journal of Interactive Multimedia and Artificial Intelligence, vol. 3, no. 7, pp. 61-69, 2016.

[10] Kumar-Choundary, S. et al. "Spiking Activity of a LIF Neuron in Distributed Delay Framework", International Journal of Interactive Multimedia and Artificial Intelligence, vol. 3, no. 7, pp. 70-76, 2016.

[11] Mehta, V. et al. "A Real Time Approach to Theft Prevention in the Field of Transportation System", International Journal of Interactive Multimedia and Artificial Intelligence, vol. 3, no. 7, pp. 77-80, 2016.

[12] Amadini, R. et al. "An Extensive Evaluation of Portfolio Approaches for Constraint Satisfaction Problems", International Journal of Interactive Multimedia and Artificial Intelligence, vol. 3, no. 7, pp. 81-86, 2016.

[13] Dey, A. et al. "Chinese-chi and Kundalini Yoga Meditations Effects on the Autonomic Nervous System: Comparative Study", International Journal of Interactive Multimedia and Artificial Intelligence, vol. 3, no. 7, pp. 87-95, 2016.

[14] Machado, J. R. et al. "Improved Shape Parameter Estimation in K Clutter with Neural Networks and Deep Learning", International Journal of Interactive Multimedia and Artificial Intelligence, vol. 3, no. 7, pp. 96-103, 2016.




DOI: 10.9781/ijimai.2016.370

TABLE OF CONTENTS



**OPEN ACCESS JOURNAL**

**ISSN: 1989-1660**

# SVM and ANN Based Classification of Plant Diseases Using Feature Reduction Technique

Jagadeesh D.Pujari, Rajesh Yakkundimath and Abdulmunaf. Syedhusain Byadgi

[1] SDMCET, Dharwad, India
[2] KLE. Institute of Technology, Hubli, India
[3] UAS, Dharwar, India

***Abstract* — Computers have been used for mechanization and automation in different applications of agriculture/horticulture. The critical decision on the agricultural yield and plant protection is done with the development of expert system (decision support system) using computer vision techniques. One of the areas considered in the present work is the processing of images of plant diseases affecting agriculture/horticulture crops. The first symptoms of plant disease have to be correctly detected, identified, and quantified in the initial stages. The color and texture features have been used in order to work with the sample images of plant diseases. Algorithms for extraction of color and texture features have been developed, which are in turn used to train support vector machine (SVM) and artificial neural network (ANN) classifiers. The study has presented a reduced feature set based approach for recognition and classification of images of plant diseases. The results reveal that SVM classifier is more suitable for identification and classification of plant diseases affecting agriculture/horticulture crops.**

***Keywords* — Plant Disease, Image Processing, Feature Selection, Classifiers, Experimentation.**

## I. Introduction

Plant disease diagnosis is an art as well as science. The diagnostic process (i.e. recognition of symptoms and signs), is inherently visual and requires intuitive judgement as well as the use of scientific methods. Photographic images of plant disease symptoms and signs used extensively to enhance description of plant diseases are invaluable in research, teaching and diagnostics etc. Plant pathologists can incorporate these digital images using digital image transfer tools in diagnosis of plant diseases. Most plant diseases are caused by fungus, bacteria, viral, nematodes etc [9]. These infections agents or pathogens are either saprophytes (also called necotrophies or heterotrophies) or autotrophies (also called parasites) or facultative. Saprophytes survive on dead tissues and parasites survive on living tissues, where as facultative (in both) which can change the behavior based on circumstances. Many disease produce symptoms which are the main tools for field diagnosis of diseases showing external systems out of a series of reactions that take place between host and pathogen. As such, several important decisions regarding safe practices, the production and processing of plant have been made in the recent past. One of the main concerns of scientists is the automatic disease diagnosis and control [10]. Keeping this in back drop, work on recognition and classification of plant diseases affecting agriculture/horticulture crops has been carried out. The following papers have been cited during the literature survey to understand the different applications of computers in allied areas of the present work carried out.

## II. A Brief Overview Of Related Work

Khoje et al., [11] have proposed fruit grading system based on discrete cosine transform (DCT). The system is developed to gauge quality of fruits, namely, guava and lemon. Texture features based on DCT are extracted from the surface of normal and affected fruit sample images and fed as input to SVM and PNN classifiers. The classification results have shown that the SVM performed as better discriminator compared with PNN classifier. Razmjooy et al., [17] have proposed a hierarchical grading method for quality evaluation of defected potatoes. The system is developed in conjunction with size sorting of potatoes. Color features are extracted from defective potato images. Experimental results have shown that the SVM has very high accuracy and speed across classifiers for defect detection. Anami and Savakar [18] have presented a neural network approach to identify effect of foreign bodies (FB) on bulk food grain image samples. Different food grains, namely, green gram, groundnut, jowar, rice, and wheat are considered for recognition and classification. The color and texture features extracted from sample images are provided as input to a neural network classifier. The average classification accuracy of 90% is obtained for the tested sample images using ANN classifier. Vibhute and Bhode [21] have done a survey on several image processing techniques applied in agricultural applications. Focus has been on techniques like remote sensing, hyper-spectral imaging, fuzzy logic, neural network, genetic algorithm, wavelet, PCA, etc. The importance of image processing techniques in automatic sorting of fruits, weed detection has also been discussed. (Prasad et al., 2012) have discussed image processing methods to detect crop diseases. The proposed imaging system consists of disease spot detection using histogram based segmentation, feature extraction using Gabor wavelet transform (GWT), and classification using SVM. Classification accuracy rate of over 89% is obtained in all the cases. Landge et al., [12] have designed an image processing system to detect maize crop diseases. Color features are extracted from disease symptoms, namely, stem borer and brown stripe downy mildew found on maize crops. An ANN classifier is developed for classification of disease type. Barbedo [3] has done a survey on several image processing methods for detecting plant diseases. The techniques discussed are useful in automatic recognition, classification, and quantifying disease severity in plants. These methods are awaited to be useful for researchers providing comprehensive overview of vegetable pathology and automatic detection of plant diseases using pattern recognition techniques. Dubey et al., [5] have presented a novel approach for the detection of defected apples based on color features with k-means clustering technique. Apple scab, apple rot, and apple blotch diseases are considered for experimentation. The potential of proposed image processing approach in evaluating the quality of defected apples is observed. The simulation results revealed that the proposed approach is promising in terms of precision and computational efficiency. Rathod et al., [16] have provided various image processing and machine vision techniques for automatic



DOI: 10.9781/ijimai.2016.371

recognition of plant leaf disease. The techniques used for image preprocessing, segmentation, feature extraction, which provide fast and accurate detection of plant leaf disease have been focused. Bauer et al. [2], and Pachecho et al. [22], have proposed image processing methods for classification of leaf diseases. The high resolution multi-spectral stereo images of healthy leaves and infected with the leaf spot pathogens, namely, cercospora beticola and uromyces betae found on sugar beet are considered for the study. The classification of disease type is performed using k-NN and an adaptive Bayes classifier using Gaussian mixture models. The classification results observed indicates that an adaptive Bayes classifier using Gaussian mixture models performed better in comparison with k-NN classifier. Sungkur et al., [20] have described the design and implementation of an automated system to recognize disease spots present on leaves of sugarcane. To recognize disease spots present on leaves of sugarcane, several descriptors, namely, aspect ratio, eccentricity, circularity, and moments analysis have been tested. The system has given a classification accuracy of 95.25% using minimum distance classifier. Bandi et al., [1] have evaluated the performance of various classifiers for classifying various citrus diseases. The disease present on citrus leaves, namely, melanose, greasy spot, and scab are considered for the study. K-nearest neighbor, naive bayes (NB), LDA, and random forest tree (RFT) classifiers are used for the classification purpose. Texture features based on CCM are extracted from the disease affected citrus leaves. The experimental results reveal that the proposed work achieved 98.75% using LDA. (Fina et al., 2013) have demonstrated various image processing methods for detection and recognition of the plant pests. The imaging system used combination of k-means clustering technique and the correspondence filter. The objects (pests) from the background (pest habitat) are separated by partitioning the dataset into voronoi cells. Different attributes between the pest and its habitat (leaf, stem) are extracted and plant pests are identified using corresponding filter. The effectiveness of corresponding filter is promising in recognition and detection of pests, which can achieve rotational invariance of pests up to 360 degrees. Cui et al., [4] have developed image processing methods for quantifying severity of rust disease found on soybean leaves. Segmentation of infected areas from multi-spectral images of soybean plant leaves is done using fast manual threshold-setting method based on HSI color model. The extracted color features with ratio of infected area (RIA) and rust color index (RCI) diagnostic parameters are used as symptom indicators for quantifying rust severity. The performance of threshold-setting method and centroid-locating method are compared. It is observed that threshold-setting method works well under laboratory conditions for detecting soybean rust severity and centroid-locating method has the better performance in field application. Fenyvesi et al., [6] have demonstrated level of damage in the fruits during harvesting, transport, and manipulating. The stress developed in fruits leading to its damage is analyzed based on general material properties and unit load using finite element method (FEM) simulations. According to the model developed, it is reported that the maximum stress is developed in the middle of the fruits which results in breakage of fruits. The literature survey has revealed that there is fair amount of scope for plant disease detection in the area of agriculture and horticulture. Fungi, bacteria, virus, nematodes, etc., are the main source of diseases in plants [9]. From the literature survey presented above, it is observed that the work on classification of plant diseases like fungi, bacteria, virus, nematodes and deficiency diseases affecting agriculture/horticulture crops reported in the literature is scarce. This being the motivation, the work on classification of plant diseases in agriculture/horticulture crops is proposed to assist the farmers technologically. In the proposed work, focus has been on early detection and classification of plant diseases like fungi, bacteria, virus, nematodes and deficiency diseases affecting different agriculture/horticulture crops. The paper is organized into five sections Section.3 gives the proposed methodology. Section.4 describes results and discussion. Section.5 gives conclusion of the work.

## III. Proposed Methodology

In the proposed work, we have focused on early detection of plant disease affecting agriculture/horticulture crops. This useful work in the real world comprises of the tasks like image acquisition, pre-processing of images, feature selection, development of methodologies for identification of different plant diseases, finally development and classification of architecture for the computer vision system The Fig. 1 shows the schematic flow diagram of the proposed work.

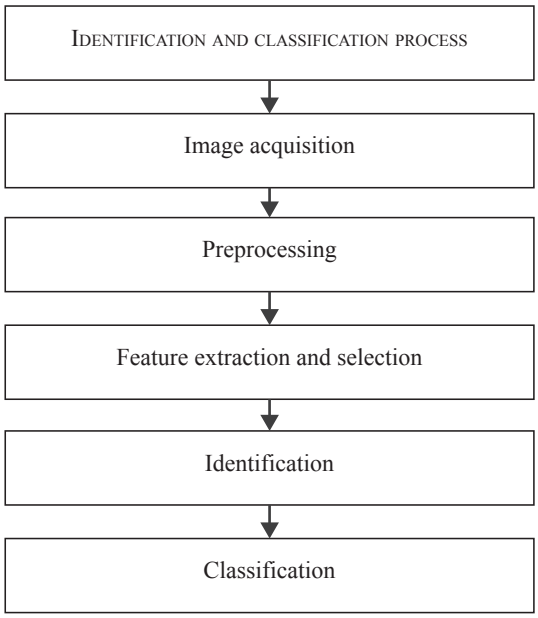


Fig. 1. Block diagram of the approach followed in the work

### A. Image data set

In the present work, plant diseases found on agriculture/horticulture crops, namely, fungal, bacterial, viral, nematodes, deficiency and normal (not affected) are considered for recognition and classification. This constitutes 6 classes. The study considers 900 sample images (150 samples of each class) for recognition and classification purpose. The set of 900 sample images used in this work was obtained from department of plant pathology, at the University of Agricultural Sciences, Dharwad, INDIA. As first signs and symptoms of disease are observed on plant leaves, methodologies for identification and classification of plant diseases affecting leaves of agriculture/horticulture crops have been developed. The Fig. 2 to 6 shows the sample images affected by plant diseases in agriculture/horticulture crops used in the present work. The classification tree is shown in the Fig. 7.

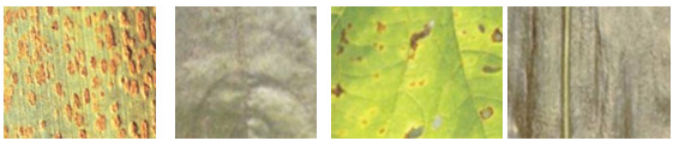

Fig. 2. Images of fungal disease affected samples a)leaf rust of wheat b) powdery mildew of sunflower c)anthracnose of grape d)downey mildew of maize

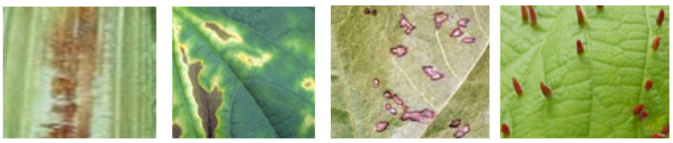

Fig. 3. Images of bacterial disease affected samples a) Stalk rot of maize b) bacterial wilt of cucumber c) angular leaf spots of cotton d) galls on lime

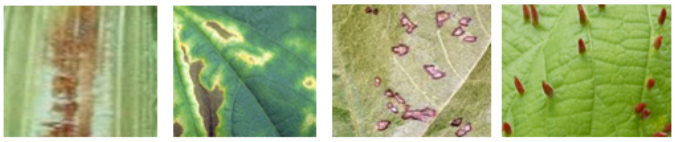

Fig. 4. Images of bacterial disease affected samples a) Stalk rot of maize b) bacterial wilt of cucumber c) angular leaf spots of cotton d) galls on lime

Fig. 5. Images of viral disease affected samples a)mosaic on cucumber b) yellow virus on grape c)veinal chlorosis on tomato d)enations on sugarbeet

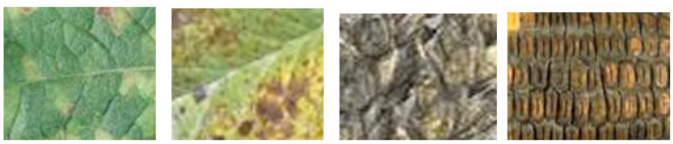

Fig. 6. Images of nematodes disease affected samples a)foliar nematode of tomato b)cyst disease on soybean c)ear cockle on wheat d)ear rot on maize

Fig. 7. Images of deficiency disease affected samples: a)magnesium deficiency on grapes b)zinc deficiency on citrus c)boron deficiency on sunflower d) potassium deficiency on tomato

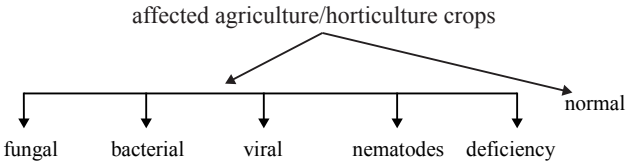


Fig. 8. Classification tree.

The symptoms of plant disease exhibit different properties like color, shape, and texture. When samples of different normal and disease affected agriculture/horticulture crops are considered, patterns vary from disease to disease. Color is an important dimension of human visual perception that allows discrimination and recognition of visual information [14]. Many natural surfaces and naturally occurring patterns reveal texture characteristic, meant to capture the granularity and repetitive forms of surfaces within an image [14]. The considered work has used some state-of-the-art color and texture features for recognition and classification of disease affected agriculture/horticulture crops to validate the accuracy and efficiency. It is apparent from the Fig.s 2 to 6 that the sample images belonging shows significant difference in terms of color and texture.

### *B. Image acquisition and preprocessing*

The image data set, used for experimentation in this thesis, comprises 9912 digital images. For image acquisition, a color camera (DXC-3000A, Sony, Tokyo, Japan) is used. The camera has a zoom lens of 10-120 mm focal length and a 72 mm close-up lens set. The camera is vertically oriented and approximately a distance of 0.5 meter is maintained while capturing the images. Image quality is definitive for the after effects of investigation, influencing both the ability to detect features under examination and accuracy of consequent estimations. Image enhancement techniques are used to emphasize features of interest and highlight certain details hidden in the image. To improve the quality of the image, preprocessing steps are applied over the image. MATLAB version 7.10 is used for implementation of the digital image processing algorithms.

Preprocessing of the image includes shade correction, removing artifacts, and formatting. Some images, originally from camera, manifest uneven lighting called shade. Due to variation in outdoor lightning conditions, some regions are brighter and some others are darker than the mean value for the whole image. This phenomenon is a consequence of inaccuracy in the system. Precise tuning of camera is done to minimize this effect. The images contain some artifacts induced like scratches, coat or mark, lumps of dust or abrasive particles. Hence, median filter and imfilter have been used to remove such artifacts. Formatting deals with storage representation and setting the attributes of the image. The images acquired from the camera are of 1920x1080 pixels and are reduced to suitable size for the reasons of reducing computational time required for feature extraction and their storage on the medium.

### *C. Feature selection*

A pattern can denote a quantitative or morphological description of an object or some other point of interest in an image, in which some organization of underlying structure can be supposed to live. In other words, a pattern is an arrangement of descriptors. Descriptors are also called features in pattern recognition literature [15]. Only significant features are extracted from the processed image. This is where the features reduction method is adopted. In the present work, feature extraction employs color features based on RGB, HSI color models, texture features based on GLCM [15] [19].

#### *Color feature extraction*

One of the primary facets of color feature extraction is the selection of a color space. A color space is a multidimensional space, in which different dimensions represent different constituents of the color. Most color spaces are three dimensional. An instance of a color space is RGB, which attributes to each pixel a three element vector, giving the color intensities of the three primary colors, namely, red (R), green (G), and blue (B). The space covered by the R, G, and B values completely describes visible colors, which are entitled as vectors in the 3D RGB color space. As a consequence, the RGB color space offers a useful starting point for representing color features of the images [14][15].

The following method is adopted in the extraction of RGB features. The foremost step is the separation of RGB components from the original color images. The next step is the computation of mean, standard deviation, variance, and range from the separated RGB components using the following Equations (1) to (6).

$$\mu \quad \underset{i=1}{\overset{N}{1/N \sum x_i}} = \frac{x_1+x_2+\ldots\ldots\ldots\ldots+x_N}{N} \qquad (1)$$

Where,
N is the total number of pixels,
$x_i$ is the $i^{th}$ pixel value

$$\text{Standard deviation } \sigma = 1/N \sum_{i=1}^{N} \sqrt{(x_i - \mu)^2} \quad (2)$$

$$\text{Variance} = \sigma \times \sigma \quad (3)$$

Maximum element and minimum elements from given input color (RGB) image is calculated using Equation (2.4).

$$max1 = max\ (image),\ max2 = max\ (max1) \quad (4)$$

The above function returns the row vector containing maximum element from each column, similarly find minimum element from whole matrix using Equation (2.5).

$$min1 = min\ (image),\ min2 = min\ (min1) \quad (5)$$

Range is the difference between the maximum and minimum elements and is given in the Equation (2.6).

$$Range = max2 - min2 \quad (6)$$

When humans see a color object, the object is depicted by its hue (H), saturation (S), and brightness or intensity (I). Hue is a good descriptor of a pure color (pure yellow, orange or red), whereas saturation refers to the amount of pure color mixed with white light. The chromatic notion of intensity (gray level) which describes brightness is the most useful descriptor of monochromatic images. The intensity component is easily quantifiable and interpretable. The HSI color model separates the intensity component from the color carrying information (hue and saturation) in a color image. As a consequence, the HSI model is an absolute aid for developing image processing algorithms based on color descriptions that are natural and instinctive to humans, who, after all, are the developers and users of these algorithms. The hue, saturation, and intensity components are extracted from these RGB components [14] [15]. RGB color space can be transformed to HSI color space using the Equations (7) to (10).

$$H = \begin{cases} \theta, & if\ B \leq G \\ 360^0 - \theta, & if\ B > G \end{cases} \quad (7)$$

With

$$\theta = \cos^{-1}\left( \frac{1/2\ [(R-G) + (R-B)]}{[(R-G)^2 + (R-B)\ (G-B)]^{1/2}} \right) \quad (8)$$

The saturation component is given by

$$S = 1 - \frac{3}{(R + G + B)}\ [min(R, G, B)] \quad (9)$$

$$I = \frac{1}{3} R\left( + G + B \right) \quad (10)$$

The concept of RGB and HSI component extraction is presented in the Algorithm 1. There are 24 color features extracted from the images and they are listed in the Table 1.

TABLE 1. COLOR FEATURES

| Sl.No. | Features | Sl.No. | Features |
|---|---|---|---|
| 1 | Red mean | 13 | Hue mean |
| 2 | Red variance | 14 | Hue variance |
| 3 | Red range | 15 | Hue range |
| 4 | Red standard deviation | 16 | Hue standard deviation |
| 5 | Green mean | 17 | Saturation mean |
| 6 | Green variance | 18 | Saturation variance |
| 7 | Green range | 19 | Saturation range |
| 8 | Green standard deviation | 20 | Saturation standard deviation |
| 9 | Blue mean | 21 | Intensity mean |
| 10 | Blue variance | 22 | Intensity variance |
| 11 | Blue range | 23 | Intensity range |
| 12 | Blue standard deviation | 24 | Intensity standard deviation |

*Color feature reduction*

It is found through experimentation that only eight color features which are common in all the sample images are significant. Hence, these eight features contribute more to the classification of plant diseases. Therefore, eight features have been considered as first-level feature reduction. The reduction is done based on threshold and delta value. Any feature values below the threshold are discarded. The threshold is chosen based on average of minimum feature value and maximum feature value. The threshold value is empirically determined as 0.2. Delta is the minimum difference between two feature values and is empirically determined as 10-3 [8]. The Fig. 8 show the histogram plot values of eight color features obtained for images of plant diseases affecting agriculture/horticulture crops. The procedure involved in color feature reduction is given in the Algorithm 1.

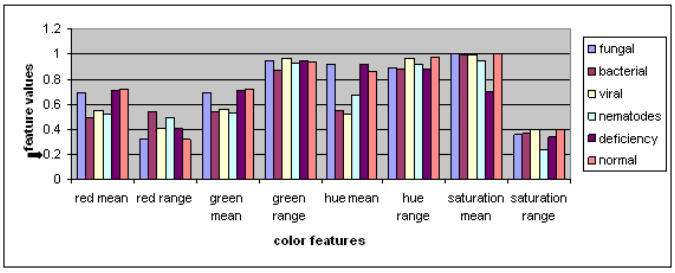


Fig. 8: color feature values of plant diseases (Threshold 0.2)

Algorithm 1: Color feature reduction

Input: Color (RGB) image.

Output: Reduced color feature vector.

Description: Delta is the minimum difference between two features and is set to 10-3. Threshold is the average of minimum and maximum feature value and is set to 0.2.

Start

Step 1: Separate the RGB components from the original 24-bit input color image

Step 2: Obtain the HSI components using the Equations (7), (8), (9), and (10)

Step 3: Compute mean, variance, and range for each RGB and HSI components using the Equations (1) through (6)

Step 4: Threshold = (minimum feature value + maximum feature value)/2

Step 5: Initialize feature vector to zeros

Step 6: For (i =1 to size of the feature vector)

If (value of feature (i) > threshold)

Select as reduced feature

Step 7: For (i=1 to size of the reduced feature vector)

Compare each feature with the other

If (features values are equal OR feature values differ by delta)

Discard the feature

Else

Select as reduced color feature

Stop.

*Texture feature extraction*

For texture features based on spatial domain analysis, one way to describe the descriptor is using a second order statistics of pairs of intensity values of pixels in an image using co-occurrence matrix method [89]. The co-occurrence matrix method of texture description is developed through the use of spatial gray level dependence matrices (SGDMs), which is based on repeated occurrence of some gray level configuration in the texture. This configuration varies rapidly with distance in fine textures and slowly with coarse textures. The GLCM Pφ, d (i, j) represents a matrix of relative frequencies describing how frequency pair of gray levels (i, j) appear in the window separated by a given distance d= (dx, dy) at an angle 'φ' [105]. Gray level co-occurrence matrices (GLCMs) method counts how often pairs of gray level of pixels separated by certain distance and oriented in a certain direction, while scanning the image from left-to-right and top-to-bottom. In the present work, a distance of 1 (d=1) when 'φ' is 0° or 90° and √2 (d= √2) when 'φ' is 45° or 135° is considered [19]. The Equations (11) to (16) are used to evaluate the textural features.

$$\text{Energy}= \sum_{i=1}^{Ng} \sum_{j=1} p^2 d(i,j) \tag{11}$$

$$\text{Entropy}= -\sum_{I,J} P(i,j)\log P(i,j) \tag{12}$$

$$\text{Homogeneity}= \sum_{i=1}^{Ng} \sum_{j=1}^{Ng} \frac{p_d(i,j)}{1+|i-j|} \tag{13}$$

$$\text{Maximum Probability} = max(P(x,y)) \tag{14}$$

$$\sigma_x = \sum_x (x-\mu_x)^2 \sum_y P(x,y) \tag{15}$$

$$\text{Contrast}= \sum_{n=0}^{Ng-1} n^2 \sum_{|i-j|} Pd(i,j) \tag{16}$$

$$\text{Inverse Difference Moment} = \sum_{x,y;x\neq y} \frac{P^{\lambda}(x,y)}{|x-y|^k} \tag{17}$$

where $\mu_x, \mu_y$ $\sigma_x, \sigma_y$ are means and standard deviations defined by,

$$\mu_x = \sum_x x \sum_y P(x,y), \quad \mu_y = \sum_y y \sum_x P(x,y),$$

$$\sigma_x = \sum_x (x-\mu_x)^2 \sum_y P(x,y) \text{ and}$$

$$\sigma_y = \sum_y (y-\mu_x)^2 \sum_x P(x,y)$$

The differentiation between sample images is carried out in the simplest way, quantifying average gray levels within the matrix, change in the gray level with respect to average level of minimum and maximum gray levels present in the matrix. Hence, basic co-occurrence features, namely, mean, variance, and range has been considered using the Equations (1) to (6). The texture features used in the work are listed in the Table 2.

TABLE 2: GLCM TEXTURE FEATURES

| Sl.No. | Features | Sl. No. | Features | Sl.No. | Features |
|---|---|---|---|---|---|
| 1 | Red GLCM mean | 11 | Green GLCM mean | 21 | Blue GLCM mean |
| 2 | Red GLCM variance | 12 | Green GLCM variance | 22 | Blue GLCM variance |
| 3 | Red GLCM range | 13 | Green GLCM range | 23 | Blue GLCM range |
| 4 | Red GLCM energy | 14 | Green GLCM energy | 24 | Blue GLCM energy |
| 5 | Red GLCM entropy | 15 | Green GLCM entropy | 25 | Blue GLCM entropy |
| 6 | Red GLCM homogeneity | 16 | Green GLCM homogeneity | 26 | Blue GLCM homogeneity |
| 7 | Red GLCM sum mean | 17 | Green GLCM sum mean | 27 | Red GLCM sum mean |
| 8 | Red GLCM correlation | 18 | Green GLCM correlation | 28 | Blue GLCM correlation |
| 9 | Red GLCM contrast | 19 | Green GLCM contrast | 29 | Blue GLCM contrast |
| 10 | Red GLCM Maximum Probability | 20 | Green GLCM Maximum Probability | 30 | Blue GLCM Maximum Probability |

*Texture feature reduction*

It is found through experimentation that only five texture features which are common in all the sample images are significant. Hence, these five features contribute more to the classification of plant diseases. Therefore, five features have been considered as first-level feature reduction. The reduction is done based on threshold and delta value. Any feature values below threshold are discarded. The threshold is chosen based on average of minimum feature value and maximum feature value. The threshold value is empirically determined as 100. Delta is the minimum difference between two feature values and is empirically determined as 10-3 [8]. The Fig. 9 show the histogram plot values of six texture features obtained for images of plant diseases affecting agriculture/horticulture crops. The procedure involved in texture feature reduction is given in the Algorithm 2.

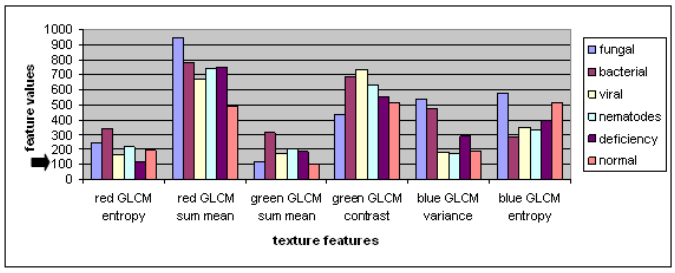


Fig. 9: texture feature values of plant diseases (Threshold 100)

Algorithm 2: Texture feature reduction

Input: Color (RGB) image.

Output: Reduced texture feature vector

Description: Pφ, d (x, y) means GLCM matrices in the direction (φ= 00, 450, 900, and 1350 ) and 'd' is the distance. Delta is the minimum difference between two features and is set to 10-3. Threshold is the average of minimum and maximum feature value and is set to 100.

Start

Step 1: For all the separated RGB components, derive the co-occurrence matrices Pφ, d (i, j) in four directions 00, 450, 900, and 1350 and d=1

Step 2: Compute mean, variance, and range for each RGB components using theEquations (1) through (6)

Step 3: Threshold = (minimum feature value + maximum feature value)/2

Step 4: Initialize feature vector to zeros

Step 5: For (i =1 to size of the feature vector)

If (value of feature (i) >threshold)

Select as reduced feature

Step 6: For (i=1 to size of the reduced feature vector)

Compare each feature with the other

If (feature values are equal OR feature values differ by delta)

Discard the feature

Else

Select as reduced texture feature

Stop.

## D. Classification

The study has adopted artificial neural network based classifiers using multilayer feed-forward with back propagation support vector machine based classifiers in the recognition of images of plant disease and studied their behavior in terms of suitability of classifiers for identification of different plant diseases.

## IV. Results And Discussion

The classifiers are trained and tested using images of plant diseases. The sample images are divided into two halves and one half is used for training and other is used for testing. The color and texture features are used to train and test neural network model.

The percentage accuracy of recognition and classification is defined as the ratio of correctly recognized sample images to the total number of sample images and is given in the Equation (17). The process of recognition and classification is given in the Algorithm 3.

$$\text{Percentage accuracy (\%)} = \frac{\text{correctly recognized sample images}}{\text{total number of test sample images}} \text{x} 100 \quad (17)$$

Algorithm 3: Recognition and classification of plant diseases affecting agriculture/horticulture crops

Input: Color (RGB) images of plant diseases affecting agriculture/ horticulture crops.

Output: Recognized and classified images.

Start

Step 1: Apply color and texture feature extraction input color image and obtain color and texture features

Step 2: Apply color and texture feature reduction Algorithms 1 and 2 to color and texture features and obtain reduced color and texture feature vector

Step 3: Train the SVM and BPNN with reduced color and texture feature vector

Step 4: Accept test images and repeat Steps 1 and 2

Step 5: Recognize and classify the images using SVM and BPNN

Stop.

*SVM based classifier*

A support vector machine (SVM) is used to recognize plant disease affecting agriculture/horticulture crops. The study has chosen SVM because of its efficient implementations and performances proved to be excellent for high dimensional problems and small data sets. Viewing training input vector in an *n*-dimensional space, SVM constructs a hyper-plane in the space, which can be used for classification that has the highest distance to the closest training data point of any class (functional margin). To compute the margin, two parallel hyper-planes are constructed, one on every side of the isolating hyper-plane, which are pushed up in opposition to the two data sets. The aim is to determine which class a new data point belongs based on data points associated to one of the two classes. In the case of support vector machines, a data point is computed as a p-dimensional vector (a list of p numbers) and it is meant to know whether such levels can be forked by a (p−1) dimensional hyper-plane. This is called a linear classifier or maximum margin classifier [123]. The core of SVM Matlab toolbox used in the present work is based on Dr. Lin's Lib SVM version 2.33. It is developed by Junshui Ma, Los Alamos National Lab and Yi Zhao, Electrical Engineering department, Ohio State University [10].

The Fig. 10 shows the graph of classification accuracy of plant diseases affecting agriculture/horticulture crops using reduced eight color features with SVM classifier. From the graph, it is observed that the maximum classification accuracy of 91% has occurred with images of normal. The minimum classification accuracy of 78% has occurred with images of nematodes disease. The average classification accuracy of 84% is achieved irrespective of the image types of plant disease affecting agriculture/horticulture crops.


Fig.10: Classification efficiency for plant diseases using color features with SVM

The Fig. 11 shows the graph of classification accuracy of plant diseases affecting agriculture/horticulture using reduced six texture features with SVM classifier. From the graph, it is observed that the maximum classification accuracy of 96% has occurred with images of normal. The minimum classification accuracy of 83% has occurred with images of bacterial disease. The average classification accuracy of 89% is achieved is achieved irrespective of the image types of plant disease affecting agriculture/horticulture crops.

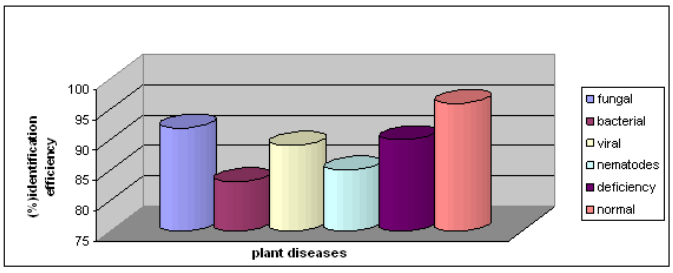


Fig. 11: Classification efficiency for plant diseases using texture features with SVM

In order to take advantages offered by both color texture features, color and texture features are combined and used as input to the SVM classifier. The training and testing are carried out with combined color and texture features. The Fig. 12 shows the graph of classification accuracy of plant diseases affecting agriculture/horticulture using combined features with SVM classifier. From the graph, it is observed that the maximum classification accuracy of 98% has occurred with images of fungal disease. The minimum classification accuracy of 86% has occurred with images of nematodes disease. The average classification accuracy of 92% is achieved irrespective of the image types of plant disease affecting agriculture/horticulture crops.

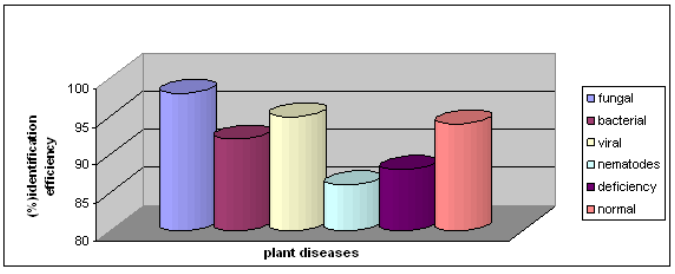


Fig. 12: Classification efficiency for plant diseases using combined features with SVM

*ANN based classifier*

In order to corroborate the accuracy of classification obtained from SVM classifier, the study has considered a multilayer BPNN as an alternate model to identify plant disease symptoms affecting agriculture/horticulture crops.

Multilayer back propagation neural network (BPNN) has been used as a classifier in the present work. A typical multilayer neural network comprises an input layer, output layer, and hidden (intermediate) layer of neurons. BPNN has the potential to classify different forms (patterns) of arbitrary complex input/output mappings or decision surfaces. Among the majority of multilayer feed-forward artificial neural network (ANN) algorithms, BPNN emerged as the most important algorithm for the supervised training and has been the workhorse for many classification problems in different applications of machine learning. The study has chosen BPNN because of its ease and strength in execution for large training data set. The number of neurons in the input layer corresponds to the number of input pattern vectors and the number of neurons in the output layer corresponds to the number of pattern types (classes). In the hidden layers sigmoid functions have been used. The number of nodes in the hidden layer is calculated using the Equation (2.32) [8].

$$n = \frac{(I+O)}{2} + y\text{^}0.5 \qquad (18)$$

Where, n= number of nodes in hidden layer,

I= number of input features,

O= number of outputs,

y= number of inputs pattern in the training set

The training and testing is carried out using reduced color and texture features. The number of nodes in the hidden layer is calculated using the Equation (18).

The ANN classifier has used eight input nodes and six output nodes corresponding to six chosen categories of plant diseases and the chosen eight color features respectively. The Fig. 13 shows the graph of classification accuracy of plant diseases affecting agriculture/horticulture using reduced eight color features with ANN classifier. From the graph, it is observed that the maximum classification accuracy of 94% has occurred with images of normal. The minimum classification accuracy of 72% has occurred with images of deficiency disease. The average classification accuracy of 82% is achieved irrespective of the image types of plant disease affecting agriculture/horticulture crops.

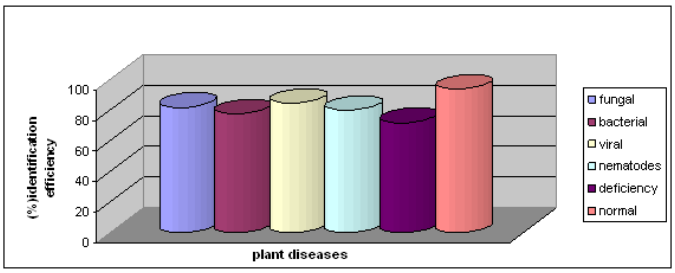


Fig. 13: Classification efficiency for plant diseases using color features with ANN

The ANN classifier has used six input nodes and six output nodes corresponding to six chosen categories of plant diseases and the chosen six texture features respectively. The Fig. 14 shows the graph

of classification accuracy of plant diseases affecting agriculture/ horticulture using reduced six texture features with ANN classifier. From the graph, it is observed that the maximum classification accuracy of 92% has occurred with images of normal. The minimum classification accuracy of 78% has occurred with images of deficiency disease. The average classification accuracy of 84% is achieved irrespective of the image types of plant disease affecting agriculture/ horticulture crops.

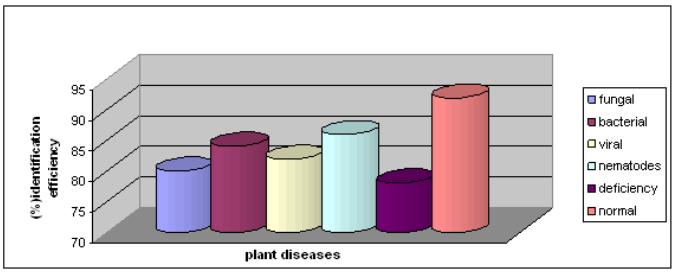


Fig. 14: Classification efficiency for plant diseases using texture features with ANN

In order to take advantages offered by both color texture features, color and texture features are combined and used as input to the BPNN classifier. The Fig. 15 shows the graph of classification accuracy of plant diseases affecting agriculture/horticulture using combined features with ANN classifier. From the graph, it is observed that the maximum classification accuracy of 92% has occurred with images of normal. The minimum classification accuracy of 82% has occurred with images of deficiency disease. The average classification accuracy of 87% is achieved irrespective of the image types of plant disease affecting agriculture/horticulture crops.

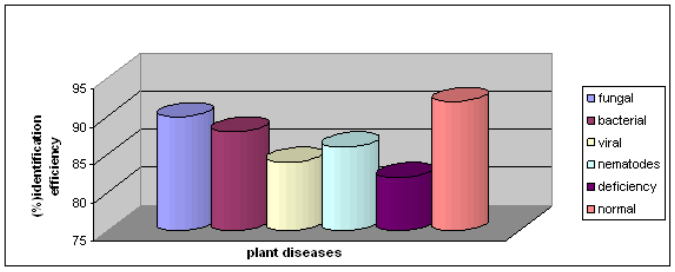


Fig. 15: Classification efficiency for plant diseases using combined features with ANN

A comparison between the performances of SVM and ANN classifiers has been done. The comparison of classification accuracies of both the classifiers using reduced color, texture and combined features is given in the Table 3. From the Table 3, it is evident that the SVM based classifier has given better classification accuracy than the ANN classifier.

TABLE 3: PERFORMANCE OF SVM AND ANN CLASSIFIERS USING COLOR, TEXTURE AND COMBINED FEATURES

| classification performance rate(%) | classifiers | | | | | |
|---|---|---|---|---|---|---|
| | SVM | | | ANN | | |
| | color | texture | combined | color | texture | combined |
| minimum accuracy | 78 | 83 | 86 | 72 | 78 | 82 |
| maximum accuracy | 91 | 96 | 98 | 94 | 92 | 92 |
| average identification accuracy | 84 | 89 | 92 | 82 | 84 | 87 |

The performance of individual classifiers with respect to true positive rate (TPR), false positive rate (FPR), precision, recall, F-measure, and average classification accuracy (ACA) using SVM and ANN classifiers with combined features is given in the Table 4. From the Table 4, it is evident that SVM classifier has given better classification accuracy than ANN for identification and classification of plant diseases affecting agriculture/horticulture crops.

TABLE 4: PERFORMANCE EVALUATION OF SVM AND ANN CLASSIFIERS USING COMBINED FEATURES

| Classifier | TP Rate | FP Rate | Precision | Recall | F-Measure | ACA (%) |
|---|---|---|---|---|---|---|
| SVM | 0.931 | 0.917 | 0.976 | 0.921 | 0.945 | 92.17 |
| ANN | 0.847 | 0.953 | 0.823 | 0.847 | 0.834 | 87.48 |

## V. Concusion

Recognizing the plant disease is mainly the purpose of the proposed approach. Thus, the proposed algorithms are tested on five plant diseases with normal which influence the agriculture/horticulture crops. The developed classifier uses color and texture features for classification of plant diseases and affecting agriculture/horticulture crops. Even though these features have given different accuracies in isolation for different images of plant disease affecting agriculture/horticulture crops, the very combination of features has proved to be effective. The main advantage of this proposed approach is that, considerably less number of features is deployed to achieve better classification accuracy and to reduce computation time. The experimental results indicate that the proposed approach is a valuable approach, which can significantly support an accurate detection of plant disease in a little computational effort. It indicates that SVM achieves a significant improvement in the classification accuracy over ANN. SVM proved to be a powerful tool for automatic classification of plant diseases considered in the present work. But, there is scope for enhancement in the classification accuracy.

## References

[1] Bandi S R., Vardharajan A. and Chinnasamy A, Performance Evaluation of Various Statistical Classifiers in Detecting the Diseased Citrus Leaves, International Journal of Engineering Science and Technology, Vol. 5, Issue.2 February 2013, pp.297-307.

[2] Bauer S D., Korc F. and Wolfgang Forstner, The Potential of Automatic Methods of Classification to Identify Leaf Diseases from Multi-spectral Images, Precision Agriculture, Vol.12, 2011, pp.361-377.

[3] Barbedo J C A, Digital Image Processing Techniques for Detecting, Quantifying and Classifying Plant Diseases, Springer Plus, Vol.2, Issue.660, 2013, pp.1-12.

[4] Cui D., Zhang Q., Li M., Hartman G L. and Zhao Y, Image Processing Methods for Quantitatively Detecting Soybean Rust from Multi-spectral Images, Biosystems engineering, Vol.107, Issue.3, 2010, pp.186-193.

[5] Dubey S R., Dixit P., Singh N. and Gupta J P, Infected Fruit Part Detection using K-Means Clustering Segmentation Technique, International Journal of Artificial Intelligence and Interactive Multimedia, Vol. 2, Issue.2, 2013, pp.65-72.

[6] Fenyvesi L., Fenyvesi D. and Csatár A, (2013), Stress Analysis in Fruits, Advances in Mechanical Engineering, Hindawi Publishing Corporation, Article ID: 874673, 2013, pp.1-6.

[7] Fina F., Birch P., Young R., Obu J., Faithpraise B. and Chris Chatwin, Automatic Plant Pest Detection and Recognition Using k-means Clustering Algorithm and Correspondence Filters, International Journal of Advanced Biotechnology and Research, Vol. 4, Issue.2, 2013, pp.189-199.

[8] Jagadeesh D. Pujari, Rajesh Yakkundimath and A.S.Byadgi, Recognition and Classification of Normal and Affected Agriculture Produce Using Reduced Color and Texture Features, International Journal of Computer Applications, Vol.93, Issue.11, 2014, pp.17-24.

[9] Jagadeesh D. Pujari, Rajesh Yakkundimath and A.S.Byadgi, Automatic Fungal Disease Detection based on Wavelet Feature Extraction and PCA Analysis in Commercial Crops, International Journal of Image, Graphics and Signal processing, Vol.6, Issue.1, 2014, pp.24-31.

[10] Jagadeesh D. Pujari, Rajesh Yakkundimath and A.S.Byadgi, Detection and Classification of Fungal Disease with Radon Transform and Support Vector Machine Affected on Cereals, International Journal of Computer Vision and Robotics, Vol.4, Issue.4, 2014, pp.261-280.

[11] Khoje S A., Bodhe S K. and Adsul A, Automated Skin Defect Identification System for Fruit Grading Based on Discrete Curvelet Transform International Journal of Engineering and Technology, Vol.5, Issue.4, September-2013, pp.3251-3256.

[12] Landge P S., Patil S A., Khot D S., Otari O D. and Malavkar U G, Automatic Detection and Classification of Plant Disease through Image Processing, International Journal of Advanced Research in Computer Science and Software Engineering, Vol.3, Issue.7, July 2013, pp.798-801.

[13] Prasad S., Piyush Kumar., Hazra R. and Ajay Kumar, Plant Leaf Disease Detection Using Gabor Wavelet Transform, Proceedings of 3rd International Conference on Swarm, Evolutionary, and Memetic Computing, Springer-Verlag, Berlin, Heidelberg, 2012.

[14] Pujari J D, Content Based Image Retrieval Using Color and Texture Features, Ph.D. Thesis, Gulburga University, Gulburga, 2008.

[15] Rafael C G., Woods R E. and Eddins S L, Digital Image Processing, Prentice Hall, 3rd edition, 2008.(92)

[16] Rathod A N., Tanawal B. and Shah V, Image Processing Techniques for Detection of Leaf Disease, International Journal of Advanced Research in Computer Science and Software Engineering, Vol.3, Issue.11, November 2013, pp.397-399.

[17] Razmjooya N., Mousavib B S. and Soleymani F, A Real Time Mathematical Computer Method for Potato Inspection Using Machine Vision, Computers and Mathematics with Applications, Vol. 63, 2012, pp.268–279.

[18] Savakar D G. and Anami B S, Improved Method for Identification and Classification of Foreign Bodies Mixed Food Grains Image Samples, International Journal of Artificial Intelligence and Machine Learning, Vol.9, Issue.1, 2009, pp.1-8.

[19] Sonka M., Hlavac V. and Boyle R, Digital Image Processing and Computer Vision, Cengage Learning, Indian Edition, 2008.(105)

[20] Sungkur R K., Baichoo S. and Poligadu A, 2013, An Automated System to Recognize Fungi-caused Diseases on Sugarcane Leaves, Proceedings of Global Engineering, Science and Technology Conference, Singapore, 3-4 October, 2013.

[21] Vibhute A. and Bhode S K, Applications of Image Processing in Agriculture: A Survey, International Journal of Computer Applications, Vol. 52, Issue. 2, August 2012, pp.34-40.

[22] Pacheco, A. et al. Reconstruction of High Resolution 3D Objects from Incomplete Images and 3D Information. International Journal of Interactive Multimedia and Artificial Intelligence, Vol. 2, Issue 6, pp. 7-16. DOI: 10.9781/ijimai.2014.261

**Jagadeesh D.Pujari** He has obtained Bachelor of Engineering in Computer Science in 1990 and MS in Software Systems (BITS PILANI) and Ph.D. in Computer Science in 2008. Currently he is working as Professor & Head in the department of Information Science & Engineering, SDMCET, Dharwad, INDIA. His research areas of interests are Image Processing Pattern Recognition and Content-Based Image Retrieval.

**Rajesh Yakkundimath** He has obtained Bachelor of Engineering in Electronics & Instrumentation in 2004(VTU, Belgaum, INDIA) and M.Tech. in Computer Science & Engineering in 2007 (VTU, Belgaum, INDIA). He is working for his doctoral degree in Computer Science under VTU, Belgaum, INDIA. Since 2008 he is working as Assistant Professor in the department of Computer Science & Engineering, KLE.Institute of Technology, Hubli, INDIA.

**Abdulmunaf. Syedhusain Byadgi** He has obtained Bachelor of Science (Agri.) in 1977(UAS, Bangalore, INDIA), M.Sc. (Agri.) in 1980(UAS, Bangalore, INDIA) and Ph.D. in 1994 (IARI, New Delhi, INDIA). Currently is working as Professor in the department of Plant Pathology, UAS, Dharwar, INDIA.

# A New Protection for Android Applications

ER-RAJY Latifa, EL KIRAM My Ahmed

*Faculty of Sciences Semlalia, University Cadi Ayyad, Marrakech, Morocco*

***Abstract* — Today, Smartphones are very powerful, and many of its applications use wireless multimedia communications. Prevention from the external dangers (threats) has become a big concern for the experts these days. Android security has become a very important issue because of the free application it provides and the feature which make it very easy for anyone to develop and published it on Play store. Some work has already been done on the android security model, including several analyses of the model and frameworks aimed at enforcing security standards. In this article, we introduce a tool called PermisSecure that is able to perform both static and dynamic analysis on Android programs to automatically detect suspicious applications that request unnecessary or dangerous permissions.**

***Keywords* — Android, Operating System Mobile, Privacy, Issues, Hackers, Permission, Solution, Protection.**

## I. Introduction

Since the first Android powered phone named The HTC Dream (also known as the T-Mobile G1 in the United States and parts of Europe, and as the Era G1 in Poland) was delivered in October 2008 [1], Android smart phones have grown to the largest global market share (76%) among all smartphones shipped in the 4th quarter of 2014 [2]. In 2014, Google announced that more than billion Android devices had been activated [3]. This important popularity of Android and the open nature of its application marketplace makes it a prime target for attackers. Malware authors can be freely upload malicious applications to the Android Play Store waiting for unsuspecting users to download and install them.

To alert users to the privacy and security ramifications of installing an application, Android employs mandatory access control (MAC) in the form of an install-time permission system [4]. At installation time, an application must request permission to access system resources such as location, Internet, or the cellular network, from the user. Then the user is presented with a screen allowing him to either grant all the permissions or cancel the installation. Since it is not possible to selectively accept or deny access privileges. Thus, many users simply accept such permission requests without considering their implications, which put their private data in the zone of danger [5]. For example if an application granted some critical permissions such as the INTERNET permission it can controls communication with remote servers and if this application was also granted access to the Android camera, nothing prevents it from sending the user's pictures to any server on the internet. May 2014, Google had done a Play Store updates to simplify the display of the permissions and allow better navigation user. They were re-grouped by categories. Therefore, from more than 150 permissions, we went to a dozen groups, including another category, which includes everything that does not fit elsewhere [6]. With the old system, each update of the application, if developer added a new permission, the Play Store posted it and the user must then accept it. With the new system, developers can add for example the permission ACCESS_SUPERUSER that allow him to take control of all the features of the phone and storage if his application had permissions in the group "another category" [7].

The rest of the paper is organized as follows. In Section 2, we give an overview on the background of our work. Section 3 describes the details on the problem caused by permissions requested by android applications and their updates. Section 4 gives an overview on related work. We proceed in Section 5 with details of the design and user interface of our tool. In Section 6, we demonstrate how our tool protects the user from permissions and updates challenges by providing the results of applying PermisSecure to 120 paid and 456 free applications from the Google Play Store. In Section 7 we conclude and summarize our results and contributions.

## II. Background

To frame the problem, we describe the Android architecture, permission system and explain how these permissions requested by an application can play an important role in spring of malwares.

### *A. Application Package*

An Android application package or apk file is an archive. It contains a Dalvik executable (dex file), which is a compiled Android program that runs on a Dalvik virtual machine, and a set of resources (non-executable files like graphics, media files, user interface components, etc.). Application packages also contain a manifest (AndroidManifest.xml), which Android contains meta-information about the application like package name, version, supported Android versions, and other attributes. These components are digitally signed with the developer's signing key. The developer's signing certificate can be self-signed and is included in the application package [8].

### *B. Deconstructing Application Installation*

Any developer (even those who have not registered with Google) can create and distribute applications through the official Google Play Store, through third-party markets (e.g., Amazon Appstore) or through developer websites (side-loading). The lack of control over the application distribution process raises the importance of enforcing security within the Android OS. During the installation of a new application, permissions are approved prior to installation, but the rest of the process remains the same. First, the application package validity is verified: the system ensures that the Android application package has not been modified or corrupted since being signed, and that it contains a valid certificate for the signing key. Then, Android decides whether the application is a new installation or should overwrite an existing application. If the application being installed has the same package attribute in the manifest (e.g., com.google.android.music) as another currently installed application, then Android will treat the installation as an update. So, the certificate (or set of certificates if signed by multiple keys) is compared to the certificate(s) of the already installed application. If both applications were signed with the same key(s), then the currently installed binary is removed (preserving any user data) and the new application is installed in its place. Otherwise, the new application is installed as an initial installation. Next Android must assign a UID to the application. In this case, the previous application's UID is used. In the case of an initial installation, Android checks if the application's manifest contains the sharedUserId directive. If so,



DOI: 10.9781/ijimai.2016.372

Android looks for any other installed applications that are signed with the same key(s) and have sharedUserId specified in their manifest. If such applications are found, the application is assigned the same UID; otherwise a new UID is created.

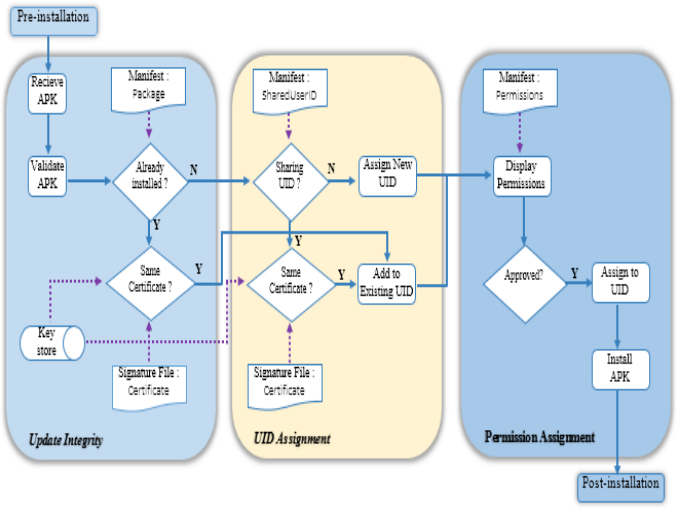


Fig 1. Abstract model of the Android installation process for an application package (apk).

Finally permissions must be assigned to the UID[9]. The user is prompted to review and approve the permission assignments before the application is installed. When UID sharing is not used, permissions listed in the application's manifest are assigned to the UID. When UID sharing is used, the UID is assigned the union of all permissions in the manifests of applications sharing the UID. If the application is updating an already installed application, the permissions listed in the updated application's manifest are assigned to the UID [10].

## III. Problem Description

*Permission System:* Android controls access to system resources with install-time permissions by using two-way process. Firstly, developer defines the required permissions that are the first requisite for performing the functionalities of an application. Secondly, during installation time, user must have approved all the requested permissions to use an application [11]. Permissions requested by each application permissions fall into four levels:

(1) Normal – These permissions protect access to API calls that cannot impart real harm to the user (e.g. SET_WALLPAPER controls the ability to change the user's background wallpaper) and, while applications need to request them, they are automatically granted.

(2) Dangerous – These control access to potentially harmful API calls, like those related to spending money or gathering private information. For example, Dangerous permissions are required to send text messages, read the list of contacts, call numbers, open Internet connections, etc.

(3) Signature – These regulate access to the most dangerous privileges, such as the ability to control the backup process or delete application packages. They are automatically granted to a requesting application if that application is signed by the same certificate (so, developed by the same entity) as that which declared/created the permission. This level is designed to allow applications that are part of a suite, or otherwise related, to share data.

(4) Signature/System – Same as Signature, except that the system image gets the permissions automatically as well. This is designed for use by device manufacturers only.

*Menace of Pileup*: The security analysis of mobile updating, focusing on Android Package Manager brings to light a new category of unexpected and security-critical vulnerabilities within Android's update installation logic. Such vulnerabilities, called Pileup (privilege escalation through updating), enable an unprivileged malicious application to acquire system capabilities once the OS is upgraded, without being noticed by the phone user. More specifically, through the application running on a lower version Android, the adversary can strategically claim a set of carefully selected privileges or attributes only available on the higher OS version. For example, the application can define a new system permission such as permission. ADD_VOICEMAIL on Android 2.3.6, which is to be added on 4.0.4. It can also use the shared user ID[12] (a string specified within an application's manifest file) of a new system application on 4.0.4, its package name and other attributes. Since these privileges and attributes do not exist in the old system (2.3.6 in the example), the malicious application can silently acquire them (self-defined permission, shared UID and package name, etc.). When the system is being updated to the new one, the Pileup flaws within the new Package Manager will be automatically exploited. Consequently, such an application can stealthily obtain related system privileges, resources or capabilities. In the above example, once the phone is upgraded to 4.0.4, the application immediately gets permission.ADD_VOICEMAIL without the user's consent and even becomes its owner, capable of setting its protection level and description. Also, the preempted shared UID enables the malicious application to substitute for system applications such as Google Calendar, and the package name trick was found to work on the Android browser, allowing the malicious application to contaminate its cookies, cache, security configurations and bookmarks, etc.

## IV. Related Work

Research related to this work can be classified into the following categories:

*Android Permissions:* Previous studies of Android applications have been limited in their understanding of permission usage. Enck et al. apply Fortify's Java static analysis tool to decompiled applications; they analyze a large set of applications and study their API use [13]. However, they are limited to studying application's use of a small number of permissions and API calls. In a recent study, Felt et al. manually classify a small set of Android applications as over privileged or not [14]. They were unable to reliably differentiate between necessary and unnecessary permissions because of limited Android documentation.

*Update behavior of Android:* The first studies has been by done Moeller et al. [15] by analyzing the updates of applications from Google Play quantitatively. An attack of the android system called Application Update Attack is studied by Tenenboim et al. [16]. Application updates might be a potential way to implant new security vulnerability and privacy data leaks to the user's phones. Chin et al. [17] studied users's confidence in security and privacy of Android. They found that users reported various concerns because of some misconceptions or misunderstandings. Android permissions provide a mechanism for users to manage the access control of applications, especially when fine-grained controls are granted.

*Privilege escalation:* XManDroid [18] was designed to prevent privilege escalation and collusion attacks by enforcing policies on the communications between applications, e.g., banning an application that has access to the user's location from interacting with an application that is allowed to access the Internet. Aurasium [19] repackages applications and introduces an intermediate layer between the framework's native code libraries and the operating system kernel inside the application process. AppSealer [20] combines static- and

dynamic-code analysis techniques to patch the applications's bytecode in order to mitigate component hijacking attacks. Xing et al.[7] Authors introduce a scanner tool for detecting applications that are vulnerable against the pileup threat.

## V. PermisSecure Introduction

In this section, we present PermisSecure, a tool sandbox based on dynamic and static analysis for Android smartphones, which increases user awareness about potentially harmful applications in install-time on his phone. The concept is based on the assumption that users are willing to take security increasing actions (such as canceling the installation of a potentially harmful application) once they gain knowledge about a potential dangerous or unnecessary permissions requested.

### A. Interface User

The design and implementation of the PermisSecure user interface follows the basic principle of warning, to provide the user with only as many pieces of information as necessary to avoid suspicious applications. Further, we designed the application to integrate seamlessly in the Android system.

When the user wants to install a new application, the software involved to perform an analysis on two levels (See Fig. 5(a)) , the first level it analyzes the permissions requested by the application, if they are dangerous it displays a warning to the user who can choose between contain or cancel the installation (See Fig. 5(b)). Otherwise, it goes to the second level of analysis and verifies the code. Therefore, if the code is suspicious, it shows to the user a warning same to that of the first level, otherwise it allows the installation of the application. PermisSecure repeat the process when an application update is available (See Fig. 5(c)).

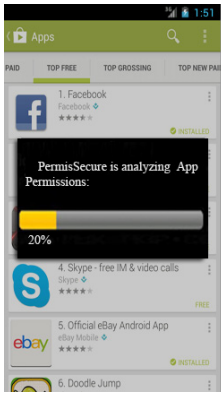


(a) PermisSecure preform an analysis in install-time of new application.

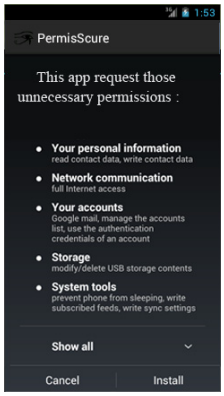


(b) PermisSecure analyzes permissions and displays a warning to the user who can choose between contain or cancel the installation.

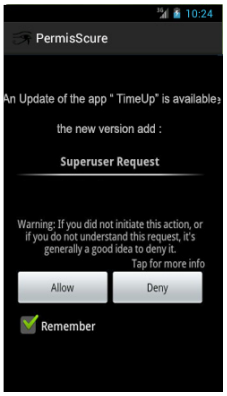


(c) Once an application is available, PermisSecure analyzes it.

## VI. Results

We applied PermisSecure to 120 paid and 456 free applications from the Google Play Store. For the applications to identify the dangerous or unnecessary permissions. PermisSecure calculates the maximum set of Android permissions that an application may need. We compare that set to the permissions actually requested by the application. If the application requests more permissions, then it is over privileged.

*Unnecessary permission*: PermisSecure identified that 45% of free and 22% of paid applications have unnecessary permissions. In some cases, we were able to determine why developers asked for unnecessary permissions.

- Permission Name: Developers sometimes request permissions with names that sound related to their application's functionality, even if the permissions are not required.
- RelatedMethods: Some classes contain a mix of permission-protected and unprotected methods. We have observed applications using unprotected methods but requesting permissions that are required for other methods in the same class. For example, android.provider.Settings.Secure includes both setters and getters. Setters require the WRITE_SETTINGS permission, and the getters do not. Two applications use the getters and not the setters, but request the WRITE_SETTINGS permission.
- Copy and Paste: Popular message boards contain Android code snippets and advice about permission requirements. Sometimes this information is inaccurate, and developers who copy it will over privilege their applications. For example, one application in our data sets registers to receive the android.net.wifi.STATE_CHANGE Intent and requests the ACCESS_WIFI_STATE permission. As of May 2011, the third-highest Google search result for that Intent contains the incorrect assertion that it requires that permission [21].
- Deputies: An application can send an Intent to another deputy application, asking the deputy to perform an operation. If the deputy makes a permission-protected API call, then the deputy needs the permission. The sender of the Intent, however, does not. We noticed instances of applications requesting permissions for actions that they asked deputies to do. For example, one application asks the Android Market to install another application. The sender asks for INSTALL_PACKAGES, which it does not need because the Market application does the installation. Another application asks the built-in camera application to take photos, yet requests the CAMERA permission for itself.
- Testing Artifacts: A developer might add a permission during testing and then forget to remove it when the test code is removed. For example, ACCESS_MOCK_LOCATION is typically used only for testing but can be seen in released applications.

Confusion over permission names, related methods, and Intents could be addressed with improved API documentation. We recommend listing permission requirements on a per-method (rather than per-class) basis. Confusion over deputies could be reduced by clarifying the relationship between permissions and pre-installed system applications.

| *Permission* | *Types* | | *Permission level* |
|---|---|---|---|
| | *Paid* | *Free* | |
| ACCESS_NETWORK_STATE | 10% | 15% | Normal |
| READ_PHONE_STATE | 9% | 15% | Dangerous |
| ACCESS_WIFI_STATE | 6% | 8% | Normal |
| WAKE_LOCK | 3% | 5% | Dangerous |
| WRITE_EXTERNAL_STORAGE | 5% | 7% | Dangerous |
| ACCESS_MOCK_LOCATION | 4% | 6% | Dangerous |
| CALL_PHONE | 4% | 5% | Dangerous |
| ACCESS_COARSE_LOCATION | 3% | 5% | Dangerous |
| CAMERA | 2% | 5% | Dangerous |
| INTERNET | 3% | 5% | Dangerous |

This table shows that almost all unnecessary requested by applications (paid and free) are dangerous.

*Dangerous permissions:* We are concerned with the prevalence of dangerous permissions. Dangerous permissions are displayed as

a warning to users during installation and can have serious security ramifications if abused. We find that 93% of free and 82% of paid applications have at least one dangerous permission, e.g., generate at least one warning. Android permissions are grouped into functionality categories. This provides a relative measure of which parts of the protected API are used by applications. A small number of permissions are requested very frequently. In particular, the INTERNET permission is heavily used. We find that 14% of free and 4% of paid applications request INTERNET as their only dangerous permission. Barrera et al. hypothesize that free applications often need the INTERNET permission only to load advertisements [22]. The disparity in INTERNET use between free and paid applications supports this hypothesis, although it is still the most popular permission for paid applications. Enck et al. found that some free applications leak personal data [23][24], this may explain the difference in ACCESS COARSE LOCATION requests. The prevalence of the INTERNET permission means that most applications with access to personal information also have the ability to leak it. For example, 97% of the 225 applications that ask for ACCESS FINE LOCATION also request the INTERNET permission. Similarly, we find that 99%, 94%, and 78% of the 306, 149, and 14 respectively applications that request ACCESS COARSE LOCATION, READ CONTACTS, and READ CALENDAR have the INTERNET permission. Although many applications ask for at least one Dangerous permission, the total number of permission requests is typically low. Even the most highly privileged application in our set asks for less than half of the available 56 dangerous permissions. Fig. 3 shows the distribution of dangerous permission requests.

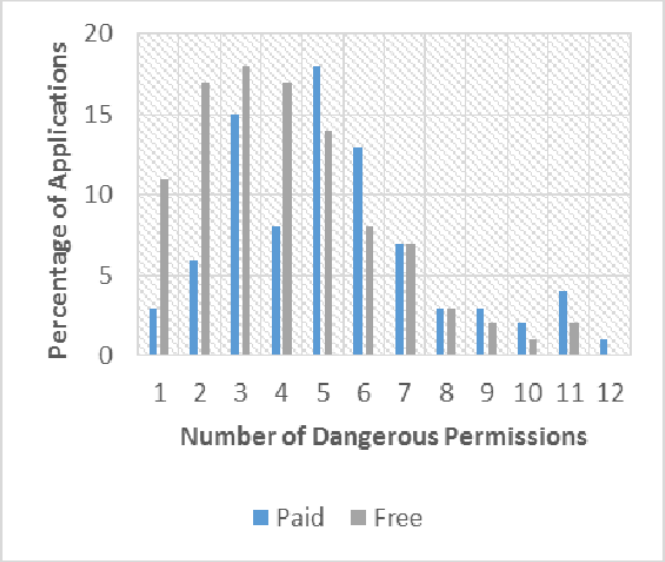


Fig 3. Dangerous permissions per application

*Analysis of updates:* The success of a privilege escalation attack on an update process depends not only on the presence of Pileup vulnerabilities, but also on the new system resources and capabilities the update adds that can be acquired by the adversary through the attack. Here we present a measurement study in which we ran our PermisSecure against a large number of applications for updates (183 Apps) to understand the exploit opportunities (new exploitable attributes and properties) they bring in.

We first looked at the overall impacts of the Pileup vulnerabilities to the Android ecosystem, in terms of update instance, which refers to the upgrade of a specific OS (from a specific manufacturer, on a specific device model and for a specific carrier) to a higher one under the same set of constraints. For each update instance, we measured the quantity of exploiting opportunities it can offer, with regards to all the Pileup flaws found in our research, such as the numbers of new permissions, packages and shared UIDs an update instance introduces to the new system. From the 383 we downloaded, we identified 241 update instances. The Statistics on their total exploit opportunities in each instance are illustrated in Fig. 4. Particularly, we found that 50% of those instances have more than 71 opportunities.

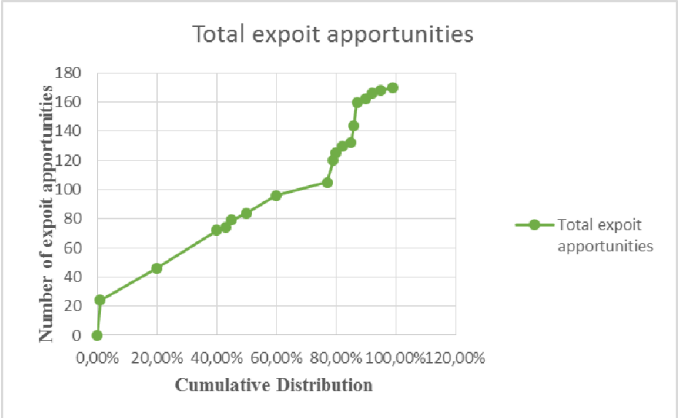


Fig 4. Cumulative Distribution of Total Exploit Opportunities in Each Update Instance.

## VII. Conclusion and Future work

In this paper, we present the design and implementation of PermisSecure that analyzes permissions requested by Android applications in installing-time and after their updates. Our reference implementation is very efficient and induces a small performance overhead. Therefore, we have developed this tool especially for users without a technical and security background. Our aim was to put permission based systems on a stable footing by informing users about dubious permission sets. There are several ways to extend the concept of creating awareness after applications are installed. First, it would be beneficial if the user would be informed before installation for suspicious applications. Preferably, the user should be given alternatives, such as this torch light app needs 124 permissions, including 15 dangerous ones. Alternatively, we have found a torch light application, that only needs 2 permissions, none of them being dangerous.

## References

[1] M. Amir, "Energy-Aware Location Provider for the Android Platform," University of Alexandria, 2010.

[2] Scientiamobile, "Mobile Overview Report October - December 2014," Reston, 2014.

[3] L. Li, A. Bartel, J. Klein, Y. Le Traon, S. Arzt, S. Rasthofer, E. Bodden, D. Octeau, and P. McDaniel, "I know what leaked in your pocket: uncovering privacy leaks on Android Apps with Static Taint Analysis," CoRR, 2014.

[4] A. P. Felt, E. Ha, S. Egelman, A. Haney, E. Chin, and D. Wagner, "Android Permissions : User Attention , Comprehension , and Behavior," 2012.

[5] M. Lange, S. Liebergeld, A. Lackorzynski, A. Warg, and M. Peter, "L4Android: A Generic Operating System Framework for Secure Smartphones," Proc. 1st ACM Work. Secur. Priv. Smartphones Mob. Devices, pp. 39–50, 2011.

[6] N. Viennot, E. Garcia, and J. Nieh, "A measurement study of google play," 2014 ACM Int. Conf. Meas. Model. Comput. Syst. - SIGMETRICS '14, pp. 221–233, 2014.

[7] L. Xing, X. Pan, R. Wang, K. Yuan, and X. Wang, "Upgrading Your Android, Elevating My Malware: Privilege Escalation Through Mobile OS Updating," IEEE Symp. Secur. Priv., 2014.

[8] T. Report, "Analysis of Dalvik Virtual Machine and Class Path Library,"

Management, pp. 1 – 42, 2009.

[9] E. Struse, J. Seifert, S. Ullenbeck, E. Rukzio, and C. Wolf, "PermissionWatcher: Creating user awareness of application permissions in mobile systems," Third Int. Jt. Conf. Ambient Intell., pp. 65–80, 2012.

[10] D. Barrera, "Securing Decentralized Software Installation and Updates," 2014.

[11] T. Vidas, N. Christin, and L. F. Cranor, "Curbing Android Permission Creep," IEEE Web 2.0 Secur. Priv. Work., 2011.

[12] L. Davi, A. Dmitrienko, A. R. Sadeghi, and M. Winandy, "Privilege escalation attacks on android," Lect. Notes Comput. Sci. (including Subser. Lect. Notes Artif. Intell. Lect. Notes Bioinformatics), vol. 6531 LNCS, pp. 346–360, 2011.

[13] W. Enck, D. Octeau, P. Mcdaniel, and S. Chaudhuri, "A Study of Android Application Security."

[14] A. Felt, K. Greenwood, and D. Wagner, "The effectiveness of application permissions," WebApps '11 2nd USENIX Conf. Web Appl. Dev., pp. 75–86, 2011.

[15] A. Möller, F. Michahelles, S. Diewald, L. Roalter, and M. Kranz, "Update Behavior in App Markets and Security Implications : A Case Study in Google Play," Proc. 3rd Int. Work. Res. Large. Held Conjunction with Mob. HCI, pp. 3–6, 2012.

[16] O. Barad, a Shabtai, D. Mimran, L. Rokach, B. Shapira, and Y. Elovici, "Detecting Application Update Attack on Mobile Devices through Network Features," pp. 2465–2466, 2013.

[17] E. Chin, A. P. Felt, V. Sekar, and D. Wagner, "Measuring user confidence in smartphone security and privacy," Proc. Eighth Symp. Usable Priv. Secur. - SOUPS '12, no. 1, p. 1, 2012.

[18] S. Bugiel, L. Davi, A. Dmitrienko, T. Fischer, and A. Sadeghi, "XManDroid: A New Android Evolution to Mitigate Privilege Escalation Attacks," System, pp. 4–7, 2011.

[19] R. Xu, H. Saïdi, R. Anderson, and H. Saıdi, "Aurasium: Practical Policy Enforcement for Android Applications," Proc. 21st USENIX Conf. …, p. 27, 2012.

[20] M. Zhang and H. Yin, "AppSealer: Automatic Generation of Vulnerability-Specific Patches for Preventing Component Hijacking Attacks in Android Applications," Symp. Netw. Distrib. Syst. Secur., no. February, pp. 23–26, 2014.

[21] Jacob West, "Software Security Goes Mobile," AppSecAsiaPac2012, 2012.

[22] D. Barrera, P. C. Van Oorschot, and A. Somayaji, "A Methodology for Empirical Analysis of Permission-Based Security Models and its Application to Android," Security, no. 1, pp. 73–84, 2010.

[23] W. Enck, P. Gilbert, B.-G. Chun, L. P. Cox, J. Jung, P. McDaniel, and A. N. Sheth, "TaintDroid: TaintDroid: An Information-Flow Tracking System for Realtime Privacy Monitoring on Smartphones.," Osdi '10, vol. 49, pp. 1–6, 2010.

[24] J. Pascual-Espada et al., "Using extended web technologies to develop Bluetooth multi-platform mobile applications for interact with smart things", Information Fusion, vol. 21, pp. 30-41, 2015

**ER-RAJY Latifa** received the B. S. in administration of computer systems from faculty of Sciences, University Mohamed V at Rabat in 2011. She obtained her master in the field of networks and computer system from faculty of sciences and techniques, University 1st Hassan at Settat in 2013. She is currently a Ph.D student in the University Cadi Ayyad, Marrakech, Morocco. Her main field of research interest is the security of android application.

**Moulay Ahmed El Kiram** is research professor at the Faculty of Science Semlalia, Cadi Ayyad University of Marrakech. He received his DES in Computer Science in 1997 at Mohammed V University of Rabat. El Kiram specializes in Security and network communication. His areas of interest include Authentication, particularly in multicast environment.

# Query Migration from Object Oriented World to Semantic World

SOUSSI Nassima, BAHAJ Mohamed

*Department of Mathematics & Computer Science, Faculty of Science and Technologies, Hassan 1st University, Settat, Morocco*

***Abstract* — In the last decades, object-oriented approach was able to take a large share of databases market aiming to design and implement structured and reusable software through the composition of independent elements in order to have programs with a high performance. On the other hand, the mass of information stored in the web is increasing day after day with a vertiginous speed, exposing the currently web faced with the problem of creating a bridge so as to facilitate access to data between different applications and systems as well as to look for relevant and exact information wished by users. In addition, all existing approach of rewriting object oriented languages to SPARQL language rely on models transformation process to guarantee this mapping. All the previous raisons has prompted us to write this paper in order to bridge an important gap between these two heterogeneous worlds (object oriented and semantic web world) by proposing the first provably semantics preserving OQL-to-SPARQL translation algorithm for each element of OQL Query (SELECT clause, FROM clause, FILTER constraint, implicit/explicit join and union/intersection SELECT queries).**

***Keywords* — OQL, SPARQL, Semantic Web, Object, OQL To SPARQL.**

## I. Introduction

THE Semantic Web [1] is an extension of the current web in which information is given well-defined meaning, better enabling computers and people to work in cooperation; it's based on the standards and protocols of the current web (http, URI and XML) and its own standards: The Resource Description Framework RDF [3] dedicated to describe data, the Web Ontology Language OWL [2] for creating structured ontology and the query language SPARQL [4] for querying data from RDF graphs.

Currently, the majority of information systems for companies databases adopt the object-oriented approach regarded as the best data organization paradigm providing the ability to represent complex entities and implement structured software with very high performance, which makes the development of methods and tools for automatic mapping from object oriented world to semantic world a very relevant need. These reasons motivated us to work on this topic so as to elaborate a first conversion query algorithm of OQL to SPARQL that translate each component of OQL SELECT query to its equivalent in SPARQL language.

## II. Related Works

Recently, several researches focus on the mapping of data, models, concepts, and queries from the existing data source content to semantic web world. The majority of these researches are interested much more to the relational systems than others; several approaches have been proposed about this mapping direction, such as: *RETRO* [6] that choose not to physically transform the data but to derive a domain specific relational schema from RDF data and its query mapping transforms an SQL query over the schema into an equivalent SPARQL query executable upon the RDF store. *R2RML* [7,8] a language for expressing customized mappings from relational databases to RDF datasets presented recently with a novel version which provides a user interface to create and edit mappings interactively even for non-experts. *D2RQ/Update* [5] is an extension of *D2RQ* [9] to enable executing SPARQL/Update statements on the mapped data, and to facilitate the creation of a read-write Semantic Web.

Regarding the object-oriented data source, the *SPOON* approach (Sparql to Object Oriented eNgine) described in [11] propose an automatic mapping between the object-oriented model (ODL) and the correspondent one at the ontological level in order to build a SPARQL endpoint. The paper [12] aims to address query rewriting by means of model transformations. In fact, it allows querying RDF data sources via an object oriented query which is automatically rewritten in SPARQL in order to access RDF data, it also translate SPARQL queries into object oriented queries so as to implement SPARQL endpoints for object oriented applications.

These studies did not propose any query translation solution for rewriting each element of Object Oriented queries into SPARQL queries semantically equivalent but they rely on models transformation process to guarantee this mapping.

## III. Query language Metamodel & Examples

In this section, we describe languages used by our translation approach from object oriented world to semantic web world in order to represent each language with its own metamodel developed from their grammars [14] [15] : the Object Query Language (OQL) for object-oriented databases and a query language for RDF data (SPARQL).

### A. OQL Metamodel

The OQL is an object-oriented query language in the Object Data Management Group standard named ODMG; this language provides an easy access to an object databases. Like SQL, the SELECT query which runs on relational tables works with the same syntax and semantics on collections of ODMG objects, which leads to search for an instance of an object rather than looking for a row of data. Several implementations of this standard exist; we quote as examples: HQL [16], JPQL [17], and others.

The metamodel schematized below is limited to SELECT Query in its simple and compound form (Intersect and Union SELECT query). The fig. 1 represents the OQL query of such a type that is composed of five clauses: SelectFromClause, WhereClause, GroupByClause, OrderByClause and HavingClause.



DOI: 10.9781/ijimai.2016.373

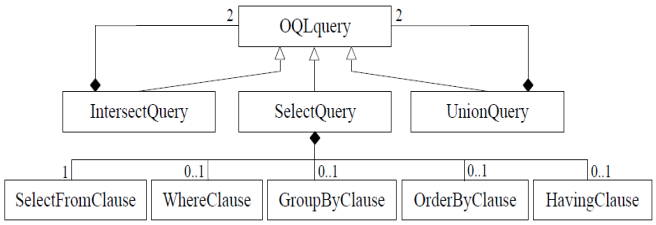


Fig. 1. The OQL Query representation

The SelectFromClause representation is given in fig 2. This clause is composed of an optional SelectClause (we can omit the SELECT clause in some implementation of OQL language such as HQL) and a mandatory FromClause. A SelectClause contains a PropertyList composed of a list of values or objects resulting from the query; these properties are described as a path that permits to browse the object model. The FromClause allows selecting properties from the object model. This clause is composed of a mandatory ClassReference and an optional ClassJoined ; the ClassReference indicates the class name ClassNameDeclaration or collection name CollectionNameDeclaration of selected objects whereas the ClassJoined indicates the set of classes which we want to join.

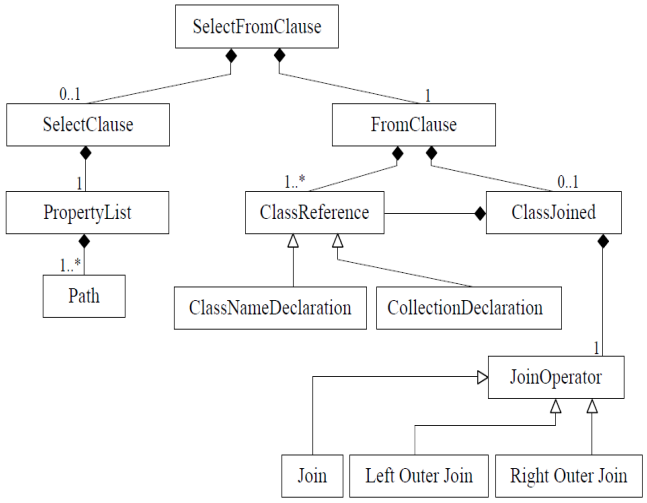


Fig. 2. Representation of the Select FROM Clause

The fig. 3 describes the WhereClause expression that represents the constraint part of the query. It can be a binary expression (and, or) or an operator expression (<,=<, >, >=,=) containing an attribute path and a value.

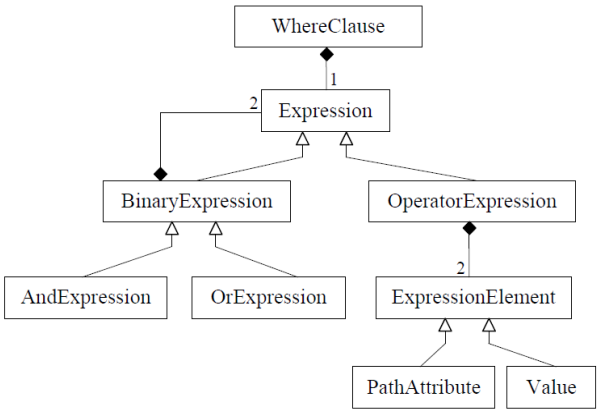


Fig. 3. Clause Representation of the Where Clause

## B. SPARQL Metamodel

The SPARQL is an RDF query language, that is, a semantic query language for databases, able to retrieve and manipulate data stored in Resource Description Framework (RDF) format [13]. The fig. 4 schematizes the SPARQL metamodel presented the different types for queries. In this paper, we are only interested by *SelectQuery*.

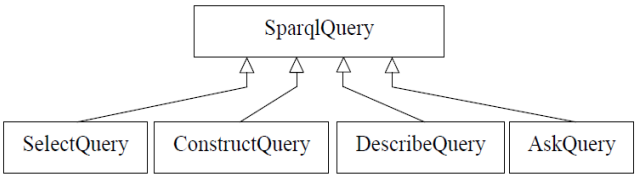


Fig. 4. The different types of Query Operation in the SPARQL metamodel

The *SelectQuery* as presented in the fig. 5 is composed of the *SelectClause* identifies the variables to appear in the results, and the *WhereClause* consists, in its turn, of *GroupGraphPattern* represents a set of *GraphPattern* identifying a various kinds of graph pattern: (a) *FilterPattern*: used to filter a set of objects using a various criteria and requirements. The filter expressions can be combined through the logical operations so as to form more complex filter, (b) *TripleSameSubject*: includes a subject and associated properties, (c) *UnionGraphPattern*: union of patterns, (d) *OptionalGraphPattern*: optional patterns.

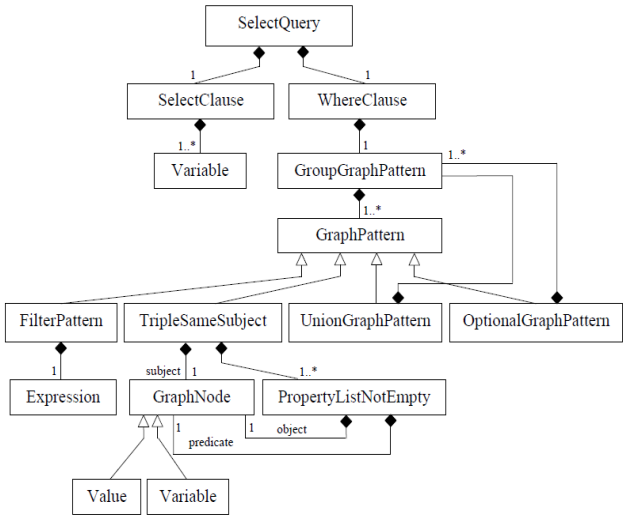


Fig. 5. Representation of the Group Graph Pattern in the SPARQL metamodel

## C. Examples

In the examples illustrated in Table I, we consider the two classes quoted bellow that list the *Person* class having as attributes: *matricule*, *name*, *age*, *degree* and *addr* which represents the declaration of *Address* class in *Person* class as an attribute; the *Address* class having as attributes: *id*, *city* and *state*. The OQL queries listed in this example have the types: Simple query (SELECT FROM clause with/without WHERE clause), implicit and explicit join, Union and intersection SELECT queries.

```
Class Person{
  attribute string matricule;
  attribute string name;
  attribute integer age;
  attribute string degree;
  relationship Address addr;
}
```

Class *Address* {
attribute integer id;
attribute string city;
attribute string state;
}

TABLE I
QUERIES EXAMPLES USING OQL AND SPARQL

| Query Type | OQL | SPARQL |
|---|---|---|
| Simple Query | SELECT p.name, p.age<br>FROM Person p<br>WHERE p.age<30 | SELECT ?name ?age<br>WHERE {<br>?who <Person#name> ?name;<br><Person#age> ?age.<br>Filter ( ?age < 30 )<br>} |
| Explicit Join | SELECT p.name, a.city<br>FROM Person p JOIN<br>Address a<br>ON p.addr = a.id<br>WHERE a.state = "MA" | SELECT ?name ?city<br>WHERE {<br>?who <Person#name> ?name;<br><Person#addr> ?addr.<br>?addr <Address#city> ?city;<br><Address#state> ?state.<br>Filter ( ?state = "MA" )<br>} |
| Implicit Join | SELECT p.name, a.city<br>FROM Person p, Address<br>a WHERE a.state =<br>"MA" | |
| Union Query | SELECT p.name<br>FROM Person p<br>WHERE p.age<20<br>UNION<br>SELECT p.name<br>FROM Person p JOIN<br>Address a<br>ON p.addr = a.id<br>WHERE a.city = "Nice" | SELECT ?name<br>WHERE<br>{ ?who <Person#name> ?name;<br><Person#age> ?age.<br>Filter ( ?age < 20 )<br>}<br>UNION<br>{ ?who <Person#name> ?name;<br><Person#addr > ?addr.<br>?addr <Person#city> ?city<br>Filter ( ?city = "Nice" )<br>} |
| Intersect Query | SELECT p.name<br>FROM Person p<br>WHERE p.age>26<br>INTERSECT<br>SELECT p.name<br>FROM Person p JOIN<br>Address a<br>ON p.addr = a.id<br>WHERE a.city = "Paris" | SELECT ?name<br>WHERE<br>{<br>{ ?who <Person#name> ?name;<br><Person#age> ?age.<br>Filter ( ?age > 26 )<br>}<br>{ ?who <Person#name> ?name;<br><Person#addr> ?addr.<br>?addr <Address#city> ?city;<br>Filter ( ?city = "Paris" )<br>}<br>} |

## IV. Query Mapping Algorithm

In this section, we will detail our main contribution by describing all procedures used in our query mapping algorithm: *ConstructSparqlSelectClause*, *ConstructTriplePattern*, *ConstructFilterExpression* *ConstructSparqlWhereClause*, *MappingOQLtoSPARQL* and *Merge*. The fig. 6 schematizes our approach as follow:

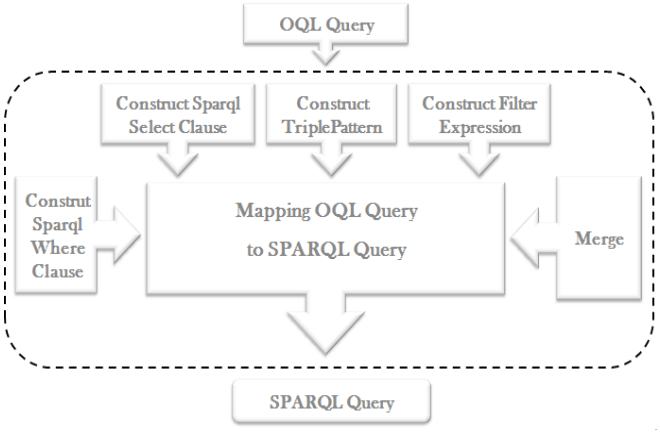


Fig. 6. Representation schema of our mapping approach

### A. ConstructSparqlSelectClause Subprocedure

The *ConstructSparqlSelectClause* subprocedure takes as input a set of attributes from an OQL SELECT Attributes (OSA) in order to glance through this set and extract the attributes name and add each one to the SPARQL SELECT clause initially blank which is returned at the end by this procedure.

Input : OSA
Output : A SPARQL SELECT Clause
**Begin**
select = ""
{A SPARQL SELECT Clause that is initially blank}
**for** each attribute attr ∈OSA **do**
attrName = getAttrName($attr_i$)
select += "?" + attrName + " "
**end for**
**return** select
**End Algorithm**

### B. ConstructTriplePattern Subprocedure

The *ConstructTriplePattern* subprocedure takes as input the OQL SELECT Attributes, OSA, Class Reference, CR, Class Joined, CJ and Where Clause Attribute, WCA so as to return at the end a set of Triple Patten of SPARQL equivalent query. Firstly, the algorithm stores the OSA in the set A (initially blank) dedicated to contain all query attributes, then it verifies the existence of join in the query by determining its type if it exists; In fact, the explicit join type is checked if the CJ variable is not null, in this case, the algorithm extract the join condition operand in order to add it to the set A, and next it also extract the *ClassReference* included in the *ClassJoined* clause in order to add them to the set CR dedicated to contain all Classes References of the query. Similarly, the implicit join type is checked if the number of elements of the set CR is strictly greater than 1, in this case, the join condition operand is added to the set A. If the query contains a where clause, its attribute is added also to the set A. Before adding attributes to the set A, the algorithm checks firstly if these attributes do not already exist in that list.

After the combination of all the query attributes in the set A and Classes references in the set CR, it glances through the set A for each Class Reference $CR_i$ in order to extract for each $a_j$ attribute its name and the alias for its class; if the $CR_i$ alias equal to the alias of the class attribute $a_j$, then it formulate the triple pattern of equivalent SPARQL query and adds it to the set TP and removing the attribute $a_j$ from the list A so as not to reprocess it in the following iterations. The attributes

that do not satisfy the above condition will be stored in a temporary list so as to add them again to the set A and switch to the next reference class and repeat the same process.

```
Input : OSA, CR, CJ, WCA
Output : A set of Triple Pattern
Begin
A = ø {Set of all query attributes initially blank}
Stack Atemp = EmptyStack
Boolean simpleJoin = False
A.add(OSA)
if (CJ != ø OR CR.size>1) then
   simpleJoin = True
   if (CJ != ø) then //Explicit Join
      JCA_l = CJ.getJoinCond().loperand()
      CR.add(CJ.getCR())
   else if (CR.size>1) then //Implicit Join
      JCA_l = CR_1.getClassName().getExternalKey()
   end if
   if (A.ExistInList(JCA_l) == False) then
         A.add(JCA_l)
   end if
end if
if(WCA!=NULL AND A.ExistInList(WCA)=False) then
   A.add(WCA)
end if
for i ← 1 to CR.size do
  for j ← 1 to A.size do
    attrClassAlias = getClassAlias(a_j)
    attrName = getAttrName(a_j)
    if (CR_i.getClassAlias() == attrClassAlias) then
      tp←{?s_i <CR_i.getClassName()#attrName> ?attrName}
      if (simpleJoin==True AND
         tp.object == CRi.getClassName().getFK()) then
      ?s_i+1 = tp.object
      end if
     TP.add(tp)
     A.remove(a_j)
    else
      Atemp.add(a_j)
    end if
  end for
  while (Atemp.size>0) do
     A.add(Atemp.remove())
  end while
end for
return TP
End Algorithm
```

### C. ConstructFilterExpression Subprocedure

The *ConstructFilterExpression* subprocedure takes as input an OQL where condition, WC, so as to extract the left operand, operator and right operand, and formulate at the end the FILTER clause expression of the SPARQL equivalent query.

```
Input : An OQL where condition, WC
Output : A Filter Expression
Begin
   filterExp = “”{A Filter Expression that is initially blank}
   if (WC != NULL) then
      leftOp = WC.lOperand
      Op = WC.Operand
      rightOp = WC.rOperand
      attrName = getAttrName(leftOp)
      filterExp =“FILTER(”+ ?attrName +Op+ rightOp +“)”
   end if
return filterExp
End Algorithm
```

### D. ConstructSparqlWhereClause Subprocedure

The *ConstructSparqlWhereClause* subprocedure takes as input the set of triple pattern TP returned by the *ConstructTriplePattern* Subprocedure and the Filter Expression *FilterExp* returned by the *ConstructFilterExpression* Subprocedure. This algorithm glances through the set of TP to concatenate the triple patterns in order to formulate the SPARQL WHERE clause equivalent. In the case where the two triple patterns have the same subject, the second one will be reduced by removing its subject and adding a comma after the first triple pattern.

```
Input : TP, FilterExp
Output : A SPARQL WHERE Clause
Begin
where = “” {A SPARQL Where Clause that is initially blank}
for i←1 to TP.size then
   if (i>1 AND TP[i].subject == TP[i-1].subject) then
         TP[i] ← {TP[i].predicate TP[i].object}
     where += “;” + TP[i]
   else
         where += TP[i]
   end if
end for
if (isEmpty(FilterExp) == False) then
    where += FilterExp
end if
return where
End Algorithm
```

### E. MappingOQLtoSPARQL Procedure

The *MappingOQLtoSPARQL* is the main procedure of our algorithm; it takes as input the OQL SELECT query, $q_{in}$ so as to return at the end the SPARQL equivalent query, $q_{out}$. A conversion tree of OQL query is generated by using the parse function. If the query type is “*SimpleQuery*”, the conversion tree generates SPARQL SELECT clause, FROM clause contained classes references and WHERE clause if it exists, then the set of triple patterns is constructed from the *ConstructTriplePattern*, and the FILTER expression from *ConstructFilterExpression* qualifying as inputs for the *ConstructSparqlWhereClause* generated the SPARQL

WHERE clause. The SPARQL SELECT clause is generated from *ConstructSparqlSelectClause*; the results of previous Subprocedures are concatenated so as to formulate the SPARQL equivalent query. We proceed with the same manner if the OQL query type is "*JoinQuery*" except that the OQL conversion tree will generates the *ClasseJoined* in addition to *ClassReference* in FROM clause. In cases where the type of the OQL query is "*UnionQuery*" or "*IntersectQuery*", the conversion tree generates two OQL SELECT queries q1 and q2 that will be used in the recursive procedure *MappingOQLtoSPARQL* so as to construct the SPARQL SELECT query of each one and concatenate them in order to have an equivalent SPARQL SELECT query.

Input : An OQL SELECT Query, $q_{in}$
Output : A SPARQL Query, $q_{out}$
**Begin**
$q_{out}$ = "" {A SPARQL query that is initially blank}
tree = parse($q_{in}$) {A parse tree obtained by parsing $q_{in}$}
$q_{in}^{SELECT}$ = tree.getSelectClause();
$q_{in}^{FROM\_CR}$ = tree.getClassReference()
$q_{in}^{FROM\_CJ}$ = tree.getClassJoined()
$q_{in}^{WHERE}$ = tree.getWhereCond()
$q_{out}^{SELECT}$ = "SELECT" $q_{out}^{WHERE}$ = "WHERE {"
TP ← ø { The set of triple patterns is initially empty}
**if** (tree.type == SimpleQuery) **then**
TP = ConstructTriplePattern($q_{in}^{SELECT}$, $q_{in}^{FROM\_CR}$, NULL, $q_{in}^{WHERE}$)
FilterExp = ConstructFilterExpression($q_{in}^{WHERE}$)
$q_{out}^{WHERE}$ += ConstructSparqlWhereClause(TP, FilterExp)
$q_{out}^{SELECT}$ += ConstructSparqlSelectClause($q_{in}^{SELECT}$)
$q_{out}$ = $q_{out}^{SELECT}$ + $q_{out}^{WHERE}$ +" }"
**else if** (tree.type == JoinQuery) **then**
TP = ConstructTriplePattern($q_{in}^{SELECT}$, $q_{in}^{FROM\_CR}$, $q_{in}^{FROM\_CJ}$, $q_{in}^{WHERE}$)
FilterExp = ConstructFilterExpression($q_{in}^{WHERE}$)
$q_{out}^{WHERE}$ += ConstructSparqlWhereClause(TP, FilterExp)
$q_{out}^{SELECT}$ += ConstructSparqlSelectClause($q_{in}^{SELECT}$)
$q_{out}$ = $q_{out}^{SELECT}$ + $q_{out}^{WHERE}$ +" }"
**else if** (tree.type == UnionQuery) **then**
$q_1$ = tree.leftSubTree(), $q_2$ = tree.rightSubTree()
$q_1^{out}$ = MappingOQLtoSPARQL($q_1$)
$q_2^{out}$ = MappingOQLtoSPARQL($q_2$)
$q_{out}$ = Merge($q_1^{out}$, $q_2^{out}$, "UNION")
**else if** (tree.type == IntersectQuery) **then**
$q_1$ = tree.leftSubTree(), $q_2$ = tree.rightSubTree()
$q_1^{out}$ = MappingOQLtoSPARQL($q_1$)
$q_2^{out}$ = MappingOQLtoSPARQL($q_2$),
$q_{out}$ = Merge($q_1^{out}$, $q_2^{out}$, "INTERSECT")
**end if**
**return** $q_{out}$
**End Algorithm**

### *F. Merge Subprocedure*

The *Merge* subprocedure takes as inputs two OQL subqueries and the merge type in order to generate a significant and valid SPARQL query. Firstly, it extracts the SELECT clauses from each subqueries and encapsulate these in S1 and S2, secondly, it extracts and encapsulate the triple patterns of each subqueries in TP1 and TP2. Finally, it extracts and stores the FILTER expressions of each the subqueries in F1 and F2. If the merge type is "UNION" then the $q_{out}$'s SELECT clause takes one of subqueries SELECT clause, and the $q_{out}$'s WHERE clause is formulated from the concatenation of the q1's WHERE clause returned by the *ConstructSparqlWhereClause* Subprocedure taking as inputs TP1 and F1 as well as the keyword UNION and the q2's WHERE clause returned also by the *ConstructSparqlWhereClause* Subprocedure taking as inputs TP2 and F2. We proceed with the same manner if the SPARQL query type is "JoinQuery" except that we remove the keyword Union.

Input: q1, q2, mergeType
Output: A SPARQL query qout
**Begin**
qout = "SELECT"
S1=q1.ExtractSelectClause();
S2=q2.ExtractSelectClause();
TP1= q1.ConstructTriplePatterns();
TP2= q2.ConstructTriplePatterns();
F1 = q1.ExtractFilter();
F2 = q2.ExtractFilter();
**if** (mergeType = "UNION") **then**
qout += ConstructSparqlSelectClause(S1)
qout+="WHERE{ {" + ConstructSparqlWhereClause(TP1, F1) + "} UNION {" + ConstructSparqlWhereClause(TP2, F2) + "} }"
**else if** (mergeType = "INTERSECT") **then**
qout += ConstructSparqlSelectClause(S1)
qout += "WHERE{ {" + ConstructSparqlWhereClause(TP1, F1) + "}{" + ConstructSparqlWhereClause(TP2, F2) + "} }"
**end if**
**return** qout
**End Algorithm**

## V. Conclusion

In summary, the main contribution of this paper in the pertinent topic of interoperability between object oriented world and relational world is the elaboration of a query conversion algorithm of the OQL SELECT queries to SPARQL equivalent queries by translating each element of OQL query (SELECT clause, FROM clause, FILTER constraint, implicit/explicit join and union/intersection SELECT queries) to its equivalent in SPARQL language so as to bridge the gap between this two world without a physical data transformation.

One obvious extension of our research is to reinforce our algorithm by supporting more concepts, such as: subqueries, collections, aggregation and composition.

## References

[1] T. Berners-Lee, J. Hendler and O. Lassila, "The Semantic Web, Scientific American", Mai 2001.
[2] S. Bechhofer, "OWL: Web ontology language". In Encyclopedia of Database Systems (pp. 2008-2009). Springer US, 2009.
[3] World Wide Web Consortium. RDF 1.1 Concepts and Abstract Syntax. 2014.
[4] J. Pérez, M. Arenas & C. Gutierrez, "Semantics and complexity of SPARQL ". ACM Transactions on Database Systems (TODS), 34(3), 16,

2009

[5] V. Eisenberg and Y. Kanza, "D2RQ/update: updating relational data via virtual RDF", In Proceedings of the 21st international conference companion on World Wide Web (pp. 497-498), 2012.

[6] J. Rachapalli, V. Khadilkar, M. Kantarcioglu, and B. Thuraisingham, "RETRO: A Framework for Semantics Preserving SQL-to-SPARQL Translation", The University of Texas at Dallas, 800 West Campbell Road, Richardson, TX 75080-3021, USA, 2009.

[7] K. Sengupta, P. Haase, M. Schmidt, and P. Hitzler, "Editing R2RML mappings made easy", 2013.

[8] S. Das, S. Sundara, and R. Cyganiak, "R2RML: RDB to RDF Mapping Language". Working draft, W3C, 2011.

[9] C. Bizer, A. Seaborne, "D2RQ: treating non-RDF databases as virtual RDF graphs", In: International Semantic Web Conference ISWC (posters), 2004.

[10] S. Auer, S. Dietzold, J. Lehmann, S. Hellmann, and D. Aumueller, "Triplify--Light-Weight Linked Data Publication from Relational Databases", In Proceedings of the 18th International World Wide Web Conference, 2009.

[11] W. Corno, F. Corcoglioniti , I. Celino and E. Della Valle, "Exposing Heterogeneous Data Sources as SPARQL Endpoints through an Object-Oriented Abstraction", In: Asian Semantic Web Conference (ASWC 2008), pp. 434–448, 2008.

[12] G. Hillairet, F. Bertrand, & J. Y. Lafaye, "Rewriting queries by means of model transformations from SPARQL to OQL and vice-versa", In Theory and Practice of Model Transformations (pp. 116-131), Springer Berlin Heidelberg, 2009.

[13] SPARQL. (2015, avril 27). Wikipedia. Retrieved from https://fr.wikipedia.org/wiki/SPARQL. Last visited January 2016.

[14] OQL Grammar. (2015, September 23). Retrieved from https://wiki.openitop.org/doku.php?id=2_2_0:oql:oql_grammar. Last visited January 2016.

[15] E. Prud'hommeaux, S. Harris, Garlik, and A. Seaborne. SPARQL 1.1 Query Language. (2013, 21 March) . Retrieved from http://www.w3.org/TR/sparql11-query/#sparqlGrammar. Last visited december 2015.

[16] S. Guruzu, and G. Mak, "HQL and JPA Query Language". Hibernate Recipes: A Problem-Solution Approach, 155-166, 2010.

[17] J. Juneau, "The Query API and JPQL". In Java EE 7 Recipes (pp. 447-470). Apress, 2013.

**N. SOUSSI** was born in 1991, in Khouribga, Morocco. She got her special higher studies degree in software engineering from National School of Applied Sciences in 2014. She is now a Phd student in the Department of Mathematics and computer sciences, Faculty of Sciences & Technology of Settat, Hassan 1st University, Settat, Morocco. Her area of interest includes web ontologies and semantic web.

**M. BAHAJ** is a full professor in the Department of Mathematics and Computer Sciences from the University Hassan 1st Faculty of Sciences & Technology Settat Morocco. He is co-chairs of IC2INT, International Conference on Software Engineering, Databases and Expert Systems (SEDEXS'12) , NASCASE'11. He has published over 80 peer-reviewed papers. His research interests are intelligent systems, ontologies engineering, partial and differential equations, numerical analysis and scientific computing. He is Editor-in-Chief for Australasian Journal of Computer Science and associate editor of Journal of Artificial Intelligence and Journal Software Engineering.

# The Silver Lining Methodology

José Miguel Castillo Chamorro[1],[2], PhD

[1]Universidad Internacional de la Rioja;
[2]SOFTCAST Consulting S.L. Madrid. Spain

***Abstract* — The way in which Strategic planning is designed is different depending on the organization. For that reason, no standard procedures can be given to develop Strategic planning. However, the scenarios analysis method is used in any field or organization. We could define a scenario as a set of variables or events that describes a future situation. Additionally, the continuous irruption of new technologies invites us to carry out a revision of the old methodologies and procedures with the intention of starting an innovation process to make them more efficient. The challenge presented in this article consists of the use of the agents technology within a new methodological approach to envision future possible scenarios more quickly and more accurately than the classical methods we currently use.**

***Keywords* — Foresight, Strategic Planning, Agents Technology, Methodology.**

## I. Introduction

Today the need for envisioning what is going to happen in the future is the same as centuries ago [1]. The developments in economy, industry, technology and society depend on the decisions we make in the present that, without any doubt, will have a direct influence in the future [2]. The more accurate the perception of what is going to happen in the future is the more correct these decisions will be.

Strategic planning is the subject responsible for the analysis of getting a future position within a future scenario. Consequently, the study and assessment of the future belong to the strategic planning analysis [3].

We should do this exercise of reflection very often with the aim of aligning our efforts towards the future final objectives whatever the application field is, entrepreneurial, industrial, social, technological, etc. The lack of this reflection exercise can unleash a chaos at any organization that will navigate with no direction as the scenario circumstances allow it to do it.

Social scenarios are very unsteady and are influenced by a big number of heterogeneous variables.

Changes in a situation will generate uncertainties; this implies the need of a new analysis when accomplishing the Strategic planning. Strategic planning does not eliminate uncertainty, but tries to reduce it with the aim of making decisions about the future with more possibilities of success.

The influence or modification of events in one scenario creates a variation in the global scenario with a major o minor intensity depending on the influence degree of each event within the scenario [4].

We can state that the success of the strategic planning depends on knowing with certain accuracy the events or variables that have a direct influence on the scenario and our capacity to eliminate, modify or foster these sensitive events. An approximate knowledge will always be better than a total ignorance or disregard for the strategic planning and its way to analyze the future.

Methodologies and techniques in Strategic planning are under the scope of IJIMAI since many of the new approaches are based on applied Artificial Intelligence. Namely, this article could be catalogued within one of the topics that are covered by IJIMAI: Heuristic and AI Planning Strategies and Tools.

This article is focused on the use of foresight to prevent and make an analysis of future scenarios by using the opinion of groups of experts.

The hypothesis that is introduced in this article consists of giving a new methodology to get future possible scenarios by using and treating adequately the opinion of human experts. Silver lining is the name given by the author of this article to the methodology. With this name the author tries to convey a positive view of hope to create and reach the future. The methodology not only includes the different phases and processes but also indicates the agent-based technologies that can be used to process human experts' opinions.

The article is divided into seven sections. A comparison between Forecast and Foresight are presented in section two. The different phases of the Silver lining methodology are introduced in section three. Section four illustrates a complete map of the processes of the Silver lining methodology. In section five the processes that can be developed by using the agent-based technologies are explained. An analysis of future works and applications is exposed in section six. Finally, section seven presents the conclusions of this article.

## II. Foresight vs. Forecast

We can gather the different methods with scientific foundation to foresee the future in two groups: Technical and Anticipatory.

Within the Technical group, we can find mathematical models [5] that are developed to extrapolate past and present data in order to predict future results [6]. The study of tendencies permits us to approximate future situations in stable dynamic systems. Econometrics, demography and meteorology are sciences that can be included in this group. All these methods and scentific branches are included in the area of Forecast. That means that we can predict future scenario behaviour by means of algorithms or models able to predict future results or behaviours.

Technical prediction techniques are efficient in the creation of future scenarios based on stable dynamic systems in which tendencies of historical data are applied.

Unfortunately, social systems don't always behave in a stable way; normally they evolve in an unstable or chaotic way. Furthermore, when a situation includes a great deal of different and heterogeneous variables, technical prediction becomes complex and unaffordable [7].

The collapse of transportation, economic crisis, natural disasters, terrorist attacks, political scenarios, internal and external national



DOI: 10.9781/ijimai.2016.374

conflicts are just a few of many examples of crisis scenarios which are difficult to estimate with techniques based upon technical prediction [8]. Normally, the crisis scenarios are created by an accumulation of events that would otherwise be ineffective in isolation; however when occurring together they create an unsustainable and critical scenario [9].

Anticipatory techniques try to avoid the problem of using technical prediction in unstable systems by using the opinion of a group of human experts [10]. The expert's opinion embodies relations among events or variables based on his/her personal experience; so complex relationships among heterogeneous events are mentally treated as a whole. The methods and techniques used to envision the future by using the opinion of groups of experts belong to the area of Foresight.

It is not until the mid of the twenty century when new techniques allow carrying out an anticipatory foresight, with the aim of giving a reliable and alternative solution to construct future possible scenarios in which the diversity, relationship and amount of variables make it impossible to process them by using forecast techniques.

Classical methodologies [1] [2] to carry out foresight exercises are still in use. It is worth mentioning the especial relevance of Godet's publications [11]. Nevertheless, it is important to remark that they are twenty years old and since that time AI technologies have evolved and reached a maturity level to be applicable in foresight studies and substitute statistical methods.

## III. Phases of Silver lining

It is common that foresight exercises are linked. Departments or centers that carry out this kind of exercises make them in a continuous way. Normally there is a feedback between foresight exercises. The main objective of a foresight department is to generate information about the future in a continuous way, correcting or adjusting lack of accuracy. It is not a final objective for such departments to develop isolated foresight exercises.

The general phases of the Silver lining methodology are the following:

- Describing objectives. Initial Processes
- Consulting experts
- Processing experts' opinions
- Analysis of inferences
- Validating results.

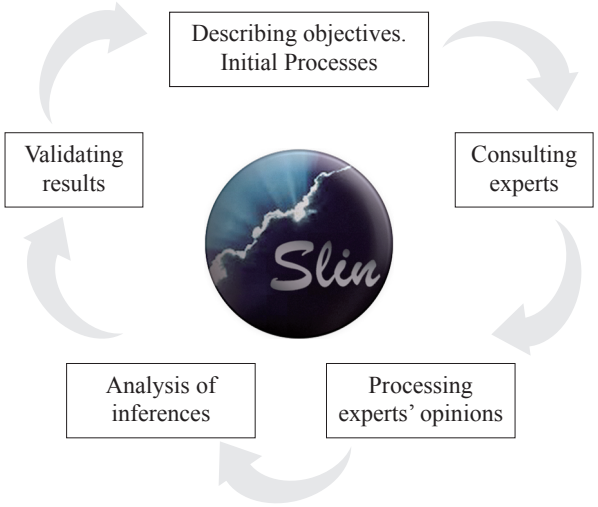


Fig. 1. Phases of the Silver lining methodology

In the first phase, 'Describing objectives' the aim of the foresight exercise is defined and the initial processes are prepared such as the selection of the temporal horizon, the events that may belong to the scenario and the selection of the group of experts. This phase can be recursive since many times it is necessary to re-define new objectives before starting the following phase.

Once the inquiries to the group of experts have been done, it is necessary to process all the information by using agent-based technologies. The result of this process has to be analyzed in order to study inferences or to give a new approach to the inquiries in case of any anomaly during the process.

The whole study finalizes with the validation phase that consists of checking the result with the scenario materialization through time. In the case that new events appear and they can influence the previewed scenario, it is necessary to accomplish a deep analysis of them to determine if a new foresight study is needed.

These five phases can be represented in an execution model that is illustrated in the following flowchart.

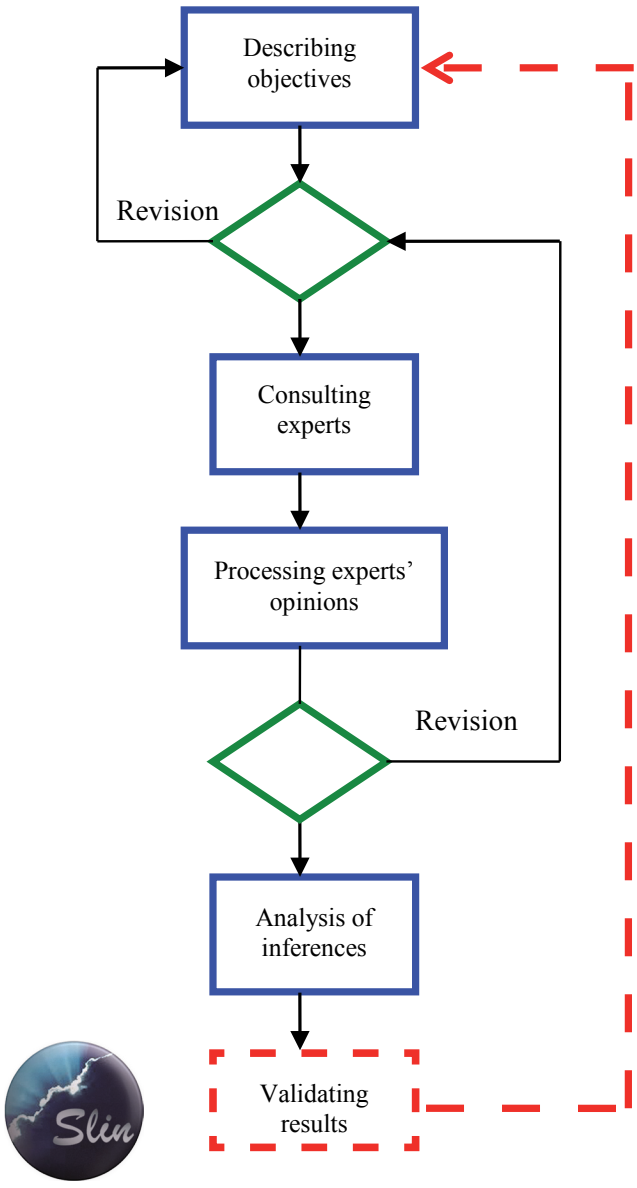


Fig. 2. Execution model flowchart

## IV. Agent-based processes

Strategic planning exercises are different depending on the application area, not only for the input data that is processed for planning but for the objectives to achieve as well as the internal rules used for the construction of different plans.

The technological evolution invites us to make a deep analysis of procedures used in foresight exercises with the aim of innovating in the case that the technology has reached the maturity level needed, facilitating more efficient results [12].

Regarding foresight studies in which human reasoning processes are dominant especially when experts gave their opinions about the possibility of achievement of a specific scenario or when gathering the opinion of all of them, the methods usually used are based on statistics and algebra. With the irruption of the Artificial Intelligence procedures we have the opportunity of developing an innovation exercise by substituting classical procedures for new technologies [13].

When doing a foresight exercise, the expression of the experts' opinions when qualifying a possible scenario and the global treatment of all answers reveal the necessity of using technologies that allow us to:

- Work with qualitative descriptions given individually by the experts, instead of quantitative answers expressed in terms of probabilities.
- Obtain the response of the group through the individual responses.
- Extrapolate the response of the whole group to envision the behavior of the rest of possible scenarios that are not possible to consult to the group of experts.

For the resolution of the problem of treating in a qualitative way the experts' opinions, it seems advisable the use of techniques based on Fuzzy Logic [14] that allow the elaboration of membership functions and rules to construct scenarios.

To get the answer of the group through the individual answers given by the experts, again it seems that Fuzzy Logic can provide a plausible solution.

Initially, to treat a set of heterogeneous variables with the aim of extrapolating the experts' opinions to the rest of scenarios within a specific domain, it seems that the use of Neural Networks [15] is adequate since it permits the classification of new scenarios after having been trained with the experts' opinions.

All these functionalities have to be developed under the Agency paradigm [16]. Agents are software entities able to develop certain cognitive capacity. That is to say that they simulate functionalities related to the human knowledge.

To construct agents in the planning environment (Strategic and Tactical), the MECIMPLAN methodology [17] could be adequate.

The following table matches the classic procedures to the substitutive technology.

TABLE 1. SUBSTITUTIVE TECHNOLOGIES

| Problem | Classic procedure | Substitutive technology |
|---|---|---|
| *Getting individual experts' opinions* | -Delphi (4 rounds)<br>-Answers in terms of probability | -Delphi (2 rounds)<br>-Answers in terms of possibility |
| *Getting opinions of the group* | -Cross impacts<br>- Bayes theorem: Conditional probabilities | Fuzzy logic |
| *Extrapolation of the rest of possible scenarios within the domain* | Without solution | Neural Networks |

## V. Map of Processes

To develop each phase it is necessary to carry out a series of processes. The list of processes that belong to every phase is the following.

- Describing objectives. Initial Processes
  *Scope selection and temporal horizon*
  *Stability study*
  *Selection of participant*
  *Selection experts group*
  *Experts group evaluation*
  *Selection of events*
- Consulting experts
  *Questionnaires 1st round*
  *Answers 1st round*
  *Qualitative Process. 1st round*
  *Sensitive events selection*
  *Questionnaires 2nd round*
  *Answers 2nd round*
  *Qualitative Process. 2nd round*
  *Sensitive events confirmation*
- Processing experts' opinions
  *Rest scenarios Interpolation*
  *Information analysis*
- Analysis of inferences
  *Analysis of inferences*
  *Final report draft*
  *Proactive actions*
- Validating results
  *Qualification metric*
  *Validation of results*

The majority of the Silver lining processes are developed in a sequential way.

The processes that belong to the first phase 'Describing objectives. Initial Processes' may be developed almost simultaneously since they are activities that do not require inputs from previous processes. Most of them begin once the study scope and temporal horizon are defined. The evaluation of the group of experts has to be done after the selection of the group components.

It is important to study the stability of the system. Dynamic systems evolve through time in three different ways: stable, unstable or chaotic. The more stable a system is the longer we can envision its behaviour. An unstable system evolves following certain tendencies between margins of stability, that is to say that the system behaviour is predictable within a margin. However, systems that evolve in a chaotic way are not predictable; in reality they are predictable but the result of the prediction has no value because many external variables could influence the system producing unexpected results.

To envision the future behaviour of a system by using the scenarios method we have to study if the system is evolving through time in a stable way or unstable with in a margin.

After finishing the first phase of Silver lining we should wonder if the exercise is well defined or if it is advisable to review some of the previous processes, such as reducing the scope of the study, increasing the number of experts or cancelling the study due to the instability of the system since the foresight study would yield uncertain results.

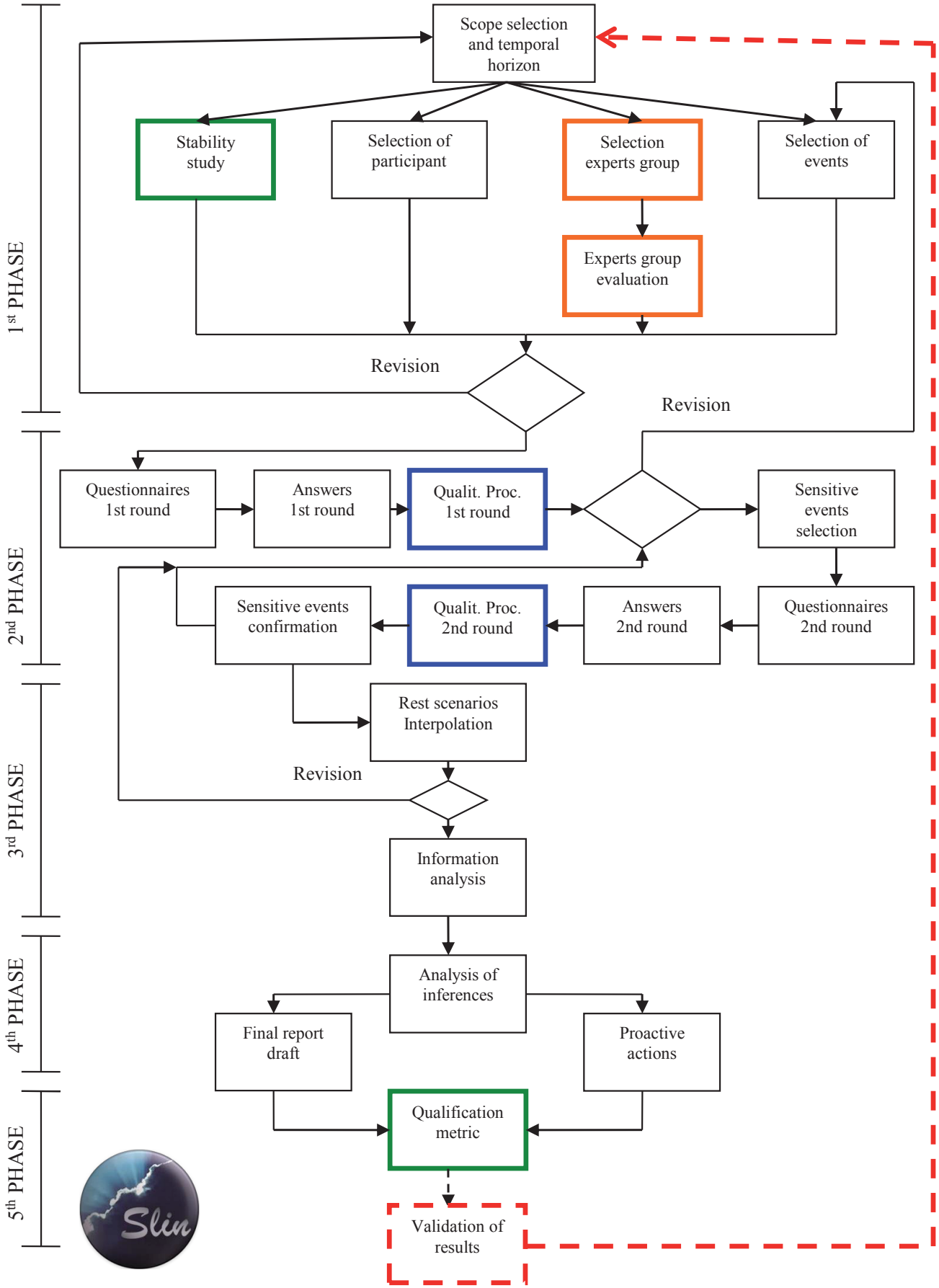


Fig. 3. Map of processes of the Silver lining methodology

The processes that belong to the second phase of the methodology are sequential, that is to say that each one receives information from the previous one, with the exception of those cases in which an incorrect selection of the event has been detected or there is certain ambiguity in the interpretation of the inquiries by the experts. In that last case it will be necessary to define and select the events again in the first inquiry round as in the second. The Delphi technique [18] is used in this phase but with a variation regarding its classical use: we do not show the results of the first round to the group of experts contrasting opposite answers and trying to gather experts' opinions within the second and third quartile. We treat the expert' opinion as a rule within a fuzzy inference module. By processing this module we extract the opinion of the expert group as a whole and we get those events that are sensitive in the scenario. The second round of the Delphi technique is carried out in the case we need to confirm the events that have been identified as sensitive after the first round.

In both, the first and the second round we use Fuzzy Logic to process in a qualitative way the answers of the experts.

Within the third phase of the Silver lining the opinion of the experts is processed and the knowledge elicited from the experts is interpolated to the rest of scenarios not consulted.

The analysis of inferences is achieved in the fourth phase of the methodology. This phase is composed of three tasks that can be developed in parallel.

Finally, the fifth phase of Silver lining is focused on checking the quality and validity of the foresight exercise. The first process measures with a biased checklist the main activities done during the exercise, providing a tool to evaluate and compare the quality among foresight studies. The second process is extended through time with the aim of checking if the foreseen future is becoming a fact in the way it was expected. This last activity will boost new foresight studies in case the prediction was wrong or some new event has suddenly appeared changing the initial conditions of the original study.

## VI. Applications and Future Works

This article shows the main achievements after seven years of research trying to obtain a methodology that uses new technologies to allow us to carry out foresight studies in a more efficient way, rather than using classical methodologies or procedures.

Up to now the methodology has been applied successfully in more than five foresight exercises with Spanish think-tank centers [19]. Detailed and complete foresight studies in which the Silver lining methodology has been applied can be consulted in 'Instituto Español de Estudios Estratégicos' web page [20].

Foresight studies and the Silver lining methodology can be applied to simulate possible future scenarios at any field [21], such as evolution of technology, social behaviour, economy scenarios, crisis scenarios, decision in politics, etc.

Nevertheless, there is work left to be done in order to improve the results of foresight studies to envision future scenarios in the most realistic way.

Some of the future works that we are willing to face are listed below:

- Forecast and foresight working together: as it has been presented in section two of this article, forecast and foresight are seen currently as different methods to predict future scenarios; one based on mathematical models and the other processing complex relations with the most sophisticated computer 'the human brains of a group of experts'. It is necessary to study in depth the possibility of using with more flexibility both methods by means of integrating specific techniques in a single methodology that is able incorporate forecast and foresight, since in many occasions some variables that belong to a specific scenario can be affected through time by tendencies. The variable itself would have a double dependency, on one hand its tendency that could be calculated with a forecast study and on the other hand its complex relationship with the rest of variables, only predicted with a foresight study.
- Fostering software tools to support the use of foresight: Software tools permit the standardization and consolidation of procedures. The development of software tools that support foresight exercises with Silver lining would facilitate the methodology consolidation process.
- Validating experts' quality: The more right guesses of human experts the more realistic results in a foresight exercise. Therefore, the veracity of a foresight study is directly related to the quality of the each expert individually. It is vital that the expert be a real expert with a wide knowledge about the matter and with a high social intelligence level. It is necessary to study the kind of tests that an expert should pass in order to assure his quality as an expert.
- New solutions to the limitation of the number of events that belongs and describes a specific scenario: A number of seven events that could belong to a specific scenario would provide 128 possible scenarios. Silver lining permits the development of scenarios in cascade. Nevertheless, it would be advisable to study new ways of eliminating the limitations of the number of events.

In summary, the most important research lines that we are eager to face in a near future with interdisciplinary research groups are:

- Forecast and foresight working together
- Validating the expert's quality
- Reducing the limitation the number of events

## VII. Conclusion

Once we have reached the initial objectives that lead to the research project, as a conclusion of this article we can sum up the main achievements of this research project in three areas:

- From a methodological point of view

  This research project provides the Silver lining methodology as a powerful tool that can guide the development of foresight studies. The methodology is agile, well-structured and applicable at any field that needs strategic planning.

- From a technological point of view

  Nowadays, there are technologies that may substitute the mathematical-statistical methods that have been used up to now to develop the use of foresight. These technologies are mainly based on Fuzzy logic and Neural networks and are developed under the Agents paradigm. Processing natural language as the normal expression of human experts has a better understanding by the participants of a foresight study and they usually provide a more realistic solution.

- From the strategic planning point of view

  Strategic planning is usually related to the long term, but there could be strategic decisions to make in the short term. For this reason, it is necessary to provide new solutions that working together with the latest technologies can give answers in the short term. This is the case of the result of this research.

## References

[1] Masini, E. (1994). *Why Futures Studies?* London: Ed. Grey Seal Books.

[2] Jarratt, J. (2003). *From Scan to Plan: Integrating Trends into the Strategy-Making Process*. American Society of Association Executives.

[3] Bell, W. (1997). *Foundations of Futures Studies. Human Science for a New Era: History, Purposes and Knowledge*. Vol. 1. New Jersey: Transaction Publishers.

[4] Bas, E.; Guillo, M. (2013). *Prospectiva e innovación* (Vol. 1: visiones). Barcelona: Plaza y Valdés.

[5] Meadows, D. (1982). *Groping in the dark; the first decade of Global Modelling*. Bristol, John & Sons.

[6] Castillo, J. M., et al. *An Agent-Based Approach for Data Fusion in Homeland Security*. International Journal of Interactive Multimedia and Artificial Intelligence, vol. 2, issue Special Issue on Improvements in Information Systems and Technologies , no. 3, pp. 44-49, 09/2013.

[7] Piedra-Calderón, J. C., et al. *Global Collective Intelligence in Technological Societies: as a result of Collaborative Knowledge in Combination with Artificial Intelligence*. International Journal of Interactive Multimedia and Artificial Intelligence, vol. 2, issue Regular Issue, no. 4, pp. 76-80, 12/2013

[8] Castillo, J.M. (2010). *A Technological Approach for Crisis Prevention*. El Algarbe (Portugal): Proceedings of the e-Society International Congress.

[9] Castillo, J.M. (2011). *An agent-based approach to envision the future*. Lisbon (Portugal): Proceedings of the 8th International ISCRAM congress.

[10] Linstone, H.A. et al. (2010). *Delphi: A brief look backward and forward*. Technol. Forecast. Soc. Change, doi:10.1016/j.techfore.2010.09.011

[11] Godet, M. (1994). *From anticipation to action*. UNESCO Publishing.

[12] Castillo, J. M., et al. *Prospecting the future with AI.* International Journal of Interactive Multimedia and Artificial Intelligence, vol. 1, issue Special Issue on Business Intelligence and Semantic Web, no. 2, pp. 1-5, 12/2009.

[13] Castillo, J.M. (2012). *Getting Experts' Agreement in Strategic Planning*. Dubrovnik (Croatia): Proceedings of the Agreement Technologies International Congress.

[14] Zadeh, L. (1993). *The role of fuzzy logic and soft computing in the conception and design of intelligent systems*. Procedings of the 8th Austrian Artificial Intelligence Conference.

[15] Rosemblatt, F. (1958). *The Perceptron: A probalistic model for information storage and organization in the brain*. Psychological Review, 65, pags. 386-408.

[16] Castillo, J. M. *A crystal ball made of agents.* International Journal of Artificial Intelligence and Interactive Multimedia, vol. 1, issue A Direct Path to Intelligent Tools, no. 3, pp. 13-17, 12/2010.

[17] Castillo, J.M., et al. (2006). *The MECIMPLAN Approach to Agent-based Strategic Planning*. Hong Kong: Workshop Proceedings, IAT International Conference on Intelligent Agents Technology.

[18] Dalkey, N. C. (1972). *The Delphi method: An experimental study of group opinion. Studies in the quality of life*. Delphi and decision-making (pp. 13-54). Lexington Books.

[19] Castillo, J.M. (2012). *Tecnología y Prospectiva: Un reto hecho realidad*. Madrid: Rev. Instituto Español de Estudios Estratégicos. NIPO: 083-12-238-7. Num 0 pags. 111 – 132.

[20] http://www.ieee.es/investigacion/#sub3

[21] Castillo, J.M. (2010). *Simulating future crisis scenarios with MAS*. Orlando (USA): Proceedings of the I/ITSEC International Congress.

**José Miguel Castillo Chamorro** is the CEO of SoftCast Consulting. Currently he is Associate Professor at the Universidad Internacional de la Rioja in Madrid. From 2011 to 2013 he was the Director of the Area of Information Systems, training and decision making support in 'Tecnalia Research and Innovation'. From 2007 to 2011 he was Director of Division in European Virtual Engineering (Tech. Center). In 2001 he earned his PhD in Telecommunications from the Universidad Politécnica in Madrid. The same year he was awarded with the 'General Fernández Chicarro' prize by the Spanish Ministry of Defence for his work on Operations Research. He has a large experience leading projects in which simulation, artificial intelligence and project management are involved. From 1999 to 2013 he was Associate Professor at the Universidad Pontificia de Salamanca in Madrid. In 2007 he obtained his PhD in the Statistics and Operational Research department from the Universidad Rey Juan Carlos in Madrid. In June 2007 he was awarded with the prize on Research by the Spanish Ministry of Defence. In the same year he was awarded with the prize on Research on the field of Security by the Directorate of Civil Protection and Emergencies (Spanish Ministry of Interior). In July 2015 he earned his PhD in Sociology from the Universidad Pontificia de Salamanca.

# Linear Temporal Logic-based Mission Planning

Anil Kumar and Rahul Kala

*Student Member, IEEE, Member, IEEE Robotics and Artificial Intelligence Laboratory, Indian Institute of Information Technology, Allahabd, India*

***Abstract* — In this paper, we describe the Linear Temporal Logic-based reactive motion planning. We address the problem of motion planning for mobile robots, wherein the goal specification of planning is given in complex environments. The desired task specification may consist of complex behaviors of the robot, including specifications for environment constraints, need of task optimality, obstacle avoidance, rescue specifications, surveillance specifications, safety specifications, etc. We use Linear Temporal Logic to give a representation for such complex task specification and constraints. The specifications are used by a verification engine to judge the feasibility and suitability of plans. The planner gives a motion strategy as output. Finally a controller is used to generate the desired trajectory to achieve such a goal. The approach is tested using simulations on the LTLMoP mission planning tool, operating over the Robot Operating System. Simulation results generated using high level planners and low level controllers work simultaneously for mission planning and controlling the physical behavior of the robot.**

***Keywords* — Temporal Logic, Linear Temporal Logic, Mission Planning, Robot Operating System, Robot Motion Planning.**

## I. Introduction

The problem of Robot Motion Planning is to enable a robot to navigate and make its way out in a complicated obstacle-prone environment. A classical motion planning problem using temporal logic [1], is described simply as "Go from A(source) to B(goal) by avoiding obstacles", where A and B may be some regions of interest in the robotic world. Since last decades robots are increasingly becoming more autonomous and are able to work in the absence of humans. Therefore simple goal specifications also become more complex and we need to plan the motion beyond a single goal problem. One of the most common dreams is that a robot should work as a *helper robot*, which obeys human instructions and never violates the robotics laws.

One must be able to robustly satisfy commands such as "Surveillance of all laboratories in any order for safety purposes", "Pick and deliver food items from cafeteria to the Robotics Laboratory and all other laboratories", "If a robot is in the robotics laboratory and any disaster occurs, then inform all research students in the laboratory and hostel". We can not always assume the navigation environment of the mobile robot to be static. It may change with the environmental conditions and can be sensed by the robot's sensors. Recently there has been increasing interest to have complicated task specifications in partially known and unstructured environments. Some common basic examples include: reach on some specific goal and convergence to that region ("reach A eventually and stay there forever"), visit a set of goals sequentially ("reach A then C then B until D is visited"), surveillance ("reach A then B and repeat the same for numerous occasions"), condition ("never go to A until regions B or C are visited"), liveliness ("move to all regions continuously"). The basic notions can be combined in numerous ways to make more complicated specifications possible. This gives a language, very similar to natural language, to the owner to control the robot. It is evident from current research that in the future robots will be able to converse with the humans and take complex specifications such as: Go to the laboratory to get the equipment from the assistant, while on the way also see how are the students doing. At some time drop a letter to Prof. X and if someone gives a letter on the way, also get that too.

Several search algorithms have been designed with complex specifications. In this paper we use Temporal Logic to represent the complex goal specifications [2] [3]. Temporal logic is a tool which can model such relations between different entities, in our case multiple regions or goal points. Temporal Logic is an extension to the conventional Logic based systems, with the difference that it can represent temporal relations which depend upon time. It is a very expressive way to define complex goal specifications with constraints, while using formal notions to enable verification checks.

The paper solves the problem of mission planning where the mission is specified by a user in terms of a LTL formula. The map comprises of regions of interest and obstacles. The map is parsed with a low level planner to get all the transitions between different regions, while satisfying any task constraints. The information is stored as an automaton. High level planning is applied on the automaton to get a strategy acceptable by the automaton, which is implemented using low level controllers.

Many mission specifications may require inputs not available or visible to the robot. As an example, consider the mission which asks a robot to go immediate to a particular place when asked for by a user, besides other specifications. The robot does not know when it would be asked to approach the place by the user and hence it can't plan in advance. Robots compute a strategy for best performance against the most adverse sensor readings, and use this strategy for navigation. The trajectory is derived from the path based on the sensor readings. It is assumed that the map with all specifications of regions of interest and obstacles is known to the robot, although obstacles may change with time, which is handled by the low level controller.

The paper is organized as follows. *Section 2* discuses and presents some related works in the literature. *Section 3* presents the overall overview of the work. *Section 4* subsequently presents a primer of LTL, which is the technique used for mission specification and planning. The specification is represented as a Bchi Automata described in *Section 5*. *Section 6* describes the simulation framework and gives the simulation results. Finally, *Section 7* gives the concluding remarks.

## II. Related Works

We are always motivated by the previous research involving robotics and other related fields. Robot motion planning is one of the most challenging domains for study and research. This section very briefly describes some of the related works. In a framework presented by Gazit et al. , the authors solved the reactive mission motion planning



DOI: 10.9781/ijimai.2016.375

problem using a hybrid controller to control the behaviors of the robot based on the environmental conditions such as rescue, coverage and obstacle avoidance. In [1], firstly the authors created a feasible discrete controller for all LTL specifications, and then captured the reactive behaviors of a single or a group of robots which is computationally feasible in complex environment. Kala et al. [27] solved the problem of robot path planning in dynamic environments using a Hierarchical Evolutionary technique, wherein the robot had to find the optimal path from the entire given map. Several moving obstacles were used on the map during the motion of the robot. Hierarchical Evolutionary algorithm optimized the extra step cost in a variety of scenarios. Kala et al. [25] solved the navigating of multiple mobile robot using cell decomposition technique and reactive planning with fuzzy logic whereas indirect communication between mobile robot is achieve through simple fuzzy-logic.

A mathematical discrete-optimization based trajectory generation using Linear Temporal Logic specification was solved by Gazit et al.[1] where the author presented an optimal control for a non-linear system using LTL specification and generated a trajectory to control. Gazit et al. [2] provided an environmental model for automatically verifiable controllers that satisfy the high level task specification for the mobile robot based on the sensors/actuators information which described the local behaviors of the robot. However for computational approach discrete controllers must satisfy General Reactivity GR(1) formulas [18]. If LTL specification is feasible then only the mobile robot will be able to complete the desired task. Svorenova et al.[9] formulated a mission planning problem for the mobile robot in partitioned environment for task specifications like surveillance mission, obstacle avoidance etc. An automaton based approach was used by the authors for model checking, for high level task accomplishment by the robot and also for collecting the rewards form the visited regions.

Sampling based motion planning using temporal goals is presented by Bhatia et al. [3], where a multi-layered synergistic approach was used for all temporal goals. In this multi-layered synergistic framework, the high level discrete structure was involved for exploring the information and suggested the high level goal plans. The authors also used geometry based multi-layered approach and continuous time-step for low level sampling of the task. In another approach Bhatia et al.[4] extended their work by using nonlinear hybrid dynamics for the high level temporal goals. Moreover a lazy-search approach was used for the high level planning thus resulting in computational speedups by 10 times for the second order non-linear hybrid controller compared with the previous method. Moreover sampling based Tree-Search motion planning with discrete abstractions for specifications using temporal logic proposed by McMahon et al. [8]. In this framework the authors suggested very low cost motion trajectories that satisfy Co-Safe LTL. A physics based engine was managed which was responsible for the robots' accurate motions with their own physical dynamics. There has been additional work using multi-robot systems. Saha et al.[5] proposed a compositional framework for motion planning based on Satisfiability Modulo Theories (SMT), which are a combination of linear constrains solvable within given motion primitives and generate an optimal trajectory. Here the behaviors of the multiple robots was specified by a set of temporal logic formulas. A controller was used to trace all trajectories for each robot in the experimental workspace. Thus an optimal cost was maintained for each trajectory based on the motion primitives for that robot and synthesize-able for the given configurations.

Although all the above discussed works are mainly on completely known environments, Guo et al.[6] solved the mission planning in partially known workspaces where the task specification was given by a Linear Temporal Logic formula. In this generic model the mission specification was done by LTL based on the previous knowledge of the system environment. Further as more information about the environment model was available, the plans for the robots were revised. This type of approach is good for an environment where the robot operates in partially known workspaces. Another approach for motion planning in unknown environment was proposed by Ayala et al. [7]. The authors solved the LTL specification for an unknown environment wherein an accurate assumption of the sensors and actuators data was made, and the environment was partitioned into finite square cells. The authors used a formal method for verification and a grid based exploration method. During the authors experiments, the initiation of the algorithm started only when the robot has enough information for processing the given task specifications.

An automated LTL based task complication for a multi-robot system was proposed by Loizou et al.[10]. In this experimental framework the author suggested an input-output module used for task specification given by LTL by considering the environmental condition such as safety, liveliness and obstacle avoidance. The authors suggested Multi-Robot Navigation Function controllers which were generated by the linear temporal logic task specifications.

Several software model based frameworks are proposed to validate the task specification using model based software toolkits which synthesize the task specification generally using GR(1) and *Büchi* Autometa. An automatically synthesizing DD (Digital Design) from LTL specification was proposed by Piterman et al.[26] wherein GR(1) was used to synthesis the specification using game planning techniques, resulting in always winning strategies and plans. Thus the number of individual states may increase during the process of the algorithm, and formal specifications of the task may lead to complexity on experimental environments. Finucane et al.[11] solved the mission planning for mobile robots using the LTLMoP toolkit. Here the mission planning specification was given through temporal logic in English structured language which was synthesized by GR(1) and the mission was further validated during the motion of the robot. Sensors and actuators were used to collect real-time information from the environment. However another approach for mission planning was proposed by Jing et al.[12] where LTLMoP software was used on the given map to analyze the users specification as either valid or invalid. Moreover for demonstration of the task specification the authors used simulations and a physical robot wherein the path planning problem was solved by the Open Motion Planning Library.

Action verification during the motion of the robot, having correct-by-constructions controllers for temporal logic based synthesis, was proposed by Raman et al.[13]. Here the physical robot was controlled and invoked by low-level behaviors. If the behaviors of the low-level were unsafe or in a different time length, then a hybrid controller was used to determine whether the behaviors are safe or unsafe. All the user-friendly specifications execute at a time, one for slow and another for fast controllers and finally both are synchronized. However several specifications may also not be synthesizeable by GR(1) due to incorrect specifications and thus Raman et al.[14] presented an autonomous behavior based controller which compared a nontrivial set of actions and decided whether the given task is feasible and acceptable by a GR(1) parser or not. These kind of algorithms are more feasible for complex behaviors where the given task may not be free from deadlock/may cause failure during the implementation of the task.

Model checking and verification of any LTL specification[26] is a commonly used operation for the specific hardware and software configurations. Using TuLiP toolkit, Wolff et al. [28] interfaced several nonlinear optimal control for LTL specifications based on game solving models. A finite-state automaton was generated by the controller that evaluated the specifications. Only synthesizable tasks in the experimental environment were processed and therefore resources were optimally used. The beautify of TuLiP model checking was that it

converted the high level specification into low level smaller problems. Thus the computational complexity of task solving becomes more efficient.

Kunze et al. [15] proposed a framework wherein every-day object manipulation problems were generated through a LTL formula. A mobile robot (PR2) was used to demonstrate the feasible of solutions by using the LTL formula. All task specifications were validate in logic programming language PROLOG. The robot behaviors and action plans depended on the results generated by PROLOG using a backtracking mechanism. All the test scenarios during the experiments were divided into three parts namely grasping, pouring pancake and truing pancake. These all experiments were done with a physical robot PR2 also in ROS environments.

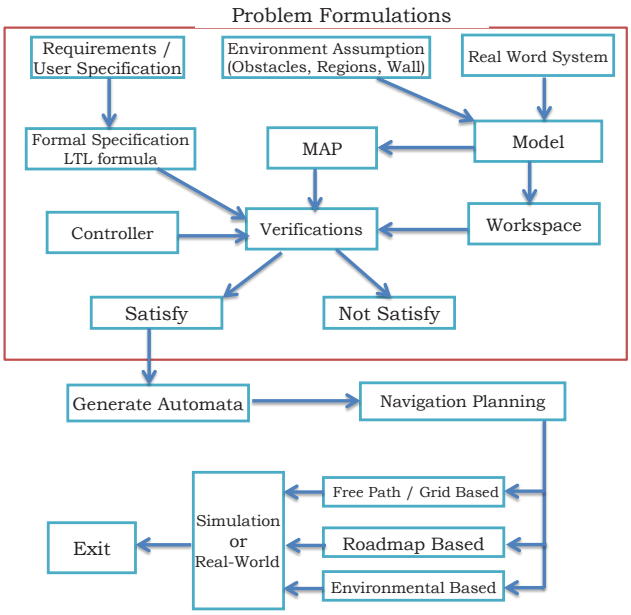


Fig. 1: Graphical Representation of Proposed Methodology

Numerous approaches have been developed to translate high-level, heterogeneous tasks to low-level continuous or discrete controllers, optimally and in a computationally efficient manner [16] [17]. Moreover Fusion of probabilistic A* and fuzzy interface system for mobile robot path planning is achieved by Kala et al.[19]. Tiwari et al.[20] present the also several algorithmic approaches for mobile robot path planning in many experimental environmental assumptions.

## III. Methodology

In this section we discuses about the general outline of the proposed work of motion planning which is also represented in Fig 1. The overall approach for solving the motion planning consists of user specifications, system modeling, environment knowledge, navigation planning etc. The system methodology in our problem represents the layout of the environmental, how we model any problem related to mission planning using temporal specifications and implementation of the motion strategy. The constituents of our methodology are given below:

- **Requirements/ User specifications :** All the robot mision related query of the user is specified in this section for all approaches used in this work. The user specifications must be written in either LTL specification format or translatable into LTL symbolic specifications. However it may possible that the requirements of the user for the robot mission may be ambiguous or invalid. Thus we need to perform verification of the given problem on some LTL verification engine.
- **Environment Assumptions:** The robotic environment may consist of obstacles (i.e. non-navigation areas for the mobile robot, walls, etc.) and regions of interests (i.e. goal points, e.g. rooms, laboratories, areas, etc.). This information is the most important while preparing the robotic navigation map for the mobile robots.
- **Real Word System Modeling:** While representing the real-world system for our navigation map in workspace configurations we need efficient techniques for representing the complicated world system. Thus sometimes we need to redesign the real-world environmental information for robotic map. The path from the source to goals is fully dependent how the real-world system is represented. Thus the real-world system needs to eventually translate into system state model representation so that we can apply LTL state verification techniques for the given user specifications. The system design of any real-world scenario can be represented with $\mathcal{M}$. If the temporal logic formula $\phi$ holds the system proposition $S_j$, the system can be represented as: $(\mathcal{M}, S_j) \models \phi$.
- **Map and Workspace:** The entire real-world system of experimental scenario is represented using a map. Map of the real-world environments may be 2D or 2.5D as in our experiments. The map conversion from real-world to workspace environment can be done through camera calibration, distance information to obstacles and regions, etc. Moreover the mapping is also required for real-world map size to workspace size reductions.
- **Verification and Satisfying Conditions:** The users requirement are in the form of LTL specifications which need to be verified before initially starting the motion execution for a given problem specification. The specifications are either satisfied by the LTL verification method or the goals are not satisfied by the LTL verification method (i.e. Go to A to B until region C does not occur is interpreted as valid; whereas Go to A and don't go to A is interpreted as an invalid specification). However for verification of LTL formula we generate an automaton based on *Büchi* Automata and GR(1) parsing method for counter-strategy generations. A strategy for navigation is generated that satisfies the LTL formula.
- **Navigation Planning:** The navigation planning generates only valid LTL specifications and synthesis of the LTL specifications. The navigation planning approach has three different methods `Grid Based`, `RoadMap Based` and `Environment Based`. In Gird based approach the map is represented in a Grid format; RoadMap Based approaches decompose the environment into several path segments or produce a roadmap so that the computation time decreases and it improve the efficiency for reaching the goals. In Environmental Based approaches a local path planner is used for the roadmap decomposition and an external sensor is used for the environmental conditions while the robot is in motion.
- **Simulations and Real-world Representations:** The experiments are done with navigation planning techniques which need a representation of the map with either simulated or a physical world representation. In all our experiments we use a simulated environment as the real-world scenario for problem solving. The Grid Based approach was used with a point sized robot in aprior work [27]. The Roadmap Based approaches are presented in this work. Moreover another efficient approach with promising result is presented by Kala et al.[24] for multirobot robot motion planning using hybrid MNHS and Genetic Algorithm(GA).

In all our assumptions the system is modeled with some environmental assumptions which undergoes verification related to goal specifications. In our model checking method the LTL formula

follows the goal-based automata approach. In our experiments we used an indoor robot navigation environment, where the Lab Regions and office areas were represented as goal regions.

## IV. Linear Temporal Logic

The LTL is extended from the propositional logic with some operators which are bound with the time interval factor. In real-world scenarios, the goal is not always constant and may change with time interval due to the external interference. Similarly the multiple goals in the problem of mission planning may have temporal relations among them. Thus, single/multi-goal specifications for any mobile robot can be expressed with LTL easily. Recently temporal logic is widely accepted and is gaining popularity for high level mission planning due to its expressive power, flexibility and mathematical framework. Formal verification model based systems are widely accepted in real-time environments to verify systems such as Air-Traffic Control, Autopilot Drive Mode, CPU design etc. We perform an examination of our problem definition system based on the LTL problem specifications and ensure that the given specification/task is reachable to the desired goal or the robot will not be able to reach on the given goal positions as per the current specifications. We also formulate a strategy of navigation which results in attaining the goal condition as specified in the LTL.

In our experimental work LTL is used to describe the complex mission specification for the robot from one region to another region. Here regions may be interpreted as any region of interest on the map like A, B, labs, offices, etc. An LTL formula $\phi$ must satisfy all specifications over the input alphabet, $\omega \rightarrow 2^{\texttt{Prop}}$ where `Prop` (Atomic Propositions) and satisfy the models at time instant $i$ used in the LTL formula. Linear Temporal Logic can formally be described by some traditional logic operators like *conjunction* ($\wedge$), *disjunction* ($\vee$), *negation* ($\neg$), *implication* ($\rightarrow$) and *equivalence* ($\Longleftrightarrow$) whereas additional temporal operators are used including *eventually* ($\Diamond$), *next* ($\bigcirc$), *always*($\Box$) and *until* ($\mathcal{U}$). The LTL has some properties with the environment assumptions. These include:

- **Safety**: It describes those conditions which must be always satisfied (e.g. always avoid obstacles). The LTL formula *negation* ($\neg$) is used to describe the conditions which must never hold. A natural safety condition is to never collide with any obstacle, that is: $\neg(O_1 \vee O_2 \vee O_3 \vee ... \vee O_n)\mathcal{U}\mathcal{R}$, means eventually reach region $\mathcal{R}$ by avoiding all obstacles $O_i, i = 1, 2, ...n$.
- **Liveness**: This specifies the goals which must be satisfied eventually by some actions in the future (e.g. "Eventually go to the region B and visit infinitely often").
- **Sequencing**: Describes the sequence of goals to be followed in any order. The LTL formula specifies that we must visit all regions (i.e. A,B,C,D,E) as per the requirement: $\Diamond$(A $\wedge$ $\Diamond$ (B $\wedge$ $\Diamond$ (C $\vee$ $\Diamond$D))).
- **Reachability**: An individual state $s_i$ is reachable from an initial present state if at least one path exists which takes the system from the initial state to the state $s_i$.

The aim is to use the realtime map to get a trajectory $\tau(t)$ which satisfies the LTL specification, based on the sensor percepts received in realtime. The initial position of the robot is assumed to be known or we can set during the problem execution, which must satisfy the LTL specification. All LTL formulas for a real-time environment are specified with the initial state $\tau(0)$ and with regions of the environment $\chi = \{\pi_1, \pi_2, \ldots, \pi_N\}$. The LTL formulas are given by the grammar.

$$\phi \quad ::= True|False|\phi|\neg\phi|\phi \vee \phi|\phi \wedge \phi|\bigcirc \phi|\phi\mathcal{U}\phi \tag{1}$$

The boolean constants (`True`, `False`) can be defined as `True` = $\phi \vee \neg\phi$ and `False` = $\neg$`True`. All the temporal and non-temporal operators are not represented in the grammar but they can be derived with these basic operators. Using the basic temporal operator, we can define additional temporal operators such as "Eventually" $\Diamond\phi = \texttt{True}\mathcal{U}\phi_1$, safety or "Always" $\Box\phi = \neg\Diamond\neg\phi$ and "Next" operator $\bigcirc\phi$. The semantics of any LTL formula can be recursively defined as:

- $\tau(t) \models_c \neg\phi$ if $\tau[t] \not\models_c \phi$
- $\tau(t) \models_c \phi_1 \vee \phi_2$ if $\tau[t] \models_c \phi_1 \vee \tau[t] \models_c \phi_2$
- $\tau(t) \models_c \phi_1 \wedge \phi_2$ if $\tau[t] \models_c \phi_1 \wedge \tau[t] \models_c \phi_2$
- $\tau(t) \models_c \bigcirc\phi$ if $\tau[t+1] \models_c \phi$
- $\tau(t) \models_c \phi_1\ \mathcal{U}\ \phi_2$ if $\exists t'' \geq t : \tau(t') \models_c \phi_1 \forall t \leq t' \leq t'' \wedge \tau(t'') \models_c \phi_2$
- $\tau(t) \models_c \Diamond\phi$ if $\exists t' \geq 0$, $\phi^{t'} \models \phi$.

***`weak-until:`*** The operator is defined as, $\phi_1$ must be true until $\phi_2$ become true and thereafter there is no bound for $\phi_2$, it may either be true or false. *`Until`* and *`weak-until`* $\mathcal{W}$ are dual in nature, expressed as:

$$\neg(\phi_1\mathcal{U}\phi_2) \equiv (\phi_1 \wedge \neg\phi_2)\mathcal{W}(\neg\phi_1 \wedge \neg\phi_2)$$
$$\neg(\phi_1\mathcal{W}\phi_2) \equiv (\phi_1 \wedge \neg\phi_2)\mathcal{U}(\neg\phi_1 \wedge \neg\phi_2)$$

***`Release:`*** The release operator $\phi_1\mathcal{R}\phi_2$, is defined as, $\phi_2$ must be true from starting where $\phi_1$ becomes true for first time. Somehow if $\phi_1$ never becomes true, then $\phi_2$ needs to be true for all future times or forever. The *`release`* $\mathcal{R}$ operator can be expressed as $\phi_1\mathcal{R}\phi_2 \equiv \neg(\neg\phi_1\mathcal{U}\neg\phi_2)$. The *`until`* $\mathcal{U}$ and *`release`* $\mathcal{R}$ are also dual and can be expressed as:

$$\phi_1\mathcal{U}\phi_2 \equiv \neg\phi_1\mathcal{R}\neg\phi_2$$
$$\phi_1\mathcal{R}\phi_2 \equiv \neg(\neg\phi_1\mathcal{U}\neg\phi_2)$$

The expansion law is also satisfies by the *`release`* $\mathcal{R}$ operator that is: $\phi_1\mathcal{R}\phi_2 \equiv \phi_2 \wedge (\phi_1 \vee \bigcirc(\phi_1\mathcal{R}\phi_2))$.

The pictorially representation of LTL operators is shown in Fig 2. $\mathbf{A}$ and $\mathbf{B}$ are two propositions used to represent the region information, $\phi_1$ and $\phi_2$ are used for LTL problem formulations. The "Next" operator $\bigcirc\mathbf{A}$ holds the next state. Similarly $\Diamond\mathbf{A}$ represent s that will eventually hold somewhere on path a subsequent path. The $\Box\mathbf{A}$ means that the formula needs to hold all future paths from the state where it belongs. $\mathbf{A}\ \mathcal{U}\ \mathbf{B}$ means $\mathbf{A}$ has to hold on all the future states until $\mathbf{B}$ does not occur. Finally $\mathbf{A}\ \mathcal{R}\ \mathbf{B}$ presents the release operator. Based on task specification we need to formulate the LTL specification for testing goal conditions, wherein a combination of the operators are used.

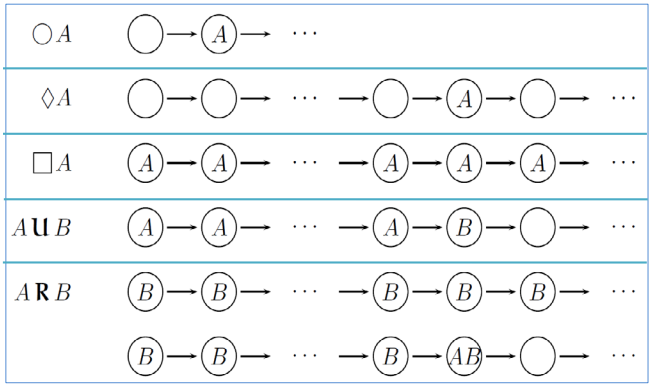


Fig. 2: Graphical Representation of LTL Operators

Syntactically the LTL formula $\phi$ is a Deterministic Finite Automaton (DFA) which can be easily contracted and always satisfies the finite traces[23]. The DFA for any given tuple can be defined as: $\mathcal{T}_\phi = (\mathcal{S}, \omega, \delta, S_0, S_F)$.

- $\mathcal{S}$ is a collection of all states
- $\omega \rightarrow 2^{\text{prop}}$ represents all input alphabets
- $\delta$ is the transition function, $\mathcal{S} \times \omega \rightarrow \mathcal{S}$
- $S_0 \in \mathcal{S}$ is the initial state
- $S_F$ is a set of accepting states or the terminal state for the defined model

Run of a tuple $\mathcal{T}_\phi$ is sequence of states $s_0, s_1, \ldots, s_n$ where $s_0 = S_0$ and $\omega_i \in \mathcal{S}$ for all $i = 1, 2, \ldots, n$, moreover the tuple will accept $\omega$ only if $\omega_n \in S_F$.

The fairness constrains in LTL may be expressed with two different assumptions, either `Action-based Fairness` or `State-based Fairness`. The conclusion of using Fairness in Transition System (TS) is that we need to determine if the entire TS for any LTL formula only needs to verify the LTL formula $\phi$ for fairness execution of LTL formula over TS. Thus assume $\Phi_1$ is defined as "Something is Enabled" and $\Phi_2$ represents "Something is Taken" then the Fairness constraints can further be expressed in following ways:

`Unconditional Fairness:` The specification does not express any conditions or circumstances for something happening on some period of time. Thus the specification becomes much easier to implement.

$$ufair = \square\diamondsuit\Phi_1$$

`Strong Fairness:` Assume that the LTL specification consists of an activity *infinitely often*. E.g. the task condition "Visit IT_LAB and stay there infinitely often. The condition may become false after some time. Although sometimes our goal reversibility is not fully satisfied for all future times then `Strong Fairness` is more general for invoking LTL specifications.

$$sfair = \square\diamondsuit\Phi_1 \rightarrow \square\diamondsuit\Phi_2$$

`Weak Fairness:` The `Weak Fairness` may be presented by those LTL specifications where an activity/task is always *continuously enabled*. If the task is continuously enabled then it does not generally allow the temporary disabling.

$$wfair = \diamondsuit\square\Phi_1 \rightarrow \square\diamondsuit\Phi_2$$

Moreover Fair paths and Traces assumptions can be expressed for any set of state/actions. Let the fairness be given by $\mathcal{F} = (\mathcal{F}_u, \mathcal{F}_s, \mathcal{F}_w)$, then Fair Path and Fair Traces can be expressed as:

$$FPath(s) = \{\tau \in Paths(s) | \tau \models fair\},$$
$$FTraces(s) = \{trace(\tau) | \tau \in FPath(s)\}$$

Therefore Path from initial state $s_0 \rightarrow s_1 \rightarrow \ldots$ $is\ \mathcal{F} - fair$ only iff there exists an $\mathcal{F}$ execution $s_0 \overset{a1}{\rightarrow} s_1 \overset{a2}{\rightarrow} \ldots.$

## V. Büchi Automata For LTL Specifications

*Büchi* automaton extends the finite automaton for infinite input word sequences. It is a variant of $\omega-$ automaton. The *Büchi* automaton accepts infinite words sequences as input for a given model and visits (at least) states from the given state to the final states infinitely often. automata is widely accepted for model checking in LTL for automata-based verification.

Formally we can define a deterministic *Büchi* automata as the quintuple $\mathcal{A} = (S, \Sigma, \delta, s_0, F)$ where the each component is defined as:

- $S$ : is a finite set of states of $\mathcal{A}$
- $\Sigma$ : is a finite set of alphabet of $\mathcal{A}$.
- $\delta$ : is $S \times \Sigma \rightarrow S$ the transition function of the tuple $\mathcal{A}$
- $s_0$ : is an initial state where $s_0 \in S$ of the tuple $\mathcal{A}$.
- **F** : $F \subseteq S$ is called as the acceptance conditions/final states and at least one state should occur from the set of final state $\{F_1, F_2, \ldots, F_n\}$.

Consider a run of *Büchi* automata over a finite alphabet $\Sigma$. The set of infinite words $w = w_0, w_1, \ldots, w_n \in \Sigma$ and the sequence of states are $s_0, s_1 \ldots, \in S$ such that $\forall\ \mathcal{A} \geq 0,\ \delta(s_i, w_i) = s_{i+1}$. The set of infinite words($w$) for which we visit at least one state in $F$ are accepted words and can be denoted by $\mathcal{L}_w(\mathcal{A})$. A *Generalized Büchi Automaton* (GBA) is used where the number of accepting state increase $F = F_1, F_2, \ldots, F_k$, where $k$ is the number of final states. Therefore GBA will accept any set of words iff, for all $1 \leq \text{i} \leq \text{k},\ S \cap F_i \neq \phi$.

We can also express the extended transition relations $\delta^w$: $S \times \Sigma^w \times S$. This relation shows that it will take as input the set of stings rather then single characters. Let us assume that an empty string is represented by $\zeta$, then $\delta^w$ can be defined recursively as $\forall s \in S,\ w \in \Sigma^w,\ \sigma \in \Sigma$ such as:

$$\delta^w(s, \zeta) = s$$
$$\delta^w(s, w\sigma) = \delta(\delta^w(s, w), \sigma).$$

Intuitively, let us assume that $\mathcal{A}_M$ and $\mathcal{A}_N$ are two different states running in parallel and synchronously to each other, then $\sigma$ is an event which is associated from the state $s_0$ to $s_0'$ from model $\mathcal{A}_M$ to $\mathcal{A}_N$ respectively at time $t = 0$ to $t = 1$ times. Thus a computation of LTL formula $\phi$ is a set of infinite words that can be represented by the alphabet $\Sigma = 2^{PROP}$, which need to accepted by the *Büchi* automata $\mathcal{A}_w$ for all sets of input sequence $\phi$.

### A. LTL to GNBA States:

Loosely speaking in formal verification methods, FSM based models need to express an equivalent *Büchi* automata for LTL formula. Generally speaking LTL formula is converted by $\omega - language$ [22] for equivalent GNBA specifications . However to convert any LTL formula into corresponding *Büchi* automata we need to find the *closure* of the given system specifications. Thus a closure of any formula $\phi$ can be found as $closure(\phi) = \{sub - formula\}$ of $\phi$ and $\{Negationofsub - formula\}$ of $\phi$. However let us assume that a LTL formula $\phi = a \wedge b$ then its subset is $\{a,\ b,\ a \wedge b, \zeta\}$ $\cup\ \{\neg a,\ \neg b,\ \neg(a \wedge b), \neg\zeta\}$ and also assume that the subset of closure ($\phi$) is represented by $B_i$, then there are some elementary set of formulas for determining the property of the GNBA represented as:

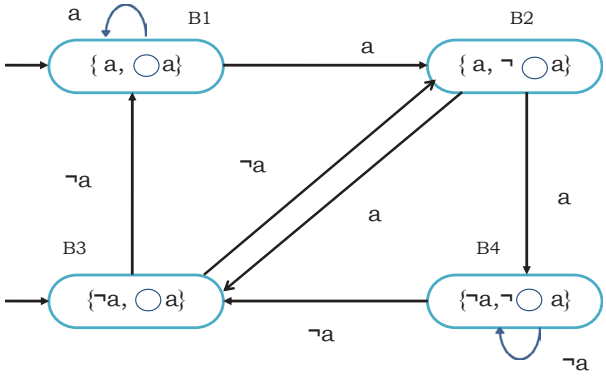


Fig. 3: LTL formula($\bigcirc\ a$) in GNBA

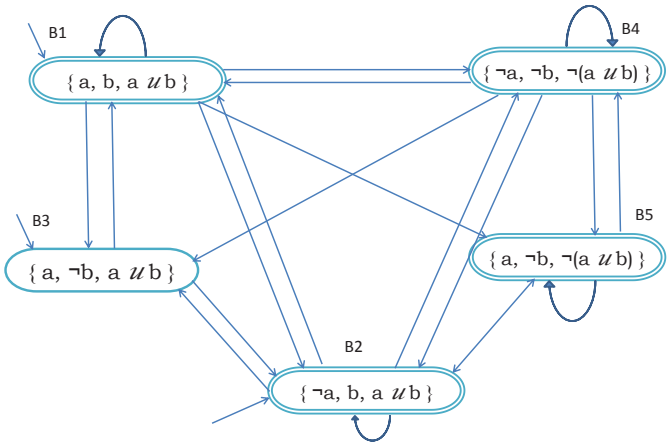


Fig. 4: LTL formula($a \mathcal{U} b$) in GNBA

1. $B$ is logically equivalent/consistent if for all $\phi_1 \wedge \phi_2,\ \zeta \in cl(\phi)$
   - if $\phi_1 \wedge \phi_2 \in B \iff \phi_1 \in B$ and $\phi_2 \in B$
   - $\zeta \in B \Rightarrow \neg\zeta \notin B$
   - $true \in cl(\phi) \Rightarrow true \in B$
2. $B$ is locally equivalent/consistent if for all $\phi_1 \mathcal{U} \phi_2 \in closure(\phi)$
   - $\phi_2 \in B \Rightarrow \phi_1 \mathcal{U} \phi_2 \in B$
   - $\phi_1 \mathcal{U} \phi_2 \in B$ and $\phi_2 \notin B \Rightarrow \phi_1 \in B$
3. $B$ is called maximal, if for all $\zeta \in closure(\phi)$, $\zeta \notin B \Rightarrow \neg\zeta \in B$

However in Fig 3 we present an automaton for the LTL formula $\bigcirc\ a$ to GNBA. The terminal $a$ may be interpreted as any region on the given map or goal specifications as per requirements. Thus the closure of $\bigcirc\ a = \{a, \neg a, \zeta\}$ and similarly in another example we present an automaton of the LTL formula $a \mathcal{U} b$ in GNBA. Moreover the formula $a \mathcal{U} b$ similarly may interpreted as "Visit IT_ LAB until visit CS_LAB". However the closure for the same formula is displayed in Fig 4 with closures of the given specifications.

### B. GNBA to GR(1) Parsing :

GR(1) parsing is generally based on two-player games played in some environment. The major goal for the parsing technique is to find the winning conditions for the LTL formula over the GNBA automaton. The goal of the system depends on the environmental actions performed while moving from one system state to another system state. A general Game structure for GR(1) can be defined as $G = (\mathcal{R}, \mathcal{I}, \mathcal{O}, \mathcal{Q}_{env}, \mathcal{Q}_{st}, \mathcal{T}_{env}, \mathcal{T}_{st}, \omega)$ and is expressed as:

- $\mathcal{R} = \{r_1, r_2, \ldots, r_n\}$ : A set of all *state variables* or a finite set over the finite domains. We also assume that all sets of states ($\mathcal{R}$) are Boolean from the environment $\mathcal{M}_{\mathcal{R}}$ for computation purposes.
- $\mathcal{I} \subseteq \mathcal{O}$ is a set of *input variables* for an environment which is controlled during the motion of the robots.
- $\mathcal{O} = \frac{\mathcal{R}}{\mathcal{I}}$ is a set of *output variables* controlled by the system $\mathcal{M}$.
- $\mathcal{Q}_{env}$ is boolean assertions for $\mathcal{I}$ and make distinct the initial states of the environment.
- $\mathcal{Q}_{st}$ is also boolean assertions for $\mathcal{O}$ and make distinct the initial states of the systems $\mathcal{M}$
- $\mathcal{T}_{env}(\mathcal{R}, \mathcal{I}')$ is the transition relation for the environment. This assertion is satisfied by any state $s \in \mathcal{M}$ to possible next input for $s_{\mathcal{I}} \in \mathcal{M}$ at the time interval $t$ to $t+1$ by putting $\mathcal{I}$. Thus transition relation $\mathcal{T}_{env}$ is $(s, s_{\mathcal{I}}) \models \mathcal{T}_{env}$.
- $\mathcal{T}_{st}(\mathcal{R}, \mathcal{I}', \mathcal{O}')$ is the transition relation for the system. This assertion is satisfied for any relation for the output value for $s_{\mathcal{O}} \in \mathcal{M}_{\mathcal{O}}$ for all combinations of $\mathcal{R}$. Thus the transition relation $\mathcal{T}_{st}$ is identifies as $s_{\mathcal{O}} \in \mathcal{M}_{\int \sqcup}$. Therefore state $s$ will read the input $s_{\mathcal{I}}$ if $(s, s_{\mathcal{I}}, s_{\mathcal{O}}) \models \mathcal{T}_{st}$.
- $\omega$ is the winning conditions for any given LTL formula orver the GNBA automaton.

However any initial state $s$ must satisfy both $\mathcal{Q}_{env}$ and $\mathcal{Q}_{st}$ i.e. $s \models \mathcal{Q}_{env} \wedge \mathcal{Q}_{st}$. Any play between two states $s$ and $s'$ respectively is a successor of $s$ only if $(s, s') \models \mathcal{Q}_{env} \wedge \mathcal{Q}_{st}$. Fig 5 shows a small example of GR(1).

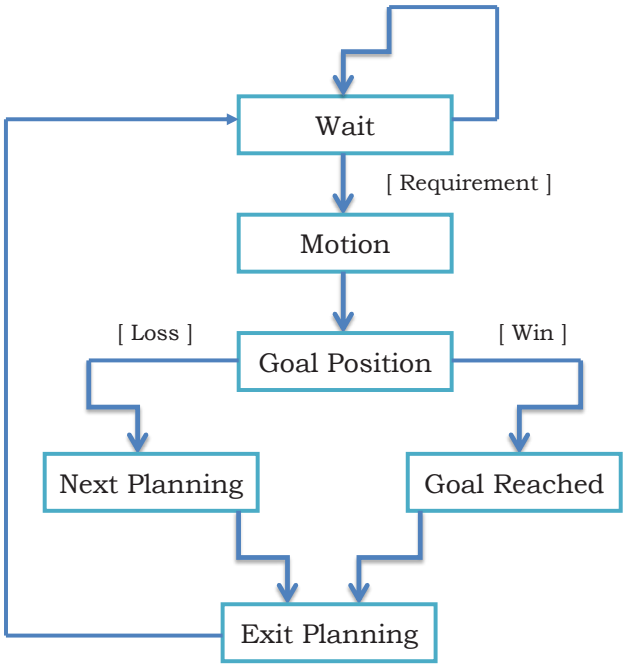


Fig. 5: GR(1) parsing example for LTL formula

## VI. Simulation Results

The simulations have been done in the LTLMoP (Linear Temporal Logic MissiOn Planning) software [21]. All our experiments are performed under Ubuntu 12.04 LTS operating system environments with Intel Core i5-5200GHz processor, 4GB RAM on a desktop computer. The software allows the user to write LTL specifications as well as define the map of the environment. We setup the map based on the lab environment of IIIT Allahabad Robotics and Artificial Laboratory, although changes were made to make the environment complex and the display more appealing. Several complex labs are setup for experimental simulation purpose. Although the current setup was 2D, LTLMoP also supports 2.5D regions. All real-time information about the current experiments and motion status of the robot with all physical information can visualized in the simulation tool.

The first set of experiments are done on a 2D map of the laboratories, in which some obstacles are added. A point robot is taken that needs to visit several places on the map based on conditional requirements given by the user as the problem specifications. The map and the regions are illustrated in Fig 6. To solve the problem we setup some custom propositions corresponding to each regions shown in Table I.

First we apply roadmap decomposition on the map. The decomposed map is shown in Fig 7.

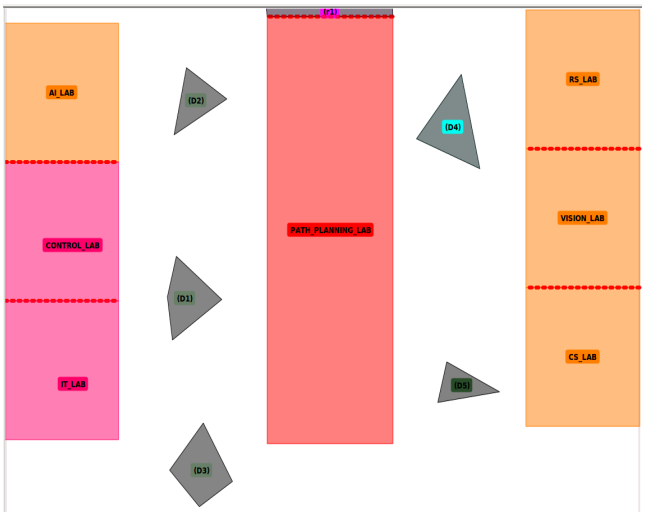


Fig. 6: Artificial map for experimental environment

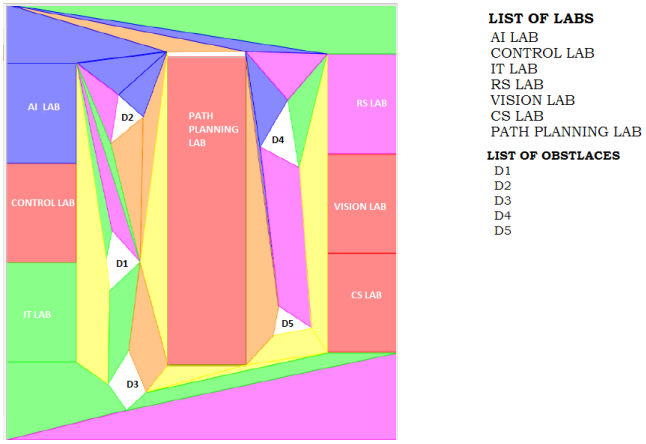


Fig. 7: Workspace Decomposition of experimental map

TABLE 1. REGION DECOMPOSITION INTO SYSTEM PROPOSITION

| MAP REGIONS | CUSTOM PROPOSITIONS |
|---|---|
| IT_LAB | it_lab_visited |
| CS_LAB | cs_lab_visited |
| VISION_LAB | vision_lab_visited |
| RS_LAB | rs_lab_visited |
| PATH_PLANNING_LAB | path_planning_lab_visited |
| CONTROL_LAB | control_lab_visited |
| AI_LAB | ai_lab_visited |
| | x,y |

In the first scenario the robot is asked to visit either `IT_LAB` or `AI_LAB` and then `RS_LAB` and `CS_LAB` until `CONTROL_LAB` is not finally visited. The LTL specification for the same problem interpreted as $\bigcirc(\bigcirc(IT\_LAB \vee AI\_LAB) \wedge \bigcirc(RS\_LAB \wedge CS\_LAB))\, \mathcal{U}\, CONTROL\_LAB$. The mission specification is given by Algorithm 1. This is a common problem in robotics, wherein the robot may be asked to talk to any student sitting in either of the two labs, and then broadcast the information to all the other labs, finally ending the journey at the home lab. The resultant trajectory displayed on the map in black color is shown on Fig 8.

**Algorithm 1** Robot Waiter Example

```
ai_lab_visited is set on AI_LAB and reset on false
rs_lab_visited is set on RS_LAB and reset on false
it_lab_visited is set on IT_LAB and reset on false
cs_lab_visited is set on CS_LAB and reset on false
x is set on (it_lab_visited or ai_lab_visisted) and reset on false
y is set on (rs_lab_visited and cs_lab_visisted) and reset on false
if x then
    Go to y
    Go to x
end if
```

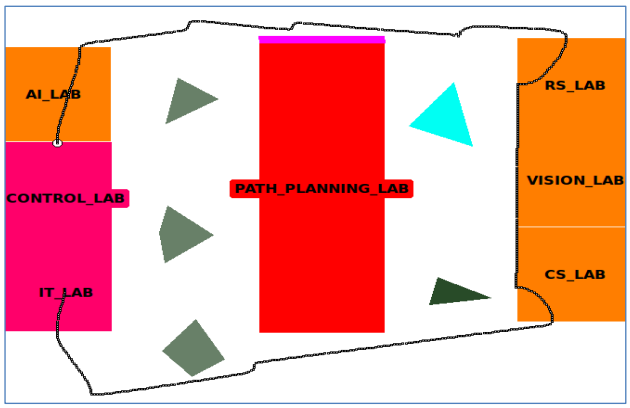


Fig. 8: Results for First Scenario

In the second scenario the robot is ask to perform some search or rescue/surveillance task in our experimental environment and it needs to visit all labs on map. In this specification we take an assumption that the robot needs to visit all the research labs in any order. The specific LTL specification is represented as: $\bigcirc(CS\_LAB \wedge VISION\_LAB \wedge RS\_LAB \wedge AI\_LAB\, CONTROL\_LAB \wedge IT\_LAB \wedge PATH\_PLANNING\_LAB)$. The resulted trajectory is shown in Fig 9. In the third scenario the robot is asked to carry some notebooks or research papers either from IT_LAB or VISION_LAB and then visit CONTROL_LAB and AI_LAB and finally visit the IT_LAB. The corresponding LTL specification interpreted as . The trajectory traced by the robot is shown in 10.

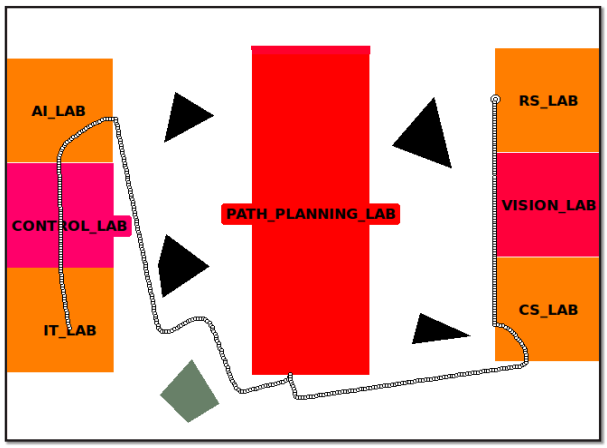


Fig. 9: Results for Second Scenario

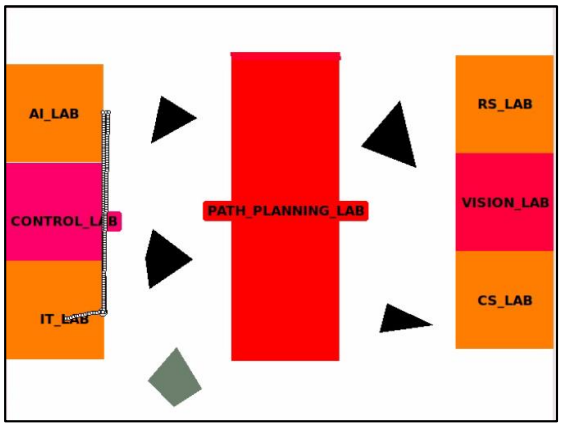


Fig. 10: Results for Third Scenario

We also setup an experimental stationary environment for a PR2 robot using LTLMoP-ROS software. The simulation result is performed under the GAZEBO-ROS GUI API. The map represents an office like environment consisting of three regions office, Lab1 and Lab2, defined as regions of interest. We also use a dummy sensor "wait", during the motion of the PR2 robot. If the dummy sensor is activated, then the robot will wait on its position infinity until the sensor is not deactivated. Fig 11 shows the map used for the experiment, while the decomposed map is shown in Fig. 12. In this scenario the robot is asked to move from initially office to Lab1 or Lab2 . The PR2 robot will only be in motion condition if the dummy sensor is disabled. The movement of the robot is shown in Figs 13, 14 and 15. Moreover as the robot visits in the office area or in a corridor a local planner will "foldArm". In Fig 16 during the motion of PR2 the robot waits as the wait sensor is enabled.

**Algorithm 2** Robot Helper Example

```
robot start in office with false
initially often not wait
Visit Lab2 or Lab1
Visit Office
if you were in office then
    Do foldArms
end if
if you are sensing wait then
    Stay there
end if
```

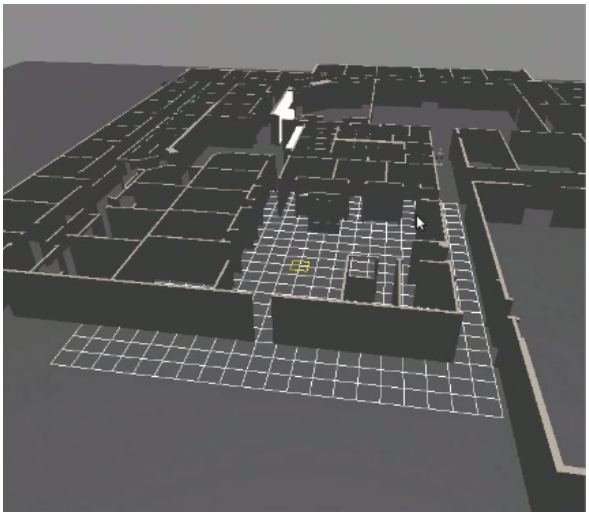

Fig. 11: Workspace of the experimental map in ROS


Fig. 12: Workspace Decomposition in ROS for PR2 Robot

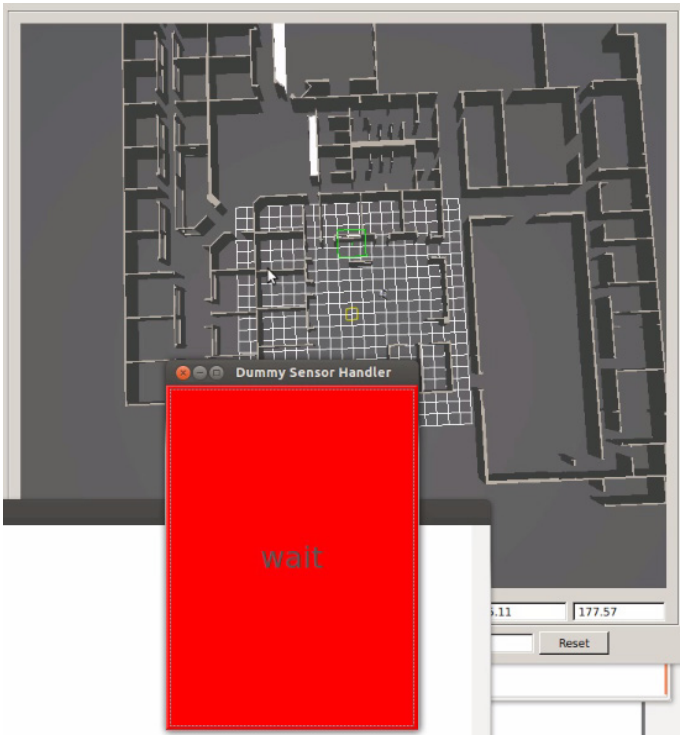


Fig. 13: PR2 robot is initially in the office area and is waiting for the sensor to be disabled

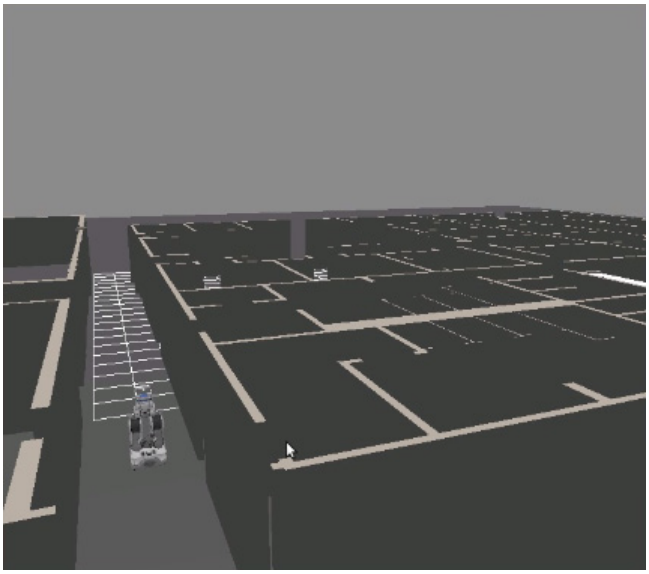

Fig. 14: PR2 robot visiting from office area to Lab1 with the Wait Sensor disabled

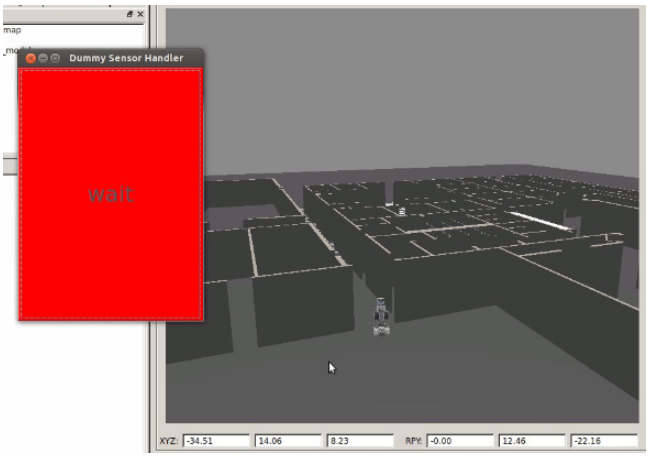


Fig. 15: PR2 robot visited Lab1 and the Wait sensor was disable

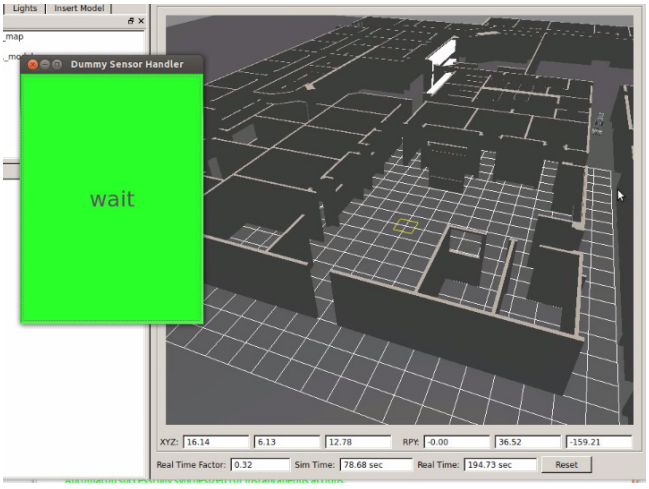


Fig. 16: PR2 robot standing on the corridor as the wait sensor was enabled

Moreover the video results of simulation can be found at:
https://www.youtube.com/watch?v=7rvbnd8MlWc,
https://www.youtube.com/watch?v=gSwOi-lJiuA,
https://www.youtube.com/watch?v=vJ2rdU2aLuE.

## VII. Conclusion and Future Scope

Mission planning is a complicated problem in robot motion planning, wherein the task required to be done by the robot can be overly complicated. In this paper we used Temporal Logic for solving the problem of Mission Planning for mobile robots. The map was decomposed into regions which made the roadmap, and the approach was thus faster than the prior approach which used grid maps. The benefit of using a decomposition of the map is that the robot follows the trajectory given by the roadmap during the motion from one region to another, rather than computing the inter-region trajectory in real time. The simulations were initially done on a point robot. Finally a demonstration on ROS environment for real-time problem specifications using a PR2 robot was provided. The simulations used sensors mounted on the PR2 robot.

Currently the experiments are done with a single robot only. The work needs to be extended for multiple robots. The use of multi-resolution techniques and sampling based search techniques can significantly improve the computational time of the algorithm, while making more realistic assumptions about the environment. The algorithm also needs to be extended to handle probabilistic behavior and vague specifications. The algorithm needs to be tested on physical robots preferably with the ROS environment.

## References

[1] Kress-Gazit, H.; Fainekos, G.E.; Pappas, G.J., "Temporal-Logic-Based Reactive Mission and Motion Planning," Robotics, IEEE Transactions on , vol.25, no.6, pp.1370,1381, Dec. 2009 doi: 10.1109/TRO.2009.2030225

[2] Kress-Gazit, H.; Fainekos, G.E.; Pappas, G.J., "Where's Waldo? Sensor-Based Temporal Logic Motion Planning," Robotics and Automation, 2007 IEEE International Conference on , vol., no., pp.3116,3121, 10-14 April 2007 doi: 10.1109/ROBOT.2007.363946

[3] Bhatia, A.; Kavraki, L.E.; Vardi, M.Y., "Sampling-based motion planning with temporal goals," Robotics and Automation (ICRA), 2010 IEEE International Conference on , vol., no., pp.2689,2696, 3-7 May 2010 doi: 10.1109/ROBOT.2010.5509503

[4] Bhatia, A.; Kavraki, L.E.; Vardi, M.Y., "Motion planning with hybrid dynamics and temporal goals," Decision and Control (CDC), 2010 49th IEEE Conference on , vol., no., pp.1108,1115, 15-17 Dec. 2010 doi: 10.1109/CDC.2010.5717440

[5] Saha, I.; Ramaithitima, R.; Kumar, V.; Pappas, G.J.; Seshia, S.A., "Automated composition of motion primitives for multi-robot systems from safe LTL specifications," Intelligent Robots and Systems (IROS 2014), 2014 IEEE/RSJ International Conference on , vol., no., pp.1525,1532, 14-18 Sept. 2014 doi: 10.1109/IROS.2014.6942758

[6] Meng Guo; Johansson, K.H.; Dimarogonas, D.V., "Revising motion planning under Linear Temporal Logic specifications in partially known workspaces," Robotics and Automation (ICRA), 2013 IEEE International Conference on , vol., no., pp.5025,5032, 6-10 May 2013 doi: 10.1109/ICRA.2013.6631295

[7] Ayala, A.I.M.; Andersson, S.B.; Belta, C., "Temporal logic motion planning in unknown environments," Intelligent Robots and Systems (IROS), 2013 IEEE/RSJ International Conference on , vol., no., pp.5279,5284, 3-7 Nov. 2013 doi: 10.1109/IROS.2013.6697120

[8] McMahon, J.; Plaku, E., "Sampling-based tree search with discrete abstractions for motion planning with dynamics and temporal logic," Intelligent Robots and Systems (IROS 2014), 2014 IEEE/RSJ International Conference on , vol., no., pp.3726,3733, 14-18 Sept. 2014 doi: 10.1109/IROS.2014.6943085

[9] Svorenova, M.; Tumova, J.; Barnat, J.; Cerna, I., "Attraction-based receding horizon path planning with temporal logic constraints," Decision and Control (CDC), 2012 IEEE 51st Annual Conference on , vol., no., pp.6749,6754, 10-13 Dec. 2012 doi: 10.1109/CDC.2012.6426041

[10] Loizou, S.G.; Kyriakopoulos, K.J., "Automated Planning of Motion Tasks for Multi-Robot Systems," Decision and Control, 2005 and 2005 European Control Conference. CDC-ECC '05. 44th IEEE Conference on , vol., no., pp.78,83, 12-15 Dec. 2005 doi: 10.1109/CDC.2005.1582134

[11] Finucane, C.; Gangyuan Jing; Kress-Gazit, H., "LTLMoP: Experimenting with language, Temporal Logic and robot control," Intelligent Robots and Systems (IROS), 2010 IEEE/RSJ International Conference on , vol., no., pp.1988,1993, 18-22 Oct. 2010 doi: 10.1109/IROS.2010.5650371

[12] Gangyuan Jing; Finucane, C.; Raman, V.; Kress-Gazit, H., "Correct high-level robot control from structured English," Robotics and Automation (ICRA), 2012 IEEE International Conference on , vol., no., pp.3543,3544, 14-18 May 2012 doi: 10.1109/ICRA.2012.6225161

[13] Raman, V.; Finucane, C.; Kress-Gazit, H., "Temporal logic robot mission planning for slow and fast actions," Intelligent Robots and Systems (IROS), 2012 IEEE/RSJ International Conference on , vol., no., pp.251,256, 7-12 Oct. 2012 doi: 10.1109/IROS.2012.6385935

[14] Raman, V.; Kress-Gazit, H., "Explaining Impossible High-Level Robot Behaviors," Robotics, IEEE Transactions on , vol.29, no.1, pp.94,104, Feb. 2013 doi: 10.1109/TRO.2012.2214558

[15] Kunze, L.; Dolha, M.E.; Beetz, M., "Logic programming with simulation-based temporal projection for everyday robot object manipulation," Intelligent Robots and Systems (IROS), 2011 IEEE/RSJ International Conference on , vol., no., pp.3172,3178, 25-30 Sept. 2011 doi: 10.1109/IROS.2011.6094743

[16] Kloetzer, M.; Belta, C., "A Fully Automated Framework for Control of Linear Systems from Temporal Logic Specifications," Automatic Control, IEEE Transactions on , vol.53, no.1, pp.287,297, Feb. 2008 doi: 10.1109/TAC.2007.914952

[17] Karaman, S.; Frazzoli, E., "Complex mission optimization for Multiple-UAVs using Linear Temporal Logic," American Control Conference, 2008 , vol., no., pp.2003,2009, 11-13 June 2008 doi: 10.1109/ACC.2008.4586787

[18] Alur, R.; Moarref, S.; Topcu, U., "Counter-strategy guided refinement of GR(1) temporal logic specifications," Formal Methods in Computer-Aided Design (FMCAD), 2013 , vol., no., pp.26,33, 20-23 Oct. 2013 doi: 10.1109/FMCAD.2013.6679387

[19] Kala Rahul, Anupam Shukla, and Ritu Tiwari. "Fusion of probabilistic A* algorithm and fuzzy inference system for robotic path planning." Artificial Intelligence Review 33.4 (2010): 307-327.

[20] Tiwari, Ritu, ed. Intelligent Planning for Mobile Robotics: Algorithmic Approaches: Algorithmic Approaches. IGI Global, 2012.

[21] C. Finucane, G. Jing, and H. Kress-Gazit. LTLMoP website. http://ltlmop.github.com/, 2015

[22] Anping He; Jinzhao Wu; Lian Li, "An Efficient Algorithm for Transforming LTL Formula to Büchi Automaton," Intelligent Computation Technology and Automation (ICICTA), 2008 International Conference on , vol.1, no., pp.1215,1219, 20-22 Oct. 2008 doi: 10.1109/ICICTA.2008.297

[23] Kiam Tian Seow; Ming Gai; Tong Lee Lim, "A Temporal Logic Specification Interface for Automata-Theoretic Finitary Control Synthesis," Robotics and Automation, 2005. ICRA 2005. Proceedings of the 2005 IEEE International Conference on , vol., no., pp.565,571, 18-22 April 2005 doi: 10.1109/ROBOT.2005.1570178

[24] Kala Rahul. "Multirobot Motion Planning using Hybrid MNHS and Genetic Algorithms" Applied Artificial Intelligence 27.3 (2013): 170-198.

[25] Kala Rahul. "Navigating Multiple Mobile Robots without Direct Communication." International Journal of Intelligent Systems 29.8 (2014): 767-786.

[26] Piterman, Nir, Amir Pnueli, and Yaniv Saâ€™ar. "Synthesis of reactive (1) designs." Verification, Model Checking, and Abstract Interpretation. Springer Berlin Heidelberg, 2006.

[27] R. Kala, A. Shukla, R. Tiwari (2010) Dynamic Environment Robot Path Planning using Hierarchical Evolutionary Algorithms. Cybernetics and Systems, 41(6): 435-454.

[28] Wolff, E. M., Murray, R. M. (2013). Optimal control of nonlinear systems with temporal logic specifications. In Proc. of Int. Symposium on Robotics Research.

**Dr. Rahul Kala** received the B.Tech. and M.Tech. degrees in information technology from the Indian Institute of Information Technology and Management, Gwalior, India in 2010. He received his Ph.D. degree in cybernetics from the University of Reading, UK in 2013. He is currently working as an Assistant Professor in the Indian Institute of Information Technology, Allahabad, India in the Robotics and Artificial Intelligence Laboratory. He is the author of three books and over 70 papers. His recent book is on robotic planning is entitled
Intelligent Planning for Mobile Robotics: Algorithmic Approaches (IGI-Global Publishers, 2013). He is a recipient of the Commonwealth Scholarship and Fellowship Program from the UK Government; the Lord of the Code Scholarship from RedHat and the Indian Institute of Technology Bombay; and the GATE scholarship from the Ministry of Human Resource Development, Government of India.

**Dr. Anil Kumar** received the M.Tech degrees in information technology from Indian In- stitute of Information Technology Allahabad, India in 2015. He is author of more then four research papers in the field of Robotics and Artificial Intelli- gence. He is the recipient of the GATE scholarship from the Ministry of Human Resource Development, Government of India.

# Comparative Study of Clustering Algorithms in Text Mining Context

Abdennour Mohamed JALIL, Imad HAFIDI, Lamiae ALAMI, ENSA Khouribga

*Laboratoire IPOSI*

***Abstract* — The spectacular increasing of Data is due to the appearance of networks and smartphones. Amount 42% of world population using internet [1]; have created a problem related of the processing of the data exchanged, which is rising exponentially and that should be automatically treated. This paper presents a classical process of knowledge discovery databases, in order to treat textual data. This process is divided into three parts: preprocessing, processing and post-processing. In the processing step, we present a comparative study between several clustering algorithms such as KMeans, Global KMeans, Fast Global KMeans, Two Level KMeans and FWKmeans. The comparison between these algorithms is made on real textual data from the web using RSS feeds. Experimental results identified two problems: the first one quality results which remain for algorithms, which rapidly converge. The second problem is due to the execution time that needs to decrease for some algorithms.**

***Keywords* — Algorithms, Clustering, Data, Text Mining.**

## I. Introduction

The advent of smartphones, social networks and cloud computing has added to the amount and sparse of data creation in the world, so much so that 90% of the world's total data has been created in the last 5 years and 70% of it by individuals. Studies predict that approximately 4 trillion gigabytes of data will exist on earth. As the world becomes increasingly digital, new techniques are requested, needed to search, analyze, and understand these huge amounts of unstructured data. This requires an automatic processing for unstructured data. This is BIGDATA R&D problematic, more specifically in the field of textual Data researches.

Text mining is a set of techniques, which aim to process those huge amounts of data and gain value from it. Introduced by Ronen and Dagan as KDT [2], we find as main branches of text mining: text extraction, summarizing, categorization, etc.

In opposite of Data mining, KDT aims to process unstructured texts, complex and over dimensioned data. Generally KDT is based on an automatic process to analyze the entire contents.

The paper is organized on three sections: In the first section, we present a text clustering system for KDT. In the second section, a number of classification algorithms are described. The third section presents a comparative study of clustering algorithms in a KDT context. At the last section some conclusions are drawn.

## II. Existing Clustering System

It is generally based on automatic method to analyze and process the whole text. Among these methods there is the process show in [10], which is spread over three main stages:

### A. Preprocessing

The aim of this step is to clean data and reduce noise: [11]:

1. Removal of empty words (defined articles, punctuation marks, etc).
2. Lemmatization: It is a lexical analysis of words that aims to bring together a number of words in the same family sorted by root.
3. Digital transformation: in this stage the text data is converted to digital data to classify them. There are many models of digital transformation, the most used are:
   a) **Boolean Model**: The representation of the content of a document is done by using a set of list method. It represents each word of the document by a Boolean value. It can be simple and efficient if used by specialists, but it loses its effectiveness when doing research on generalized corpus (lack of user experience)
   b) **Probabilistic Model**: the representation of the content of a document is made in the context of a probabilistic method [13]. Compared to a given query, this model gives a probability estimation of document relevance.
   c) **Vector Model**: sometimes called semantic Vector [14]**.** It is the representation of a document contents through and algebraic method that consider the semantics. Very famous method, Vector model is used to represent documents in a vector shape. The application of clustering with this model becomes easy.

### B. Processing

In this step, we use one of the clustering algorithms to create the corpus [15]. Alternatively we will distribute documents on several clusters. The elements of each cluster have a common characteristic. Clustering algorithms is presented in the next section.

### C. Post Processing

Some works uses the ontologies to give meaning to clusters. They use labeling **[8]** and visualization of clustering results to present hierarchical relations between the resulting clusters and evaluation. They are generally looking for the most frequent terms in each cluster to present them using semantic relations of ontologies.

## III. Clustering Algorithms KMeans

Partitioning Algorithms put data in a predetermined number of clusters. The clustering approaches can be divided into two categories according to their input parameters:

1. Algorithms that take explicitly the number of input clusters **K**.
2. Algorithms that take a threshold $\tau$ as an input, Used to determine indirectly the number of clusters.



DOI: 10.9781/ijimai.2016.376

KMeans is the most known algorithm in the first category. The second category includes Two-Level-KMeans for example.

All partitioning algorithms use the following concepts:

We note:

- group of data : $X = \{X1, X2, ..., Xn\}$
- partitions : $S = \{S1, S2, ..., Sk\} k \leq n$

**K** is the number of desired clusters, n is the cardinality of data.

It aims to minimize the distance between points belonging to each cluster (score).

$$Args \min S \sum_{i=1}^{K} \sum_{Xj \in Si} \left\| Xj - \mu i \right\|^2$$

With $\mu i$ is the center of the cluster $i$. $Xj$ is an element of the set.

Alternatively, we try to find clusters with minimum of inter-cluster distance and the maximum of intra-class distance.

### A. Algorithms KMeans

Based on the previous concept, five partitioning algorithms are presented in the following:

a) **K Means**

The classic and most widely used algorithm is KMeans [4]. It takes two input parameters: the number of clusters K and a set of data.

This algorithm initializes arbitrarily the center of these clusters. Before running in several iterations, KMeans affected data to the nearest cluster, and the centers are recalculated at the end of each iteration. The algorithm stops once there are no more new assignments.

b) **Global-K Means**

The majority of proposed solutions previously cannot ensure the convergence to a global optimum, Global KMeans [3] proposed a new version, which overcomes this problem.

The main idea of the algorithm is to start with a single cluster that contains all the data set.

Then each iteration creating a new cluster with the center that minimizes the squared error. The algorithm stops once reached the number of clusters specified by the user.

c) **Fast Global KMeans**

This algorithm is proposed by **Jim Z.C and all** [6], to improve the Global KMeans. The fast global k-means algorithm constitutes a straightforward method to accelerate the global k-means algorithm. Suppose we are in $k - 1$ iteration, the new center ($x_n$) will allocate all points $x_j$ whose squared distance from $x_n$ is smaller than the distance $d_{k-1}^{j}$ from their previously closest center. $d_{k-1}^{j}$ Is the squared distance between $x_j$ and the closest center among the $k - 1$ cluster centers Therefore, for each such data point $x_j$ the clustering error will decrease by $d_{k-1}^{j} - |x_n - x_j|^2$

d) **Two-Level-KMeans**

Taking a threshold τ as an input parameter, the Two-level-KMeans [7] is executed in two steps. The implementation of the classic KMeans is made first. After clusters that do not verify the threshold condition, are selected for subdivision into $(r_i \div \tau) \times n$ subclasses with $(r_i)$ is the radius of the cluster and $n$ is the data cardinality.

e) **FW-KMeans**

FW-KMeans applies on the vector space model (VSM). Unlike KMeans that treats all elements of the set fairly, the FWK-Means uses the notion of weight to highlight the most common elements. In addition, FW-Means introduced a constant (very low value) to avoid the noise problem.

$$F(W,Z,\Lambda) = \sum_{l=1}^{k} \sum_{k=1}^{n} \sum_{i=1}^{m} w_{l,j} \lambda \beta_{l,i} \left[ d(z_{l,i}, x_{j,i}) + \sigma \right]$$

Where σ is a constant, k (≤ n) is the number of clusters; β (> 1) is an exponent; W = [$w_{l,j}$] is a k × n integer matrix; $Z = [Z_1, Z_2, ..., Z_k] \in R^{k \times m}$ are the k cluster centers; $\Lambda = \left( \Lambda_1, \Lambda_2, ..., \Lambda_K \right)$ is the set of weight vectors for all clusters in which each $\Lambda_l = (\lambda_{l,1}, \lambda_{l,2}, ..., \lambda_{l,m})$ is a vector of weights for $m$ features of the $l_{th}$ cluster; $d(Z_{l,i}, X_{j,i}) \geq 0$ is a distance or dissimilarity measure between the $j_{th}$ document and the center of the $l_{th}$ cluster on the $i_{th}$ feature. In text clustering, they use the Euclidean distance because the frequencies of terms are numeric values.

The proposal [8] FW KMeans had the aim of reducing the noise. This reduction is made by a weighting method to decrease the influence of noise, by the concentration of comparisons on the main axes.

## IV. Works and Results

At first, we recover items from RSS feed in XML format. Then, we transform the whole to flat files. After removing empty words, we proceed to lemmatization stage: for each word we look for its root using the TreeTagger Tool [9] and the last part of the preprocessing is reserved to convert results into vectors Using **TF-IDF** formula:

$$TF - IDF_{ij} = TF_{i,j} \times IDF_{ij}$$

Where $TF_{i,j} = \frac{n_{ij}}{\sum_k n_{ik}}$

And $IDF_{ij} = \log(|D|) / (|d_j : t_i \in d_j|)$

Where $n_{ij}$ is the occurrence of the word $n_i$ in the document $j$. $\sum_k n_{ik}$ Is the total number of words in the document : $|D|$: total number of documents in the corpus and $|d_j : t_i \in d_j|$: Number of documents where the term $t_i$ appears.

An example of vector is in Fig. 1

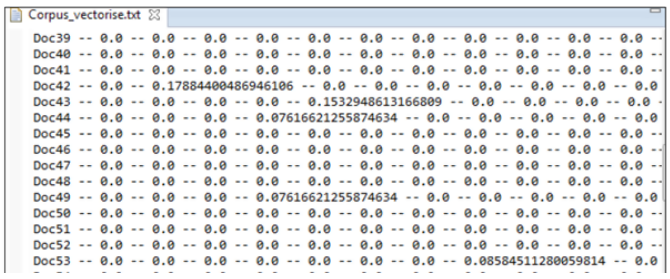


Fig 1: part of the vector file

### A. Runtime Environment

The data used are taken from the actual web processed in a machine 2.5 GHz CPU (Core i5) and 8 GB of Ram, running on Windows 7.

### B. Used Data

The actual used data is retrieved from several info websites (le monde, 01net, JDN etc.) Usually the documents do not have the same size (number of words), or the same natural category (political subject, computer etc.). In total 727 documents were recovered.

These documents went through a preprocessing cycle before the application of the clustering step.

### C. Results

Table 1 presents obtained results using the five partitioning algorithms described previously. The time execution is also reported in this table.

TABLE 1: CLUSTERING RESULTS

| Algorithm | Clusters Number | DB index | Square error | Iteration number | Execution time (s) |
|---|---|---|---|---|---|
| **KMeans** | 10 | 1.469 | 0.867 | 2 | 0.411 |
| | 20 | 1.70 | 0.66 | 3 | 0.126 |
| | 100 | 2.03 | 0.59 | 2 | 1.247 |
| **Global KMeans** | 10 | 0.462 | 0.45 | 10 | 25384062 |
| | 20 | 0.155 | 0.43 | 20 | 48480265 |
| **Fast GKMeans** | 10 | 1.16 | 0.74 | 9 | 3344 |
| | 20 | 1.02 | 0.73 | 19 | 4454 |
| | 100 | 0.80 | 0.61 | 99 | 24627 |
| **Two-Level-KMeans** | 10 | 4.09 | 0.86 | 2 | 0.455 |
| | 20 | 1.41 | 0.75 | 1 | 0.517 |
| | 100 | 1.23 | 0.69 | 3 | 4.204 |
| **FW-KMeans** | 10 | 1.73 | 0.46 | 9 | 321400 |
| | 20 | 1.41 | 0.46 | 19 | 1995788 |
| | 100 | 0.75 | 0.42 | 53 | 29686708 |

All algorithms are launched five times (except Global KMeans: one time) and took the average value of the index in Tables 1. For the Two-Level- KMeans algorithm, we fix threshold as the average value of all vectors. The initialization of the centers of all algorithms (except Global KMeans) is made arbitrarily. For the β parameter of FW-KMeans, it was set at 1.5.

By analyzing the results in Table 1, we find that the classic KMeans is the fastest in terms of execution time.

This rapid convergence to a local optimum lets results become heuristic.

For the global KMeans present the longest (execution time). It is normal because it treats all possible cases. The application of this method in a real-time context is not possible. Fast Global KMeans is very quick in comparison to the Global KMeans, and gives an interesting result compared to the execution time. Two level KMeans clustering is very useful if it used for large volume of data.

A reduction in the processing time is confirmed. This reduction according to the literature [7] maintains the quality of the clustering. But it was tested on uniform data. In our case we tested them on various data. This application showed that the two level KMeans is inefficient in this case.

The FW-KMeans presents good results compared to the majority of tested algorithms. It takes into account the concept of weighting in its partitioning which increases the quality of the results but the execution time is bit little high.

## V. Conclusion

In this paper, we have implemented a process of text mining. Initially, we have performed a preprocessing on the data from the web, and then we applied five clustering algorithms (KMeans Global KMeans, Fast Global KMeans, Two-level KMeans and FW-KMeans) on the data. The evaluation of the classification results is performed with Squar erreur and DBIndex.

We found similar results in the literature on our data: rapid convergence of the KMeans clustering and less performance of two level KMeans clustering without having good quality. Medium or high quality with Global KMeans, fast GKMeans and FWKmeans, but with a long execution time.

It has been found that Two-level-KMeans is ineffective in a KDT context, and its results are closed to KMeans ones. In addition, the choice of the threshold value is still a problem

The FW KMeans improves the k-means algorithm by adding a new step, in which the weights of features for different groups are calculated. The experiences show that FW KMeans can deal with a large and sparse data. The results of own experiment on text data provided from the real world show that the FW KMeans is better than the TWO Level KMeans.

The indices used for clustering evaluation are less specific and depend on the treated area. In future research, we will work on two axes:

- Integration of ontologies in different stages of the process to improve our results in terms of quality and execution time.
- The parallelization algorithms for the different stages.

## References


[1] WeAre Social, http://wearesocial.fr/blog/2015/01/digital-social-mobile-les-chiffres, 2015/ 2015.

[2] Ronen and Dagan: Knowledge Discovery in Textual Databases (KDT). 2005.

[3] Aristidis Likas, Nikos Vlassis, Jakob J. Verbeek: The Global K-Means Clustering Algorithm., 2003.

[4] J. B. MacQueen: Some Methods for classification and Analysis of Multivariate Observations. 1967.

[5] Kaufman, L. And Rousseeuw, P.J. Clustering by means of Medoids, in Statistical Data Analysis Based on the L_1–Norm and Related Methods, edited by Y. Dodge, north-Holland, 1987. pp.405–416.

[6] Jim Z.C. Laia, Tsung-Jen Huanga: Fast global KMeans clustering using cluster membership and inequality. 2009.

[7] Radha Chitta, M. Narasimha Murty JournalPattern Recognition archive Volume 43 Issue 3, March 2010 pp. 796-804.

[8] Liping Jing, Michael K. Ng, Xinhua Yang, Joshua Zhexue Huang : A Text clustering System based on k-means Type Subspace Clustering and Ontology, World Academy of Science, Engineering and Technology Vol: 2 2008

[9] Helmut Schmid, Improvements in Part-of-Speech Tagging with an Application to German. 2005.

[10] Joel Azzopardi, Christopher Staff, Incremental Clustering of News Reports, 2012.

[11] IBEKWE-SANJUAN Fidelia, SANJUAN Eric, Ingénierie linguistique et Fouille de Textes, 2007.

[12] Davies, DavidL Bouldin W, A Cluster Separation Measur. IEE Transaction on Pattern Machine Intelligence. PAMI-1(2), 2012, pp.224-227

[13] [Stephen E.Roberston ; Karen Sparrck Jones], Revelence weighting of search terms, Journal of the American Society, vol 27, n°3, main-juin 1976, pp.129-146

[14] [G.Salton, A.Wong, C.S Yang], Avector space model for automatic

indexing, Communication of the ACM, v18 n°11, 1975, pp. 613-620

[15] Khan K, Sahai A. A fuzzy c-means bi-sonar-based Metaheuristic Optimization Algorithm, International Journal of Interactive Multimedia and Artificial Intelligence. 2012;1(7), pp.26-32

**Mohamed Abdennour JALIL** was born in Khouribga, Morocco, in 1989. He received the Bachelor degree in mathematics and computer sciences from the University of Hassan I, Morocco, in 2011, and the Master degree in computer sciences from the national school of applied sciences (ENSA), Khouribga, Morocco, in 2013. In 2015, he joined the Department of Computer sciences Engineering, University of Hassan first, as a PhD student, Abdennour worked as technical consultant in ERP industry (implementing Microsoft Dynamics Ax) at Accenture Services Morocco & TVH Consulting(2013-2015). He consulted on a variety of projects, involving quantitative analysis, Processing Huge amounts of unstructured Data and Reporting. He developed an interest in Big Data, Text Mining and sophisticated clustering algorithms.

**Imad HAFIDI** PhD is a professor (since 2009) and the Head of IT and Telecom Department, at the national school of applied sciences Khouribga. He gets accreditation to supervise research in 2013. Before coming to Khouribga, he completed many programs: PhD degree (2005) in Applied Mathematics at the National institute of applied sciences Lyon (INSA), and the MS degree (2008) in Software Engineering at the School of Mines Saint-Etienne. Before that he received the MS degree in numerical analysis (2001) from Lyon I university, and the bachelor degree in Applied Mathematics (1999) from the University of Hassan II Ain Chock. His research focuses on processing heterogeneous data, Text Mining and Big Data.

**Lamiae ALAMI**, is a PhD student working at National School of Applied Sciences Khouribga. She received the Master degree in Business intelligence and statistics from the University of Lyon II, France, in 2010.Prior to beginning the PhD program, Lamiae worked as a Business intelligence consultant in the insurance Industry at Sopra Group. She consulted on a variety of projects for France's largest insurance companies (La Mutuelle Générale, IPECA prévoyance…), involving Data warehousing, Master Data Management (MDM), building repositories, KPI's and Dashboards. Her research interests cover conception and optimization of Data warehouses, Data cleansing & integration algorithms and text Mining.

# Design Methodology for Self-organized Mobile Networks Based

John Petearson Anzola, Sandro Javier Bolaños and Giovanny Mauricio Tarazona Bermúdez

*Universidad Distrital Francisco José de Caldas, Bogotá D.C., Colombia*

***Abstract* — The methodology proposed in this article enables a systematic design of routing algorithms based on schemes of biclustering, which allows you to respond with timely techniques, clustering heuristics proposed by a researcher, and a focused approach to routing in the choice of clusterhead nodes. This process uses heuristics aimed at improving the different costs in communication surface groups called biclusters. This methodology globally enables a variety of techniques and heuristics of clustering that have been addressed in routing algorithms, but we have not explored all possible alternatives and their different assessments. Therefore, the methodology oriented design research of routing algorithms based on biclustering schemes will allow new concepts of evolutionary routing along with the ability to adapt the topological changes that occur in self-organized data networks.**

***Keywords* — Self-Organizing Networks, Routing Methodology, Biclustering Algorithms.**

## I. Introduction

ONE of the everyday questions in self-organized data networks is this: are the groupings needed?. The answer is evident in the increase in overall performance that presents cluster topologies in comparison with non-clustered topologies. When using a routing protocol, mobile nodes are organized into cluster structures that facilitate access and global management of the network. With a cluster structure, the network can answer topological changes caused by the mobility of the nodes [1]–[6]. Below are several advantages in this type of structures:

1. A structure of groups facilitates the reuse of resources in space to increase the capabilities of the system. Non-overlapping, unconnected multi-cluster arrangements inside can be deployed with the same frequency or channel of communications to reduce collisions of data transmission in the network [7]–[9].
2. Structure of groups routing schemes use a set of nodes called clusterheads. These function as gateways that distribute the traffic to the inside of each group and allow interoperability with neighboring groups, so dissemination of data is decentralized [10]–[12].
3. Structure of groups make a network that is smaller and more stable, according to the employed group heuristics [13]–[15].
4. For events of admission of a node to a group, nodes residing in the group that have just entered and the group from nodes, update information routing. In this way, for groups not involved, nodes do not observe these changes, which reduces the burden of traffic generated in the network.

Another technique in a different context that allows for grouping are Microarrays, which represent a new way of measuring levels of gene expression under different biological conditions in multiple data. These data are successfully analyzed by methods of biclustering, which removes a number of genes and conditions that show a similar behavior [16]–[18].

Biclustering techniques are conventional clustering techniques for simultaneous genes and conditions grouping characteristics, as well as by relations of overlap between groups. In simultaneous clustering of genes and conditions, the groups found by a biclustering method are called biclusters and refer to the genes that act similarly under a given set of conditions. This observation of the biological condition in a group of genes behavior characterized relationships between genes to a number of conditions and its decoupling under other conditions. In the overlap feature, you can see genes in more than one bicluster, which is interesting, since in biological observations, a gene can have more than one role and relationship associated with different sets of genes and conditions.

In this article, we propose a routing methodology based on an algorithm of biclustering for self-organized data networks, under an evolutionary approach that allows biclusters to be highly correlated. The evaluation of the methodology proposed by a researcher is a function of the conception of the heuristics of grouping under the conditions of the types of data and services that are to be used, which for the case study intended to stage the Internet of Things (IoT). Throughout the article, there is an isomorphism between the biclustering algorithms employed in the analysis of gene expression; similarly, it can assimilate in the clustering of nodes in mobile networks ad hoc, referred to as self-organized data networks, showing how the proposed methodology can build a routing protocol.

## II. Problems In Self-Organized Data

One of the problems treated in self-organized data networks relates to obtaining location, tracking and metrics deployment of nodes based on the spatial coverage, highlighting the example of fire detection, where you can ask as a particular case:

- With that can quality of service (QoS) nodes in the network monitor a specific area?
- Can the network draw out info from the specific location of the fire and determine the propagation time?
- How should nodes be distributed to monitor the largest possible coverage area?
- Can a structure in groups reply in the shortest time compared with individual collaborative work from all nodes?

Each of the above questions can reveal weaknesses in physical coverage areas and suggest a scheme of movement, deployment and reconfiguration of position, the motion of the nodes can improve the quality of the information provided. For the above example, not only the physical location involved in improving the response time and the quality of information, there are other factors that affect communication between nodes, which may arise directly or indirectly:



DOI: 10.9781/ijimai.2016.377

- How to access the communications channel, if all nodes to transmit at the same time?
- What is the proper path to send the information to minimize data loss?

These questions cover issues treated at the physical layer, link and network, whose model in layers and interaction carried out among them respond to most of the problems encountered in data networks, being a communication protocol which brings the interactions between layers to mitigate these problems.

In terms of data transmission according to the routing, the path of greater power and range of coverage between two end-to-end terminals facilitates communication and efficiency, to minimize power consumption and maximize the throughput. These features of coverage in terms of space and range of data transmission, have multiple problems that have been addressed by grouping schemes [19]–[21].

On the other hand, accessibility in self-organized data networks is limited by interference from simultaneous transmissions to share a unique medium, which affected the performance by the constant struggle of the channel, without adding effects and delays caused by the topological changes related to mobility. These problems were discussed with clustering schemes that enhance the results of the scalability of routes depending on the density of the network, since they minimize the effects of on long-haul routes in contrast to routing without clusters schemes [21], [22].

Another problem in self-organized data networks is due to planning and booking of resources. One must consider the medium access control (MAC) protocols, which are responsible for coordinating access to the active nodes to a wireless environment that is prone to errors, not to mention that the search and discovery of routes with high frequency and coverage presents the hidden terminal problem [23], [24]. Therefore, these actions may be considered problems of planning policies to access the environment and provision of resources. In the link layer, planning is treated by the prioritization of packages and services, which is the case of the mechanism enhanced distributed channel access (EDCA) [25], [26]. In the network layer protocols that are based on clustering, routing schemes allow for addressing problems of planning in large networks in order to achieve better quality of service.

In this section, the problems in self-organized networks of data have been synthesized and classified into four categories: mobility, coverage, planning, and topology control, as shown in Fig. 1. The problems of classification shown in Fig. 1 are common pattern routings [53], which become a transverse solution to the problems presented. At the same time, routing protocols are classified according to the way of discovery and selection of routes in:

- Proactive: In this type of protocols, periodically a server node issues a "Hello" packet to the network to investigate that nodes are born, live, and die in the network, through the construction of a route towards them, with the assumption that at some point the alternative routes will be needed and used. The "Hello" package allows you to update the routing tables either by changing the position or death of a node in the network.
- Reactive: The reactive part of a protocol occurs when a node wants to find a path to a node destination through flood processes; this process is called route discovery. Once the proper path, it remains there until the destination node becomes unavailable, usually by a topological change or loss of the trajectory. The occurrence of a change or loss event obligates the route discovery process to start again.
- Hybrid: hybrid protocols combine the processes carried out by approaches to routing proactive and reactive, simultaneously leading routing for the intragroup and intergroup [27], [28].

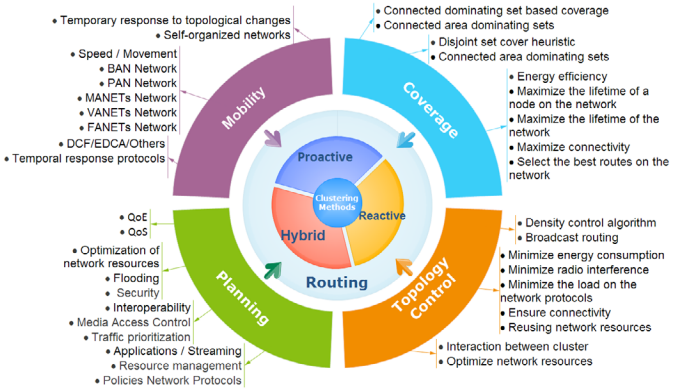


Fig. 1. Classification of problems in networks of data self-organized.

Many are the problems encountered in self-organized data networks. Fig. 1, the periphery, summarizes most of these problems, which were classified as planning, topology control, coverage, and mobility. These problems have in common the shape, which is addressed through an approach of routing and optimization of clustering schemes.

Problems in self-organized data networks have been treated using these models: mobility [29], [30], quality of service [31], [32], power consumption [33]–[35], clustering [9], [10], [19], among others, being that there are few methodologies of routing that can respond to the problems synthesized in Fig. 1, whose routing approach is based on biclustering.

## III. Infrastructure IoT

The proposed infrastructure is framed within the paradigm of the IoT and describes a scenario that contains users and "things" that have internet connectivity through edge devices globally. These edge devices are responsible for interoperability between wireless mobile networks and the internet. Fig. 2, illustrates an end user, that regardless of the last mile connectivity technology have access to the internet, and from there you can access a device or "thing" that is called node source.

One of the trends in this type of network is the convergence of devices with connectivity IEEE802.11x by penetration of the market and range of coverage, without excluding technologies such as Bluetooth or ZigBee [36]. These last two have had no great impact due to lack of IP connectivity. The raised stage of the IoT in this article, sets a device interoperability between heterogeneous networks whose functionality resembles a gateway, which can manage and control devices on the network. This device is called a target node and in the communication of end user with the node source is completely transparent, as shown in Fig. 2.

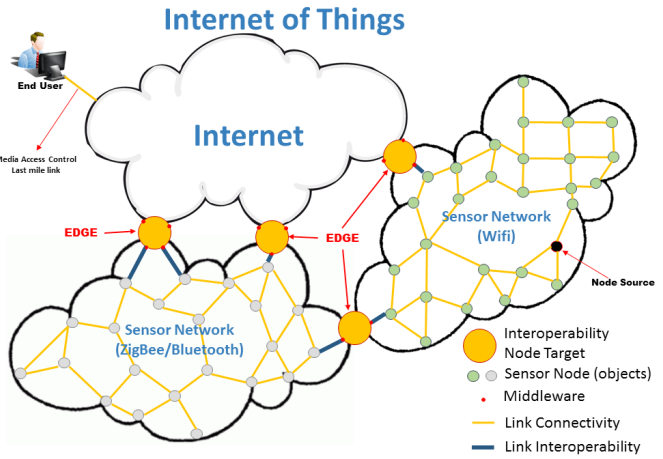


Fig. 2. Proposed scenario for the IoT.

Self-organized data networks within the source nodes are wireless mobile devices that are added to the network, allowing the growth of "things." These devices are added and adapt autonomously after an ad hoc configuration, if they have been conFig.d in infrastructure mode. These devices are also candidates to serve as target nodes by the organization's edge that are present within the network.

The scenario described in Fig. 2, is represented in Fig. 3, through an enterprise architecture that generally refers to the type of work that takes place in an organization, that describes, are not only technological parts of hardware and software, but also users and processes. At this point, the architecture of business models using the technology, users and processes in the full context of an organization and its interaction with the business[37]. The case tried in Fig. 2, the interoperability between wireless networks and the internet of things is described as a model of enterprise architecture in Fig. 3.

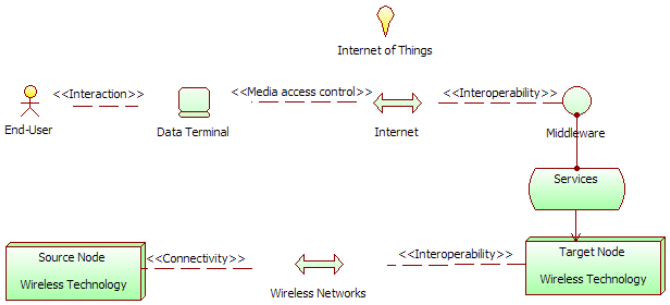


Fig. 3. ArchiMate Infrastructure model.

## IV. Dynamic Infrastructure Model Behavior

In order to understand the dynamic behavior of the model Fig. 3, describes the internal processes of communication protocols. Communication from the end user to the target node is an IP communication. Communication from the target to the source node consists of processes of flooding, clustering heuristics, data transfer, exceptions, maintenance and completion of the transfer of data, which are represented from Fig. 5 to Fig. 9, using sequence diagrams in unified modeling language (UML). In Fig. 4, each of the interactions and processes is shown in the time, detailing the flow of different packages that are carried in a self-organized data network or ad hoc mobile network, with clarifications to the level of messages from existing objects.

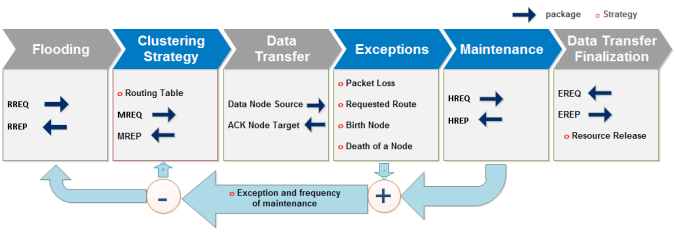


Fig. 4. General processes in a mobile wireless network.

Model Fig. 3, is based on the premise that "the end-user has internet connectivity". Once connectivity is guaranteed, we proceed to implement the general application design model client/server, following the establishment, data transfer, and completion of the communication processes. This model is known as a three-way handshake, creating a virtual logical circuit from end to end between the end user and the target node. On the model of Fig. 3, the server node is the target that centralizes the following services represented by sequence diagrams:

**Flood process**: Consists of two packages, the package Request Route (RREQ), which is intended to build a path forward from the target node to the source node. Once the RREQ packet arrives at the source node, this returns a Route Reply (RREP) response packet to the node target, building a route back. Once the RREP packet arrives at the target node, it generates an array of routing with genes that are the data collected in the course of back and forth, becoming an information input into the process of biclustering.

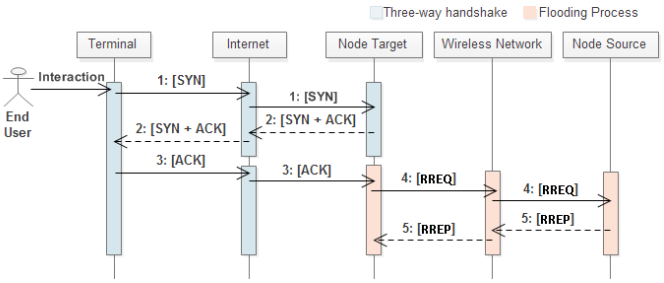


Fig. 5. Flood process.

**Heuristic grouping process**: Once the target node has received the package RREP containing genes or data collected, in the process of flooding an array of routing is built in conjunction with the conditions of the service that is required in the network. These conditions determine the end user making the request for service to the target nodes, which are distributed at the edges of the network and evaluate the proximity of the node source consulted by the end user.

The node target with the service conditions and the genes collected in the process of flooding, builds a matrix which subsequently applies a biclustering algorithm for biclusters, which then identifies clusterhead nodes by the feature overlap between groups. The nodes that make up each bicluster are associated and related to the genes and conditions of the network, whose distribution is coordinated with the clusterhead in routing, supported in the heuristics that respond to the solution of one or several of the problems recorded in Fig. 1.

Once the heuristics of grouping is complete, proceed to flood the network with package Map REQuest (MREQ). This flood is directed to locate nodes clusterhead and establish the routes and nodes inside each bicluster. Thus, the nodes that make up the bicluster sent a package Map Reply (MREP) to the node clusterhead and this sends a MREP packet to the node target, maintaining this way the communication. Once the target node receives the confirmation of all leading group nodes, you can start the process of data transfer.

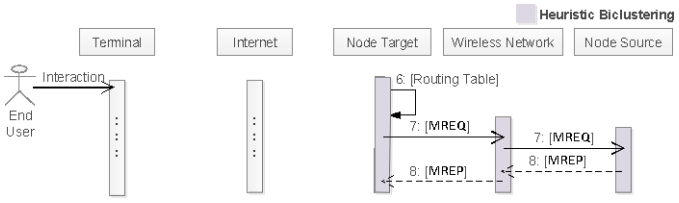


Fig. 6. Process of clustering heuristics.

As heuristics, in the implementation of the biclustering algorithm you can select a two nodes clusterhead, in order to provide redundancy in each bicluster, given the case that if one of them fails, you have routing information backed up on a second node that would become clusterhead. This second node subsequently must run within the bicluster a clusterhead of backup node selection process.

**Data transfer process**: This process is responsible for starting the bi-directional communication between the target and source nodes. Data transfer is initiated by the target node since it chooses the path to the node source through the issuance of a packet Data REQuest (DREQ). Once the service request is serviced by the source node to

receive the package DREQ, it emits a packet Data Reply (DREP) with the response of the service requested by the target node. The target through a process of interoperability node sends the end user terminal DREP package with the data required by the user. This process can occur several exceptions, which is the loss of packets, routes, and events for the birth and death of a node in the network.

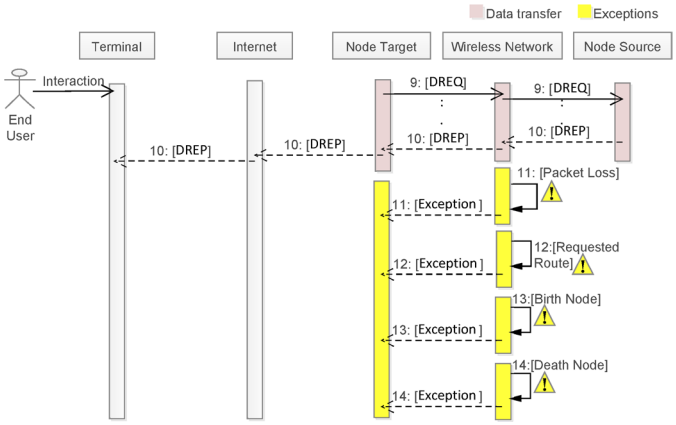


Fig. 7. Transfer of data.

**Maintenance process:** This process is conducted by clusterhead and target nodes, consists in maintenance of routes and the collection of information of genes within each bicluster, programming a local and periodic flooding of packets Hello REQuest (HREQ) shipments. This package allows you to get the information of genes within the bicluster to monitor routes and active nodes, as well as events of admission, birth, and death of a node. In the event of a node to the bicluster entry, the node receives HREQ package and generates a package Hello Reply (HREP) with genes, informed its current state within the bicluster to the target node. This process makes it possible to act like a lasso feedback between nodes clusterhead, source, and target, allowing the target node to execute the algorithm of biclustering generated a lapse feedback, which subsequently allows the node target adjustments or decisions.

This maintenance process allows foreseeing events within the bicluster feedback with HREQ and HREP packages. This feedback allows you to monitor states of links, the different routes and different metrics that can extract the package HREQ. When presenting an event that leads to the network on the brink of chaos, part of the overall structure is lost, either by overflow of data, a drop of energy in several nodes, abrupt movements of nodes or any other event that generates chaos, in any case, the network should be able to adapt to the new changes or gradual transformations seeking a balance and a reorganization. This maintenance process allows the network to evolve.

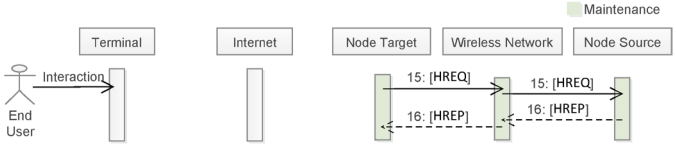


Fig. 8. Process of maintenance.

**Finalization process data:** In this process the source node sends a packet REQuest End (EREQ) to the target node and the target node responds with a package End Reply (EREP) to the source node by the main routes and alternative routes active, in order to free up resources if these were used. At the same time, the target node sends a DREP packet that tells the end user terminal that the data transfer has been completed.

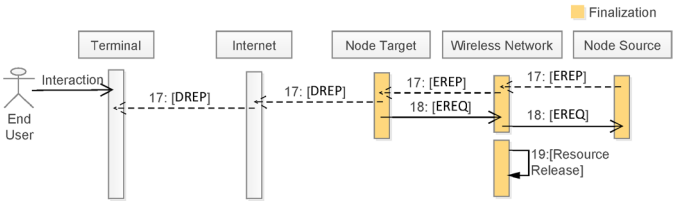


Fig. 9. Process of maintenance.

## V. Biclustering Algorithm

Biclustering is an unsupervised data analysis technique that has been applied in studies of gene expression. This technique is a natural evolution of the clustering [38] and its term was introduced by Mirkin [39], later strengthened by Cheng and Chu-Hsing [40]. This technique comprises sets of genes with a similar genetic profile in all the experimental conditions tested.

The analytical capacity of the biclustering analysis of gene expression is greater than the results obtained by techniques of traditional clustering, clustering simultaneous genes and conditions, and the overlap that may occur.

The groups found by simultaneous clustering of genes and conditions are referred to genes that act in a similar way under a single set of conditions, not necessarily all, which fits with the observed biological behavior. Under these conditions gene groups can work together to attend a particular circumstance, but be uncoupled under others.

Overlap allows handling genes into more than one bicluster simultaneously, since the biological reality of one or several genes may have more than one associated function and work with different sets of genes under different conditions.

Similar to traditional clustering techniques, the possibilities for the calculation of similarity within a bicluster have been identified in four main structures within the sub-arrays groups, as shown in Fig. 10.

The package of the levels of expression of genes with a condition or sample form a vector called the profile of that condition. Gene expression profiles are powerful sources of information that are organized in a matrix whose rows correspond to genes and columns to the conditions. One or more objectives of common analysis are a group of conditions and genes are subsets that convey a meaning of biological [41].

The resulting subsets called bicluster can be computationally interpreted as clusters allowing you to group a set of genes, which are linked to certain conditions of similarity measures simultaneously intragroup and intergroup, whose overlapping provides information of relations between groups, as with traditional clustering techniques they are not able to identify.

**constant values overall**

| | | | |
|---|---|---|---|
| 1.1 | 1.1 | 1.1 | 1.1 |
| 1.1 | 1.1 | 1.1 | 1.1 |
| 1.1 | 1.1 | 1.1 | 1.1 |
| 1.1 | 1.1 | 1.1 | 1.1 |

**constant values rows**

| | | | |
|---|---|---|---|
| 1.1 | 1.1 | 1.1 | 1.1 |
| 1.9 | 1.9 | 1.9 | 1.9 |
| 3.1 | 3.1 | 3.1 | 3.1 |
| 3.9 | 3.9 | 3.9 | 3.9 |

**constant values columns**

| | | | |
|---|---|---|---|
| 1.1 | 2.1 | 3.5 | 4.1 |
| 1.1 | 2.1 | 3.5 | 4.1 |
| 1.1 | 2.1 | 3.5 | 4.1 |
| 1.1 | 2.1 | 3.5 | 4.1 |

**coherent values additive**

| | | | |
|---|---|---|---|
| 1.1 | 2.1 | 5.1 | 0.0 |
| 2.1 | 3.2 | 6.2 | 1.1 |
| 4.1 | 5.3 | 8.3 | 3.2 |
| 5.1 | 6.2 | 9.2 | 4.1 |

**coherent values multiplicative**

| | | | |
|---|---|---|---|
| 1.0 | 2.0 | 0.5 | 0.1 |
| 2.0 | 4.0 | 1.0 | 0.2 |
| 4.0 | 8.0 | 4.0 | 0.4 |
| 3.0 | 6.0 | 1.5 | 0.3 |

**coherent evolution overall**

| | | | |
|---|---|---|---|
| E.1 | E.1 | E.1 | E.1 |
| E.1 | E.1 | E.1 | E.1 |
| E.1 | E.1 | E.1 | E.1 |
| E.1 | E.1 | E.1 | E.1 |

**coherent evolution rows**

| | | | |
|---|---|---|---|
| E.1 | E.1 | E.1 | E.1 |
| E.2 | E.2 | E.2 | E.2 |
| E.3 | E.3 | E.3 | E.3 |
| E.4 | E.4 | E.4 | E.4 |

**coherent evolution columns**

| | | | |
|---|---|---|---|
| E.1 | E.2 | E.3 | E.4 |
| E.1 | E.2 | E.3 | E.4 |
| E.1 | E.2 | E.3 | E.4 |
| E.1 | E.2 | E.3 | E.4 |

Fig. 10. Different bicluster types.

Then is an isomorphism of biclustering algorithms implemented in problems of gene expression with the problems encountered in self-organized data networks, linking them in the following form:

- Genes are isomorphic to the metrics of input, such as:
  - Number of hops
  - Received Signal Strength Indicator (RSSI)
  - Round-Trip delay Time (RTT)
  - Packet delivery ratio (PDR)
  - Bit Error Ratio (BER)
  - Energy consumption
  - Coordinates GPS

Note: At this point, the researcher can propose metrics or heuristics of input.

- Conditions are related to restrictions of service or network, such as:
  - Latency
  - Throughput
  - Peak Signal-to-Noise Ratio (PSNR)
  - Shortest route
  - Quality of Service (QoS)
  - Quality of Experience (QoE)

Note: At this point, the researcher can propose restrictions of heuristics that will require service.

Genes are obtained by flooding and maintenance processes, the target node collects the RREP and HREP packages to feed the matrix of routing, which subsequently applies a routing algorithm for biclustering restrictions that are needed to manage the network.

The biclustering algorithm compiles a set of genes that form a matrix of attributes of each node, when applying the algorithm proposed by the investigator, to get one or several sets of nodes are called biclusters, which are commonly disjointed edge or border nodes called nodes clusterhead, whose function is the interoperability between clusters. To evolve the biclustering algorithm are overlapping biclusters presenting similar and shared attributes between the biclusters obtained previously. Overlap found in these biclusters feature allows them to respond to given conditions or restrictions routing heuristics that demand services and network traffic.

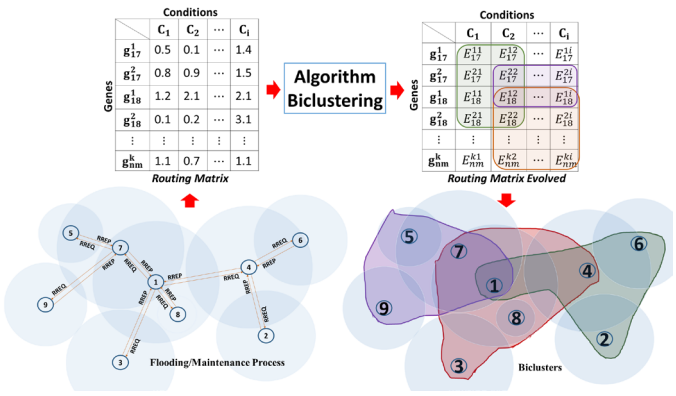


Fig. 11. General scheme of routing by biclustering.

## VI. Result: Proposed Methodology

General conditions of the IoT exist within contextualization border elements that enable the interoperability of heterogeneous networks to the internet. These elements and functionality are the gateway that acts as a bridge between networks. In the context discussed in this article referred to the mobile ad hoc network (MANET), wireless sensor network (WSN) and their variations, as self-organized data networks. The main feature of self-organized networks is the adaptability due to the contemplation of one or more nodes that may appear or disappear at any time and in any place with a degree of uncertainty in their behavior.

From the point of view of efficiency, a clustering scheme allows you to manage the traffic on the network, being this manageable, scalable, and robust scheme generated topological changes. The proposed model is taken for granted as the end user and the target node that have connectivity to the internet. The target node is conceived as a device for the provision of services that addresses features in all layers of the OSI model, from the physical layer to the application layer interoperability services focusing in the routing layer [42], [43]. The model proposed in Fig. 11, emphasis is placed on techniques, heuristics, and approaches that a researcher can qualify on the algorithms of routing as a central process in communication, ranging from an initial process of flood routing planning with metrics minimization, maximization, or balance problems to solve.

### A. Approaches the methodology

Research in self-organizing networks in recent years has focused on evolutionary algorithms and cooperation, which optimize problems synthesized in Fig. 1. In this respect, the networks of MANETs, vehicular ad hoc networks (VANETs), flying ad hoc networks (FANETs), WSN, and hybrid networks require a keen sense and knowledge in the design of evolutionary algorithms in order to contribute to the common problems affecting QoS through self-organized networks optimization parameters [44]–[49].

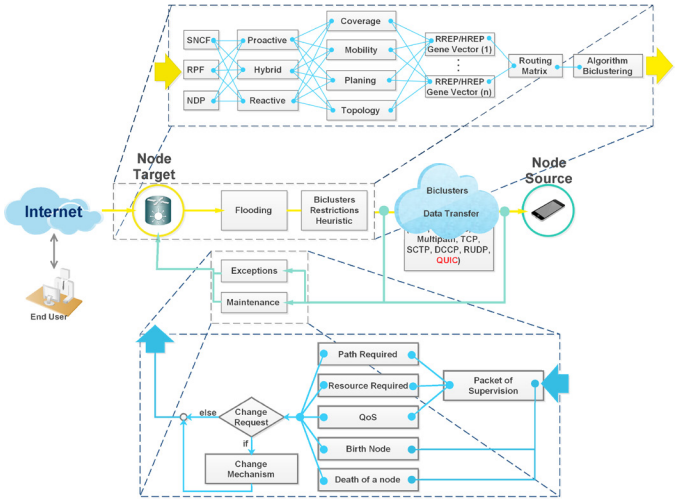


Fig. 12. Design methodology of self-organized networks.

The methodology proposed in Fig. 12 responds to the problems posed by the complexity of self-organized data networks, ranging from the search for the best route to the optimization of multiple targets, which can work under approaches to evolutionary algorithms specializing in clustering [50], as those recorded in Table 1 and/or under the classical approach of evolutionary techniques [51] recorded in Table 2.

TABLE I
EVOLUTIONARY ALGORITHMS FOR HARD PARTITIONAL CLUSTERING

| | Fixed k | Variable k |
|---|---|---|
| Label-Based | Krovi Murthy/<br>Chowdhury Krishna/<br>Murty | Cole<br>Cowgill<br>Hruschka<br>Hruschka<br>Alves |
| Centroid-Based | Scheunders<br>Fränti<br>Merz/Zell<br>Kivijärvi<br>Bandyopadhyay/Maulik | Bandyopadhyay/Maulik |
| Medoid-Based | Kuncheva/Bezdek<br>Lucasius<br>Estivill-Castro/Murray<br>Sheng /Liu | |
| Others | Bezdek | Casillas<br>Tseng/Yang Handl/<br>Knowles<br>Pan and Cheng |

TABLE II
TECHNIQUES OF EVOLUTIONARY ALGORITHMS

| | Evolutionary Programming | Evolutionary Strategy |
|---|---|---|
| Applied to | Traditional EP: machine learning tasks by FSM contemporary EP: numerical optimization | Numerical optimization |
| Representation | Real-valued vectors | Real-valued vectors |
| Representation | None | Discrete or Intermediary |
| Mutation | Gaussian perturbation (Adaptive) | Gaussian perturbation (Adaptive) |
| Parent selection | Uniform Random | Deterministic |
| Survivor selection | Probabilistic (u+u) | (u*l) or (u-l) |
| Size of chomosome | Fixed length | Fixed length |
| Evolutionary pressure | Extinctive | Extinctive |
| Attributed feature | Very open framework: any representations and mutations operators is fine | Good optimizer for real valued optimization & relatively much theory & fast |

## *B. Description of the methodology*

The characterization of the IoT part of principle than anything else anywhere has connectivity to the internet, based on the above, within the methodology proposed in Fig. 12. The end-user has connectivity to the target node. Self-organization of a network is given by "things", or wireless mobile nodes, that adaptively can connect to the internet as a principle of functionality in self-organized data networks.

Target nodes are nodes that are organized to the edge or border of the internet and allow interoperability between self-organized networks and the internet. The establishment of communication between the source node and the target node is given by a series of algorithms that the designer of networks should consider until a communication point to point is established. This communication is not done by human beings, but is a communication made by two machines; therefore, communication protocols can be considered an M2M (Machine to Machine) communication.

Consideration 1, algorithm of flood. The initial section of the methodology is composed of a series of floods that are estimated as simple routing algorithms. The methodology consists of two types of available flood: uncontrolled flood and controlled flood.

In the uncontrolled floods, all nodes send packets to their neighbors indefinitely and with more than two neighbors, create a storm of broadcasting.

In controlled floods, there are reliability rules, such is the case of sequence number controlled flooding (SNCF) and reverse path flooding (RPF). In SNCF, nodes are attached to an address and number sequence in a package and are to be transmitted. These are stored in the buffer for each node by attaching your address and your sequence number, so that when you receive a package with the same address and number of the origin node stream, this is rejected. On the other hand, in RPF the nodes send the package forward, if the packet is received by a node this is sent back to the sender node and emitted a series of package forward, if this is received, a package to return to the node which sent him and this in turn emits the same package to the node that sent the first package.

Neighbor discovery protocol (NDP) used in IPv6 is similar to address resolution protocol (ARP) used in IPv4. Both protocols allow a node to determine the direction of link layer (MAC address) of a node which is just entering the network; the issuance of this broadcast package allows you to discover the presence of other nodes on the same channel, determine their addresses MAC and the maintenance of the information of the active nodes on the network connectivity. The main objective of flooding is to collect the largest amount of information; collected information metrics become genes and an increase in the number of genes is likely to become a more selective and adaptive bicluster.

Consideration 2, type of routing. The design of self-organized networks requires a perspective of routing that can be proactive, reactive or hybrid. A proactive routing perspective is characterized by search paths regularly with the assumption that these will be useful in the future, while the reactive perspective only seeks a route when it is necessary, on the other hand, the researcher can give a tint hybrid combined the two perspectives.

Consideration 3, selection problems in self-organized networks. The next part of the design required to select one or more of the problems seen in Fig. 1, which are classified in coverage, mobility and topology planning. Once you choose the problem, it is associated to a set of genes; the conditions requiring a biclustering algorithm that controls action is estimated at routing and why controlled release means you can manage the topology.

Consideration 4, construction of the routing matrix. The construction of the routing matrix is based on the conditions of the network and type of service. At this point, you select the heuristics that allow the creation of biclusters to optimize the routes depending on the problems addressed in the consideration 3. The selected genes become monitoring metrics that monitor the state of resources of the biclusters; the conditions become restrictions on the parameters of quality of service. This consideration allows conceiving with an overview of the design of the routing algorithm.

Consideration 5, type of transport. The type of transport is associated with the service that you want to get from the source Usually within the networks node IP are two types guidance, protocols such as transmission control protocol (TCP) connection-oriented and not as user datagram protocol (UDP) connection-oriented. This methodology aims to experiment on the quick UDP internet connections (QUIC) protocol that was conceived by Google in 2012 and implemented in the

year 2013 [52]. QUIC supports a set of UDP connections multiplexed which reduces latency and estimate the bandwidth on a link. QUIC and its implementation in self-organized mobile networks has been a low received by researchers, but with a proper conceptual appropriation can generate a new transmission control protocol in wireless networks.

Consideration 6, feedback. In the feedback loop there is a module of packet monitoring that assesses flood packages that monitor the state of the network, with a frequency of monitoring defined by the researcher. Request a route, reservation of resources, evaluation of QoS, birth, life, and death of a node parameter is identified within this module. Feedback is only made by clusterhead nodes and target nodes to avoid the overload of information on the net.

## VII. Conclusions

An approach using hybrid allows you to seize the advantages of proactive approach intragroup, allowing nodes clusterhead to obtain genetic information in some few jumps. On the other hand, maintenance of the bicluster nodes decreases overload of information across the network, to monitor the status of the routes, failure in links, processes of birth, events in life such as admission or exclusion of a node to a group or the death of the same are events that recharged clusterhead nodes.

The focus hybrid to appropriate approach reagent intergroup enables the target nodes limit the total number of nodes clusterhead since the global routing information is maintained between nodes target and clusterhead, reducing the size of the matrices of routing between nodes of the bicluster. Because of the use of hybrid approaches to routing, weaknesses in latency for routes in nodes clusterhead restoration process are introduced in the methodology and win robustness in adaptability and scalability processes.

Regardless of the problems in data networks, self-organizing, clustering structure always improves the overall performance in the network from structures that are not composed of clustering, therefore the proposed routing methodology brings the advantages of using a biclustering algorithm compared to traditional methods, given by clustering techniques simultaneously gene presenting relations under certain network conditions, similarity measures operate intragroup and intergroup, finding overlap that provide information of relationships between groups that fail to identify with traditional clustering techniques.

An advantage of the biclustering algorithms is related to the consistent evolution, a product of a similar behavior in forming operations of bicluster, which through the feedback process treated in consideration 6 of the methodology, algorithm based information from genes and conditions can adapt to the changes that are occurring.

## References


[1] L. E. Quispe and L. M. Galan, "Behavior of Ad Hoc routing protocols, analyzed for emergency and rescue scenarios, on a real urban area," Expert Syst. Appl., vol. 41, no. 5, pp. 2565–2573, 2014.

[2] H. Cheng, S. Yang, and J. Cao, "Dynamic genetic algorithms for the dynamic load balanced clustering problem in mobile ad hoc networks," Expert Syst. Appl., vol. 40, no. 4, pp. 1381–1392, 2013.

[3] D. Gutiérrez-Reina, S. L. T. Marín, P. Johnson, and F. Barrero, "An evolutionary computation approach for designing mobile ad hoc networks," Expert Syst. Appl., vol. 39, no. 8, pp. 6838–6845, 2012.

[4] N. Nezamoddin and S. S. Lam, "Reliability and topology based network design using pattern mining guided genetic algorithm," Expert Syst. Appl., vol. 42, no. 21, pp. 7483–7492, 2015.

[5] H. Wang, H. Chen, and L. Song, "Improved AOW clustering algorithms for wireless self-organized network and performance analysis," in Cross Strait Quad-Regional Radio Science and Wireless Technology Conference (CSQRWC), 2012, 2012, pp. 142–146.

[6] Q. Zheng, Z. Liu, L. Xue, Y. Tan, D. Chen, and X. Guan, "An Energy Efficient Clustering Scheme with Self-Organized ID Assignment for Wireless Sensor Networks," in Parallel and Distributed Systems (ICPADS), 2010 IEEE 16th International Conference on, 2010, pp. 635–639.

[7] M. Krunz, M. Z. Siam, and D. N. Nguyen, "Clustering and power management for virtual {MIMO} communications in wireless sensor networks," Ad Hoc Networks, vol. 11, no. 5, pp. 1571–1587, 2013.

[8] J. P. O. Lopez and J. E. O. Trivino, "Stochastic model for the characterization of a cluster and its resources in an ad-hoc network," in Communications and Computing (COLCOM), 2014 IEEE Colombian Conference on, 2014, pp. 1–5.

[9] F. D. Malliaros and M. Vazirgiannis, "Clustering and community detection in directed networks: A survey," Phys. Rep., vol. 533, no. 4, pp. 95–142, 2013.

[10] M. M. Afsar and M.-H. Tayarani-N, "Clustering in sensor networks: A literature survey," J. Netw. Comput. Appl., vol. 46, pp. 198–226, 2014.

[11] M. R. Brust, A. Andronache, S. Rothkugel, and Z. Benenson, "Topology-based Clusterhead Candidate Selection in Wireless Ad-hoc and Sensor Networks," in Communication Systems Software and Middleware, 2007. COMSWARE 2007. 2nd International Conference on, 2007, pp. 1–8.

[12] J. A. Torkestani and M. R. Meybodi, "Clustering the wireless Ad Hoc networks: A distributed learning automata approach," J. Parallel Distrib. Comput., vol. 70, no. 4, pp. 394–405, 2010.

[13] L. Aslanyan, H. Aslanyan, and H. Khosravi, "Optimal node scheduling for integrated connected-coverage in wireless sensor networks," in Computer Science and Information Technologies (CSIT), 2013, 2013, pp. 1–13.

[14] A. H. Kashan, A. A. Akbari, and B. Ostadi, "Grouping evolution strategies: An effective approach for grouping problems," Appl. Math. Model., vol. 39, no. 9, pp. 2703–2720, 2015.

[15] M. Striki, A. McAuley, and R. Morera, "Modeling topology dissemination for routing in future force networks," in Military Communications Conference, 2008. MILCOM 2008. IEEE, 2008, pp. 1–7.

[16] B. Pontes, R. Giráldez, and J. S. Aguilar-Ruiz, "Biclustering on expression data: A review," J. Biomed. Inform., vol. 57, pp. 163–180, 2015.

[17] D. Vu and M. Aitkin, "Variational algorithms for biclustering models," Comput. Stat. Data Anal., vol. 89, pp. 12–24, 2015.

[18] D. Yan and J. Wang, "Biclustering of gene expression data based on related genes and conditions extraction," Pattern Recognit., vol. 46, no. 4, pp. 1170–1182, 2013.

[19] E. Astier, A. Hafid, and A. Benslimane, "Energy and Mobility Aware Clustering Technique for Multicast Routing Protocols in Wireless Ad Hoc Networks," in Wireless Communications and Networking Conference, 2009. WCNC 2009. IEEE, 2009, pp. 1–6.

[20] F. Torrent-Fontbona, V. Muñoz, and B. López, "Solving large immobile location–allocation by affinity propagation and simulated annealing. Application to select which sporting event to watch," Expert Syst. Appl., vol. 40, no. 11, pp. 4593–4599, 2013.

[21] R. Torres, L. Mengual, O. Marban, S. Eibe, E. Menasalvas, and B. Maza, "A management Ad Hoc networks model for rescue and emergency scenarios," Expert Syst. Appl., vol. 39, no. 10, pp. 9554–9563, 2012.

[22] C. Gui and P. Mohapatra, "Hierarchical multicast techniques and scalability in mobile Ad Hoc networks," Ad Hoc Networks, vol. 4, no. 5, pp. 586–606, 2006.

[23] D. Rodenas-Herraiz, F. Garcia-Sanchez, A.-J. Garcia-Sanchez, and J. Garcia-Haro, "On the influence of the hidden and exposed terminal problems on asynchronous {IEEE} 802.15.5 networks," Comput. Stand. Interfaces, vol. 42, pp. 53–70, 2015.

[24] K. Kosek-Szott, "A survey of {MAC} layer solutions to the hidden node problem in ad-hoc networks," Ad Hoc Networks, vol. 10, no. 3, pp. 635–660, 2012.

[25] J. Anzola, A. Jiménez, and J. Cuellar, "Evaluation of QoS in the Transmission of Video H. 264/SVC for Ad Hoc Networks of Two Jumps," Int. J. Comput. Appl., vol. 108, no. 19, pp. 1–8, 2014.

[26] J. P. Anzola and A. C. Jimenez, "Evaluation of QoS and QoE for H.264/SVC Video Transmission with DCF and EDCA," Int. J. Appl. Eng. Res., vol. 9, no. 22, pp. 16109–16124, 2014.

[27] W.-L. Shen, C.-S. Chen, K. C.-J. Lin, and K. A. Hua, "Autonomous Mobile Mesh Networks," Mob. Comput. IEEE Trans., vol. 13, no. 2, pp. 364–376, Feb. 2014.

[28] M. Xie, S. Han, B. Tian, and S. Parvin, "Anomaly detection in wireless sensor networks: A survey," J. Netw. Comput. Appl., vol. 34, no. 4, pp. 1302–1325, 2011.

[29] J. Lin, H. Jung, Y. J. Chang, J. W. Jung, and M. A. Weitnauer, "On cooperative transmission range extension in multi-hop wireless ad-hoc and sensor networks: A review," Ad Hoc Networks, vol. 29, pp. 117–134, 2015.

[30] N. Padmavathy and S. K. Chaturvedi, "Reliability Evaluation of Mobile Ad Hoc Network: With and without Mobility Considerations," Procedia Comput. Sci., vol. 46, pp. 1126–1139, 2015.

[31] M. C. Domingo and D. Remondo, "QoS support between ad hoc networks and fixed {IP} networks," Comput. Commun., vol. 31, no. 11, pp. 2646–2655, 2008.

[32] A. Malik, J. Qadir, B. Ahmad, K.-L. A. Yau, and U. Ullah, "QoS in {IEEE} 802.11-based wireless networks: A contemporary review," J. Netw. Comput. Appl., vol. 55, pp. 24–46, 2015.

[33] S. Ayad, O. Kazar, and N. Benharkat, "Evaluating the Energy Consumption of Web Services Protocols in Ad Hoc Networks," {AASRI} Procedia, vol. 7, pp. 8–13, 2014.

[34] I. A. Modupe, O. O. Olugbara, and A. Modupe, "Minimizing Energy Consumption in Wireless Ad hoc Networks with Meta heuristics," Procedia Comput. Sci., vol. 19, pp. 106–115, 2013.

[35] M. Omar, S. Hedjaz, S. Rebouh, K. Aouchar, B. Abbache, and A. Tari, "On-demand source routing with reduced packets protocol in mobile ad-hoc networks," {AEU} - Int. J. Electron. Commun., vol. 69, no. 10, pp. 1429–1436, 2015.

[36] J. P. Espada, V. G. Díaz, R. G. Crespo, O. S. Martínez, B. C. P. G-Bustelo, and J. M. C. Lovelle, "Using extended web technologies to develop Bluetooth multi-platform mobile applications for interact with smart things," Inf. Fusion, vol. 21, pp. 30–41, 2015.

[37] S. J. Javier, R. Gonzalez Crespo, and V. H. Medina, "Software Processes and Methodologies Modeling Language SPMML, A Holistic Solution for Software Engineering," Lat. Am. Trans. IEEE (Revista IEEE Am. Lat., vol. 12, no. 4, pp. 818–824, 2014.

[38] J. A. Hartigan, "Direct clustering of a data matrix," J. Am. Stat. Assoc., vol. 67, no. 337, pp. 123–129, 1972.

[39] H. Bacelar-Nicolau, "Mathematical Classification and Clustering. Boris Mirkin, Kluwer Academic Publishers, 1996. No. of Pages: xv+ 428. Price:{\pounds} 140. ISBN 0-7923-4159-7," Stat. Med., vol. 20, no. 6, pp. 987–988, 2001.

[40] F.-C. Jiang, C.-H. Lin, and H.-W. Wu, "Lifetime elongation of ad hoc networks under flooding attack using power-saving technique," Ad Hoc Networks, vol. 21, pp. 84–96, 2014.

[41] S. Papadimitriou, S. Mavroudi, and S. D. Likothanassis, "Mutual information clustering for efficient mining of fuzzy association rules with application to gene expression data analysis," Int. J. Artif. Intell. Tools, vol. 15, no. 02, pp. 227–250, 2006.

[42] E. T. Franco, J. D. García, O. S. Martínez, L. J. Aguilar, and R. G. Crespo, "A Quantitative Justification to Dynamic Partial Replication of Web Contents through an Agent Architecture," IJIMAI, vol. 3, no. 3, pp. 82–88, 2015.

[43] S. Ríos-Aguilar and F.-J. Lloréns-Montes, "A mobile business information system for the control of local and remote workforce through reactive and behavior-based monitoring," Expert Syst. Appl., vol. 42, no. 7, pp. 3462–3469, 2015.

[44] N. Battat, H. Seba, and H. Kheddouci, "Monitoring in mobile ad hoc networks: A survey," Comput. Networks, vol. 69, no. May, pp. 82–100, Aug. 2014.

[45] İ. Bekmezci, O. K. Sahingoz, and Ş. Temel, "Flying Ad-Hoc Networks (FANETs): A survey," Ad Hoc Networks, vol. 11, no. 3, pp. 1254–1270, 2013.

[46] V. Gulati, R. Tiwari, and A. Dumka, "Evaluation of routing protocols in congested VANET environment," in Computing for Sustainable Global Development (INDIACom), 2015 2nd International Conference on, 2015, pp. 1235–1238.

[47] R. Di Pietro, S. Guarino, N. V. Verde, and J. Domingo-Ferrer, "Security in wireless ad-hoc networks – A survey," Comput. Commun., vol. 51, no. June, pp. 1–20, Sep. 2014.

[48] D. G. Reina, S. L. Toral, P. Johnson, and F. Barrero, "A survey on probabilistic broadcast schemes for wireless ad hoc networks," Ad Hoc Networks, vol. 25, Part A, pp. 263–292, 2015.

[49] J. Santa, P. J. Fernandez, F. Pereniguez, F. Bernal, and A. F. Skarmeta, "A vehicular network mobility framework: Architecture, deployment and evaluation," in Computer Communications Workshops (INFOCOM WKSHPS), 2015 IEEE Conference on, 2015, pp. 127–132.

[50] E. R. Hruschka, R. J. G. B. Campello, a. a. Freitas, and a. C. P. L. F. de Carvalho, "A Survey of Evolutionary Algorithms for Clustering," IEEE Trans. Syst. Man, Cybern. Part C (Applications Rev., vol. 39, no. 2, pp. 133–155, Mar. 2009.

[51] H. A. Sally and M. Rafie, "A survey of Game Theory using Evolutionary Algorithms," in Information Technology (ITSim), 2010 International Symposium in, 2010, vol. 3, pp. 1319–1325.

[52] S. R. Das, "Evaluation of QUIC on web page performance," Massachusetts Institute of Technology, 2014.

[53] S. J. Bolaños, "Patterns of software development process", International Jorunal of Interactive Multimedia and Artificial Intelligence, 2014, vol. 1, pp. 33-40

**John Petearson Anzola** Teaching program of Electronic Engineering University Fundación Universitaria Los Libertadores, MSc in Information Sciences and Communications University Distrital Francisco José de Caldas, is currently studying the first year of PhD Engineering of the University Distrital Francisco José de Caldas, Bogotá D.C., Colombia. Integral is Research groups GICOECOL and GUIAS.

**Sandro Javier Bolaños** Doctor of the Pontifical University of Salamanca in Madrid, Spain and PhD Prize awarded by the university; entitled as a systems engineer and magister in teleinformática of the University Francisco Jose de Caldas in Bogota Colombia; a member of the international research group GICOGE researcher in Software Engineering, Software Engineering faculty at undergraduate, postgraduate and expertise in the area of Software Engineering; curricular projects director of undergraduate and graduate, now runs the graduate in Software Engineering and Computer Project at the University Francisco José de Caldas.

**Giovanny M. Tarazona Bermudez**: is a Ph.D. ABD in systems and computer services for internet at the Oviedo University, Asturias, Spain (2012). He acquired a Diploma of advanced studies November 2009 of the Pontifical University of Salamanca. He is an Industrial engineer and Professor of the Francisco José de Caldas District University. Director Research Group on Electronic Commerce Colombian GICOECOL. His research interests include eBusiness, eCommerce, DSL and MDA.

# Uncertainty Model For Quantitative Precipitation Estimation Using Weather Radars

A. Ernesto Gómez Vargas, B. Nelson Obregón Neira, C. Lindsay Álvarez Pomar

*Universidad Distrital Francisco José de Caldas, Bogotá D.C., Colombia*

***Abstract* — This paper introduces an uncertainty model for the quantitatively estimate precipitation using weather radars. The model considers various key aspects associated to radar calibration, attenuation, and the tradeoff between accuracy and radar coverage. An S-band-radar case study is presented to illustrate particular fractional-uncertainty calculations obtained to adjust various typical radar-calibration elements such as antenna, transmitter, receiver, and some other general elements included in the radar equation. This paper is based in "Guide to the expression of Uncertainty in measurement" [1] and the results show that the fractional uncertainty calculated by the model was 40 % for the reflectivity and 30% for the precipitation using the Marshall Palmer Z-R relationship.**

***Keywords* — Quantitative Precipitation Estimation, Radar Measurements, Uncertainty, Weather Radar.**

## I. Introduction

Most methods to quantitatively estimate precipitation often fail to provide information about the type of uncertainty associated to the corresponding measurement technique; therefore it seems compelling to quantify the technique-associated uncertainty together with the actual estimation results [2].

The general purpose of measuring is to determine the actual value of a particular magnitude (i.e. the variable), which in our case corresponds to precipitation. According to [3], measurement uncertainty is a way to express the idea whereby for a magnitude and its given measurement there is no unique value but an infinite number of values scattered in the vicinity of the suggested result; additionally, these values are consistent with all observations, data and knowledge gathered from the physical world, and so can be attributed to the measured magnitudes with different degrees of reliability.

Just like other measurement instruments, weather radars rely on indirect measurements of actual precipitation; that is, radar receivers use antennas to perceive information associated to hydrometeors-echo power. This information is subsequently transformed using the radar equation (for radar reflectivity) and then, a whole data interpretation process begins in order to finally yield a quantitative precipitation estimation by means of a given algorithm (or method). From this point onwards, there are a considerable number of aspects that affect radar measurements and so influence data; therefore such aspects have a great impact on the final result (i.e. precipitation levels). These aspects include the radar equation itself, calibration issues associated to the observation system (antenna, receiver and transmitter), space-time variability of the measurements and precipitation's own micro-physics, which cause quantitative precipitation estimations to have considerable uncertainty associated to its measuring process.

This paper provides a comprehensive uncertainty analysis intended for radar measurement procedures. A particular case study is analyzed in order to show quantitative results on the amount of uncertainty in the measurement system (the extent of such uncertainty). Section 2 of the paper illustrates the methodology applied to obtain the uncertainty model and section 3 shows specific case-study results. Conclusions are drawn in the final part of the paper.

## II. Methodology

The methodology applied in this work involves various stages. There is an initial specification of the variable to be measured (i.e. precipitation), which is a function of other variables that are previously defined in the radar equation. Subsequently, the uncertainty sources associated to this process are identified e.g. anomalous propagation, attenuation, ground echo, beam partial filling, resolution, beam height, calibration, type of rain, DSD variety, evaporation and condensation [4].

### A. Conceptual Model

Once the uncertainty sources were identified, a sub-set of uncertainty sources was selected, namely those related to radar calibration (i.e. antenna, transmitter and receiver), attenuation and the distance-sensitive radar resolution loss. Fig. 1 shows the conceptual map associated to the model:

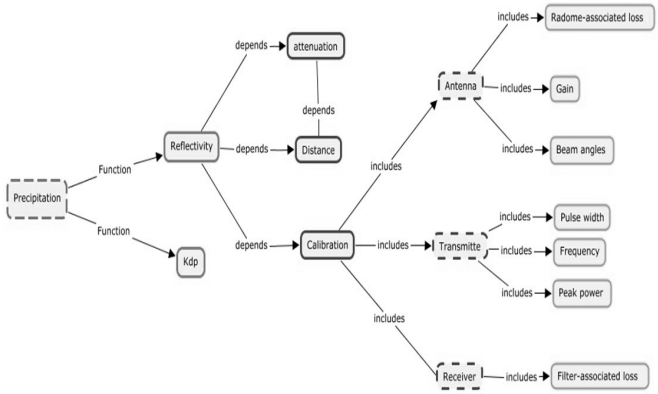


Fig, 1. Conceptual Model

### B. Mathematical Model

The mathematical uncertainty-measuring model was taken from "Guide to the expression of Uncertainty in measurement". The following is a description of the model [1]:

In most cases the value of variable Y (precipitation) is not measured directly; instead, such a value results from measuring other N magnitudes, namely $X_1, X_2, X_3, \ldots..X_N$ , using a functional relationship as follows:

$$Y = f(X_1, X_2, X_3, \ldots\ldots X_N) \quad (1)$$



DOI: 10.9781/ijimai.2016.378

In some cases, the best estimation "y" of variable "Y" can be obtained from gathering "n" observations, namely:

$$y = \bar{Y} = \frac{1}{n}\sum_{k=1}^{n} Y_{k=} \frac{1}{n}\sum_{k=1}^{n} f(X_{1,k}, X_{2,k}, X_{3,k}, \ldots . X_{N,k}) \quad (2)$$

The type of uncertainty associated to output estimation "y" is referred to as combined typical uncertainty and it is denoted by $u_c$ .This particular uncertainty can be determined from the estimated typical deviation associated to each input estimate $x_i$, referred to as typical uncertainty and denoted by $\mathrm{u}(x_i)$.

Each of the input estimations $x_i$ as well as their corresponding uncertainty $\mathrm{u}(x_i)$ is obtained from a distribution of possible values of each input magnitude $x_i$. This probability distribution might be based on a series of "n" observations $\mathrm{x_{i,k}}$ taken from the set of observations $x_i$ (type A), or else, the distribution may be assumed (type B).

The type-A uncertainty assessment is obtained from various observations and it is calculated using the following expression:

$$u(x) = \sqrt{\frac{\sum_{j=1}^{n}(x_j - \bar{x})^2}{n(n-1)}} \quad (3)$$

Where:

$$\bar{x} = \frac{1}{n}\sum_{j=1}^{n} x_j$$

For a single estimation $\mathrm{x_i}$ associated to an input magnitude $\mathrm{x_i}$ that was not obtained from repeated observations, the corresponding associated estimated variance, namely $\mathrm{u^2(x_i)}$, or the typical uncertainty $\mathrm{u(x_i)}$, can be established through scientific decision that is based on all the available information about the possible variability of $X_i$. The sort of information gathered may include:

- Results from previous measurements.
- Experience or general knowledge about the behavior and the properties of the specific materials and instruments.
- Manufacturing specifications (from suppliers).
- Data provided by certified calibrations or other types of certified processes
- Uncertainty previously assigned to reference values, which may be taken from books and manuals.

The values of $u^2(x_i)$ and $u(x_i)$ that are assessed as stated are called Type-B variance and Type-B typical uncertainty, respectively.

The uncertainty of $x_i$ is not always expressed as a multiple of a typical deviation. Instead, it is possible to define a specific interval that corresponds to a particular reliability level (e.g. 90%, 95% or 99%). Unless stated otherwise, it can be assumed that a normal distribution has been used to calculate uncertainty; this yields the typical uncertainty of $x_i$ simply by dividing the given uncertainty value by the corresponding factor in the normal distribution. Such a factor for the three aforementioned reliability levels is 1.64, 1.96 and 2.58, respectively.

In order to obtain the combined typical uncertainty estimation, namely $\mathrm{u_c(y)}$, in the case where all input magnitudes are independent, we take the positive square root of combined variance $\mathrm{u_c^2(y)}$, given by:

$$u_c^2(y) = \sum_{i=1}^{N} \left[\frac{\partial f}{\partial x_i}\right]^2 u^2(x_i) \quad (4)$$

Where f is the function that defines the variable itself as a function of variables $X_i$.

Each $\mathrm{u}(x_i)$ represents a single typical uncertainty that is assessed as previously described (either Type-A assessment or Type-B assessment). The combined typical uncertainty $\mathrm{u_c(y)}$ is a typical deviation that is estimated and characterized according to the dispersion of the potential reasonable values that can be attributed to variable "Y".

Partial derivatives (i.e. ∂f/∂xi), also known as sensitivity coefficients, describe the variation of output estimation "y" as a function of the variations in the input estimation values $x_1, x_2, x_3, \ldots x_N$.

It is worth mentioning that the previous equation holds only if the input magnitudes $x_i$ are independent or uncorrelated. In case some of the values of $x_i$ are highly correlated, it is essential to consider such correlations as follows:

$$\begin{aligned} u_c^2(y) &= \sum_{i=1}^{N}\sum_{j=1}^{N} \frac{\partial f}{\partial x_i}\frac{\partial f}{\partial x_j} u(x_i, x_j) \\ &= \sum_{i=1}^{N} \left[\frac{\partial f}{\partial x_i}\right]^2 u^2(x_i) \\ &\quad + 2\sum_{i=1}^{N-1}\sum_{j=i+1}^{N} \frac{\partial f}{\partial x_i}\frac{\partial f}{\partial x_j} u(x_i, x_j) \end{aligned} \quad (5)$$

Where $x_i$ and $x_j$ correspond to the estimations of $\mathrm{X_i}$ and $\mathrm{X_j}$; and $\mathrm{u}(x_i, x_j) = \mathrm{u}(x_j, x_i)$ represents the estimated covariance associated to $x_i$ and $x_j$. The extent of the correlation between $x_i$ and $x_j$ is determined by the correlation coefficient as follows:

$$r(x_i, x_j) = \frac{u(x_i, x_j)}{u(x_i)\, \mathrm{u}(x_j)} \quad (6)$$

Where $r(x_i, x_j) = r(x_j, x_i)$ and $-1 \le r(x_i, x_j) \le +1$. If estimations $x_i$ and $x_j$ are independent, $r(x_i, x_j) = 0$, and so a variation in one of the estimation values does not imply a variation in the other value.

Fractional uncertainty is defined as the ratio of typical uncertainty to the value of the best magnitude estimate, namely:

$$Fractional\ Uncertainty = \frac{u(x_i)}{x_i} \quad (7)$$

Although $u_c(\mathrm{y})$ can be generally employed as an expression of uncertainty for a particular measurement result, it is often necessary (in certain commercial, industrial or regulatory applications as well as in the fields of health and security) to provide uncertainty measurements that clearly define an interval in which most of the distribution (reasonably attributed values) of the variable are expected to fall.

The new expression for uncertainty, which satisfies the interval-definition requirement, is referred to as expanded uncertainty and is denoted by U. Expanded uncertainty (U) is obtained by multiplying the combined typical uncertainty $u_c(\mathrm{y})$ by a given coverage factor (k):

$$U = ku_c(y) \tag{8}$$

In general, k takes values between 2 and 3. Experience and broad knowledge about the way measurement results should be handled may facilitate choosing a convenient value for k.

### C. Uncertainty due to calibrations involving radar, distance and attenuation

Taking the radar equation defined by Probert Jones [5] as a starting point, a standard uncertainty calculation can be stated as follows:

$$P_r = \frac{\pi^3 P_{tx} G^2 \theta \phi h |K|^2 Z}{1024 \ln(2)\, \lambda^2\, r^2} \tag{9}$$

Where : $P_r$: received power at the radar

$P_{tx}$: radiated power from the transmitter

$\lambda$ : wavelength (c/f)

$Z$ : Radar-reflectivity factor

K : refraction complex index

h : spatial pulse length (c $\tau$ )

G: antenna gain

r: distance between the target and the radar's antenna

$\theta, \phi$ : beam angles of the radar

By solving for reflectivity, and also considering that h=c $\tau$, $\theta = \phi$ and $\lambda$ =c/f, the following expression is obtained:

$$Z = \frac{2^{10} \ln(2)\, c}{\pi^3 |K|^2 G^2 \theta^2 P_{tx} \tau\, f^2} P_r r^2 \tag{10}$$

The addition of some terms that were not included by Jones, such as propagation loss ($L_p$), receiving filter loss ($L_{MF}$) [6][7] and a radome-associated loss ($L_{RD}$), yields the following expression:

$$Z = \frac{2^{10} \ln(2)\, c}{\pi^3 |K|^2} \frac{L_{RD}^2}{G_A^2 \theta^2} \frac{L_{MF}}{P_{tx} \tau f^2} L_p^2 P_r r^2 \tag{11}$$

For radars that are in normal operation conditions, it is always possible to simplify the radar equation since most of the terms are constants; thus the following expression can be used:

$$Z = C_R L_p^2 P_r\, r^2 \tag{12}$$

Where $C_R$ is the radar constant, defined by:

$$C_R = \frac{2^{10} \ln(2) c}{\pi^3 |K|^2} \frac{L_{RD}^2}{G_A^2 \theta^2} \frac{L_{MF}}{P_{tx} \tau f^2} \tag{13}$$

By further elaborating on the previous expression, we obtain:

$$CTE = \frac{2^{10} \ln(2) c}{\pi^3 |K|^2} \tag{14}$$

Where:

$$CTE = \frac{2^{10} \ln(2) c}{\pi^3 |K|^2} \quad \text{y} \quad C_{ANT} = G_A^2 \theta^2$$

Aspects such as antenna gain, beam angles, frequency accuracy, pulse length, and loss estimations (in radome and in the receiving filters) constitute some of the many factors that should be considered in a radar calibration process [8]. The following is a list of the most relevant factors to radar calibration:

TABLE I
FACTORS TO BE CONSIDERED IN UNCERTAINTY MODELS [8].

| Elements | Factors to be considered in calibration | Standard uncertainty |
|---|---|---|
| Radar Calibration Antenna | • Gain ($G_A$).<br>• -3dB beam-width angles ($\theta$, $\phi$).<br>• Antenna constant $C_{ANT} = G_A^2 \theta^2$.<br>• Radome-associated loss ($L_{RD}$). | • $U(G_A)$<br>• $U(\theta, \phi)$<br>• $U(C_{ANT})$<br>• $U(L_{RD})$ |
| Radar Calibration Transmitter | • Pulse length ($\tau$).<br>• Frequency (f) and PRF.<br>• Peak power ($P_{tx}$). | • $U(\tau)$<br>• $U(f)$<br>• $U(P_{tx})$ |
| Radar Calibration Receiver: | • Gain (G).<br>• Filter-associated loss ($L_{MF}$). | • $U(G)$<br>• $U(L_{MF})$ |
| Attenuation | • Propagation loss ($L_p$). | • $U(L_p)$ |
| Resolution Space | • Coverage range (r). | • $U(r)$ |
| Physical constants: | • Wave speed c=2.9978*10^8 m/s.<br>• Dielectric constant $\|K_W\|^2$=0.93. | • $U(c)$<br>• $U(K_W)$ |
| Measurements | • Reflectivity (Z).<br>• Received power ($P_r$). | • $U(Z)$<br>• $U(P_r)$ |

Regarding the various uncertainty sources that appear in the table above as independent (except for the existing correlation between the transmitting antenna gain and its -3 dB beam angles, which are handled together within the antenna constant), the following general expression is thus obtained in order to determine the combined uncertainty that lies in the corresponding reflectivity (Z) measurement:

$$u_c^2(Z) = \left[\frac{\partial Z}{\partial C_R}\right]^2 u^2(C_R) + \left[\frac{\partial Z}{\partial P_r}\right]^2 u^2(P_r) + \left[\frac{\partial Z}{\partial L_p}\right]^2 u^2(L_p) + \left[\frac{\partial Z}{\partial r}\right]^2 u^2(r) \tag{15}$$

Similarly, for $C_R$:

$$u_c^2(C_R) = \left[\frac{\partial C_R}{\partial C_{ANT}}\right]^2 u^2(C_{ANT}) + \left[\frac{\partial C_R}{\partial L_{RD}}\right]^2 u^2(L_{RD}) + \left[\frac{\partial C_R}{\partial \tau}\right]^2 u^2(\tau) + \left[\frac{\partial C_R}{\partial f}\right]^2 u^2(f) + \left[\frac{\partial C_R}{\partial P_{tx}}\right]^2 u^2(P_{tx}) + \left[\frac{\partial C_R}{\partial L_{MF}}\right]^2 u^2(L_{MF}) \tag{16}$$

The following table shows the results in terms of partial derivatives:

TABLE II
PARTIAL DERIVATIVES FOR THE UNCERTAINTY MODEL

| $Z = C_R L_p^2 P_r\, r^2$ | | | |
|---|---|---|---|
| $C_1$ | $\frac{\partial Z}{\partial C_R}$ | $L_p^2 P_r\, r^2$ | $\frac{Z}{C_R}$ |
| $C_2$ | $\frac{\partial Z}{\partial L_p}$ | $2 C_R L_p P_r\, r^2$ | $2\frac{Z}{L_p}$ |
| $C_3$ | $\frac{\partial Z}{\partial P_r}$ | $C_R L_p^2\, r^2$ | $\frac{Z}{P_r}$ |
| $C_4$ | $\frac{\partial Z}{\partial r}$ | $2 C_R L_p^2 P_r\, r$ | $2\frac{Z}{r}$ |
| $C_R = CTE \frac{L_{RD}^2 L_{MF}}{C_{ANT} P_{tx} \tau f^2}$ | | | |
| $C_A$ | $\frac{\partial C_R}{\partial C_{ANT}}$ | $-2CTE \frac{L_{RD}^2 L_{MF}}{C_{ANT}^2 P_{tx} \tau f^2}$ | $-2\frac{C_R}{C_{ANT}}$ |
| $C_B$ | $\frac{\partial C_R}{\partial L_{RD}}$ | $2 * CTE \frac{L_{RD} L_{MF}}{C_{ANT} P_{tx} \tau f^2}$ | $2\frac{C_R}{L_{RD}}$ |
| $C_C$ | $\frac{\partial C_R}{\partial \tau}$ | $-CTE \frac{L_{RD}^2 L_{MF}}{C_{ANT} P_{tx} \tau^2 f^2}$ | $-\frac{C_R}{\tau}$ |
| $C_D$ | $\frac{\partial C_R}{\partial f}$ | $-2 * CTE \frac{L_{RD}^2 L_{MF}}{C_{ANT} P_{tx} \tau f^3}$ | $-2\frac{C_R}{f}$ |
| $C_E$ | $\frac{\partial C_R}{\partial P_{tx}}$ | $-CTE \frac{L_{RD}^2 L_{MF}}{C_{ANT} P_{tx}^2 \tau f^2}$ | $-\frac{C_R}{P_{tx}}$ |
| $C_F$ | $\frac{\partial C_R}{\partial L_{MF}}$ | $CTE \frac{L_{RD}^2 L_p^2}{C_{ANT} P_{tx} \tau f^2}$ | $\frac{C_R}{L_{MF}}$ |

By using the partial derivatives, the combined uncertainty that occurs when measuring reflectivity Z can be expressed as follows:

$$u_c^2(Z) = \left[\frac{Z}{C_R}\right]^2 u^2(C_R) + \left[2\frac{Z}{L_p}\right]^2 u^2(L_p) + \left[\frac{Z}{P_r}\right]^2 u^2(P_r) + \left[2\frac{Z}{r}\right]^2 u^2(\mathrm{r}) \quad (17)$$

The previous expression can be rewritten as follows:

$$\left[\frac{u_c(z)}{Z}\right]^2 = \left[\frac{u(C_R)}{C_R}\right]^2 + \left[2\frac{u(L_p)}{L_p}\right]^2 + \left[\frac{u(P_r)}{P_r}\right]^2 + \left[2\frac{u(r)}{r}\right]^2 \quad (18)$$

This expression serves to compute the fractional uncertainty associated to reflectivity measurements by assuming independence of all the variables involved. However, given the direct relation between attenuation and the radar's coverage range, and also assuming a corresponding correlation coefficient of 1, the following is obtained:

$$\left[\frac{u_c(z)}{Z}\right]^2 = \left[\frac{u(C_R)}{C_R}\right]^2 + \left[2\frac{u(L_p)}{L_p} + 2\frac{u(r)}{r}\right]^2 + \left[\frac{u(P_r)}{P_r}\right]^2 \quad (19)$$

Similarly, for the radar constant, the following is obtained:

$$u_c^2(C_R) = \left[-2\frac{C_R}{C_{ANT}}\right]^2 u^2(C_{ANT}) + \left[-2\frac{C_R}{L_{RD}}\right]^2 u^2(L_{RD}) + \left[-\frac{C_R}{\tau}\right]^2 u^2(\tau) + \left[-2\frac{C_R}{f}\right]^2 u^2(\mathrm{f}) + \left[-\frac{C_R}{P_{tx}}\right]^2 u^2(\mathrm{P_{tx}}) + \left[\frac{C_R}{L_{MF}}\right]^2 u^2(\mathrm{L_{MF}}) \quad (20)$$

$$\left[\frac{u_c(C_R)}{C_R}\right]^2 = \left[\frac{2u(C_{ANT})}{C_{ANT}}\right]^2 + \left[\frac{2u(L_{RD})}{L_{RD}}\right]^2 + \left[\frac{u(\tau)}{\tau}\right]^2 + \left[\frac{2u(\mathrm{f})}{f}\right]^2 + \left[\frac{u(\mathrm{P_{tx}})}{P_{tx}}\right]^2 + \left[\frac{u(\mathrm{L_{MF}})}{L_{MF}}\right]^2 \quad (21)$$

The uncertainty associated to the antenna constant, which depends on the gain and also on the -3db angles, is assumed as a correlated uncertainty with a correlation coefficient equal to 1, thus the corresponding expression y computed as follows:

$$C_{ANT} = G_A^2\theta^2 \quad (22)$$

$$\left[\frac{u_c(C_{ANT})}{C_{ANT}}\right]^2 = \left[\frac{u(G_A)}{G_A} + \frac{u(G_A)}{G_A}\right]^2 \quad (23)$$

Considering that the actual variable of interest is precipitation (R), instead of reflectivity (Z), and also involving the Marshall & Palmer Z-R relation together with an algorithm that uses both reflectivity and the specific phase differential (for precipitation estimation), the following uncertainty expressions are obtained:

$$R = f(Z, K_{dp}) \quad o \quad R = f(Z) \quad (24)$$

$$u_c^2(R) = \left[\frac{\partial R}{\partial Z}\right]^2 u^2(Z) + \left[\frac{\partial R}{\partial K_{dp}}\right]^2 u^2(K_{dp})$$

$$u_c^2(R) = \left[\frac{\partial R}{\partial Z}\right]^2 u^2(Z) \quad (25)$$

## III. Case Study

For this particular case study, technical information of radar, located in Brisbane-Australia, was considered (see Table II).

TABLE II
CHARACTERISTICS OF RADAR BRISBANE-AUSTRALIA

| Frequency | Band | PPI | Latitude | Longitude | Altitude | PRF | Range |
|---|---|---|---|---|---|---|---|
| 2,753 GHz | S | 10 | -27,669 | 152,862 | 168 | 999 | 150 Km |

Fractional uncertainty for each of the variables involved in the radar equation was assessed as Type-B uncertainty, also considering the information provided by suppliers (manufacturers).

In the cases where suppliers provide the maximum error for a particular variable, the following expression serves to compute the fractional uncertainty of a triangular distribution:

$$\frac{u(x)}{x} = \frac{\Delta X}{\sqrt{6}} \quad (26)$$

Similarly, for a normal distribution we can use:

$$\frac{u(x)}{x} = \frac{\Delta X}{3} \quad (27)$$

On the other hand, if suppliers provide relative uncertainty in dB, it becomes necessary to calculate the corresponding fractional uncertainty as follows [9]:

$$\frac{u(x)}{x} = 10^{\frac{u(x)dB}{10}} - 1 \quad (28)$$

### *A. Antenna*

TABLE III
ANTENNA UNCERTAINTY

| Parameter | Value | Error ±ΔX | Relative uncertainty u(x) | Linear scale Error ±ΔX | Fractional uncertainty Triangular $\frac{u(x)}{x}$ | Fractional uncertainty Normal $\frac{u(x)}{x}$ |
|---|---|---|---|---|---|---|
| Gain | 45 dB | ----- | 0.5 dB | ---- | 0.122 | 0.122 |
| Angle | 1 ° | 0.03 ° | | 0.03 | 0.012 | 0.01 |

### *B. Radome Associated Loss*

Regarding the information provided by antenna suppliers, the standard uncertainty due to radome loss is about 0.02 dB.

TABLE IV
RADOME LOSS

| Parameter | Value | Relative Uncertainty u(x) | Linear scale | Fractional uncertainty $\frac{u(x)}{x}$ |
|---|---|---|---|---|
| Radome Loss | 0.5 dB | 0.02 dB | 0.0046 | 0.0046 |

### *C. Pulse length τ*

TABLE V
PULSE-LENGTH UNCERTAINTY T.

| Parameter | Value | Error ±ΔX | Fractional uncertainty Triangular $\frac{u(x)}{x}$ | Fractional uncertainty –Normal $\frac{u(x)}{x}$ |
|---|---|---|---|---|
| Pulse length τ | 0,0002185979 seg | 0.000020 seg | 0.037 | 0.03049 |

### D. Frequency

TABLE VI
FREQUENCY UNCERTAINTY

| Parameter | Value | Error ±ΔX | Linear scale | Fractional uncertainty Triangular $\frac{u(x)}{x}$ | Fractional uncertainty Normal $\frac{u(x)}{x}$ |
|---|---|---|---|---|---|
| Frequency | 2,753 GHz | 0.004GHz | 0.004 | 0.0016 | 0.0013 |

### E. Transmitted power

TABLE VII
TRANSMITTED-POWER UNCERTAINTY

| Parameter | Value | Relative uncertainty $u(x)$ | Fractional uncertainty $\frac{u(x)}{x}$ |
|---|---|---|---|
| Power | 250 KW | 25KW | 0.10 |

### F. Receiving-filter loss

TABLE VIII
RECEIVING-FILTER LOSS (UNCERTAINTY)

| Parameter | Value | Relative uncertainty $u(x)$ | Linear scale | Fractional uncertainty $\frac{u(x)}{x}$ |
|---|---|---|---|---|
| Receiving-filter loss | | 0.02 dB | 0.0471 | 0.0471 |

Finally, by using equation 21, it is possible to calculate the fractional uncertainty associated to that radar constant, as shown in Table IX:

TABLE IX
RADAR-CONSTANT UNCERTAINTY

$$\left[\frac{u_c(C_R)}{C_R}\right]^2 = \left[\frac{2u(C_{ANT})}{C_{ANT}}\right]^2 + \left[\frac{2u(L_{RD})}{L_{RD}}\right]^2 + \left[\frac{u(\tau)}{\tau}\right]^2 + \left[\frac{2u(f)}{f}\right]^2 + \left[\frac{u(P_{tx})}{P_{tx}}\right]^2 + \left[\frac{u(L_{MF})}{L_{MF}}\right]^2$$

| Fractional Uncertainty | Triangular value | Normal value |
|---|---|---|
| $\frac{u(C_{ANT})}{C_{ANT}}$ | 0.134 | 0.132 |
| $\frac{u(L_{RD})}{L_{RD}}$ | 0.0046 | 0.0046 |
| $\frac{u(\tau)}{\tau}$ | 0.037 | 0.030 |
| $\frac{2u(f)}{f}$ | 0.0016 | 0.0013 |
| $\frac{u(P_{tx})}{P_{tx}}$ | 0.10 | 0.10 |
| $\frac{u(L_{MF})}{L_{MF}}$ | 0.0471 | 0.0471 |
| $\frac{u_c(C_R)}{C_R}$ | 0.2924 | 0.2879 |

Using one example of the received power, namely -85 dBm at a distance of 10 kilometers, the following uncertainty calculations were obtained in terms of reflectivity:

### G. Received power

TABLE X
RECEIVED-POWER UNCERTAINTY

| Parameter | Value | Relative uncertainty $u(x)$ | Fractional uncertainty $\frac{u(x)}{x}$ |
|---|---|---|---|
| Potencia | -85 dBm | 0.7dB | 0.17 |

### H. Distance to target

TABLE XI
RADAR-DISTANCE UNCERTAINTY

| Parameter | Value | Relative uncertainty $u(x)$ | Fractional uncertainty $\frac{u(x)}{x}$ |
|---|---|---|---|
| Distance | 10 Km | 0.1 km | 0.10 |

### I. Attenuation loss

The reciprocal value of $L_p$ ranges from 0 to 1, and, when having ideal conditions, this factor is assumed to be equal to 1; $L_p$ is defined as follows:

$$L_p(r_o) = e^{\int_0^{r_o}(k_g + k_n + k_p)dr} \quad (29)$$

Where $k_g$ $(\frac{dB}{Km})$ is the attenuation coefficient of gases, $k_n$ (dB/Km ) corresponds to the absorption coefficient of clouds, and $k_p$ $(\frac{dB}{Km})$ is the attenuation coefficient of rain. All these coefficients take approximate values intended for an S-band radar [10]:

Specifically, for an S-band radar, attenuation of gases is negligible, thus, $k_g = 0\ dB/Km$, $k_n$ = 0.004 dB/Km, and $k_p$ = 0.004 dB/Km, for precipitations of about 12 mm/h [11] .According to these values, we obtain $L_p = 1.072$ together with its reciprocal $L_p^{-1} = 0.9323$.

TABLE XII
UNCERTAINTY DUE TO ATTENUATION

| Parameter | Value $L_p^{-1}$ | Relative Uncertainty $u(x)$ | Fractional Uncertainty $\frac{u(x)}{x}$ |
|---|---|---|---|
| Attenuation loss | 0.9323 | 0.01 | 0.010 |

In order to calculate the fractional uncertainty of reflectivity, we use equation (19). These results can be observed in Table XIII.

TABLE XIII
REFLECTIVITY UNCERTAINTY

$$\left[\frac{u_c(z)}{Z}\right]^2 = \left[\frac{u(C_R)}{C_R}\right]^2 + \left[2\frac{u(L_p)}{L_p} + 2\frac{u(r)}{r}\right]^2 + \left[\frac{u(P_r)}{P_r}\right]^2$$

| Fractional Uncertainty | Triangular Value | Normal Value |
|---|---|---|
| $\frac{u(C_R)}{C_R}$ | 0.2924 | 0.2879 |
| $\frac{u(L_p)}{L_p}$ | 0.010 | 0.010 |
| $\frac{u(r)}{r}$ | 0.10 | 0.10 |
| $\frac{u(P_r)}{P_r}$ | 0.17 | 0.17 |
| $\frac{u_c(z)}{Z}$ | 0.4034 | 0.4002 |

By using these data and also considering a sample reflectivity measurement of 40 dB (10000 mm^6/m^3), the following values are obtained:

Linear scale:

$$z = 10000 \pm 4002 \ \frac{mm^6}{m^3}$$

Logarithmic scale:

$$Z = 40dB \pm 1.5 \ dB$$

Provided there is considerable reflectivity uncertainty, it is worth noting that all this uncertainty propagates over the final precipitation estimation.

For the computation of precipitation uncertainty, the most common Z-R empirical relation is adopted [12]

$$Z = aR^b \tag{29}$$

Solving for R, we obtain:

$$R = (\frac{Z}{a})^{\frac{1}{b}} \tag{30}$$

Teni Using equation (25), the following expression is obtained to compute the precipitation uncertainty:

$$u_c^2(R) = [\frac{\partial R}{\partial Z}]^2 u^2(Z) + [\frac{\partial R}{\partial a}]^2 u^2(a) + [\frac{\partial R}{\partial b}]^2 u^2(b) \tag{31}$$

The following table shows the results obtained from the partial derivatives:

TABLE XIV
PARTIAL DERIVATIVES FOR THE PRECIPITATION UNCERTAINTY MODEL

$$R = (\frac{Z}{a})^{\frac{1}{b}} = \sqrt[b]{\frac{Z}{a}}$$

| | | | |
|---|---|---|---|
| $C_1$ | $\frac{\partial R}{\partial Z}$ | $\frac{1}{bZ}\sqrt[b]{\frac{Z}{a}}$ | $\frac{R}{bZ}$ |
| $\overline{C_2}$ | $\overline{\frac{\partial R}{\partial a}}$ | $-\frac{1}{ba}\sqrt[b]{\frac{Z}{a}}$ | $\overline{-\frac{R}{ba}}$ |
| $C_3$ | $\frac{\partial R}{\partial b}$ | $-\frac{1}{b^2}\sqrt[b]{\frac{Z}{a}} ln[\frac{Z}{a}]$ | $-\frac{R}{b^2} ln[\frac{Z}{a}]$ |

By substituting the partial derivatives we obtain:

$$u_c^2(R) = [\frac{R}{bZ}]^2 u^2(Z) + [\frac{R}{ba}]^2 u^2(a) + [\frac{R}{b^2} \ ln[\frac{Z}{a}]]^2 u^2(b)$$

$$[\frac{u_c(R)}{R}]^2 = [\frac{u^2(Z)}{bZ}]^2 + [\frac{u^2(a)}{ba}]^2 + [\frac{u^2(b)}{b^2} \ ln[\frac{Z}{a}]]^2 \tag{32}$$

Finally, the following expression can be obtained to find the fractional uncertainty of precipitation using the Z-R relation:

$$\frac{u_c(R)}{R} = \frac{1}{b}\sqrt{[\frac{u^2(Z)}{Z}]^2 + [\frac{u^2(a)}{a}]^2 + [ln[\frac{Z}{a}]]^2 [\frac{u^2(b)}{b}]^2} \tag{33}$$

Based on the previous expression, it is possible to calculate the Type-A fractional uncertainty for constants "a" and "b" from the data provided in the literature regarding various Z-R relations.

TABLE XV
A SUMMARY OF DIFFERENT VALUES FOR "A" AND "B" REGARDING Z-R RELATIONS [13], [14].

| a | b | a | b | a | b |
|---|---|---|---|---|---|
| 200 | 1,6 | 300 | 1,4 | 124 | 1,64 |
| 300 | 1,35 | 21 | 1,71 | 667 | 1,33 |
| 176,5 | 1,29 | 486 | 1,37 | 500 | 1,5 |
| 215,9 | 1,35 | 300 | 1,5 | 450 | 1,46 |
| 171,9 | 1,19 | 250 | 1,2 | 200 | 1,6 |
| 172,8 | 1,33 | 130 | 2 | 800 | 1,6 |
| 371 | 1,24 | 75 | 2 | 348 | 1,81 |
| 162 | 1,48 | 140 | 1,5 | 134 | 1,55 |
| 167,8 | 1,26 | 250 | 1,2 | 162 | 1,48 |
| 65,5 | 1,69 | 436 | 1,43 | 371 | 1,24 |

To calculate the Type-A standard uncertainty of "a" and "b" equation (3) was used, yielding the following values:

TABLE XVI
PRECIPITATION UNCERTAINTY

| Fractional Uncertainty | Triangular value | Normal value |
|---|---|---|
| $\frac{u_c(z)}{Z}$ | 0,4034 | 0,4002 |
| $\frac{u^2(a)}{a}$ | 0,1197 | 0,1197 |
| $\frac{u^2(b)}{b}$ | 0,02624 | 0,02624 |
| $\frac{u_c(R)}{R}$ | 0.2920 | 0.290 |

Specifically, when reflectivity is equal to 10000 $\frac{\text{mm}^6}{\text{m}^3}$, a=271.58, and b = 1.476, the following uncertainty values can be calculated for precipitation (R):

$$R = (\frac{10000}{271.58})^{\frac{1}{1.476}}$$

$$R = 11.49 \ mm \pm 29\%$$

$$R = 11.49 \ \pm 3.33 \ mm$$

## IV. Conclusions

The antenna represents the element that most contributes to introducing uncertainty in the radar's constant; therefore, antennas play a crucial role in calibration processes. Additionally, a lot of effort should go into estimating the actual antenna gain and beam-width angles due to the nature of these variables as well as to the external uncertainty sources involved.

Although the fractional uncertainty associated to the radar's constant is 40%, when propagating towards the Marshall & Palmer Z-R relation used herein (for precipitation estimation), its value decreases down to 29%. The previous result follows from the very nature of the resulting expression for estimating precipitation in the Z-R relation.

The present work does not deal with all the possible uncertainty sources that affect quantitative precipitation estimation using radars. Specifically, aspects such as the space-time variation of the drop size distribution (dsd) would undoubtedly contribute to having greater

uncertainty in the final results of similar studies. Furthermore, other uncertainty sources were also omitted, e.g. the uncertainty related to the non-linearity of transmitters and receivers, the partial beam filling, evaporation and condensation. These other uncertainty sources represent an interesting challenge for future research on precipitation estimation uncertainty using weather radars.

## References


[1] BIPM, IEC, IFCC, ILAC, ISO, IUPAC, IUPAP, and OIML, "Evaluation of measurement- Guide to the expression of uncertainty in measurement (JCGM 100:2008)," 1ª ed, Sep, 2008. [Online]. Available: http://www.bipm.org/utils/common/documents/jcgm/JCGM_100_2008_E.pdf

[2] G. Villarini, F. Serinaldi, F. Witold, and A. Krajewski, "Modeling radar-rainfall estimation uncertainties using parametric and non-parametric approaches," Advances in Water Resources, vol. 31, pp. 1675-1685, April, 2008.

[3] B. Taylor, Barry N. Chris, and E. Kuyatt. "Guidelines for Evaluating and Expressing the Uncertainty of NIST Measurement Results. NIST Technical Note 1297," National Institute of Standards and Technology-Physics Laboratory, Sep, 1994. [Online]. Available: http://physics.nist.gov/Pubs/guidelines/TN1297/tn1297s.pdf

[4] I. Zawadski, "Factors affecting the precisión of radar measurements of rain," Preprints 22 nd Conf. of Radar Meteorology, Zurich, Switzerland, pp. 251-256, Sept, 1984.

[5] P. Jones, "The radar equation in meteorology," Quarterly Journal of the Royal Meteorological Society, pp. 485-495, Oct,1962.

[6] R. Doviak, and D. Zrnic, "Matched filter criteria and range weighting for weather radar", IEEE Transactions Aerospace Electronic System, vol. AES 14, no. 6, pp. 925-929, Nov, 1978.

[7] R. Doviak and D. Zrnic, "Receiver Bandwidth effect on Reflectivity and Doppler Velocity estimates," Journal of Applied Meteorology, pp: 69-76, Jan, 1979.

[8] F. Gekat, M. Hille, H. Niese, and M. Pool, "Accuracy of the engineering calibration of weather radars," Geoscience and Remote Sensing Symposium (IGARSS), IEEE International, pp. 1096-1099, Nov, 2010.

[9] R. E. Rinehart, "Radar for Meteorologist", Nevada, Rinehart Publ, 6ª ed, pp. 365-380, Dec, 2006.

[10] R. Wexler, and D. Atlas, " Radar reflectivity and attenuation of rain," Journal of Applied Meteorology, vol. 2, pp. 276-280. Oct, 1963.

[11] K. L. Gunn, and T.W. East, "The microwave properties of precipitation particles," Quarterly Journal of the Royal Meteorological Society, pp.522-545, Jul,1954.

[12] J. Marshall and W. Palmer, "The distribution of raindrops with size," Journal of Meteorology, McGill University, Montreal, vol 5, pp. 165-16, Oct, 1948.

[13] L.J. Battan, " Radar observation of the atmosphere," University of Chicago Press, pp. 323-324, 1973.

[14] J. Copete, "Herramientas matemáticas e informáticas aplicables en la calibración y funcionamiento de un radar meteorológico concebido para el estudio del drenaje urbano de la ciudad de Bogotá," Universidad Nacional de Colombia, Maestría en ingeniería y recursos Hidráulicos, pp 56-58, Jul, 2009.


**A. Ernesto Gómez Vargas** was born in Duitama, Colombia, in 1978. He received the B.S. degree in electronic engineering from Distrital Francisco Jose de Caldas University, Bogota, Colombia, in 2000 and the M.S. degree in telecommunications from Distrital Francisco Jose de Caldas University, Bogota, Colombia, in 2004 and the Ph.D. degree in engineering from Javeriana University, Bogota, Colombia in 2015. From 2001, he has been an Assistant Professor with the Engineering Department, University of the District, Bogota, Colombia. He is the author of one book, and some articles. His research interests include weather radars, satellites and tele-communications.

**B. Nelson Obregón** was born in Cúcuta City, Colombia, in 1967. He received the B.S. in Civil Engineering from Francisco de Paula Santander University of, Cúcuta, Colombia, in 1991; the M.S. degrees in Civil Engineering from the Andes University, Bogotá, Colombia, in 1998 and the Ph.D. degree in Hydrological Sciences from University of California, Davis, USA in 1998. From 1999, he has been an Full Professor with the Civil Engineering Department at Javeriana University, Bogotá, Colombia. From 2006 to date he also has been the head of Geophysical Institute at the same University. He is the author of several chapter books and more than 50 articles. His research interests include non-linear dynamics and chaos theory, hydroinformatics, complexity, artificial inteligence in geosciences and engineering.

**Lindsay Álvarez Pomar** was born in Florencia, Colombia, in 1978. She received the B.S. degree in industrial engineering from Distrital Francisco Jose de Caldas University, Bogota, Colombia, in 2000 and the M.S. degree in industrial engineering from Andes University, Bogota, Colombia, in 2004. She is currently pursuing the Ph.D. degree in engineering at Distrital Francisco Jose de Caldas University, Bogota, Colombia. From 2001, she has been an Assistant Professor with the Industrial Engineering Department, University of the District, Bogota, Colombia. She is the author of three books, and some articles. Her research interests include simulation, industrial dynamics and stochastic processes. Mrs. Alvarez awards the first Latin American simulation competition in 2008.

# Human Activity Recognition in Real-Times Environments using Skeleton Joints

Ajay Kumar, Anil Kumar, Satish Kumar Singh,Rahul Kala

*Robotics and Artificial Intelligence Laboratory, Indian Institute of Information Technology, Allahabd, India*

***Abstract* — In this research work, we proposed a most effective noble approach for Human activity recognition in real-time environments. We recognize several distinct dynamic human activity actions using kinect. A 3D skeleton data is processed from real-time video gesture to sequence of frames and getter skeleton joints (Energy Joints, orientation, rotations of joint angles) from selected setof frames. We are using joint angle and orientations, rotations information from Kinect therefore less computation required. However, after extracting the set of frames we implemented several classification techniques Principal Component Analysis (PCA) with several distance based classifiers and Artificial Neural Network (ANN) respectively with some variants for classify our all different gesture models. However, we conclude that use very less number of frame (10-15%) for train our system efficiently from the entire set of gesture frames. Moreover, after successfully completion of our classification methods we clinch an excellent overall accuracy 94%, 96% and 98% respectively. We finally observe that our proposed system is more useful than comparing to other existing system, therefore our model is best suitable for real-time application such as in video games for player action/gesture recognition.**

***Keywords* — Human Activity, Kinect, Skeleton Joints, Principle Component Analysis, Artificial Neural Network, Gesture Recognition**

## I. Introduction

Automatic activity recognition in real-time environment for Intelligent Device or Robotics has been automatic interpretation between human activities and perception. However, integrating them by using controls, machines, and electronics enhance its artificial intelligence efficiently. Recently, Robotics and intelligent devices has been used in more areas such as field medical robotics, service robotics, or human enlarge. The idea that has been proposed in our work targets for generate human like skills to execute a task, identifying the human activities and learning with their movements. Many researchers have been demonstrated related work in large scale since the 1050 in these areas such as robotics research and computer vision. The goal of smart device vision is to extract the information from a particular scene and design it. The recognition task can be classified in to three stages: feature representation, feature extraction and action classification. This paper aims to present a humanoid robot having the skill of observing, training and representing actions operated by humans for generating new skills. This system has been implemented in such a way that it will distinguish different actions along with grants the permission to robot for regenerating their actions. Being able to identify and recognize human actions is most essential for many applications such as smart homes and assistive robots. Human robot interaction (HRI) has been implemented in the view of real world applications. Human activity recognition is an important functionality in any intelligent system designed to support human daily activities. The measurement of image or camera motion and more on the labeling of the action taking place in the scene. We have to select most informative frame and design one another action feature, which are able to remove all noisy frames and minimize the computational cost.

Activity recognition activity detection does not provide the label however attempts to distinguish one activity from another by using classifier technique PCA/ANN for the action recognition and these are nonparametric classifiers having property to avoid the over fitting problems and advantages to take the large numbers of the classes. Our work mostly concentrates on the activity recognition of the videos, which are captured by the RGB camera. The video, which are taken by camera in 2dimension frames having RGB images in the sequential order. Moreover, many research in literature survey on the topic activity recognition for 2D videos. The spatio temporal approach has mostly used to measure the similarity between two activities. To find the accurate similarity calculation, the spatio temporal detection method and representation have proposed [8, 16]. NBNN and HMM methods widely used for the human activity recognition [8, 5]. In these approaches, human activity can explain by the combinations of the key joints and other points. On the other way, take advance technique RGBD cameras of the Microsoft Kinect have to practically capture the RGB videos in real time as well as in depth map.

Many research works has been developed related to recognizing the actions of human. Human actions can be recognized in the form of skeleton [9], silhouettes [6], and in the form of images [7]. Visual surveillance technique is used for identifying packages of human actions [2]. Researchers used different techniques to recognize human actions such as hierarchical probabilistic approach [3], multi-modality representation of joints [4], HDP-HMM which is multi-level [5], Eigen-joint based method [8] using NBNN classifier. All the mentioned work is not reliable for real world application. Researchers have been explored different varieties of compact representation for human actions. However, authors has developed a technique to recognize the human actions which is independent of human action duration and starting location of actions [10]. A lot of work is developed by researchers to identify human actions from the sequence of images of captured human actions video [11], [12], [14] and [15]. In such type of technique, the main disadvantage is the prediction of parts of body in the sequence of actions. Several authors have developed method based on image processing using histograms [13] of 3D joints to recognize human actions. In [16] it has been demonstrated that how many frames are collected and required to execute action recognition. Apart from this, many other methodologies have been implemented in [17], [18], [19] and [20].

Temporal templates is a new approach to represent the human action[ 23 ] The representation of temporal templates is a stable vector images having every points vector values and task of the motion belonging in mage sequence. Two components of templates, sample the first value is a function of regency of motion in a sequence. After that we have to construct a recognition method which



DOI: 10.9781/ijimai.2016.379

has two matching with temporal templates against the stored action. The develop method automatically perform temporal templates segmentation and its run in real time and independent linear changes in speed of standard platform. In this paper [24]authors have to take only required frames which are enough to 90% correct activity recognition and we conclude that the 10-20 frames or 7-10 snippets are more than sufficient to perform similar than the entire videos based on experiments. These methods are used both form and motion features sampled densely over the image plane. The method investigates the question, how long video snippets are required to serve the basic unit for action recognition. The advantage of extracting both form further this method perform well on different database without changes any parameter. The main advantage of this paper the action recognizes well with a very short snippet of frames (frame rate 25Htz) which are not applicable for invariance to rotation scale and viewpoint. The Activity recognition using several hardware devices is used in several previous motivational research works. Several more human activity/ action recognitions are discussed using gait patterns [28-33].

*A. Activity recognition in videos captured with single camera:* In this paper [3] the author presents an approach to activity recognition, video matching and localization based on hierarchical code book model to local temporal video volume. This method based on "bag" of the video word representation and its does not require knowledge about the action, motion estimation, background subtraction or tracking. It's also robust to the temporal and spatial scale changes as some deformation. The algorithm code video as a compact set of the temporal and spatio volume, while consider spatio-temporal composition order to account of spatial and temporal context information. The hierarchy achieved by constructing a codebook of its video volumes. Then large context volume contains many spatiotemporal volume has to consider. These ensembles used to construct probabilistic models of video volume and its spatio-temporal composition. The algorithm applied in three available videos dataset for the action recognition over different complexity (Weizmann, MSR and KTH). The result is superior to other approach and better in case of single training data example and the cross-data activity recognition. The result is highly competitive over state of art method. However, major advantage of this approaches, does not required foreground and background tracking and segmentation, it is susceptible to the analysis on line real time. The proposed method could easily extend to the multi action localization and action retrieval by modifying inference mechanism. Since the proposed method code the video used to spatio-temporal volumes and its compositional information, it could not impose any type of constraints over the video content. Therefore, it may be extended unconstraint video matching and the content based search. The main advantage of the propose algorithm for activity recognition in the video it's not required a model of event. However, it has some drawback that does need to address in future work.

*B. Activity recognition model with joint representation in 3D space* : In this paper [4] recognized that the multi-level modality and perspective to representation of the joints and the 3D action recognition. In certain the RGB sequences and the depth images, construct the best differences motion history image and after recognize many perspective calculation for getting motion processes, then these histograms extract the gradient from the each calculation to explain the target motion, finally multiperspective and the multi projections joint represent, the recognition and discriminant model proposed challenges for human activity recognition. The MSR 3D actions mostly experiment to showing the difference between two motion images, two modalities history and the performances are better than the MHI at the same time, these descripted technique also efficient and very strong what's more to represent and recognize model to improve the further performances.

## II. Proposed Methodology

We have to build a new approach on the basis of the differences of the skeletal joint in spatial domain and temporal domains. Moreover, after on normalized data, we are applying principal component analysis (PCA) to finding the Eigen joints by reducing the noises and redundancy on joint differences. Thus, after extracting the set of frames we implements classification techniques Principal Component Analysis (PCA) and Artificial Neural Network (ANN) respectively with some variants for classify our all different gesture models. Accordance with the image classification we avoided quantization of the frames to class distances and descriptor, alternatively of the videos to videos distances. In addition the efficient method performed activity recognition by operated whole video sequences. The scope of these work is widely applied many number of the real world application like as human computer interaction, health issues, video surveillances and video search based on contents. The entire work mainly concentrate on video sequences of activities which captured by the RGB cameras.

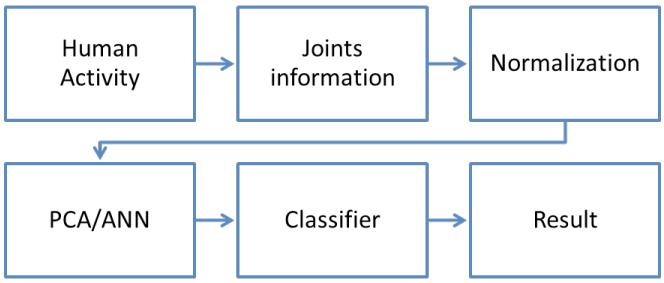


Fig.1 Graphical representation of proposed methodology

### *A. Human Activity:*

Fig.2- Corresponding activity and depth image of dataset top to down and left to right (1-Brushing teeth. 2-Working on computer. 3- Cooking (chopping). 4-Talking on the phone. 5- Drinking water. 6- Opening pill container. 7- Talking on couch. 8- Writing on whiteboard)[27].

Human activity recognition is an important functionality in any intelligent system designed to support human daily activities. the measurement of image or camera motion and more on the labeling of the action taking place in the scene.Moreover the several activity is performed in real-time environment shown in Fig 1 where subject person is perform daily routine work such as Brushing teeth, working on computer etc. while our kinet is capturing the activity with help of joint angles information. During our experiment we use all male dataset in kitchen and corridor environments. We are assuming that a kinet is mounted on wall in the front of subject user to capture the activity perform by user. However our kinet start recording the activity of humans from initial starting to until activity is not completed. Thus we have set of video image data for each individual activity. We have currently 25 joint angles for human body .

### *B. Joint information from Kinect:*

However, the total number of joints is 15. Where 11 joints have both the joint orientation value and the joint position value, and 4 have only positions value. The values of orientation and position are in following format

F = Po(1), Pp(1), Po(2), Pp(2).....Po(11), Pp(11)....Pp(15)

Where F is the frames and Po = orientation values of the joints which are 3×3 matrix stored and follows by

= 0, 1, 2, 3, 4, 5, 6, 7, 8, Co

Co is the Boolean confidence values which are o or 1

The joints which are used in to taking the data through the Microsoft kinect are given as follow: (a) Head (b) Neck (c) Torso (d) Left Shoulder (e) Left Elbow (f) Right Shoulder (g) Right Elbow (h) Left Hip (i) Left Knee (j) Right Hip (k) Right Knee (l) Left Hand (m) Right Hand (n) Left Foot (o) Right Foot .

1. *Differences between orientations and joint positions :*

The joints positions value is more accurate than the joints angle. The explanation of this point we have to compare two methods of computing a hand position in game. First method is taking the position of hand joint in API. The other method is to take torso position and orientation, both shoulder and elbow joints angle. Typically the result of hand position will different from from one returned by API because avatar will have will different lengths than model used in skeleton API (specially consider previous mentioned point that skeleton allow body segments length to vary the time where avatar model in game have fix length).the position will be match if segment length match exactly same at all time. The hand positions compute using angle driven method typically noisier other than the hand positions return direct from API. The result we have recommend by using joint position when possible.Unfortunally this method is not practical for game which based on avatar that's have need to drive using the joints angle. In that case the available option is to use either joint angle and deal the noisy hand and feet, one more way to use the joint position are constraint in post processing which have compute modify the joint angle better tuned avatar.

2. *Acquisition Module :* Microsoft Kinect - An active stereo device which is having basically three important modules. Which Shown in Fig. 3

- RGB Camera
- Depth Sensor
- Array of four mics( provides four streams of the data).
- Color Stream: In this stream its provide captured live video stream.
- Depth Stream: It's captured the each pixel with the depth information having image acquired by the kinect sensor.
- Skeletal: Stream: In our work we have to take data of different–different person for perform different activity through this we get the X, Y and Z coordinates for 15 skeleton joints which are head, neck, right shoulder, right elbow, right hand, left shoulder, left elbow, left hand, torso centre, right hip, right knee, right foot, left hip, left knee and left foot.
- Audio Stream: Kinect has 4 mics array which are used to capture and gives 4 channel audio.

The most important stream provided is the skeleton stream. Kinect has the capability to infer the body positions. It is capable to do so with the help of structured light with which it created the depth map which was discussed earlier and a machine learning algorithm. The light used by the kinect is infrared laser which. This pattern of light is projected on the object which is then analyzed by infrared camera on the kinect to create the depth map. Kinect can be initialized In these streams the most important stream is skeleton stream. Kinect is capable to find the body position. It's also capable to do more with help of structure light which are created the depth map discussed in machine learning algorithm. The lights which are used in kinect are the infrared laser light. The infrared lights are projected on object which analysed by the kinect camera to create depth map.

The light which is used in kinect is infrared light. This infrared light projected on object which is analysed by the camera and creates the depth map of the object. Kinect could be able to analysed capture colour of the frames under different resolutions and different speeds.

- 12 FPS: 1280x960 RGB
- 15 FPS: Raw YUV 640x480
- 640x480
- 30 FPS: 80x60, 320x240, 640x480

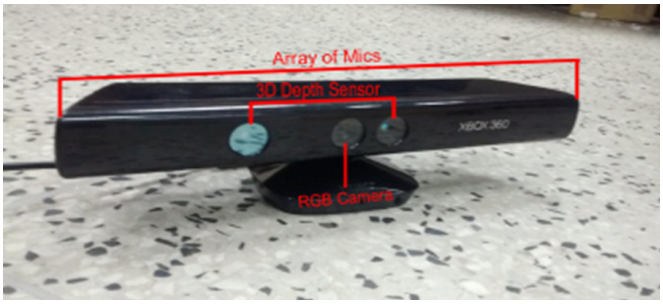


Fig 3 Microsoft kinect XBOX260

This method to finding the body position is not sufficient. Therefore to find them machine learning algorithm used which called randomize decision forest [21] which are trained by using more than thousand samples which has been skeletons associated. These algorithms learned to find the 3D joint position gives depth image. Microsoft Kinect used for the image acquition.

### *C. Image Acquisition :*

In this section we describe that the how static activity image is obtained in the real time. For the acquisition of the activity gesture, Microsoft kinet used. The following steps are in image acquisition:

(1) Colour image frames extraction: Out of various resolutions available we have to obtained only 640x480 resolution images.

(2) Depth image frame extraction: It is also obtained at the resolutions of 640x480 images.

(3) Skelton data used to track and extract the activity of user.

(4) Background subtraction

For calculation of distance to the pixel from kinect sensor actual value of the pixel are shifted 3 places in depth frame (depth point) to

right [22]. The below statements are in C language to show the work.

$$\text{Depth= depth point} << 3 \quad (1)$$

The depth values calculated in the millimetres and the range of the Microsoft kinect sensor is 0.4 meters to 8 meters. If the object is closer or outer than this range can't be resolved.

Skelton streams are the most important features of Microsoft kinect. Its provide the position and location of the persons whether they tracked or not. The skeletons which are not tracked are given to zero value returned. Kinect tracked the skeleton in two modes:

- Seated mode
- Default mode

Default mode tracked the all 15 joints and in seated mode the person could be tracked only the upper body part having 10 joint positions is obtained. The most important uses of the depth map are background subtraction from the frames. That pixel which doesn't belonging to region of the interests subtracted. So only that pixel remains which have redundant to zero intensity value.

(1) Background subtraction: Kinect is used to extract region of the interest and background subtraction. The data available in the form of skeleton to get position of the left hand i.e (xh ,yh) and left wrist (xw , yW).

$$\text{Hand length} = 3* \max\{Xabs(xh- xw),Yabs(yh- yW)\} \quad (2)$$

Where, the max is the maximum values and Xabs,Yabs is the absolute value. We have to set the minimum size of the hand is 95×95 pixel so same hand image will be determined even that both hands and wrist pixel values are coincide.

One more thing noted that in the kinect there have two camera RGB and other is infrared. There have some distance between them the region of that is depth image have not aligned. Now what meant that some pixels are in both images but that's would be at different location. Let's assume that pixel A is in color image located at (x, y), and the pixel in depth images located at ( x + δx, y + δy) i.e this should be slightly shifted. Therefore, after taking the depth region of interest (ROI) frames, the each separate pixels mapped in the color frame. That's every pixels in depth image , we have to find location in the color image and then color intensity. Then the background subtraction process is done. Now we have to set pixels and depth information about that, replace depth information corresponding to color information and that's are in the following range.

$$\text{Depth-cutoff} < \max(\text{hand\_depth}, \text{wrist\_depth}) \quad (3)$$

All the pixel value, which has the depth value, is above than the depth cutoff shown in the black color (zero intensity). Now the resultant image that's shown without the unwanted background pixel. Kinect programmed to only track the skeleton, which are nearest to kinect sensor. Therefore, its recognize the activity of one users at one time.

### *D. Normalization Technique*

Normalization [26]is a process to change the range of the pixels intensity value. Normalization also called the histogram stretching or contrast stretching. In general field of data processing such as the image processing, it refers to as the dynamic range expansion. The purpose of the dynamic range expansion in various applications usually to bring image or the other type of the signal into the range, which are normal or more familiar to sense hence the terms normalization. Often motivation is to achieve consistency in the dynamic range for set of data, images or signal to avoid the mental distractions or fatigue.

Normalization transform the n-dimensional grayscale images with the intensity values in range (min, max) into the new image with the intensity value in range (new min, new max). All the elements are scaled in the range of -1 to +1 in the normalization technique. The main advantage to normalization is to remove the infraclass variation between the data if the same activity is performed by different persons.

$$In=(I-Imin)\ ((\text{new max}[-\text{newmin})])/\max[-\min]+ \text{newmin} \quad (4)$$

Furthermore, we have the intensity range between 50-180 of the images and we have to normalize that into the range of 0-255. In the processing of normalization we have to subtract 50 from given intensity values, then the final range are between 0-130. After that, all pixel intensity multiplied 255/130 to making in a given range. Normalization technique is a nonlinear process, these are done when the values are not in a linear relationship, in that case following formula are used,

$$In = (\text{newmax-newmin})1/(1+e\hat{}(((\beta-I))/\alpha))+\text{newmin} \quad (5)$$

Where α defines the width of input intensity range and the β defines the intensity around which range is centered.

In our experiments, we are trying to normalize the Fc based on videos, which are taken by the Microsoft kinect camera, which based on entire activity videos. As given in Fig. 4 every frames we have N joints that's may result in large feature dimensions Fcc, Fcp, Fci containing N(N - 1)/2,

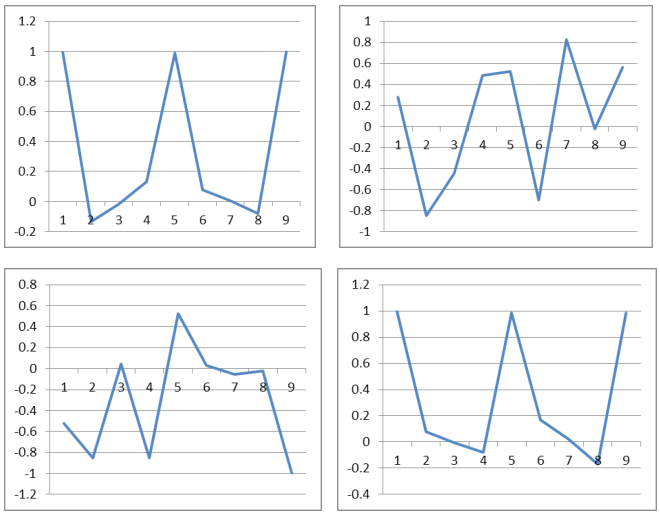

Fig 4. Normalized data joints from top to down and left to right(head, left shoulder, right shoulder, left hip).

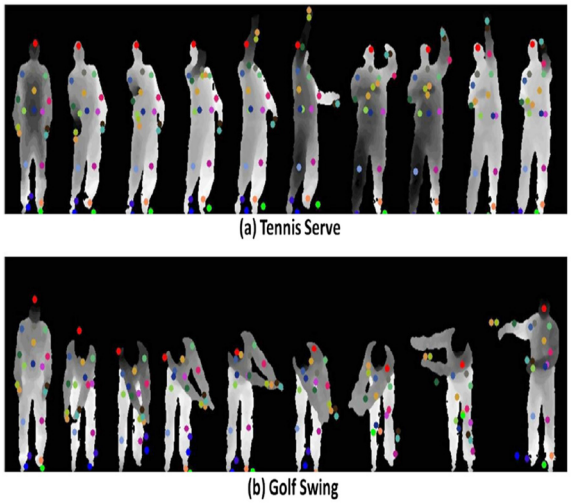


Fig 5. sequences of sampled depth images and skeleton joints of activity (a) Tennis Serve along with (b) Golf Swing. Each depth image consists of 20 joints. [26]

N^2, N^2 pairwise comparison. Each comparison generates the 3 element (Du, Dv, Dd). in end Fnorm is with dimensions of 3*(N(N-1)/2 + N^2 + N^2).

However, if we have to find 20 skeletal joints in the every frame then the Fnorm have the 2970 length. As the skeletal joints have earlier high level information recover by depth maps, these larger dimensions having noises and redundant. After that we have to apply principal component analysis to reduce the noises in generalized Fnorm. The final representations are Eigen joints which are action descriptor of each frame. We are observing that the most of Eigen values are covered by first few leading eigenvector.

### *E. Classification Methods*

We have to use Principal component analysis for the feature extraction from the kinect dataset and different classification technique like Euclidean, negative and Manhattan as a classifier and neural network technique

#### *1) Principal Component Analysis :*

Principal component analysis is a feature extraction technique from the data sets. New set of variable component are generated that's principal component. In the terminology of information, we want to find out significant information in images with several steps as givn followings.

**Step1**: Zero Mean: Suppose we have the data X has N variable and M observation to find the mean of data across M observation to find a mean vector $\bar{X}$. After that subtract the mean from data i.e.

$$A=X-X \tag{6}$$

Now the data have zero mean.

**Step2**: Find covariance matrix: The next step is find the covariance matrix from the above data having size of the data matrix A is N×M. The covariance matrix given by $C=A.A^T$ have the size N×N. If the variable larger i.e. of order of ten thousand, then the covariance matrix will be very large. After that find Eigen vector will be computationally tough task have Eigen vector V1 will be size of N×1.So slightly different method to utilized to finding Eigenvectors which is next.

**Step3**: Finding Eigen vector: To easily finding the Eigen vector/ principal component of the covariance matrix mapped from a lower dimension subspace. Instead of $C=A.A^T$ are used. Consider M is less than the N then that's give a very small covariance's matrices having the size of M×M and every Eigen matrix V1 having size of M×1. Then Eigen vectors have needs to mapped original higher dimension space, the Eigen vectors V1 multiplied by the original normalize data matrix A. there for the Eigenvectors U1 is given by U1=A.V1. Now these eigen vector have size of N×N.

**Step4**: Dimension Reduction: Now, the $\phi$ eigen matrix in columns sorted in the descending order from the eigen values. First p columns taken as principal components. Then the size of $\phi$ is N×p. For reducing the dimension of the data these operation having used,

$$A' = \phi^T T; \tag{7}$$

Where the size of matrix A′ is p×M that are reduced dimensionality.

**Step5**: Variance Conservation: To find the how many principal components having sufficient to represented the data to less losses method for variance conservation [21]. We are more interested to retaining the many components conserve the 99% variances' of the data. If p= 0 means no principal components retained, then 0% of data retained. To generalized, consider that {λ1,λ2, λ3, λ4……. λn} are eigen values across the eigen vectors U1 of the $\phi$ matrix column wise sorted eigenvalues according that matrices. If p is the retained principal components then the percentage of the variance retained/ conserved are calculated as,

$$\text{Variance}=(\sum_{j=1}^{p}\lambda j)/(\sum_{j=1}^{p}\lambda j) \tag{8}$$

Our target is to choose smallest value of p such as variance>= 0.99.

**Step 6**: Reconstruct the data: the original data could be constructed by A′ as,

$$\bar{A} = \phi A' \tag{9}$$

It's noted that the $\bar{A}$ have dimension N×M have an approximation of original data A.

However, We have to use following difference based classification techniques.

- Euclidean distance

If the two points A, B is having Cartesian coordinates A ( A1 , A2 , A3,……An) & B (B1 , B2 , B3…….Bn), then the Euclidean distance between them ,

$$D(A, B) = D(B, A)=\sqrt{([[(A]_1-B_1)]]^2+ [[[(A]_2-B_2)]]^2+ [[[(A]_n-B_n)]]^2}$$

If Euclidean vector is a position of points a Euclidean n-space. So A & B are eigen vector.

$$\| A \| = \sqrt{([A1]]^2+[[A2]]^2 \ldots [[An]]^2} = \sqrt{(A.A)}$$

A vector also described a line segment from origin of Euclidean space to the point at that space.

- Manhattan distance

Manhattan distance basically the distance between two points which is measured along with axes at right angles.

$$D(A, B) = \| A - B \| = \sum_{i=0}^{n}[[| Ai-Bi|]] \tag{10}$$

Where (A, B) are vectors, A = (A1, A2, A3… An) &

B = (B1, B2, B3… Bn), for example distance between points (A1, A2) & (B1, B2) is the,

$$= | A1 - A2 | + | B1 - B2 | \tag{11}$$

- Negative distance

Negative distances are the weighted function which applies to input to get the weighted inputs. For example if we have to random weight matrix A and B then the negative distance X defind as

$$X = -\text{sqrt}(\text{sum}( A - B)^2) \tag{12}$$

We use several distances based classifiers to compare the distance between dataset.Therefore, the variance of data actions more efficiently evaluated.

#### *2)* **Artificial Neural Network :**

This section elaborates decision making procedure of a well-known classification technique i.e ANN (artificial neural network).A classification procedure generally encountered when a predefined p class/group has to be assigned to an object over a number of calculating attributes associated with that object. ANN demonstration requires the processed data set mentioned earlier. We have chosen 70% from the activity dataset for training while 30% of the testing data set. We have developed eight classes having fourteen samples each afterwards ANN Mat lab toolbox has been utilized we have generated the final class i.e. target class.

The class having a maximum score to the remainder of the classes is determined of the output neuron. The back propagation performs the task of train/retrain artificial network. Feed forwarding action has been applied to an input provided to the artificial network. As a result we are getting better output for iterations S.

Errors in all the iterations S are analysed and again feed forwarded to the artificial neural network to adjust all the weights along with biases.

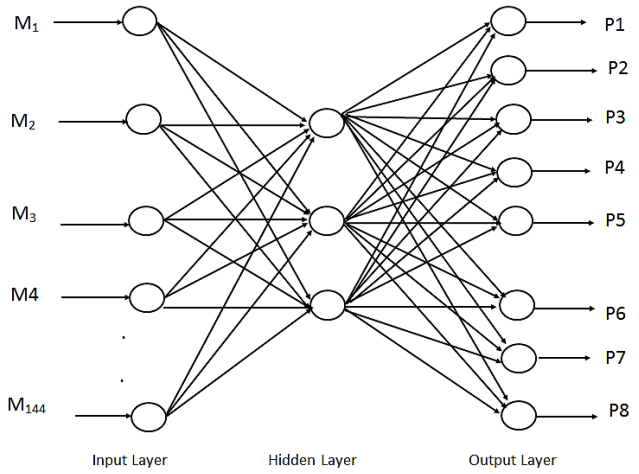


Fig.6 The functioning diagram of artificial neural network

Let Mij(s) be a weight for interface neuron i and j.

Let the result generated with neuron j be Pj.

The error is evaluated with the help of equation 13

$$Ej(s) = K(s) - pj(s) \quad (13)$$

Where K, E and q represents desired output, error and output respectively weights can be modified with the help of equation 14

$$Mij(s+1) = Mij(s) + \alpha\beta i(s)pj(s) \quad (14)$$

Where α indicates a real constant number, also called learning rate and its range is less than 1. βjis evaluated with the help of equation 13 and 14 respectively.

$$Bj\ (s) = Ej(s)\phi j'(\mu j(s)) \quad (15)$$

$$\mu j\ (s) = \sum iMij\ (s)\ qj\ (s) \quad (16)$$

Where ϕ indicates transfer function.

In the architecture of neural network consist 3 type neuron layers input, hidden and output layer.In the feed forward network(FFN) the signals are flow from input units to output unit strictly in FFD. The processing of the data extend from multiple layers of the units but there are no any feedback connection available and in recurrent network consist of feedback connections. Activation value of units undergoes the relaxations process of network involves to stable state in that activation doesn't change more. In one other application changes of activation value of neuron significant, such as dynamical output of the network.

The neural network is configuring as the application combination of input produce the desire group of the output. There are various method set strength of connection, exit. One other way to set weight finally by using forward knowledge. One other method to train the neural network to feed it teach pattern and change it weight according some learning rule. The learning situation classified into three sorts in neural network.

## III. Result analysis

In this section, results of proposed system have been demonstrated considering the different parameters such as performance and percentage accuracy of classification. We have also calculated the errors in terms of mean square error (MSE) of training samples of dataset.

- *Dataset used*

Cornell based dataset having video sequences of human activities in the form of RGB images has been captured by Microsoft Kinect camera associated with depth map. Where each frame consists of fifteen skeleton joints available in world coordinates. All the action videos are of thirty Hz, each of 640×480 resolution. Dataset is having eight different activities in different environment on a single subject. All the eight activities have been selected from the human common activities as depicted in Fig. 2.

- *Platform used*

All the proposed system for automatic human action recognition using Eigen vectors have been implemented and analysed in matlab toolbox on version R2013a successfully. Further we have compared the result with existing related publications that has been done so far.

- *Class Variations among data*

Here we have done comparative analysis of inter class variations and intra class variations of the Cornell dataset of human activities. Intra class variation is defined as the variation exists within class and Inter class variation is defined as the variation exists between two different classes. A set of classes is said to be well if there is a low intra class variation and high inter class variation as our dataset classes are having the low intra class variation and high inter class variation mentioned in Fig. 7. Regions in red are a class different from the green region class. It has been clearly observed that both the classes is well separated to each other.

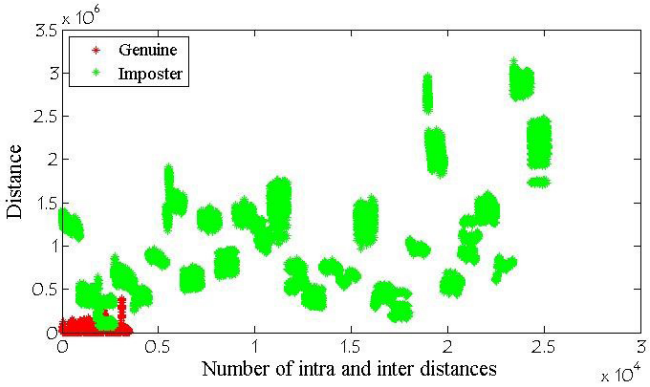


Fig. 7. intra and inter class distance distribution

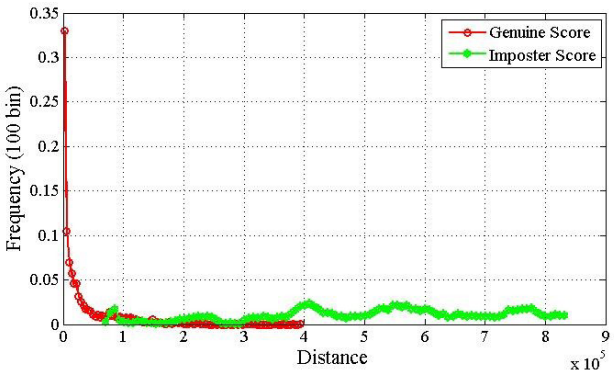


Fig. 8 intra and inter class distance histogram

- **Result comparisons**

Here are the details of all the comparative results by using different techniques such as Euclidean distance, Negative distance, Manhattan distance and ANN shown in Fig. 9. We have trained the dataset with 15 frames, 25 frames and 30 frames and tested by 3 samples from each class. While we are getting more accuracy when number of samples

are increased from 3 to 6 as Fig. 10 has achieved more accurate result when number of sample is increased to 6.

TABLE I.
RESULTS COMPARISONS WITH 3 SAMPLES USING PCA

| Methods Vs Results | Tested frames (15 for each class ) | Tested frames (25 for each class ) | Tested frames (30 for each class ) | Aggregate results |
|---|---|---|---|---|
| **Euclidean distance** | 79.2 % | 83.3 % | 91.66 % | 84.72 % |
| **Negative distance** | 75.0 % | 79.2 % | 83.3 % | 79.5 % |
| **Manhattan distance** | 79.2 % | 83.2 % | 87.5 % | 83.3 % |
| **ANN** | 92.5 % | 94.5 % | 98.2 % | 95.1 % |

TABLE II.
RESULTS COMPARISONS WITH 6 SAMPLES USING PCA

| Methods Vs Results | Tested frames (15 for each class ) | Tested frames ( 25 for each class ) | Tested frames ( 30 for each class ) | Aggregate results |
|---|---|---|---|---|
| **Euclidean distance** | 87.5 % | 91.6 % | 95.8 % | 91.66 % |
| **Negative distance** | 87.5 % | 91.6 % | 93.7 % | 90.9 % |
| **Manhattan distance** | 87.5 % | 91.6 % | 93.7 % | 90.9 % |
| **ANN** | 92.5 % | 94.5 % | 98.2 % | 95.1 % |

- **Confusion matrix**

The given Confusion matrix is a tabular representation of classification between actual and predicted classes. Each row and column shows the different class of human activity. In confusion matrix correct entries are represented by diagonal cell and incorrect entries is represented by off-diagonal entries. Rows and column indicates the actual and predicted output of the classifier.

TABLE III.
CONFUSION MATRIX OF ACTIVITY USING ANN

| Gesture type | Brushing teeth | Working on the computer | Cooking | Talkig on the phone | Drinking Water | Opening pill Container | Talking on the couch | Writing on the whiteboard |
|---|---|---|---|---|---|---|---|---|
| Brushing teeth | **100%** | 0% | 0% | 0% | 0% | 0% | 0% | 0% |
| Working on the computer | 0% | 98% | 2% | 0% | 0% | 0% | 0% | 0% |
| Cooking | 0% | 0% | 99% | 1% | 0% | 0% | 0% | 0% |
| Talking on the phone | 0% | 0% | 2% | 97% | 1% | 0% | 0% | 0% |
| Drinking Water | 0% | 0% | 2% | 0% | 98% | 0% | 0% | 0% |
| Opening pill Container | 0% | 0% | 0% | 0% | 0% | 100% | 0% | 0% |
| Talking on the couch | 0% | 0% | 0% | 0% | 3% | 0% | 97% | 0% |
| Writing on the whiteboard | 0% | 0% | 0% | 0% | 0% | 0% | 0% | 100% |

- **Accuracy assessment**

Accuracy assessment is one of the important task for analyzing the accuracy of proposed system. Fig. 4.5 is showing the mean square error at different epoch levels as the graph has achieved the best performance at epoch level 51 in terms of validation that is 0.0065999 MSE.

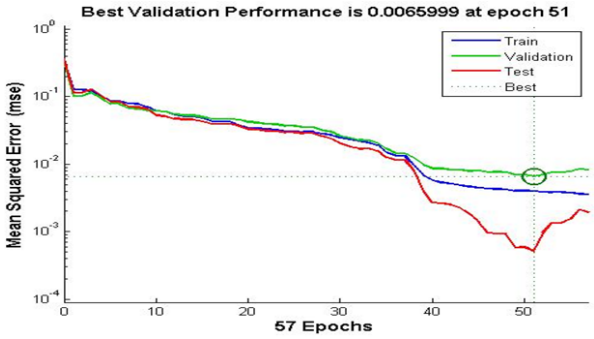


Fig. 9 Performance Analysis with MSE.

## IV. Conclusion And Future Work

In this research work we proposed a activity recognition technique which are based on the Eigen joint captured by the Microsoft kinect camera for different distance based classifier technique. Three distances are used in my work and compared the result by the other classification techniques. We have to see that the 10-12 % frames are more than enough to recognize the activity with the best accuracy from the activity video. In other computer vision systems, mostly the human activity recognitions are highly depends on context. The activities are different in every situation. Besides, what composes an activity is a part of the perception. It would be interesting to debate we have a wide range of scenarios can define a common set of action or not. Any recognition problem is finding the key to strong representative facility Pattern sets. Action a 4D event, coordinates (3D) points in the human body shape is travelling with direction of time. On abstraction facility level, variance for style changes, anthropometry changes, see the dressing changes Speed changes, noise tolerance, feature extraction and ease of calculation speed etc. For dynamic time system are problem to be seen2D or 3D representations by various trade -offs of the details that are associated with human motion another interesting problem is therefore, above all possibility to obtaining a group of common properties, which will act better in view of the challenging problem. Other interesting aspects are the questions that must be taken in part to system to better performance receive. Example ,variance On the scene by finding invariant features, feature extraction level can be controlled working with different approaches in the training level of the training include samples dataset or view level classifier using invariant matching technique. Like this, the complexity of the system which blocks up that way must be introduced the best performance of integrated system is better topic matter for investigate. Speed, accuracy, and robustness are typical contradictory of vision systems. That preference should be given to the order depending on the application area of these three performances measures. In the end, whether it will work satisfactorily, which is possible to build a common identification system battle for various applications to answer thought-annoying question is which are still exploring abroad amount of analysis in that area is needed.

In our recognition approach we have to recognize the activity of single object. My approach assumes that single person have present and only one act perform at a time. In future we have to extend the work for the multi object to perform different activities at a time, and each human activity recognize separately. The technique can be advanced to angle changes of different types of activity by different camera in the dataset.

## V. Conclusion

A conclusion section is not required. Although a conclusion may review the main points of the paper, do not replicate the abstract as the conclusion. A conclusion might elaborate on the importance of the work or suggest applications and extensions.

## References


[1] Cedras, Claudette, and Mubarak Shah. "Motion-based recognition a survey."Image and Vision Computing 13.2 (1995): 129-155.

[2] Ye, Juan, Simon Dobson, and Susan McKeever. "Situation identification techniques in pervasive computing: A review." Pervasive and mobile computing8.1 (2012): 36-66.

[3] Augustyniak, Piotr, et al. "Seamless tracing of human behavior using complementary wearable and house-embedded sensors." Sensors 14.5 (2014): 7831-7856.

[4] Liu, An-An, et al. "Coupled hidden conditional random fields for RGB-D human action recognition." Signal Processing 112 (2015): 74-82.

[5] Raman, Natraj, and Stephen J. Maybank."Action classification using a discriminative multilevel HDP-HMM." Neurocomputing 154 (2015): 149-161.

[6] Foggia, Pasquale, GennaroPercannella, and Mario Vento."Graph matching and learning in pattern recognition in the last 10 years." International Journal of Pattern Recognition and Artificial Intelligence 28.01 (2014): 1450001.

[7] Li, Y. F., Jianwei Zhang, and Wanliang Wang. Active sensor planning for multiview vision tasks.Vol. 1. Heidelberg: Springer, 2008.

[8] Xiaodong Yang; YingLiTian, "EigenJoints-based action recognition using Naïve-Bayes-Nearest-Neighbor," Computer Vision and Pattern Recognition Workshops (CVPRW), 2012 IEEE Computer Society Conference on , vol., no., pp.14,19, 16-21 June 2012.

[9] Xia, Lu, Chia-Chih Chen, and J. K. Aggarwal. "View invariant human action recognition using histograms of 3d joints." Computer Vision and Pattern Recognition Workshops (CVPRW), 2012 IEEE Computer Society Conference on.IEEE, 2012.

[10] Vantigodi, S.; Babu, R.V., "Real-time human action recognition from motion capture data," Computer Vision, Pattern Recognition, Image Processing and Graphics (NCVPRIPG), 2013 Fourth National Conference on , vol., no., pp.1,4, 18-21 Dec. 2013

[11] Vantigodi, Suraj, and VenkateshBabuRadhakrishnan. "Action recognition from motion capture data using meta-cognitive rbf network classifier." Intelligent Sensors, Sensor Networks and Information Processing (ISSNIP), 2014 IEEE Ninth International Conference on. IEEE, 2014.

[12] Kao, Wei-Chia, Shih-Chung Hsu, and Chung-Lin Huang."Human upper-body motion capturing using Kinect." Audio, Language and Image Processing (ICALIP), 2014 International Conference on.IEEE, 2014.

[13] Liang, Yan, et al. "Action Recognition Using Local Joints Structure and Histograms of 3D Joints." Computational Intelligence and Security (CIS), 2014 Tenth International Conference on.IEEE, 2014.

[14] Ijjina, Earnest Paul, and C. Krishna Mohan. "Human action recognition based on motion capture information using fuzzy convolution neural networks."Advances in Pattern Recognition (ICAPR), 2015 Eighth International Conference on.IEEE, 2015.

[15] H. Gunes, M. Piccardi, Automatic temporal segment detection and affect recognition from face and body display, IEEE Trans. Syst. Man Cybern. B 39 (1)(2009) 64–84.

[16] H. Liu, M. Sun, R. Wu, S. Yu, Automatic video activity detection using compressed domain motion trajectories for H.264 videos, J. Visual Commun.Image Represent. 22 (5) (2011) 432–439.

[17] H. Pirsiavash, D. Ramanan, Detecting activities of daily living in first-person camera views, in: Proc. IEEE Conference on Computer Vision and Pattern Recognition, 2012, pp. 2847-2854

[18] K. Schindler, L. Gool, Action snippets: how many frames does human action recognition require? in: Proc. IEEE Conference on Computer Vision and Pattern Recognition, 2008, pp. 1–8.

[19] L. Xia, C. Chen, J. Aggarwal, View invariant human action recognition using histograms of 3D joints, in: IEEE CVPR Workshop on Human Activity nderstanding from 3D Data, 2012.

[20] Z. Zhang, D. Tao, Slow feature analysis for human action recognition, IEEE Trans. Pattern Anal. Mach. Intell. 34 (3) (2012) 436–450.

[21] Andrew Ng. Cs229 machine learning autumn 2013. http://cs229. stanford. edu. Accessed: 2014-06-20.

[22] J. Sun, X. Wu, S. Yan, L. Cheong, T. Chua, J. Li, Hierarchical spatio-temporal context modeling for action recognition, in: Proc. IEEE Conference on Computer Vision and Pattern Recognition, 2009, pp. 2004–2011.

[23] A. Bobick, J. Davis, The recognition of human movement using temporal templates, IEEE Trans. Pattern Anal. Mach. Intell. 23 (3) (2001) 257–267.

[24] K. Schindler, L. Gool, Action snippets: how many frames does human action recognition require? in: Proc. IEEE Conference on Computer Vision and Pattern Recognition, 2008, pp. 1–8.

[25] O. Boiman, E. Shechtman, M. Irani, In defense of Nearest-Neighbor based image classification, in: Proc. IEEE Conference on Computer Vision and Pattern Recognition, 2008, pp. 1–8.

[26] Yang, Xiaodong, and YingLiTian. "Effective 3d action recognition using

[27] eigenjoints." Journal of Visual Communication and Image Representation 25.1 (2014): 2-11.

[28] Online Access http://pr.cs.cornell.edu/humanactivities/data.php

[29] Semwal, Vijay Bhaskar, et al. "Biped model based on human Gait pattern parameters for sagittal plane movement." Control, Automation, Robotics and Embedded Systems (CARE), 2013 International Conference on. IEEE, 2013.

[30] Semwal, Vijay Bhaskar, Manish Raj, and G. C. Nandi. "Biometric gait identification based on a multilayer perceptron." Robotics and Autonomous Systems 65 (2015): 65-75.

[31] Semwal, Vijay Bhaskar, et al. "Biologically-inspired push recovery capable bipedal locomotion modeling through hybrid automata." Robotics and Autonomous Systems 70 (2015): 181-190.

[32] Gupta, Jay Prakash, et al. "Human activity recognition using gait pattern."International Journal of Computer Vision and Image Processing (IJCVIP) 3.3 (2013): 31-53.

[33] Semwal, Vijay Bhaskar, Manish Raj, and G. C. Nandi. "Multilayer perceptron based biometric GAIT identification." Robotics and Autonomous Systems. Available online 21 (2014).

[34] Gupta, Jay Prakash, et al. "Analysis of Gait Pattern to Recognize the Human Activities." arXiv preprint arXiv:1407.4867 (2014).


**Ajay Kumar** received the M.Tech degrees in information technology from Indian Institute of Information Technology Allahabad, India in 2015. He is the recipient of the GATE scholarship from the Ministry of Human Resource Development, Government of India. His area of interests are Control System, Control Robotics, Image Processing, Digital Electronics.

**Anil Kumar** received the M.Tech degrees in information technology from Indian Institute of Information Technology Allahabad, India in 2015. He is author of more than four research papers in the field of Robotics and Artificial Intelligence. He is the recipient of the GATE scholarship from the Ministry of Human Resource Development, Government of India. His area of interests are robot motion planning, Temporal Logic, Path Planning.

**Satish Kumar Singh** (M'11-SM'14) is currentlyworking as an assistant professor in Indian Institute of Information Technology, Allahabad, India. He has completed his Ph.D., M. Tech. & B. Tech in 2010, 2005 and 2003 respectively. He is having more than 10 years of experience in academic and research institutions. He has several publications in international journal and conference proceedings of repute. He is member of various professional societies like, IEEE and IETE etc. He is an Executive Committee Member of IEEE Uttar Pradesh Section. He is serving as editorial board member and reviewer for many international journals. His current research interests are in the areas of digital image processing, pattern recognition, multimedia data indexing and retrieval, watermarking and biometrics.

**Dr. Rahul Kala** received the B.Tech. and M.Tech. degrees in information technology from the Indian Institute of Information Technology and Management, Gwalior, India in 2010. He received his Ph.D. degree in cybernetics from the University of Reading, UK in 2013. He is currently working as an Assistant Professor in the Indian Institute of Information Technology, Allahabad, India in the Robotics and Artificial Intelligence Laboratory. He is the author of three books and over 70 papers. His recent book is on robotic planning is entitled Intelligent Planning for Mobile Robotics: Algorithmic Approaches (IGIGlobal Publishers, 2013). He is a recipient of the Commonwealth Scholarship and Fellowship Program from the UK Government; the Lord of the Code Scholarship from RedHat and the Indian Institute of Technology Bombay; and the GATE scholarship from the Ministry of Human Resource Development,Government of India.

# Spiking Activity of a LIF Neuron in Distributed Delay Framework

Saket Kumar Choudhary, Karan Singh, *Vijender Kumar Solanki

*Anna University, Chennai, Tamilnadu, India*

***Abstract* — Evolution of membrane potential and spiking activity for a single leaky integrate-and-fire (LIF) neuron in distributed delay framework (DDF) is investigated. DDF provides a mechanism to incorporate memory element in terms of delay (kernel) function into a single neuron models. This investigation includes LIF neuron model with two different kinds of delay kernel functions, namely, gamma distributed delay kernel function and hypo-exponential distributed delay kernel function. Evolution of membrane potential for considered models is studied in terms of stationary state probability distribution (SPD). Stationary state probability distribution of membrane potential (SPDV) for considered neuron models are found asymptotically similar which is Gaussian distributed. In order to investigate the effect of membrane potential delay, rate code scheme for neuronal information processing is applied. Firing rate and Fano-factor for considered neuron models are calculated and standard LIF model is used for comparative study. It is noticed that distributed delay increases the spiking activity of a neuron. Increase in spiking activity of neuron in DDF is larger for hypo-exponential distributed delay function than gamma distributed delay function. Moreover, in case of hypo-exponential delay function, a LIF neuron generates spikes with Fano-factor less than 1.**

***Keywords* — Distributed Delay Framework, Fokker-Planck Equation, Gamma Distribution, Hypo-exponential Distribution, Stationary Probability Distribution, Spiking Activity.**

## I. Introduction

There are a number of neuron models depending on biophysical and electrical properties of a neuron suggested in literature [1–5]. Among these neuron models, Leaky integrate-and-fire (LIF) model has become a backbone for theoretical as well as experimental investigation of neuronal dynamics due to its simplicity and analytical solvable capability [5, 6, 7]. This model is an RC-circuit equivalent representation of a neuron with additional spiking constraint and is widely used for mathematical explanation of bio-physical mechanism and information processing of neurons [1, 2, 4, 8, 9]. Based on some specific properties, many variants of LIF model are suggested in literature [1, 5, 7, 8]. These neuron models explain neuronal dynamics adequately, but when we talk about memory, we have to rely on group of few neurons or neural networks. None of these single neuron models capture memory element. Recently, Karmeshu et. al. [10] have suggested a distributed delay framework for incorporating the effect of previous values of membrane potential (memory) on neuronal dynamics, in which, a kernel function is included in LIF model to capture the aggregate effect of previous values of membrane potential on its further evolution. It is a challenging problem to find an appropriate kernel function so that the resulting model can explain most of the variability in neuronal responses. To this end, Karmeshu et. al. [10] have investigated their proposed framework with exponential distributed delay kernel and noticed exponential inter-spike-interval (ISI) distribution, whereas Sharma and Karmeshu [11] have obtained transient bi-modality in ISI distribution for gamma distributed delay kernel. Choudhary et. al. [12] have studied LIF model in DDF with hypo-exponential distributed delay kernel and observed huge variability in spiking pattern of a LIF neuron as obtained in empirical data. These investigations [10, 11, 12] reflect the novelty and robustness of distributed delay framework for neuronal dynamics, but none of them suggests about the actual effect of distributed delay (memory) on membrane potential evolution and spiking activity of a neuron.

Ermentrout and Terman [2], Rudolph and Destexhe [13] have suggested methods for estimating the moments of excitatory and inhibitory conductances from stationary probability distribution of membrane potential (SPDV) for a neuron. Ruan and Filfil [14] have suggested about stability of steady state distribution of membrane potential for discrete delay case and calculated the critical values of discrete delay for stable steady state distribution of membrane potential. We are interested in investing the effect of memory element on evolution of membrane potential and spiking activity of a neuron in distributed delay framework [10]. To achieve the objectives, we have investigated the LIF model in DDF with two different memory kernel functions namely; (i) gamma distributed function (ii) hypo-exponential distributed function, and compared the findings with standard LIF neuron with stochastic input stimulus. SPDV for considered model is calculated in sub-threshold regime of a neuron, whereas, to notice the effect of memory kernel on neuronal information processing, firing rate of neuron and Fano-factor corresponding to spike-sequences is obtained.

The present article is divided in mainly five sections. After a brief discussion about literature survey and objective of article in Section 1, a massive discussion about DDF for a neuron is discussed in Section 2. This section also contains mathematical formulation of LIF model with gamma distributed kernel function and hypo-exponential distributed kernel function. Section 3 deals with SPDV of considered neuron models. Simulation based investigation for spiking activity of LIF neuron in DDF and their result interpretation is given in Section 4. Section 5 contains analysis of findings and conclusion.

## II. Distribution Delay Framework of a Neuron

Generalized form for describing the rate of change of membrane potential reads [2, 8]

$$\frac{dV}{dt} = f(V,t) + I \tag{1}$$

where $I$ is applied input stimulus and $f(V,t)$ is membrane potential-current relationship functions. Choices of $f(V,t)$ result into different kind of neuron models. The simplest representation of



DOI: 10.9781/ijimai.2016.3710

Eq. (1) is the LIF model which can be obtained by substitution of the $-\beta V$ for $f(V,t)$ LIF model with stochastic input stimulus is given as:

$$\frac{dV}{dt} = -\beta V(t) + \mu + \xi(t) \tag{2}$$

where $V(t)$ is membrane potential, $\beta$ is membrane decay constant, $\mu$ is mean input stimulus, $\xi(t)$ is delta correlated Gaussian white noise with intensity $\sigma$, i.e. $<\xi(t)>=0$ and $<\xi(t_i)\xi(t_j)>=\frac{\sigma^2}{2}$.

Karmeshu et. al. [10] assumed that the evolution of membrane potential not only depends on applied input stimulus but also on its previous values (memory) and proposed a distributed delay framework to investigate neuronal dynamics. Memory kernel function $\int_0^t K(t-\tau)V(\tau)d\tau$ is substituted for function $f(V,t)$ in Eq. (1) in DDF [10]. LIF model with distributed delay function $K(t)$ takes the form:

$$\frac{dV(t)}{dt} = -\beta\int_0^t K(t-\tau)V(t)d\tau + \mu + \xi(t) \tag{3}$$

Karmeshu et. al. [10], Sharma and Karmeshu [11] have investigated this DDF model in the presence gamma distributed delay kernel. Choudhary et. al. [12] have studied LIF model incorporating hypo-exponential distributed delay kernel in DDF. Mathematical formulations of these studies [10–12] are described in following subsections.

### *A. LIF Model with Gamma Distributed Delay Function*

Following Karmeshu et. al. [10], LIF model including gamma distributed delay reads as:

$$\frac{dV}{dt} = -\beta\int_0^t \frac{\eta^{m+1}(t-\tau)^m e^{-\eta(t-\tau)}}{m!}V(\tau)d\tau + \mu + \xi(t) \tag{4}$$

where $\eta$ and $m$ are delay and shape parameters, respectively. For $m=0$ Eq. (4) results neuron model with weak delay, which also a termed as neuron model with exponential distributed delay function, whereas, for $m \geq 1$ Eq. (4) results neuron model with strong delay [10, 11]. Incorporation of memory kernel in LIF model results a non-Markovian membrane potential process $\{V(t); t \geq 0\}$ which can be transformed into Markovian process in extended space [10].

Substitution of $U_m(t) = \int_0^t \frac{\eta^{m+1}(t-\tau)^m e^{-\eta(t-\tau)}}{m!}V(\tau)d\tau$ into Eq. (4) and further simplification results a system of coupled SDE

$$\begin{aligned}
\frac{dV}{dt} &= -\eta\beta U_m(t) + \mu + \xi(t) \\
\frac{dU_i(t)}{dt} &= -\eta\{U_i(t) - U_{i-1}(t)\} \\
\frac{dU_0(t)}{dt} &= -\eta\{U_0(t) - \eta V(t)\}
\end{aligned} \tag{5}$$

for $i \in \{1,2,...,m\}$, with initial condition $[V(t)=0$ and $U_j(t)=0 \forall j \in \{0,1,2,...,m\}$ at $t=0]$.

### *B. LIF with Hypo-Exponential Distributed Delay Function*

Sum of synaptic excitatory and inhibitory input stimulus at spike-generator-locus (SGL) in soma determines the spike generation in a neuron [15]. These excitatory and inhibitory input stimulus result excitatory and inhibitory membrane potential, respectively [16]. Choudhary et. al. [12] has applied hypo-exponential distributed kernel function to incorporate the SGL mechanism in DDF. Following Choudhary et. al. [12], LIF model with hypo-exponential distributed delay function becomes

$$\frac{dV}{dt} = -\frac{\beta\lambda_E\lambda_I}{\lambda_E-\lambda_I}\int_0^t (e^{-\lambda_E(t-\tau)} - e^{-\lambda_I(t-\tau)})V(\tau)d\tau + \mu + \xi(t) \tag{6}$$

with initial condition $V(t)$ at $t=0$, where $\lambda_E$ and $\lambda_I$ are arrival rate of excitatory membrane potential and inhibitory membrane potential.

In extended space, substitution of $U_1(t) = \int_0^t e^{-\lambda_E(t-\tau)}V(\tau)d\tau$ and $U_2(t) = \int_0^t e^{-\lambda_I(t-\tau)}V(\tau)d\tau$ into Eq. (6), model takes the form [12]

$$\begin{aligned}
\frac{dV}{dt} &= -\frac{\beta\lambda_E\lambda_I}{\lambda_I-\lambda_E}(U_1 - U_2) + \mu + \xi(t) \\
\frac{dU_1(t)}{dt} &= -\lambda_E U_1 + V \\
\frac{dU_2(t)}{dt} &= -\lambda_I U_2 + V
\end{aligned} \tag{7}$$

with initial condition $V(t) = U_1(t) = U_2(t) = 0$ at $t=0$.

## III. Stationary Probability Distribution of Membrane Potential (SPDV)

SPDV is an interesting feature in theoretical studies due to the easier experimental verification than other neuro-physiological features [17, 18]. Neuron models in DDF, represented as in Eq. (5) and Eq. (7), are systems of coupled stochastic differential equations. Calculation of probability distribution of membrane potential requires corresponding Fokker-Planck equation. Fokker-Planck equation plays a vital role in investigation of stochastic formulation of a neuron [6, 19, 20]. Fokker-Planck equations are helpful in solving the first passage time problem, calculation of firing rate of neuron and in estimation of moments of stochastic conductance. Solution of Fokker-Planck equations depends on initial and boundary conditions in a great extent [20]. There are many boundary conditions, but two of them are more useful in neuronal model context, ***(i)*** absorbing boundary ***(ii)*** reflecting boundary [2]. When membrane potential of neuron reaches at boundary (threshold value), immediately a spike is generated with the condition $p(V^{th},t)=1$, in former boundary case, whereas in later case, probability flux $J(V,t)$ remains equal to zero, i.e. membrane potential of neuron never reaches at its firing threshold. We consider the reflecting boundary conditions to calculate the stationary probability distribution of membrane potential in different cases given below.

### A. Neuronal Model Gamma Distributed Memory Kernel

Let $p^G(V,U_0,U_1,...,U_m,t)$ be the spatial probability distribution of membrane potential for LIF model with gamma distributed delay kernel. Fokker-Planck equation associated with Eq. (5) is

$$\frac{\partial p^G}{dt} = \frac{\partial}{\partial V}\{\eta\beta U_m - \mu\}p^G + \prod_{i=1}^{m}\frac{\partial}{\partial U_i}\eta(U_i - U_{i-1})p^G + \frac{\partial}{\partial U_0}\eta(U_0 - V)p^G + \frac{\sigma^2}{2}\frac{\partial^2 p^G}{\partial V^2} \tag{8}$$

with boundary conditions:

$$p^G(V,U_0,U_1,...,U_m,t \mid t=0) = \delta(t-t_0)\prod_{i=0}^{m}\delta(u_i(t) - U_i(t_0))$$

and

$$p^G(V,U_0,U_1,...,U_m,0) = Vp^G(V,U_0,U_1,...,U_m,t \mid t=0) = 0$$

as $V \to \infty$.

Define a differential operator $\nabla = (\frac{\partial}{\partial V}\frac{\partial}{\partial U_m}...\frac{\partial}{\partial U_0})$ as a row vector, and then Eq. (8) can be written as

$$\frac{dp^G}{dt} = \nabla(A_G + (\nabla(B_G p^G))^T) \tag{9}$$

where

$$A_G = \begin{pmatrix} \eta\beta U_m - \mu \\ \eta(U_m - U_{m-1}) \\ ..... \\ \eta(U_1 - U_0) \\ \eta(U_0 - V) \end{pmatrix}_{(m+2)\times 1} \text{ and } B_G = \begin{pmatrix} \frac{\sigma^2}{2}0...0 \\ 0.....0 \\ ..... \\ 0.....0 \end{pmatrix}_{(m+2)\times(m+2)}$$

Therefore, probability current flux for gamma distributed kernel becomes

$$J = \nabla(A_G p^G + (\nabla(B_G p^G))^T) \tag{10}$$

For stationary probability distribution $\frac{\partial p^G}{\partial t} = 0$, $p^G = p_S{}^G$ and for reflecting boundaries, Eq. (10) gives

$$A_G p^G + (\nabla(B_G P^G))^T = 0 \tag{11}$$

Substituting the values of $A_G, B_G$ and using matrix calculation in Eq. (11), after simplification, we get

$$\frac{1}{p_S{}^G}\frac{\partial p_S{}^G}{\partial V} = -\frac{\sigma^2}{2}(\beta V - \mu) \tag{12}$$

Integration of Eq. (12) yields stationary probability distribution

$$p_S{}^G = k_G \exp\{-\frac{\beta}{\sigma^2}\{(V-\mu)^2 - \mu^2\}\} \tag{13}$$

Where $k_G$ is normalization constant.

### B. Neuronal Model Hypo-Exponential Distributed Memory Kernel

Let $pH(V,U_1,U_2,t)$ be the spatial probability distribution of membrane potential for LIF model with hypo-exponential distributed delay. Fokker-Planck equation associated with Eq. (7) becomes

$$\frac{\partial p^H}{dt} = \frac{\partial}{\partial V}\{\beta(U_1 - U_2) - \mu\}p^H + \frac{\partial}{\partial U_1}\eta(\lambda_E U_1 - V)p^H + \frac{\partial}{\partial U_2}\eta(\lambda_I U_2 - V)p^H + \frac{\sigma^2}{2}\frac{\partial^2 p^H}{\partial V^2} \tag{14}$$

with boundary conditions:

$$p^H(V,U_1,U_2,t \mid t=0) = \delta(t-t_0)\delta(U_1(t) - U_1(t_0))\delta(U_2(t) - U_2(t_0)) \text{ and}$$

$$p^H(V,U_1,U_2,0) = Vp^H(V,U_1,U_2,t \mid t=0) = 0 \text{ as } V \to \infty.$$

Define a differential operator $\nabla = (\frac{\partial}{\partial V}\frac{\partial}{\partial U_1}\frac{\partial}{\partial U_2})$ as a row vector, and then Eq. (14) can be written as

$$\frac{dp^H}{dt} = \nabla(A_H + (\nabla(B_H p^H))^T) \tag{15}$$

where $A_H = \begin{pmatrix} \beta(U_1 - U_2) - \mu \\ \eta(\lambda_E U_1 - V) \\ \eta(\lambda_I U_2 - V) \end{pmatrix}$ and $BH = \begin{pmatrix} \frac{\sigma^2}{2} & 0 & 0 \\ 0 & 0 & 0 \\ 0 & 0 & 0 \end{pmatrix}$.

Therefore, probability current flux becomes

$$J = \nabla(A_H + (\nabla(B_H p^H))^T) \tag{16}$$

For stationary probability distribution $\frac{\partial p^H}{\partial t} = 0$, $p^H = p_S{}^H$ and for reflecting boundaries, Eq. (10) gives

$$A_H p^H + (\nabla(B_H p^H))^T = 0 \tag{17}$$

Substituting the values of $A_H, B_H$ and using matrix calculation in Eq. (17), after simplification, we get

$$\frac{1}{p_S{}^H}\frac{\partial p_S{}^H}{\partial V} = -\frac{\sigma^2}{2}(\beta V - \mu) \tag{18}$$

Integration of Eq. (18) yields stationary probability distribution

$$p_S{}^H = k_H \exp\{-\frac{\beta}{\sigma^2}\{(V-\mu)^2 - \mu^2\}\} \tag{19}$$

Where $k_H$ is normalization constant.

*C. LIF Model*

Let $p^L(V,t)$ be the spatial probability distribution of membrane potential for LIF model. Following Frank [20] and Burkitt [6, 19], Fokker-Planck equation associated with Eq. (2) is

$$\frac{\partial p^L}{dt} = \frac{\partial}{\partial V}\{\beta V - \mu\} p^L + \frac{\sigma^2}{2}\frac{\partial^2 p^L}{\partial V^2} \tag{20}$$

with boundary conditions: $p^L(V, t \mid t = 0) = \delta(t - t_0)$ and $p^L(V) = Vp^L(V, t \mid t = 0) = 0$ as $V \to \infty$.

Probability current flux ( $J$ ) associated with Eq. (20) becomes

$$J = (\beta V - \mu) p^L + \frac{\sigma^2}{2}\frac{\partial^2 p^L}{\partial V^2} \tag{21}$$

For stationary probability distribution $\frac{\partial p^L}{\partial t} = 0$, $p^L = {p_S}^L$ and for reflecting boundaries, Eq. (21) results

$$\frac{1}{{p_S}^L}\frac{\partial {p_S}^L}{\partial V} = -\frac{\sigma^2}{2}(\beta V - \mu) \tag{22}$$

Integration of Eq. (22) yields stationary probability distribution

$${p_S}^L = k_L \exp\{-\frac{\beta}{\sigma^2}\{(V-\mu)^2 - \mu^2\}\} \tag{23}$$

where $k_L$ is normalization constant and can be calculated by using law of conservation of probabilities [19].

## IV. Spiking Activity of a Neuron in DDF

Spiking activity of a neuron exhibits a high level of variability [12, 21, 22]. This variability in spiking activity is essential for encoding information in form of spikes sequences [1, 21, 23]. Rate code scheme and temporal code scheme are two important strategies used by a neuron to encode information into spikes [3, 23–29]. Spike-count and Fano-factor related to the spike sequences are two important statistical measures of variability for rate code scheme [22, 29, 30]. Spike-count is used to encode information whereas Fano-factor provides a measure of variability in spike sequence, which can be computed as fallow [22, 29, 30].

Following Eden and Kramer [30], let spiking activity of a neuron is observed for $T$ time duration, and, if $t_1, t_2, t_3, \ldots.$ be the spike time in observed spike sequence, divide time interval $[0, T]$ into $K$ sub-interval of equal size $\delta(t)$ and count the number of spikes in each sub-interval. Let $n_1, n_2, \ldots, n_K$ be the number of spike in subintervals, respectively. Then

$$\text{Mean Spike Count: } \bar{N} = \frac{1}{K}\sum_{i=1}^{K} n_i \tag{24}$$

Fano-factor for this spike-sequence can be computed as

$$\text{Fano-factor: } F(\delta t) = \left(\frac{K}{K-1}\right)\frac{\sum_{i=1}^{K}(n_i - \bar{N})^2}{\sum_{i=1}^{K} n_i} \tag{25}$$

Fano-factor for a homogeneous Poisson process is exactly 1 [29], whereas, experimental data has Fano-factor distant from 1 [4, 5, 17]. In order to examine the effect of membrane potential delay on spiking activity and information processing of a neuron, we assume the rate code scheme of neuronal encoding and investigating the spike-count and the Fano-factor associated with spike sequence for considered neuron models. We apply Euler-Maruyama scheme in Monte-Carlo based simulation method [31, 32].

Let $dX(t) = Y(X(t)) + Z(X(t))dW(t)$ be a stochastic differential equation, where $X$, $Y$ and $Z$ are state variables and $dW(t)$ is the Wiener process. Using Euler-Maruyama approximation in time sequences $\{t_0 = 0, t_1 <, \ldots, t_n = t\}$, the considered SDE can be simulated as [32]

$$X(t_{i+1}) = X(t_i) + Y(X(t_i))(t_{i+1} - t_i) + Z(X(t_i))\sqrt{t_{i+1} - t_i}\, w_{i+1} \tag{26}$$

where $w_1, w_2, w_3, \ldots$ are independent normal variates and for fixed step size $(h)$: $t_i = ih$, thus Eq. (26) takes the form

$$X(i+1) = X(i) + Y(X(i))h + Z(X(i))\sqrt{h}\, w_{i+1} \tag{27}$$

By applying above stated simulation strategy, we simulate neuron models given in Eqns. (2), (5) and (7). Eq. (5) is simulated for weak delay and strong delay, both, i.e. for $m = 0$ and $m = 1$. Spike-count and Fano-factor of our interest during simulation based study for various combination of parameter values are illustrated in Figs. 1-4 and in Figs. 5-7, respectively. In these Fig.s, legends SLIF, LIFG: m = 0, LIFG: m = 1 and LIFH are used which stand for simple LIF model, LIF model with gamma distributed delay having $m = 0$, LIF model with gamma distributed delay having $m = 1$ and LIF model with hypo-exponential distributed delay. Spike-count for neurons are calculated at fixed $\mu = 0.1$, $\sigma = 0.1$ and $\beta$ ranging from 0 to 0.25 with the step size of 0.01, whereas, rest parameter values are given in Fig. caption. For $\beta = 0$, considered neuron models becomes pure integrate-and-fire model, thus initial values of spike-count in Figs. 1-4 are same which is approximately about 100 spikes per second. This spiking activity of neurons decreases as $\beta$ increases, but, decrease in spiking activity in LIF models in DDF is smaller than simple LIF model due to presence of delay parameters. Critical value of delay parameters (i.e. $\eta = 1$, $\lambda_E = 1$ and $\lambda_I = 1.01$ with input stimulus of small intensity) where all considered neuron models exhibit similar spiking activity is depicted in Fig. 1. When the value of $\eta$, $\lambda_E$ and $\beta$ is reduced, a neuron emits more spike as compared to simple LIF model due to dependency on past membrane potential values which works as memory element. LIFH neuron exhibits more spiking activity then other three neuron models due to the presence of delay in both excitatory parameter ( $\lambda_E$ ) and inhibitory parameters ( $\lambda_I$ ), which is well illustrated in Fig.s 2-4.

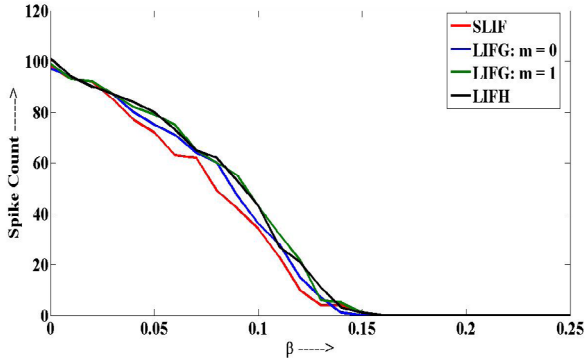


Fig. 1 Spike Count for $\eta = 1$, $\lambda_E = 1$ and $\lambda_I = 1.01$.

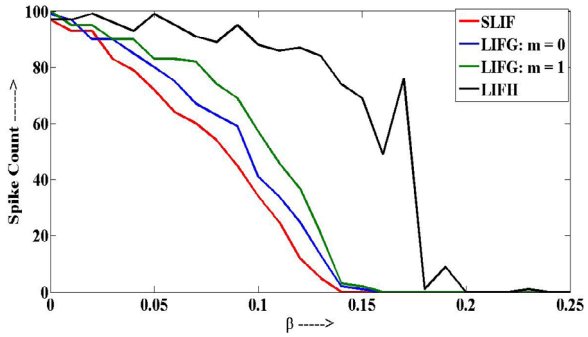


Fig. 2 Spike Count for $\eta = 0.5$, $\lambda_E = 0.5$ and $\lambda_I = 1.01$.

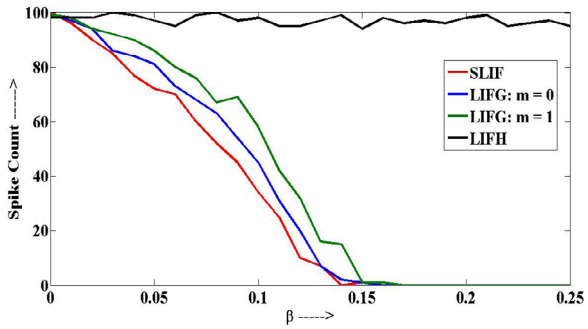


Fig. 3 Spike Count for $\eta = 0.5$, $\lambda_E = 1$ and $\lambda_I = 0.1$.

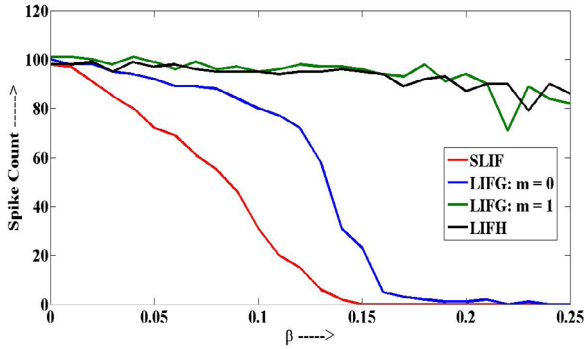


Fig. 4 Spike Count for $\eta = 0.1$, $\lambda_E = 0.1$ and $\lambda_I = 0.11$.

These observations suggest that the spiking activity of a neuron increases in presence of memory kernel functions, and in this context, hypo-exponential distributed kernel function is more robust than gamma distributed kernel function. Now, a pertinent question arises that among these considered models, which neuron model is capable to generate the greater variability in its spiking activity. To this end, we have computed the Fano-factor of spike sequences obtained from simulation of considered neuron models.

Fano-factor (also known as index of dispersion) is defined as the ratio of variance to the mean number of spike generated by a neuron in a fixed time period $\delta(t)$ which can be computed in many repetition of simulation of model with same input stimulus [5]. We have applied 100 times of repetition in our simulation based study for different combination of parameter values and corresponding results are illustrated in Figs. 5-7.

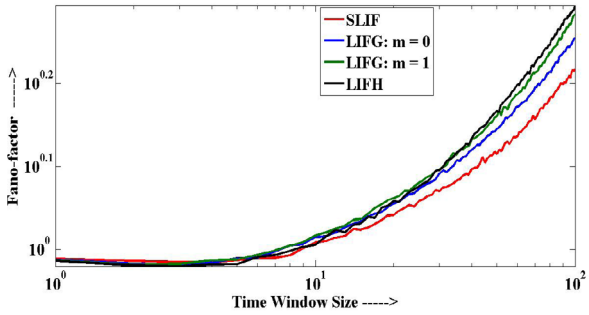


Fig. 5 Fano-factor for $\beta = 0.1$, $\mu = 0.1$, $\sigma = 0.15$, $\eta = 1$, $\lambda_E = 1$ and $\lambda_I = 0.99$.

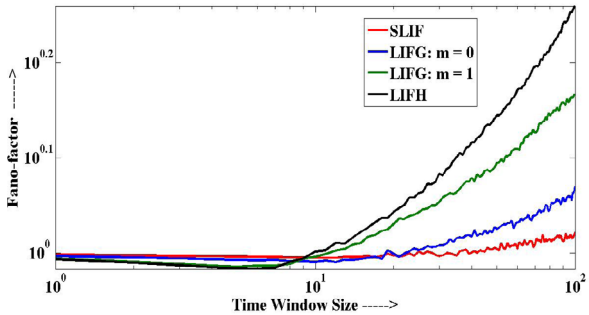


Fig. 6 Fano-factor for $\beta = 0.25$, $\mu = 0.2$, $\sigma = 0.05$, $\eta = 1$, $\lambda_E = 1$ and $\lambda_I = 0.9$.

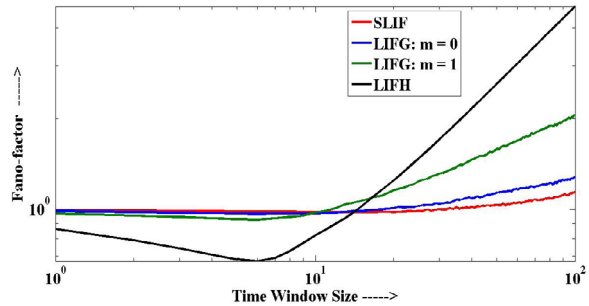


Fig. 7 Fano-factor for $\beta = 0.25$, $\mu = 0.2$, $\sigma = 0.05$, $\eta = 0.5$, $\lambda_E = 0.5$ and $\lambda_I = 0.1$.

For critical parameter values where LIF model in DDF exhibits spiking activities similar simple LIF model, their Fano-factor also exhibits the similar behavior as illustrated in Fig. 5. It is shown in Fig. 5 and 6 that Fano-factor for considered neuron models are closer to 1

for small time window, which is in a nice agreement with the Poisson hypothesis [5], whereas its value increases with respect to increase in time window. Increment in the Fano-factor is due to the long-term correlation in spiking activity [5], which is higher in LIF neuron with hypo-exponential distributed kernel function.

Various experimental studies have suggested that sensory systems exhibit the value of Fano-factor less than 1 [5]. We have noticed that when delay parameter values are smaller than critical values (as given in Fig. 1), LIF neuron with hypo-exponential kernel function is capable of generating spikes with less than 1 Fano-factor as shown in Fig. 7. Such kind of spiking in LIFH neuron is possible when difference between $\lambda_E$ and $\lambda_I$ is large.

## V. Result Analysis and Conclusion

Unlike other bio-physical neuron models, analytically solvable capability of LIF neuron is higher due to its linear representation though it is distant from a real neuron in many bio-physical mechanisms. Non-linearity in LIF neuron model arises due to threshold constraint [7]. Spiking activity of visual sensory system of many insects, fly etc., where spiking-rate is higher, cannot be captured by standard LIF neuron. Memory element of a neuron is incorporated in LIF neuron by kernel function in DDF [10–12]. We have analyzed these updated LIF model and noticed that memory functions do not affect the SPDV. Analytical calculation for SPDV of considered neuron models in sub-threshold regime are found asymptotically similar and exhibiting Gaussian-distribution, i.e. from Eqns. (13), (19) and (23), it is clear that when $V \to \infty$, $p_S{}^G \square p_S{}^H \square p_S{}^L$. This finding suggests that the LIF neuron with such kind of delay kernel functions has no effect on its stationary state probability distribution of membrane potential. Therefore, delay kernel functions, which can be extended to form the membrane potential evolution process, as a Markovian process, will exhibit Gaussian distribution for membrane potential, in sub-threshold regime and one can't notice the effect of memory in SPDV of experimental data. Moreover, parameter estimation techniques which are applicable for LIF models (see [13]), can also be applied for considered models in distribution delay framework. A pioneering question in studies of such kind of stochastic problems is solve the associated first passage time (FPT) problem, i.e. to find the distribution of time interval, when the membrane potential of a neuron first time reaches to its threshold value. Analytical solution of FPT associated with the simple LIF neuron model is an unsolved problem, however in some special case, one can obtain the solution of simple LIF neuron [10, 11]. In addition to the unsolved FPT problem associated with simple LIF neuron, FPT problem associated with LIF neuron in DDF becomes the challenges in future.

Masas [33] has demonstrated that how the network of spiking neurons attains self origination and learning form noise. DDF also provides a way capture the noise values in term of previous values of membrane potential. From simulation based study, it is notable that the spiking activity of a neuron increases in DDF due to the dependency on its previous values. The delay kernel function works as a memory function and membrane potential of a neuron attains threshold value in quicker time due to memory effect, i.e. previous values of membrane potential works as learning. Such kind of spiking activity is helpful to describe experimental and physiological data more accurately especially where higher firing rate is required. We have also noticed that hypo-exponential kernel function is more robust and reliable in term of spiking activity and neuronal information processing as compared with gamma distributed kernel function, but it is still a challenging problem to find a suitable kernel function which can replicate most of the experimental data *in-vivo* and *in-vitro*.

Lim et. al. [34] has shown the implementation of the artificial neural network (ANN) at hardware level by applying neuristor-based leaky integrate-and-fire neuron model. LIF neuron model in DDF can be an alternate model for such kind of hardware level implementation of ANN due to the increase in spiking activity.

## VI. Acknowledgment

The authors are extremely grateful to the reviewers whose comments have led to significant improvement in the quality of the paper.

## References

[1] P. Dayan, and L.F. Abbott "Theoretical Neuroscience: Computational and Mathematical Modeling of Neural Systems", The MIT Press, 2001.

[2] G.B. Ermentrout, and D.H. Terman, "Mathematical Foundations of Neuroscience", Springer, 2010.

[3] W. Gerstner, R. Naud, "How Good are Neuron Models?" Science, vol. 326, no, 5961, 2009, pp. 379-380.

[4] M.I. Rabinovich, P. Varona, A. I, Selverston, and H.D.I. Abarbanel, "Reviews of Modern Physics", vol. 78, no. 4, 2006, pp. 1213-1256.

[5] C. Koch, "Biophysics of Computation: Information Processing in Single Neurons", Computational Neuroscience, Oxford University Press, 1998.

[6] A.N. Burkitt, "A Review of the Integrate-and-Fire Neuron Model: I. Homogeneous Synaptic Input", Biological Cybernatics, vol. 95 no.1, 2006, 1-19.

[7] E.M. Izhikevich, "Dynamical Systems in Neuroscience: The Geometry of Excitability and Bursting", Computational Neuroscience, MIT Press, 2007.

[8] F. Gabbiani, and S.J. Cox, "Mathematics for Neuroscientists", Academic Press, 2006.

[9] C.F. Lo, and T.K. Chung, "Neural Information Processing: Lecture Notes in Computer Science", vol. 4232, 2006, pp. 324-331.

[10] Karmeshu, V. Gupta, and K.V. Kadambari, "Neuronal model with Distributed Delay: Analysis and Simulation Study for Gamma Distribution Memory Kernel", Biological Cybernatics, vol. 104, no. 6, 2011, pp. 369-383.

[11] S.K. Sharma, and Karmeshu, "Neuronal Model with Distributed Delay: Emergence of Unimodal and Bimodal ISI Distributions", IEEE Transactions on Nanobiosciences, vol. 12, no. 1, 2013, pp. 1-12.

[12] S.K. Choudhary, K. Singh, and S.K. Bharti, "Variability in spiking pattern of leaky integrate-and-fire neuron due to excitatory and inhibitory potentials", Computing for Sustainable Global Development

[13] (INDIACom), 2015, pp. 2025–2030.

[14] M. Rudolph, and A. Destexhe, "On the Use of Analytical Expressions for the Voltage Distribution to Analyze Intercellular Recordings", Neural Computation, vol. 18, 2006, pp. 2917-2922.

[15] S. Ruan, and R.S. Filfil, "Dynamics of a Two-Neuron System with Discrete and Distributed Delays", Physica D, vol. 191, 2004, 323-342.

[16] R.B. Northrop, "Introduction to Dynamic Modeling of Neuro-Sensory Systems", CRC Press, 2000.

[17] Srdjan Ostojic, "Two types of asynchronous activity in networks of excitatory and inhibitory spiking neurons", Nature Neuroscience, Vol. 17, No. 4, pp. 594-602. 2014.

[18] N. Ho, and A. Destexhe, "Synaptic Background Activity Enhances the Responsiveness of Neocortical Pyramidal Neurons", The American Physiological Society, vol. 84, no. 3, pp. 1488-1496.

[19] A. Destexhe, and D. Pare, "Impact of Network Activity on the Integrative Properties of Neocortical Pyramidal Neurons In Vivo", The American Physiological Society, vol. 81, no. 4, 1999, pp. 1531-1547.

[20] A.N. Burkitt, "A Review of the Integrate-and-Fire Neuron Model: II. Inhomogeneous Synaptic Input and Network Properties", Biological Cybernatics, vol. 95, no. 2, 2006, pp. 97-112.

[21] T.D. Frank, "Nonlinear Fokker-Planck Equations: Fundamentals and Applications", Springer Series in Synergetics, Springer, 2005.

[22] F.Y.M. Wan, and H.C. Tuckwell, "Neuronal Firing and Input Variability", Journal of Theoretical Neurobiology, vol. 1, 1982, pp. 197-218.

[23] M.P. Nawrot, C. Boucsein, V.M. Rodriguez, A. Riehle, and A.A.S. Rotter, "Measurement of Variability Dynamics in Cortical Spike Trains", Journal

of Neuroscience Methods, vol. 169, 2008, 374-390.
[24] F. Rieke, D. Warland, R.R. Steveninck, and W. Bialek, "Spikes: Exploring The Neural Code", MIT Press, 1997.
[25] A.B. Arcas, A.L. Fairhall, and W. Bialek, "Computation in a Single Neuron: Hodgkin and Huxley Revisited", Neural Computation, vol.15, 2003, pp. 1715-1749.
[26] A. Fairhall, E.S. Brown, and A. Barreiro, "Information Theoretic Approaches to Understanding Circuit Function", Neurobiology, vol. 22, 2012, pp. 653-659.
[27] S. Haykin, J.C. Principe, T.J. Sejnowski, and J. Mcwhirter, "New Directions in Statistical Signal Processing: From Systems to Brains", MIT Press, 2007.
[28] S. Sinanovic, and D.H. Johnson, "Toward a theory of information processing", Signal Processing, vol. 87, 2007, pp. 1326-1344.
[29] W. Gerstner, A.K. Kreiter, H. Markram, and A.V.M. Herz, "Neural Code: Firing Rate and Beyond", Proceedings National Academy of Science, USA, vol. 94, 1997, 12740-12741.
[30] W. Gerstner, and W.M. Kistler, "Spiking Neuron Models: Single Neurons, Populations, Plasticity", Cambridge University Press, 2002.
[31] U.T. Eden, and M.A. Kramer, "Drawing Inferences from Fano Factor Calculations", Journal of Neuroscience Methods, vol. 190, 2010, pp. 149-152.
[32] D.J. Higham, "An Algorithmic Introduction to Numerical Simulation of Stochastic Differential Equations", SIAM Review, vol. 46, no. 3, 2001, pp. 525-546.
[33] P. Glasserman, "Monte Carlo Methods in Financial Engineering", Springer, 2004.
[34] W. Maass, "Noise as a Resource for Computation and Learning in Networks of Spiking Neurons", Proceedings of the IEEE , Vol. 102, No. 5, 2014, pp. 860-880.
[35] H. Lim, V. Kornijcuk, J. Y. Seok, S. K. Kim, I. Kim, C. S. Hwang and D. S. Jeong, "Reliability of neuronal information conveyed by unreliable neuristorbased leaky integrate-and-fire neurons: a model study", Nature: Scientific Reports 5, 5, Article number: 9776, 2015.

**Saket Kumar Choudhary** obtained his master degrees in Mathematics from the University of Allahabad, Allahabad, India in 2005, Master of Computer Application (MCA) from UPTU, Lucknow, India in 2010, Master of Technology (M.Tech) from Jawaharlal Nehru University, New Delhi, India in 2014. He is finishing his doctorate in School of Computer and Systems Sciences, Jawaharlal Nehru University, New Delhi, India. His research interest includes mathematical modeling and simulation, dynamical systems, computational neuroscience: modeling of single and coupled neurons, computer vision and digital image processing.

**Karan Singh** (M-1981) received the Engineering degree (Computer Science & Engineering) from Kamala Nehru Institute of Technology, Sultanpur, UP, India and the M.Tech (Computer Science & Engineering) from Motilal Nehru National Institute of Technology UP, India. He is Ph.D. (Computer Science & Engineering) from MNNIT Allahabad deemed university. Currently, he is working in school of Computer & Systems Sciences, Jawaharlal Nehru University, New Delhi. His primary research interests are in computer network and computer network security. He is reviewer of IEEE & Elsevier conferences and reviewer of International journals. He is organizer of various workshop, Conference and training. Recently, Dr. Karan work as General Chair of Qshine 2013. Dr. Singh has been joined as Professional member of IEEE, ACM, CSTA, CSI, IACSIT, ICST, IAENG, ACEEE, ISOC and IEEE computer society.

**Vijender Kumar Solanki** received the Master in Computer Application and Master in Engineering degree (Computer Science & Engineering) from Maharishi Dayanand University, Rohtak, Haryana, India.(2004 & 2007). He is pursuing Ph.D. (Computer Science & Engineering) from Anna University, Chennai, Tamilnadu, India. His primary research interests are in Network Security, Smart Cities and Big Data. He is reviewer of IEEE, Springer & Elsevier conferences and reviewer of International journals. He is the Guest Editor of IJRSDA, Spl Issue on "Recent Approaches on Internet of Thing, Next Generation Networks, Smart Cities and Cloud Computing" and Editor for Book on "Big Data Management and Analytics with Modern Tools & Technologies" Published by Universities Press, India. He has delivered many Lectures in FDP, Workshop and Confrences. He can be contacted at spesinfo@yahoo.com

# A Real Time Approach to Theft Prevention in the field of Transportation System

Vartika Mehta[1], Deepak Punetha[2], Vishwanath Bijalwan[3]

[1]Department of Electronics & Communication Engineering, SIT, Pithoragarh
[2]Department of Electronics & Communication Engineering, Tula's Institute, Dehradun
[3]Department of Electronics & Communication Engineering, IT, Gopeshwar

***Abstract* — This paper report discusses a theft prevention system, which can prevent the theft and also can be track the object. This system is capable to tracking the vehicle as well as theft prevention. An R.F. module is use to exchange the information regarding vehicle and owner of the vehicle with police control room or SOS services. The vehicle can be track with the help of R.F. receiver. A DTMF based fuel lock has been attached in this system. A cell phone with SIM card has been attached with DTMF IC. The fuel flow in the vehicle can be controlled by give a call to this cell phone. This system has been controlled by a microcontroller which can make the system cost effective, low power consumption, effective and reliable.**

***Keywords* — Theft Preventation, Tracking, RF Module,DTMF, Microcontroller, Mobile Phone.**

## I. Introduction

Vehicle Prevention system is primary concern for everyone to prevent robberies of vehicle. Research shows that there are thousands of vehicles have stolen every year. These crimes are increasing day by day. In this paper report a system has been developed by use of RFID and DTMF. This process is called Dual Tone Multiple Frequency based Vehicle Prevention System using RFID.

There are two type of prevention system exist "Active system and Passive system". Active System transfers all information about the vehicle to police control room via cellular. Passive devices are used for knowing about the location and it is also used as trigger for ON/OFF the fuel or door of the vehicle.

Vehicle Prevention System is the solution to overcome this problem. By using RFID people can know about the location of the vehicle and with the help of Dual Tone Multiple Frequency people can lock the fuel of vehicle.

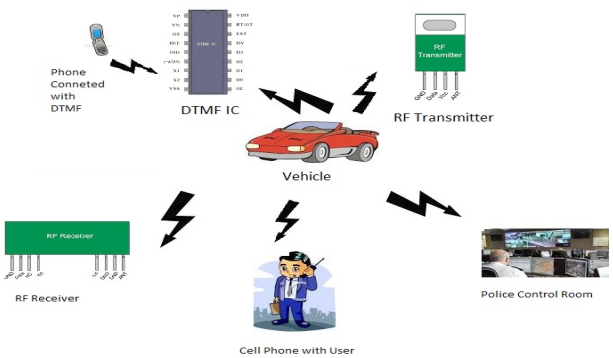


Fig. 1. Vehicle Tracking System Procedure

Vehicle Prevention System is a system which provides the effective, reliable and real time vehicle location. So many organization and researcher are working in the field of transportation system [1-3].

## II. Motivation

Around the world thousands of vehicles theft occur because of low security. If the people go somewhere in its vehicle due to some work then they want to their vehicle should be safe. For every problem RTO is making the case study. Research shows that above from thousands vehicle has been stolen in one state. Because of Lake of awareness the crime is increasing day by day. Report of government shows the robberies occurs in Haryana state. Following table is showing the detail of vehicle which has been stolen.

**TABLE 1.** TABLE OF STOLEN VEHICLE AND ITS DETAIL

| S. No. | Type of vehicle | Make | Regd. Num | Place of occurrence | Date of occurrence |
|---|---|---|---|---|---|
| 1 | M/CYCLE | SPL | HR07M-4915 | COMMERCIAL AREA | 04-05-15 |
| 2 | M/CYCLE | SPL+ | HR02U-7402 | COMMERCIAL AREA | 14-05-15 |
| 3 | CAR | MARUTI DESIRE | D13A1604344 | COMMERCIAL AREA | 25-05-15 |
| 4 | CANTER | TATA 407 | HR46A-4057 | COMMERCIAL AREA | 26-05-15 |
| 5 | TRACTOR | MAHINDRA 605 | RAR5603 | COMMERCIAL AREA | 26-05-15 |
| 6 | JEEP | PICK UP | M28984 | COMMERCIAL AREA | 26-05-15 |

## III. Problem Definition

The strategy of solving these problems is use the tracking system the vehicle. This tracking system should inbuilt in the vehicle. Stolen vehicle can be track easily by its area of police station. According to govt. report robberies is increasing very fast. Further reducing these issues government will take the step to use this system.

## IV. Related Work

Montaser N. Ramadan et. al describe the anti-theft system, which can detect the location of vehicle by using GPS module. It gives approximately 10 meter difference to detect object from exact location. Detecting location using GPS is also very costly [3]. K. P. Kamble elaborate the system which can save petrol, gas, time and also optimize the driver route and can control the function of vehicle. The accuracy



DOI: 10.9781/ijimai.2016.3711

of this system is not good [4]. D. Narendar Singh et.al illustrate real time vehicle theft identity for recognize the face of driver of vehicle by using PCA. With the help of face detection people can detect the face of thief but in case of wearing mask PCA can't detect the face [5]. Some system describes the study of auto theft prevention in which system makes use of microcontroller and it is connected to interfacing GSM for controlling the theft of vehicle. GSM work on AT command, sometime GSM can't read these commands and can't work properly [6-9]. A methodology defined the Vehicle Accident Alert and Locator which can detect the vehicle when it meet with accident. This system is reliable for people. It can detect vehicle when there will be a little vibration in vehicle [10]. Some systems present concise overview of detecting and tracking of vehicle. This system plays a vital role in civilian and military environment such as in management and urban traffic planning, highway traffic surveillance control by video. In this system protection of camera is very important [11-14]. Many systems have been proposed which can detect the crash detection and a lot of work done in the field of transportation system.

## V. System Overview

This system can give the great contribution in the field of vehicle tracking in army, navy and somewhere in police department. This system contains the RF module, DTMF, cell phone and controlled device [16-18].

### A. RF module

The RF transmitter is able to transmit the radio frequency containing the information about the vehicle.

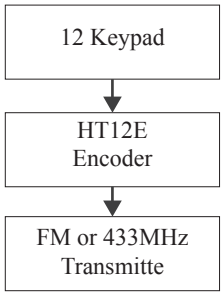


Fig. 2. Block diagram of RF transmitter

HT12E encoder and HT12D decoder is used by RF transmitter and RF receiver respectively. Operating voltage of these encoder and decoder is 2.4V to 12V.

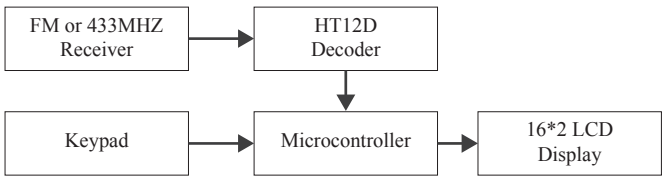


Fig. 3. Block diagram of RF receiver

### B. DTMF

DTMF stand for Dual Tone Multiple Frequency. Moving object can be control by using mobile phones. This system requires two phones. Amongst them one with SIM card connected with RF transmitter and another phone will keep the vehicle owner. Phone connected with RF transmitter is put in such a mode that it automatically picks up the call. When the owner will call on that number, the call can activate automatically and owner can lock the fuel with help of DTMF. Solenoid can use for locking the fuel.


Fig. 4. DTMF Transmitter and DTMF based fuel lock.

### C. System Setup

This system is defined as the tracking of moving object. The proposed system contains RFID which has a specific range. It can be categorized in different sections such as RF transmitter, RF receiver and DTMF fuel lock. RF transmitter can attach with the vehicle. Transmitter uses the HT12E encoder and transmits the 12 bit code. This encoder is the series of CMOS LSIs and also capable for encoding data. These data have N numbers of address bit and 12 data bit. The programmed address/data are conveyed together. Its operating voltage is 2.4V to 12V. The second section in this system is RF receiver. HD12D uses in the receiver section. It is a series of CMOS LSI and receives serial address and data and compares it continuously with local address. If there are any unmatched code then the input data code are decoded and transfer it to output pin. DTMF based fuel lock is the third section of this system which installed in vehicle which can be activated and deactivated by mobile. It encoded the hybrid frequency DTMF code, IC 8870 decode it and transform it into BCD code [15].

TABLE 2. ENCODED OUTPUT

| **Pressed Mobile key** | 1 | 2 | 3 | 4 | 5 | 6 | 7 | 8 | 9 | * | 0 | # |
|---|---|---|---|---|---|---|---|---|---|---|---|---|
| **D3** | 0 | 0 | 0 | 0 | 0 | 0 | 0 | 1 | 1 | 1 | 1 | 1 |
| **D2** | 0 | 0 | 0 | 1 | 1 | 1 | 1 | 0 | 0 | 0 | 0 | 1 |
| **D1** | 0 | 1 | 1 | 0 | 0 | 1 | 1 | 0 | 0 | 1 | 1 | 0 |
| **D0** | 1 | 0 | 1 | 0 | 1 | 0 | 1 | 0 | 1 | 1 | 0 | 0 |

## VI. Experiment Results

For explaining this project first of all sees the hardware part. There is a power supply which consist of two pin connector, four diode that is also called bridge rectifier, one ON OFF switch, capacitor is of 1000 µF, voltage regulator is of 5V and 12V and LED is also be there. Next is basic circuit of microcontroller which consists of 89S52 microcontroller, a reset circuit and a crystal oscillator. Reset circuit consists of 10 µF capacitor and 10KΩ register. Crystal oscillator provides a clock frequency to microcontroller. After seeing the Fig. there is a GSM modem which is connected to microcontroller through serial port.

Fig. 5. Snapshot of the device

First of all connect power supply to the circuit for initializing the modem. After connecting the power supply it takes some moment for initialization and sends an acknowledgement on the mobile. Mobile receives a message which is "Welcome to Vehicle Tracking System"


Fig. 6. Modem Initialization

If the vehicle passed through the RFID reader then LCD displays the position of vehicle and simultaneously a message sends to the mobile. This message displays on the mobile that "A vehicle name XY-0000 has been stolen and this is in your area". At another place if the vehicle is tracked then another message sends on the mobile.

## VII. Conclusion

Tracking system is becoming important in countries. This system is integrated in vehicle. This system is very fast, accurate and robust. It is very securing then other system. Once it will integrate in the vehicle then tracking can be very easy. After stolen the vehicle this system is capable to find the area of the vehicle where it has located with the help of RFID. Receiver part is placed in police station of every area. After tracking the vehicle first it lock the fuel by DTMF then find out the vehicle. With the help of this system vehicle can be tracked very easily.

## References

[1] Cueva-Fernandez, Guillermo, Jordán Pascual Espada, Vicente García-Díaz, Rubén González Crespo, and Nestor Garcia-Fernandez, "Fuzzy system to adapt web voice interfaces dynamically in a vehicle sensor tracking application definition," Soft Computing : 1-14, 2015.

[2] García, Carlos Martín, and Gonzalo Martín Ortega, "Route planning algorithms: Planific@ project," IJIMAI 1, no. 2 (2009): 57-66.

[3] Gechter, Franck, Bruno Ronzani, and Fabien Rioli, "Sphericall: A Human/ Artificial Intelligence interaction experience," IJIMAI 3, no. 1 (2014): 49-58.

[4] Montaser N. Ramadan, Mohammad A. Al-Khedher and Sharaf A. Al-Kheder, "Intelligent Anti-Theft and Tracking System for Automobiles," International Journal of Machine Learning and Computing, Vol. 2, No. 1, February 2012.

[5] K.P.Kamble,"SMART VEHICLE TRACKING SYSTEM," International Journal of Distributed and Parallel Systems (IJDPS) Vol.3, No.4, July 2012.

[6] D.Narendar Singh, K.Tejaswi, "Real Time Vehicle Theft Identity and Control System Based on ARM 9," International Journal of Latest Trends in Engineering and Technology, Vol. 2 Issue 1 January 2013.

[7] Deepak Punetha, Vartika Mehta, "A Wireless Approach to Real Time Remote Monitoring System consisting of Environmental Parameters using feasibility of a GSM module," IEEE International Conference on Advances in Engineering & Technology Research (ICAETR'14), Unnao, Kanpur, Uttar Pradesh, 1-2 August 2014.

[8] Deepak Punetha, Vartika Mehta, "Protect the Child/ Elderly/ Disabled/ Pet by Smart and Intelligent GSM and GPS based Automatic Tracking and Alert System," IEEE International Conference on Advances in Computing, Communications and Informatics (ICACCI'14), Second International Symposium on Women in Computing and Informatics, Galgotias, Greater Noida, Uttar Pradesh, pp: 2349-2354, 24-27 September 2014.

[9] Deepak Punetha, Deepak Kumar and Vartika Mehta, "Design and Realization of the Accelerometer based Transportation System (ATS)," International Journal of Computer Applications 49(15):17-20, July 2012. Published by Foundation of Computer Science, New York, USA.

[10] Deepak Punetha, Neeraj Kumar, Vartika Mehta, "Development and Applications of Line Following Robot Based Health Care Management System," International Journal of Advanced Research in Computer Engineering & Technology, Vol. 2, no. 8, pp. 2446-2450, August-2013.

[11] M. Zafri Baharuddin, Izham Z. Abidin, S. Sulaiman Kaja Mohideen, Yap Keem Siah, Jeffrey Tan Too Chuan,"Analysis of Line Sensor Configuration for the Advanced Line Follower Robot",University Tenaga Nasional.

[12] Pakdaman, M.; Sanaatiyan, M.M., "Design and Implementation of Line Follower Robot," Computer and Electrical Engineering, 2009. ICCEE '09. Second International Conference on , vol.2, no., pp.585-590, 28-30 Dec. 2009.

[13] T. Gomi, K. Ide,"Evolution of gaits of a legged robot", IEEE International Conference on Fuzzy Systems 06/1998; DOI:10.1109/ FUZZY.1998.687476 ISBN: 0-7803-4863-X In proceeding of: Fuzzy Systems Proceedings, 1998.

[14] Deepak Punetha, Divakar Mani Tripathi, Ashish Kumar, "A Wireless Approach with Sensor Network for Real Time Railway Track Surveillance System," International Journal of Engineering Trends and Technology (IJETT), Vol. 9, Number 9, 426-429 March 2014.

[15] Deepak Punetha, Pratyush Jha, Shweta Singh, "An Intelligent Transportation System with Computer System Architecture approaching Safe Passage in Adaptive Traffic Light," International Journal of Computer Networks and Wireless Communications, Vol. 4, Number 2, pp. 143- 149, April 2014.

[16] Datasheets of microcontroller AT89C51, LDR sensor, IR proximity sensor, Motor driver L293D, Comparator, 16*2 LCD, Available: http:// www.alldatasheet.com

[17] Miller Peter , "Building a Two Wheeled Balancing Robot", University of Southern Queensland, Faculty of Engineering and Surveying. Retrieved Nov 18, 2008.

[18] Nor Maniha Abdul Ghani, Faradila Naim, Tan Piow Yon , "Two Wheels Balancing Robot with Line Following Capability," World Academy of Science, Engineering and Technology, pp-634-638, 2011.

[19] Román Osorio," Inteligent Line Follower Mini-Robot System", International Journal of Computers, Communications & Control Vol. I, No. 2 ,pp. 73-83 ,2006.

**Ms. Vartika Mehta** is serving SIT, Pithoragarh as an Assistant Professor in E.C.E. department. He has an experience of more than 4.5 years in teaching and Software companies. She has completed her B.Tech in ECE from Dehradun Institute of Technology and M.Tech in Communication System from Graphic Era Hill University, Dehradun, Uttarakhand, India. Signals and Systems. She has published so many research papers in various National and International conferences and journals. She is also the member of many research organizations. Her area of interest is Joomla, Opencart frame work, Executing test cases, Jmeter tools, Xampp server, Wireless Communication,

**Mr. Deepak Punetha** is serving Tula's Institute, Dehradun as an Assistant Professor in E.C.E. department. He has an experience of more than 5.5 years in teaching and research (Including research experience in CDAC, Mohali). He has completed his B.Tech in ECE from Dehradun Institute of Technology and M.E. (8.5 CGPA) in EPDT from PEC University of Technology, Chandigarh. His area of interest is Electronics Product Design and Technology, Face Recognition and Compression, Radiation Pattern analysis of different Antennas, Navigation and Emergency Alerting System, Robotics and Embedded Systems. He has published more than 35 research papers in reputed conferences and International Journals. He is the member of reviewing and technical program committee of IEEE Explorer, Springer (Journal of Intelligent & Robotics Systems), Hindawi and various international Journals. He is also an active member of different National and International Association of Electronics and Communication Engineers and Editorial Boards.

**Mr. Vishwanath** bijalwan obtained his B.Tech degree in ECE, from Dehradun Institute of Technology (UPTU) in 2009. He received his M.TECH degree from Uttarakhand Technical University in Digital Communication stream in 2012. Currently he is working as an Assistant Professor & head of the department ECE at IT,Gopeshwar (State Government Institute). Besides this he has been also serving some more academic duties of Examination controller, & Dean Student's welfare at IT Gopeshwar. He has more than 5 years of teaching experience and 1 year industry experience. He has worked for various organizations, such as HCL Info system, Doon Institute of Engg. & Technology Rishikesh, Uttaranchal University Dehradun, and Institute of Technology, Gopeshwar. In Research domain he has published various research papers in international journals. His research area of interest is Wireless adhoc network, IEEE 802.15.4, & Machine learning. He has served as a PC member for many national & International conferences in the region; he is also serving as a reviewing board member for various international journals like OMICS group and various IEEE conferences. He is also an active member of IAENG, UACEE. His teaching area of Interest is Digital Electronics, Electromagnetic field theory, Antenna & wave propagation & digital signal processing.

# An Extensive Evaluation of Portfolio Approaches for Constraint Satisfaction Problems

[1]Roberto Amadini, [2]Maurizio Gabbrielli and [3]Jacopo Mauro

[1]*University of Melbourne, Australia*
[2]*University of Bologna, Italy*
[3]*University of Oslo, Norway*

***Abstract*— In the context of Constraint Programming, a portfolio approach exploits the complementary strengths of a portfolio of different constraint solvers. The goal is to predict and run the best solver(s) of the portfolio for solving a new, unseen problem. In this work we reproduce, simulate, and evaluate the performance of different portfolio approaches on extensive benchmarks of Constraint Satisfaction Problems. Empirical results clearly show the benefits of portfolio solvers in terms of both solved instances and solving time.**

***Keywords* — Algorithm Selection, Algorithm Portfolios, Constraint Programming, Constraint Satisfaction Problems.**

## I. Introduction

In the context of *Constraint Programming* (CP) [40] a portfolio approach [13,17] combines $m > 1$ different solvers $S_1, ..., S_m$ to get a globally better solver, dubbed a *portfolio solver*. When a new, unseen problem $p$ comes, the portfolio solver seeks to predict and run the best constituent solver(s) $S_{i_1}, ..., S_{i_k}$ (with $1 \leq i \leq m$ for $j = 1, ..., k$) for solving $p$. Portfolio approaches can be seen as instances of the *Algorithm Selection* problem [39] where, as reported by [25], the algorithm selection is performed case-by-case according to the problem to solve.

Portfolio solvers have proven to be very efficient, especially for solving the Boolean satisfiability (SAT) problem. For instance, the SAT portfolio solvers 3S [21] and CSHC [30] won gold medals in the SAT Competition 2011 and 2013, while SATZilla [53] won the SAT Challenge 2012. Unfortunately, in the CP field fewer portfolio solvers have been proposed. In this regard, worth mentioning are CPHydra [35] that won the International Constraint Solver Competition 2008 [49] and `sunny-cp` [5] that won the MiniZinc Challenge 2015 [48]. This witnesses that portfolio approaches can be effective also in the CP domain [6], and that the research in this field is not merely theoretical: many real life applications might take advantage of portfolio solvers for solving daily life problems such as, for example, task scheduling or resource allocation problems [1, 36].

With the aim of deepening the study of portfolio solving in the CP field, in this paper we extend the research initiated by [2] by presenting a more recent and exhaustive evaluation of portfolio approaches for solving Constraint Satisfaction Problems (CSPs). Improvements are manifold: we evaluate more recent solvers, more features, we fully support the MiniZinc language [33], and we use a larger dataset of CSP instances. The obtained results are encouraging and confirm the effectiveness of portfolio solvers in terms of both solved instances and solving time.

Unfortunately, due to the difficulties in using and adapting to the CSP domain some approaches originally designed for SAT, most of the portfolio solvers we tested have been reimplemented as faithfully as possible. Hence, the goal of this paper is not to present a (possibly unfair) competition between portfolio solvers. We want instead to shed further light on CSP portfolio approaches by means of empirical evaluations. In this regard, we submitted the data and the results we computed to the *Algorithm Selection library* [9], an open-access library providing a standardized format for representing, evaluating, and comparing different portfolio approaches without the effort of rebuilding all the experimental environment.

*Paper structure.* Section 2 gives some background notions on CSP portfolio solvers. Section 3 explains the experimental methodology, while Section 4 describes the obtained results. In Section 5 we report the related literature and the concluding remarks.

## II. Background

A *Constraint Satisfaction Problem* (CSP) is a triple consisting of a set of variables each of which associated with a domainof values thatcould take, and a set of constraints defining all the admissible assignments of values to variables [27]. The goal is normally to find a solution, i.e., a variable assignment satisfying all the constraints of the problem, by using a suitable constraint solver. In this context, a *portfolio solver* can be seen as a meta-solver consisting of $m > 1$ different solvers $S_1, ..., S_m$. *When a new, unseen CSP instance p comes, the portfolio solver seeks to predict and run the best constituent solver(s) for solving p. In the rest of the section we give a brief overview of the main ingredients characterizing a CSP portfolio solver, namely: the dataset of CSPs used to make (and test) predictions, the solvers of the portfolio, the features characterizing each CSP, and the selection algorithms used for deciding the solver(s) to run on a given CSP.*

### A. Dataset, Solvers and Features

In order to build and test a good portfolio approach it is fundamental to gather an adequate *dataset* of CSPs. The data sample should capture a significant variety of problems encoded in the same language. Although nowadays the CP community has not yet agreed on a standard modelling language, *MiniZinc* [33] is probably the most used and supported language to model CP problems. However, the biggest existing dataset of CSPs we aware is the one used in the 2008 International Constraint Solver Competition (ICSC) [49]. These instances are encoded in the XML-based language XCSP [41]. In [2] an empirical evaluation on such a dataset was conducted. Here we take a step forward by exploiting the `xcsp2mzn` [3] compiler we developed for converting XCSP to MiniZinc. This allowed us to use a bigger benchmark of 8600 CSPs: 6944 instances of ICSC converted by `xcsp2mzn`, and 1656 native MiniZinc instances coming from the MiniZinc 1.6 benchmarks and the MiniZinc Challenge 2012.

A portfolio solver contains a number of different constituent solvers that clearly should be as effective as possible. However, the individual performance of a solver is not the only key to success: what really matters is the contribution of a solver to the portfolio performance [51]. For this reason, increasing the number of constituent solvers does not necessarily mean increasing the performance of a portfolio. Conversely,



DOI: 10.9781/ijimai.2016.3712

having too many candidates solvers can make the solvers prediction inefficient and especially inaccurate. In this work we consider (subsets of) a collection of 11 different solvers that attended the MiniZinc Challenge, namely: BProlog, Fzn2smt, CPX, G12/FD, G12/LazyFD, G12/CBC, Gecode, iZplus, MinisatID, Mistral, and OR-Tools.

Usually portfolio solvers decide the solver(s) to run according to a set of *features* extracted from the instance to solve. Features are specific attributes characterizing a given problem instance, and are clearly of paramount importance for the success of a portfolio approach [39]. Features can be divided in *static* (computed off-line according to the problem specification) and *dynamic* (computed at runtime by monitoring the problem resolution). In this paper we used `mzn2feat` [3] to extract a set of 155 features (144 static, 11 dynamic) from a MiniZinc instance. For more details about such features we refer the interested reader to [3].

### B. Algorithm Selection

There are several ways to select one or more constituent solver(s) for solving a given instance. A primary distinction can be done between the approaches that require training and the so-called *lazy* approaches [25] that do not need it. For the former, the training phase is usually performed off-line and empirical evidences prove that a good training can lead to very good performance (e.g., see [50,21,31,30]). However, avoiding the training phase can be clearly advantageous in terms of simplicity and flexibility: new information can be used to improve the predictions without rebuilding the prediction model. For this reasons some lazy approaches have been proposed in the literature (e.g., see [35,37,34,11,43,4]). A further distinction can be made between algorithms that run just one solver and those that schedule more solvers. These may have some practical advantages since they reduce the risk of choosing a wrong solver. Furthermore, scheduling more solvers enables the communication of potentially relevant information such as bounds [6] or nogoods [23].

In this work we considered different selectors disparate in their nature. We implemented and adapted them to the CSP domain trying to be as faithful as possible to their original concept. In particular, we compared the performance of off-the-shelf *Machine Learning* (shortly, ML) classifiers against some well-known portfolio approaches, namely: CPHydra [35], ISAC [22], 3S [21], SATzilla [50], and SUNNY [4]. In the following we provide a brief overview of such approaches.

***Off-the-shelf*** (OTS) are selectors that rely on off-the-shelf ML classification algorithms to predict the best solver to run for a given instance. Thanks to WEKA [14] we implemented a number of well-known OTS selectors based on well-know classifiers, namely: *IBk* (*k*-Nearest Neighbours), *J48* (4.5 decision trees), *PART* (PART decision lists), *RF* (Random Forests), and *SMO* (Support Vector Machines).

*CPHydra* [35] is the first general CSP portfolio solver proposed in the literature. It uses a *k*-Nearest Neighbour (*k*-NN) algorithm for computing a schedule of its constituent solvers according to the *k*-neighbours runtimes. The schedule is computed by solving a generalization of a knapsack problem. CPHydra won the ICSC 2008.

*ISAC* [22] is a configuration tool that aims at optimally configuring a highly parametrized algorithm. In this work we use the ISAC ``*Pure Solver Portfolio*'' approach following what done by [31] in the SAT field. The training instances are clustered and the solver that solves the most instances in the cluster closer to the instance to be solved is selected.

*3S* [21] is a SAT solver conjugating a fixed-time static solver schedule (computed off-line) with the dynamic selection of one long-running solver. This solver is chosen with a *k*-NN algorithm and is eventually executed after the static schedule. 3S was the best dynamic portfolio in the SAT Competition 2011.

*SATzilla* [52] is a SAT solver relying on runtime prediction models. Its last version [51] uses a weighted random forest approach provided with a cost-sensitive loss function for punishing misclassifications in direct proportion to their performance impact. SATzilla won the SAT Challenge 2012.

*SUNNY* [4] is a lazy algorithm portfolio using a *k*-NN algorithm for selecting a sub-portfolio of solvers to run. Solvers are scheduled according to their performance in the neighbourhood. `sunny-cp` [5], a parallel portfolio solver built on top of the SUNNY algorithm [4], won the MiniZinc Challenge 2015.

## III. Methodology

In this section we explain the methodology used for conducting the experiments. Following what is usually done by most of the approaches, we first removed all the constant features and we scaled all the non-constant ones in the range [-1, 1], ending up with a reduced set of 114 features. Fixed a timeout of $T = 1800$ seconds[1], we then filtered the dataset of the 8600 CSPs mentioned in Section II-A by removing the ``easiest'' instances (i.e., those solved when computing the dynamic features) and the ``hardest'' ones (i.e., those for which the feature extraction required more than $T/2 = 900$ seconds). We discarded the easiest since if an instance is already solved during the feature extraction, then no solver prediction is needed. The hardest ones were instead discarded since if the extraction takes more than $T/2$ seconds, then recompiling the MiniZinc model into FlatZinc (a step needed to run the solvers) would take at least other $T/2$ seconds, therefore consuming all the time slot available. The final dataset $\Delta$ on which we conducted the experiments was constituted by 4642 MiniZinc instances (3538 from ICSC, 6 from MiniZinc Challenge 2012, and 1098 from MiniZinc 1.6 benchmarks).

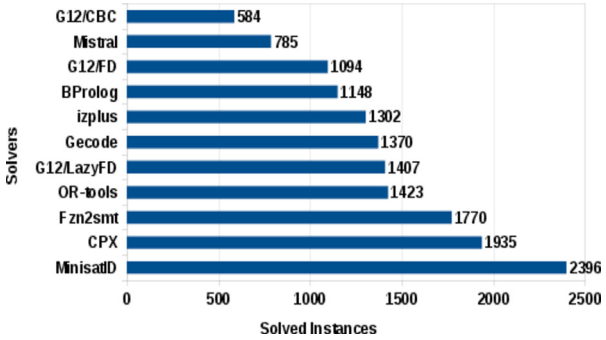


Fig. 1. Total number of solved instances for each solver of the portfolio.

We ran all the 11 solvers listed in Section II-A on each of the 4642 instances of $\Delta$, thus solving 51062 CSPs[2]. We ran all of the solvers with their default parameters, their specific FlatZinc redefinitions, and keeping track of their performance within the timeout $T$. We then built ten portfolios $\prod_m$ of different size $m = 2, \ldots, 11$ where $\prod_m$ is the portfolio with cardinality $m$ maximizing the number of solved instances in $\Delta$ (we used the average solving time for breaking ties). Unlike other approaches, following [2], we decided to keep in $\Delta$ the 944 CSPs not solvable by any solver. We took this decision since these instances could affect the behavior of a portfolio approach. For example, SUNNY allocates to a predesignated backup solver an amount of time proportional to the instances of the *k*-neighborhood that no solver can solve.

The single solvers performance are listed in Fig. 1. The *Single Best Solver* (SBS) of the portfolio is MinisatID [10] since it solves

1 The same timeout used in the ICSC (the timeout of MiniZinc Challenge is lower).
2 We used Intel Dual-Core 2.93GHz computers with 2 GB of RAM and Ubuntu operating system.

the greatest number of instances. Each of the portfolio approaches described in Section II-B has been simulated and evaluated using a 5-repeated 5-fold cross validation [8]. We evaluated the performance of each approach in terms of *Average Solving Time* (AST)[3] and *Percentage of Solved Instances* (PSI) within *T* seconds.

## IV. Results

This section presents the obtained results. In addition to the SBS and the portfolio approaches, we add to the evaluation the *Virtual Best Solver* (VBS) baseline. The VBS is an "oracle" solver always selecting the best solver of the portfolio for any given instance. For all the reimplemented approaches (i.e., ISAC, 3S, and SATzilla) we use the *'-like'* suffix. For the OTS approaches we tried different techniques like oversampling, parameters tuning, meta-classifiers, and feature selection. The best results were obtained by RF (with 250 decision trees) and SMO (with a RBF kernel and the $C$, $\gamma$ parameters set to $2^9$ and $2^{-8}$ respectively). In the rest of the section, for better viewing, we report only their performance among all the OTS variants we experimented. For all the approaches relying on $k$-NN algorithm we fixed $k = 10$ and used the Euclidean distance metric.

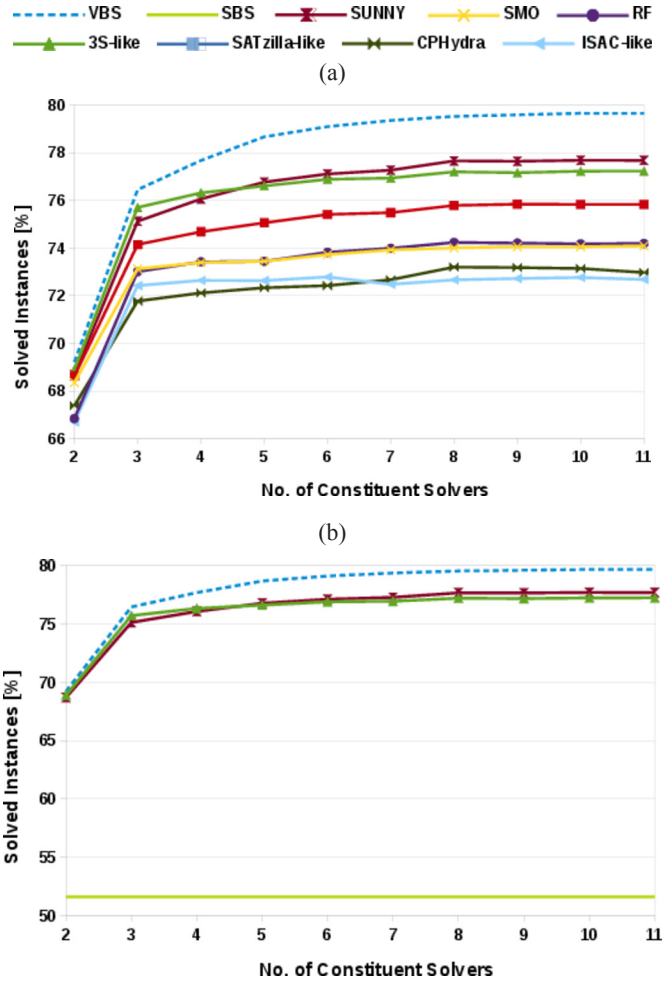


Fig. 2: PSI performance.

Fig. 2a shows the Percentage of Solved Instances for the aforementioned approaches. All of them have good performance. As already observed by [2], 3S-like and SATzilla-like are better than the best OTS approaches, which in turn solve more instances than ISAC-like and CPHydra. We do not notice the performance deterioration observed by [2] when increasing the portfolio size: the addition of a new solver is almost always beneficial, or at least not so harmful. Being the methodology of the experiments basically the same of [2], we deem that such a behavior is due to the different nature of the dataset, the features, and the solvers we used in this evaluation.

The peak performances are reached by 3S-like (77.23% with 11 solvers) and SUNNY (77.69% with 10 solvers) while in this case SATzilla-like is slightly worse (75.85% with 9 solvers). Fig. 2b depicts the performance of 3S-like and SUNNY only, together with the SBS and the VBS. It is immediately visible the performance difference between the best portfolio approaches and the SBS, which solves just 51.62% of the instances. In particular, SUNNY is able to close up to 92.95% of the gap between the SBS and the VBS.

Fig. 3a shows the Average Solving Time for each approach. As also noted by [2] the AST is highly anti-correlated with the PSI for all the approaches except CPHydra. 3S-like however is slower if compared to its performance in the work by [2]. A plausible explanation is that CPHydra and 3S-like do not employ any heuristic for sorting the selected solvers. Let us explain this with a simple example. Let us suppose that a solver $S_1$ solves a given CSP in 10 seconds, while another solver $S_2$ fails to solve it. Now consider two portfolio approaches $P_1$ and $P_2$. $P_1$ schedules $S_1$ for the first 900 seconds, and then $S_2$ for the remaining 900 seconds. Symmetrically, $P_2$ schedules $S_2$ for 900 seconds and then $S_1$ for the remaining time. Despite both $P_1$ and $P_2$ solves the CSP —so the different schedules do not influence the PSI— the solving time of $P_1$ will be 10 seconds, while the one of $P_2$ will be 910 seconds. Clearly, this difference might have a great influence on the AST.

3S-like is better than CPHydra since it solves more instances and schedules the solvers in a reduced time window ($T/10 = 180$ seconds). Conversely, the heuristic used by SUNNY (which sorts the selected solvers by increasing solving time in the $k$-neighbourhood) is fruitful in this context. SATzilla-like is not far from SUNNY, confirming that it can minimize the AST more than 3S-like, even if it solves less instances. Also in this case the difference with the SBS is remarkable (see Fig. 3b). The best AST performance is reached by SUNNY (568.84 seconds) which by using 10 solvers is able to close the 77.52% of the gap between the SBS and the VBS. The strong anti-correlation between AST and PSI is confirmed by the low Pearson coefficient (about –0.79). There is instead a linear correlation between the PSI and the AST of CPHydra. Nonetheless, its worst performance (884.81 seconds) is however better than the one of the SBS. For better viewing, Table 1 and Table 2 report the actual values of PSI and AST respectively.

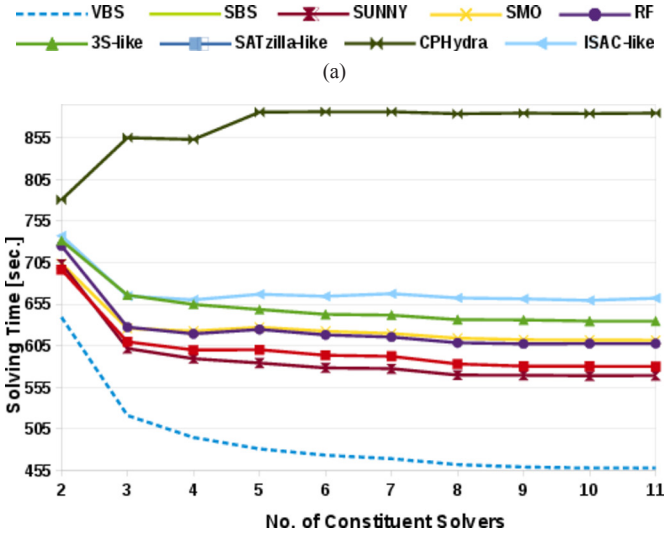


3. If a (portfolio) solver can not solve an instance in T seconds, its solving time is set to T. This choice is also adopted in the MiniZinc Challenge, while in other contexts (e.g., SAT competitions) a penalization of $10 \times T$ seconds is given (PAR10 score).

TABLE 1: PSI VALUES

| No. Solvers | SBS | VBS | RF | SMO | SATzilla | 3S | ISAC | CPHydra | SUNNY |
|---|---|---|---|---|---|---|---|---|---|
| 2 | 51.62 | 69.22 | 66.84 | 68.35 | 68.63 | 68.9 | 66.7 | 67.38 | 68.69 |
| 3 | 51.62 | 76.45 | 73.01 | 73.13 | 74.15 | 75.71 | 72.43 | 71.78 | 75.13 |
| 4 | 51.62 | 77.68 | 73.43 | 73.4 | 74.69 | 76.32 | 72.65 | 72.12 | 76.07 |
| 5 | 51.62 | 78.67 | 73.45 | 73.45 | 75.07 | 76.61 | 72.64 | 72.34 | 76.77 |
| 6 | 51.62 | 79.1 | 73.83 | 73.73 | 75.42 | 76.89 | **72.79** | 72.43 | 77.11 |
| 7 | 51.62 | 79.36 | 73.99 | 73.93 | 75.49 | 76.95 | 72.48 | 72.67 | 77.28 |
| 8 | 51.62 | 79.53 | **74.24** | 74.01 | 75.79 | 77.21 | 72.67 | **73.21** | 77.66 |
| 9 | 51.62 | 79.6 | 74.21 | 74.05 | **75.85** | 77.17 | 72.73 | 73.18 | 77.65 |
| 10 | 51.62 | 79.66 | 74.18 | 74.06 | 75.84 | **77.23** | 72.77 | 73.15 | **77.69** |
| 11 | 51.62 | 79.66 | 74.2 | **74.09** | 75.84 | **77.23** | 72.68 | 72.98 | **77.69** |
| ***MIN*** | *51.62* | *69.22* | *66.84* | *68.35* | *68.63* | *68.9* | *66.7* | *67.38* | *68.69* |
| ***MAX*** | *51.62* | *79.66* | *74.24* | *74.09* | *75.85* | *77.23* | *72.79* | *73.21* | ***77.69*** |
| ***AVG*** | *51.62* | *77.9* | *73.14* | *73.22* | *74.68* | *76.02* | *72.05* | *72.12* | *76.17* |

TABLE 2: AST VALUES

| No. Solvers | SBS | VBS | RF | SMO | SATzilla | 3S | ISAC | CPHydra | SUNNY |
|---|---|---|---|---|---|---|---|---|---|
| 2 | 950.91 | 639.36 | 725.12 | 703.85 | 696.53 | 731.54 | 737.21 | **780.5** | 703.39 |
| 3 | 950.91 | 521.23 | 627.35 | 625.96 | 609.81 | 666.06 | 664.79 | 855.24 | 601.78 |
| 4 | 950.91 | 494.77 | 619.35 | 622.61 | 599.94 | 654.8 | 660.3 | 853.04 | 589.41 |
| 5 | 950.91 | 481.04 | 624.61 | 627.17 | 600.32 | 648.65 | 666.9 | 885.84 | 584.2 |
| 6 | 950.91 | 473.47 | 618.08 | 622.54 | 593.55 | 642.83 | 664.55 | 886.39 | 578.4 |
| 7 | 950.91 | 469.18 | 615.43 | 619.72 | 592.3 | 641.8 | 667.57 | 886.35 | 577.54 |
| 8 | 950.91 | 462.17 | 608.54 | 614.11 | 583.1 | 636.47 | 662.57 | 883.89 | 569.7 |
| 9 | 950.91 | 459.25 | **607.28** | 612.15 | 580.43 | 636.09 | 661.39 | 884.75 | 569.51 |
| 10 | 950.91 | 458.12 | 607.63 | 611.96 | 580.35 | **634.72** | **659.54** | 884.19 | **568.84** |
| 11 | 950.91 | 458.03 | 607.68 | **611.68** | **580.3** | 634.83 | 662.27 | 884.81 | 569.3 |
| ***MIN*** | *950.91* | *458.03* | *607.28* | *611.68* | *580.3* | *634.72* | *659.54* | *780.5* | ***568.84*** |
| ***MAX*** | *950.91* | *639.36* | *725.12* | *703.85* | *696.53* | *731.54* | *737.21* | *886.39* | *703.39* |
| ***AVG*** | *950.91* | *491.66* | *626.11* | *627.17* | *601.66* | *652.78* | *670.71* | *868.5* | *591.21* |

(b)

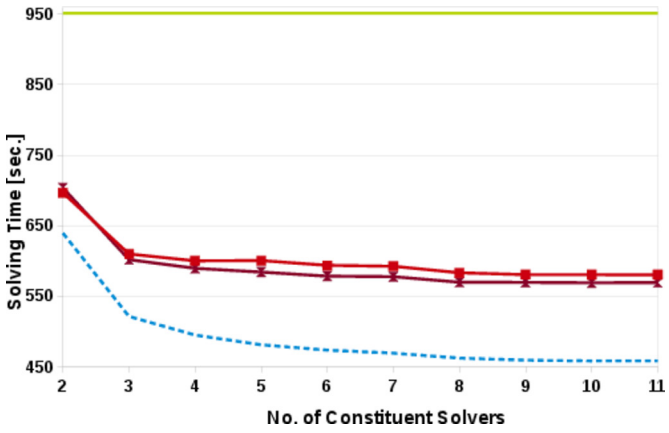


Fig. 3: AST performance.

Reproducibility The problem of effectively reproducing and comparing different approaches is a well-known issue that also affected this work. Indeed, some of the approaches we tested were not publicly available or extremely hard to use and adapt when available. There are several different ways to adapt an approach to CSP, and many other solver selectors exists. Clearly, comparing them all is a daunting task. To address this problem, the Algorithm Selection Library (ASlib) [9] has been recently introduced. ASlib provides a standardized format for representing very heterogeneous portfolio scenarios with the aim of effectively sharing and comparing different approaches. Unfortunately, at the time we conducted the experiments the ASlib had not been developed yet. We then submitted to ASlib the data and the results described in this paper, hoping that this will foster the creation of further and better portfolio approaches for the CSP field. Furthermore, the source code we developed for conducting the experiments is available at: http://www.cs.unibo.it/~amadini/csp_portfolio.zip

## V. Conclusions

In this paper we presented an empirical analysis of different portfolio approaches for solving Constraint Satisfaction Problems (CSPs). We simulated and evaluated different approaches on extensive benchmarks of CSPs encoded in MiniZinc language. The obtained results are encouraging and confirm the effectiveness of CSP portfolio solvers in terms of both solved instances and solving time.

Since the impossibility of using the original code, most of the approaches have been reimplemented trying to be as faithful as possible. However, for making our experiments reproducible and comparable, we submitted the evaluation scenario to the Algorithm Selection library [9]. Indeed, in addition to the approaches evaluated in this paper, a plethora of other CSP portfolio approaches have been proposed in the literature [32,12,46,18,2]. For more comprehensive surveys about algorithm selection and runtime prediction we refer the interested reader to [25,45,20].

The possible extensions of this work are manifold. From the CSP point of view, the gap with SAT portfolio solvers is still pronounced. An immediate research direction is therefore to encourage the construction, the experimentation, and the dissemination of effective and portable CSP portfolio solvers by devising new techniques and strategies. Moreover, even if in this work we focused only on sequential approaches, the multi-solver nature of portfolios naturally leads to the parallelization of the solvers execution [29,24,42,16,5].

A well-known problem concerns the selection of the most informative features for removing redundant information and improving the prediction accuracy [19,26]. Reducing the training times [47] and exploiting incoming knowledge [28] are also promising directions for having more dynamic portfolios. Finally, we remark that portfolio approaches can be successfully applied in the most disparate domains. Besides SAT and CSP fields, successful portfolio solvers have been developed also for Answer-Set Programming (ASP) [15], Quantified Boolean Formula (QBF) [38], Planning [44], Constraint Optimization Problems (COPs) [6].

## VI. References


[1] Roberto Amadini, Maurizio Gabbrielli, and Jacopo Mauro. A Constraint-Based Model for Fast Post-Disaster Emergency Vehicle Routing. *IJIMAI*, vol. 2, num. 4, pp. 67-75, 2013.

[2] Roberto Amadini, Maurizio Gabbrielli, and Jacopo Mauro. An Empirical Evaluation of Portfolios Approaches for Solving CSPs. In *CPAIOR*, vol. 7874 of LNCS, pp. 316-324. Springer, 2013.

[3] Roberto Amadini, Maurizio Gabbrielli, and Jacopo Mauro. An Enhanced Features Extractor for a Portfolio of Constraint Solvers. In *SAC*, pp. 1357-1359. ACM, 2014.

[4] Roberto Amadini, Maurizio Gabbrielli, and Jacopo Mauro. SUNNY: a lazy portfolio approach for constraint solving. *TPLP*, vol. 14, num. 4-5, pp. 509-524, 2014.

[5] Roberto Amadini, Maurizio Gabbrielli, and Jacopo Mauro. A Multicore Tool for Constraint Solving. In *IJCAI*, pp. 232-238. AAAI Press, 2015.

[6] Roberto Amadini and Peter J. Stuckey. Sequential Time Splitting and Bounds Communication for a Portfolio of Optimization Solvers. In *CP*, vol. 8656 of *LNCS*, pp. 108-124. Springer, 2014.

[7] Roberto Amadini, Maurizio Gabbrielli, and Jacopo Mauro. Why CP Portfolio Solvers are (under)Utilized? Issues and Challenges. In *LOPSTR*, vol. 9527 of *LNCS*, pp. 349-364. *Springer*, 2015.

[8] S. Arlot and A. Celisse. A survey of cross-validation procedures for model selection. *Statistics Surveys*, vol. 4, pp. 40-79, 2010.

[9] Bernd Bischl, Pascal Kerschke, Lars Kotthoff, Marius Thomas Lindauer, Yuri Malitsky, Alexandre Fréchette, Holger H. Hoos, Frank Hutter, Kevin Leyton-Brown, Kevin Tierney, and Joaquin Vanschoren. Aslib: A benchmark library for algorithm selection. *CoRR*, abs/1506.02465, 2015.

[10] Broes de Cat, Bart Bogaerts, Jo Devriendt, and Marc Denecker. Model Expansion in the Presence of Function Symbols Using Constraint Programming. In *ICTAI*, pp. 1068-1075, 2013.

[11] Cormac Gebruers, Alessio Guerri, Brahim Hnich, and Michela Milano. Making Choices Using Structure at the Instance Level within a Case Based Reasoning Framework. In *CPAIOR*, vol. 3011 of *LNCS*, pp. 380-386. Springer, 2004.

[12] Ian P. Gent, Christopher Jefferson, Lars Kotthoff, Ian Miguel, Neil C. A. Moore, Peter Nightingale, and Karen E. Petrie. Learning when to use lazy learning in constraint solving. In *ECAI*, vol. 215 of *FAIA*, pp. 873-878. IOS Press, 2010.

[13] Carla P. Gomes and Bart Selman. Algorithm portfolios. *Artif. Intell.*, vol. 126, num. 1-2, pp. 43-62, 2001.

[14] Mark Hall, Eibe Frank, Geoffrey Holmes, Bernhard Pfahringer, Peter Reutemann, and Ian H. Witten. The WEKA data mining software: an update. *SIGKDD Explor. Newsl.*, vol 11, num. 1, November 2009.

[15] Holger Hoos, Marius Thomas Lindauer, and Torsten Schaub. claspfolio 2: Advances in algorithm selection for answer set programming. *TPLP*, vol. 14, num. 4-5, pp. 569-585, 2014.

[16] Holger H. Hoos, Marius Thomas Lindauer, and Frank Hutter. From Sequential Algorithm Selection to Parallel Portfolio Selection. In *LION*, vol. 8426 of *LNCS, pp. 21-35,* 2015.

[17] Bernardo A Huberman, Rajan M Lukose, and Tad Hogg. An economics approach to hard computational problems. *Science*, vol. 275, num. 5296, pp. 51-54, 1997.

[18] Barry Hurley, Lars Kotthoff, Yuri Malitsky, and Barry O'Sullivan. Proteus: A Hierarchical Portfolio of Solvers and Transformations. In *CPAIOR*, vol. 8451 of *LNCS*, pp. 301-317. Springer, 2014.

[19] Frank Hutter, Holger H. Hoos, and Kevin Leyton-Brown. Identifying Key Algorithm Parameters and Instance Features Using Forward Selection. In *LION*, vol. 7997 of *LNCS*, pp. 364-381. Springer, 2013.

[20] Frank Hutter, Lin Xu, Holger H. Hoos, and Kevin Leyton-Brown. Algorithm runtime prediction: Methods & evaluation. *Artif. Intell.*, vol. 206, num. 79-111, 2014.

[21] Serdar Kadioglu, Yuri Malitsky, Ashish Sabharwal, Horst Samulowitz, and Meinolf Sellmann. Algorithm Selection and Scheduling. In *CP*, vol. 6876 of *LNCS*. Springer, 2011.

[22] Serdar Kadioglu, Yuri Malitsky, Meinolf Sellmann, and Kevin Tierney. ISAC - Instance-Specific Algorithm Configuration. In *ECAI*, vol. 215 of *FAIA*. IOS Press, 2010.

[23] George Katsirelos and Fahiem Bacchus. Generalized NoGoods in CSPs. In *AAAI*, pp. 390-396, 2005.

[24] George Katsirelos, Ashish Sabharwal, Horst Samulowitz, and Laurent Simon. Resolution and parallelizability: Barriers to the efficient parallelization of SAT solvers. In *AAAI*. AAAI Press, 2013.

[25] Lars Kotthoff. Algorithm Selection for Combinatorial Search Problems: A Survey. *AI Magazine*, vol. 35, num. 3, pp. 48-60, 2014.

[26] Christian Kroer and Yuri Malitsky. Feature Filtering for Instance-Specific Algorithm Configuration. In *ICTAI*, pp. 849-855. IEEE, 2011.

[27] Alan K. Mackworth. Consistency in Networks of Relations. *Artif. Intell.*, vol. 8, num. 1, pp. 99-118, 1977.

[28] Yuri Malitsky, Deepak Mehta, and Barry O'Sullivan. Evolving instance specific algorithm configuration. In *SOCS*. AAAI Press, 2013.

[29] Yuri Malitsky, Ashish Sabharwal, Horst Samulowitz, and Meinolf Sellmann. Parallel SAT solver selection and scheduling. In *CP*, vol. 7514 of *LNCS*, pp. 512-526. Springer, 2012.

[30] Yuri Malitsky, Ashish Sabharwal, Horst Samulowitz, and Meinolf Sellmann. Algorithm Portfolios Based on Cost-Sensitive Hierarchical Clustering. In *IJCAI*. IJCAI/AAAI, 2013.

[31] Yuri Malitsky and Meinolf Sellmann. Instance-Specific Algorithm Configuration as a Method for Non-Model-Based Portfolio Generation. In *CPAIOR*, vol. 7298 of *LNCS*. Springer, 2012.

[32] Steven Minton. Automatically configuring constraint satisfaction programs: A case study. *Constraints*, vol. 1, num. 1/2, pp. 7-43, 1996.

[33] Nicholas Nethercote, Peter J. Stuckey, Ralph Becket, Sebastian Brand, Gregory J. Duck, and Guido Tack. MiniZinc: Towards a Standard CP Modelling Language. In *CP*, 2007.

[34] Mladen Nikolic, Filip Maric, and Predrag Janicic. Instance-Based Selection of Policies for SAT Solvers. In *SAT*, vol. 5584 of *LNCS*, pp. 326-340. Springer, 2009.

[35] Eoin O'Mahony, Emmanuel Hebrard, Alan Holland, Conor Nugent, and Barry O'Sullivan. Using case-based reasoning in an algorithm portfolio for constraint solving. In *AICS*, 2008.

[36] Zahra Pooranian, Mohammad Shojafar, Jemal H. Abawajy and Mukesh Singhal. GLOA: A New Job Scheduling Algorithm for Grid Computing. *IJIMAI*, vol. 2, num. 1, pp. 59-64, 2013.

[37] Luca Pulina and Armando Tacchella. A Multi-engine Solver for Quantified Boolean Formulas. In *CP*, vol. 4741 of *LNCS*, pp. 574-589. Springer, 2007.

[38] Luca Pulina and Armando Tacchella. A self-adaptive multi-engine solver for quantified boolean formulas. *Constraints*, vol. 14, num. 1, pp. 80-116, 2009.

[39] John R. Rice. The Algorithm Selection Problem. *Advances in Computers*, vol. 15, pp. 65-118, 1976.

[40] F. Rossi, P. van Beek, and T. Walsh, editors. *Handbook of Constraint Programming*. Elsevier, 2006.

[41] Olivier Roussel and Christophe Lecoutre. XML Representation of Constraint Networks: Format XCSP 2.1. *CoRR*, abs/0902.2362, 2009.

[42] Ashish Sabharwal and Horst Samulowitz. Insights into parallelism with

intensive knowledge sharing. In *CP*, vol. 8656 of *LNCS*, pp. 655-671. Springer, 2014.

[43] Horst Samulowitz, Chandra Reddy, Ashish Sabharwal, and Meinolf Sellmann. Snappy: A simple algorithm portfolio. In *SAT*, vol. 7962 of *LNCS*, pp. 422-428. Springer, 2013.

[44] Jendrik Seipp, Silvan Sievers, Malte Helmert, and Frank Hutter. Automatic configuration of sequential planning portfolios. In *AAAI*, pp. 3364-3370. AAAI Press, 2015.

[45] Kate Smith-Miles. Cross-disciplinary perspectives on meta-learning for algorithm selection. *ACM Comput. Surv.*, vol. 41, num. 1, 2008.

[46] Kostas Stergiou. Heuristics for dynamically adapting propagation in constraint satisfaction problems. *AI Commun.*, vol. 22, num. 3, pp. 125-141, 2009.

[47] Mirko Stojadinovic, Mladen Nikolic, and Filip Maric. Short portfolio training for CSP solving. *CoRR*, abs/1505.02070, 2015.

[48] Peter J. Stuckey, Ralph Becket, and Julien Fischer. Philosophy of the MiniZinc challenge. *Constraints*, vol. 15, num. 3, pp. 307-316, 2010.

[49] MRC van Dongen, Christophe Lecoutre, and Olivier Roussel. Third International CSP Solver Competition, 2008.

[50] L. Xu, F. Hutter, J. Shen, H. Hoos, and K. Leyton-Brown. SATzilla2012: Improved algorithm selection based on cost-sensitive classification models. Solver description, SAT Challenge 2012, 2012.

[51] Lin Xu, Frank Hutter, Holger Hoos, and Kevin Leyton Brown. Evaluating Component Solver Contributions to Portfolio-Based Algorithm Selectors. In *SAT*, vol. 7317 of *LNCS*, pp. 228-241. Springer, 2012.

[52] Lin Xu, Frank Hutter, Holger H. Hoos, and Kevin Leyton-Brown. The design and analysis of an algorithm portfolio for sat. In *CP*, vol. 4741 of *LNCS*, pp. 712-727. Springer, 2007.

[53] Lin Xu, Frank Hutter, Holger H. Hoos, and Kevin Leyton-Brown. Satzilla: Portfolio-based algorithm selection for SAT. *JAIR*, vol. 32, pp. 565-606, 2008.

**Roberto Amadini** received a Bachelor (2007) and Master (2011) degree in Computer Science from the University of Parma. In 2015 he received a Ph.D. in Computer Science from the University of Bologna. He is interested in Constraint Programming, Operations Research, Algorithm Selection, Software Anallysis and Verification. Currently is a Research Fellow at the Department of Computing and Information Systems of the University of Melbourne, Australia.

**Maurizio Gabbrielli** is professor of Computer Science at the University of Bologna, member of the INIRIA team FOCUS and Director of the EIT Digital Doctoral School. He received his Phd. in Computer Science in 1992 from the University of Pisa and worked at CWI (Amsterdam) and at the University of Pisa and of Udine. His research interests include constraint programming, formal methods for program verification and analysis, service oriented programming.

**Jacopo Mauro** received a bachelor and master degree in computer science from Udine University. In 2012 he receive a PhD in computer science from the University of Bologna. From 2010 to 2015 he was member of the Focus Research Group at INRIA (France). He has been involved in numerous Italian, French, and European research projects and a visiting student at CWI (Netherlands). He is currently working at the University of Oslo and interested in Concurrent Languages, Service Oriented Computing, Constraint Programming, Constraint Handling Rules, AI Planning and Distributed Application Deployment.

# Chinese-chi and Kundalini yoga Meditations Effects on the Autonomic Nervous System: Comparative Study

Anilesh Dey, D. K. Bhattacharya, D.N. Tibarewala, [7] Nilanjan Dey, [5] Amira S. Ashour, [6] Dac-Nhuong Le, [7] Evgeniya Gospodinova, [7] Mitko Gospodinov

[1] *Department Electronics and Communication Engineering at The Assam Kaziranga University, India*
[2] *Department of Pure Mathematics University of Calcutta, India*
[3] *School of Bioscience & Engineering at Jadavpur University, India*
[4] *Department of Information Technology in Techno India College of Technology, India*
[5] *Computers Engineering Department, Computers and Information Technology College*
[6] *Faculty of Information Technology, Haiphong University, Vietnam.*
[7] *Computer Systems Engineering at Institute of Systems Engineering and Robotics of Bulgarian Academy of Sciences, Bulgaria*

***Abstract* — Cardiac disease is one of the major causes for death all over the world. Heart rate variability (HRV) is a significant parameter that used in assessing Autonomous Nervous System (ANS) activity. Generally, the 2D Poincare′ plot and 3D Poincaré plot of the HRV signals reflect the effect of different external stimuli on the ANS. Meditation is one of such external stimulus, which has different techniques with different types of effects on the ANS. Chinese Chi-meditation and Kundalini yoga are two different effective meditation techniques. The current work is interested with the analysis of the HRV signals under the effect of these two based on meditation techniques. The 2D and 3D Poincare′ plots are generally plotted by fitting respectively an ellipse/ellipsoid to the dense region of the constructed Poincare′ plot of HRV signals. However, the 2D and 3D Poincaré plots sometimes fail to describe the proper behaviour of the system. Thus in this study, a three-dimensional frequency-delay plot is proposed to properly distinguish these two famous meditation techniques by analyzing their effects on ANS. This proposed 3D frequency-delay plot is applied on HRV signals of eight persons practicing same Chi-meditation and four other persons practising same Kundalini yoga. To substantiate the result for larger sample of data, statistical Student t-test is applied, which shows a satisfactory result in this context. The experimental results established that the Chi-meditation has large impact on the HRV compared to the Kundalini yoga.**

***Keywords* — 2D and 3D Poincaré Plot, 3D Frequency Delay Plot, Hypothesis Testing By Student t-Test.**

## I. Introduction

Meditation is considered an ancient spiritual practice that has potential benefit on health and well-being [1, 2]. It is a complex physiological process, which affects neural, psychological, behavioral, and autonomic functions. It is considered as an altered state of consciousness, which differs from wakefulness, relaxation at rest, and sleep [3, 4]. Most of the meditation techniques affect the ANS, thus indirectly regulate several organs and muscles. Accordingly, functions of heartbeat, sweating, breathing, and digestion are controlled by the ANS. Recent studies highlighted the psycho-physiological aspects of meditation and its effect [5-15].

Typically, the HRV is a popular non-invasive tool to assess different conditions of heart [16-19]. Nowadays, it is observed that HRV reflects some psychological conditions [20, 21]. The HRV analysis studies the period variation between consecutive heart beats to provide valuable information for the ANS assessment. There are two branches of the ANS, namely i) the sympathetic branch, which increases the heart bits, and ii) the parasympathetic branch, which decreases the heart bits. Thus, the observed HRV is an indicator of the dynamic interaction and balance between these two nervous systems. In the resting condition, both the sympathetic and parasympathetic systems are active with parasympathetic dominance. The balance between both systems is constantly varying to optimize the effect of any internal/external stimuli [22]. Accordingly, the HRV can be significantly affected by physiological state changes and various diseases. Due to the non-invasive character of the HRV, it becomes an attractive tool for the study of human physiological response to different stimuli.

There are a variety of mathematical techniques used to analyze HRV. Peng *et al*. [23] were interested with the effect of the Chinese Chi and Kundalini Yoga meditation techniques in healthy young adults. It was reported an extremely major heart rate oscillations related to slow breathing during these meditation techniques. The authors applied the spectral analysis along with a new analytic technique based on the Hilbert transform to quantify these heart rate dynamics. The experimental results reported greater oscillations' amplitude during theses meditation compared to the pre-meditation control state and in three non-meditation control groups as well.

Kheder *et al*. [24] introduced an analysis of HRV signals using wavelet transform (WT). The WT assessment as a feature extraction approach was employed to represent the electrophysiological signals. The authors studied the effect on the ANS system of subjects who did some meditation exercises such as the Chi and Yoga. The calculated detail wavelet coefficients of the HRV signals were used as the feature vectors that represented the signals. Kheder *et al*. [25] suggested a novel proficient feature extraction technique based on the adaptive threshold of wavelet package coefficients. It is used to evaluate the ANS using the background variation of the HRV signal. The proposed method provided the HRV signal representation in a time-frequency form. This provided better insight in the frequency distribution of the HRV signal with time. The ANOVA statistical test was employed for the evaluation of proposed algorithm.

Consequently, in the current work, the effect of meditation on HRV signals under pre-meditative and meditative states is analyzed. A proposed method is applied [26] for this analysis and thereby distinguishes between two different meditation techniques, namely the


DOI: 10.9781/ijimai.2016.3713

Chinese chi-meditation and Kundalini yoga. Traditional 2D and 3D Poincaré plots [27-33] with proper delay are constructed for the analysis of the effect of meditation on HRV signals under pre-meditative and meditative states. However, no differences can be visual even by fitting an ellipse/ellipsoid in the respective cases to the cloud region of the Poincare′ plot of the HRV signals [34]. Consequently, the signal is analyzed in the frequency domain by transferring the signal from the time domain to the frequency domain using Fast Fourier Transform (FFT) [35]. The notion of three-dimensional (3D) frequency-delay plot [26] is applied. Furthermore, student t-test [36] is performed to substantiate the result for larger sample of data statistical.

The structure of the remaining sections is as follows. Section II included the materials and methods used in the proposed system. Afterwards, the results and discussion are represented in Section III. Finally, the conclusion is depicted in Section IV.

## II. Materials and Methods

During resting conditions, the RR interval variations characterize a fine tuning of beat-to-beat control. Typically, the HRV signals analysis is very significant for the ANS study to evaluate the stability between the sympathetic and parasympathetic effects on the heart rhythm. Since, the physical activity level is obviously specified in the HRV power spectrum. Thus, the current work proposed a method to effectively analyze the HRV as an indication the ANS system of subjects who are performing meditation exercises such as the Chinese-chi and Kundalini yoga.

### A. Subjects and Meditation Techniques

In this study, two popular meditative techniques, namely Chinese Chi (Qigong) meditation and the traditional Kundalini yoga are concerned. All the data are collected from PhysioNet [37]. The Chi meditators were all graduate and post-doctoral students. They were relatively novices in their practice of Chi meditation; most of them began their meditation practice about 1–3 months before this study. All the subjects were healthy, who sign consent in accord with a protocol approved by the Beth Israel Deaconess Medical Centre Institutional Review Board.

Eight Chi meditators, who are 5 women and 3 men (age range 26–35 yrs), wore a Holter recorder for 10 hours during their ordinary daily activities were engaged in this study. During approximately 5 hours into the recording, each of the meditators practiced one hour of meditation. Beginning and ending of meditation times were delineated with event marks. During these sessions, the Chi meditators sat quietly, listening to the taped guidance. The meditators were instructed to breathe spontaneously. The meditation session lasted after about one hour.

For Kundalini Yoga meditation, four meditators (2 women and 2 men: age range 20–52 yrs), wore a Holter monitor for approximately one and half hours. Fifteen minutes of baseline quiet breathing were recorded before the 1 hour of meditation. The meditation protocol consisted of a sequence of breathing and chanting exercises, performed while seated in a cross-legged posture. The beginning and ending of the various meditation sub-phases were delineated with event marks.

### B. Poincaré plots for HRV Analysis

To explore the HRV dynamics on 'beat-to-beat' basis, the original idea of 2D Poincaré plot included a delay of one beat only with non-unit lag is developed. In order to obtain comparatively better form of 2D Poincaré plot, proper quantification of the 2D Poincaré plot is required for the purpose of interpretation of the behavior of the data. For example, when quantification of 2D Poincaré Plot is performed by the process of 'ellipse fit', then for this ellipse, independent coordinates are required from the data itself. Generally, for quantifying the Poincaré plot, it should not have irregular shape. Hence, it is necessary to select proper lag for constructing best 2D Poincaré plot. Therefore, the minimum auto-correlation method and the Average Mutual Information (AMI) method can be employed for obtaining the proper delay [38]. Since, the HRV signal is nonlinear, thus the AMI method is used to construct the Poincaré Plot as follows.

The AMI method is employed to determine useful delay coordinates for plotting. Suppose $\{x(t)\}_{t=1}^{N}$ is given time series. Given the state of the system $x(t)$, a good choice for the delay $\tau$ is significant to provide maximum new information with measurement at $x(t+\tau)$. For too short delay value, then $x(t)$ is very related to $x(t+\tau)$, thus the plot of the data will stay near the line $x(t)=x(t+\tau)$. For too long delay value, then the coordinates are basically independent, thus no information can be gained from the plot. Therefore, the better choice of the delay $\tau$ can be done by calculating the Mutual information function $I(\tau)$ defined by:

$$I(\tau)=\sum_{t=1}^{N-\tau} P\left[x(t),x(t+\tau)\right]\log\left(\frac{P\left[x(t),x(t+\tau)\right]}{P\left[x(t)\right]P\left[x(t+\tau)\right]}\right) \quad (1)$$

It was suggested in [38] that the value of the delay, where $I(\tau)$ reaches its first minimum be used for the Poincaré reconstruction as illustrated in Fig.1.

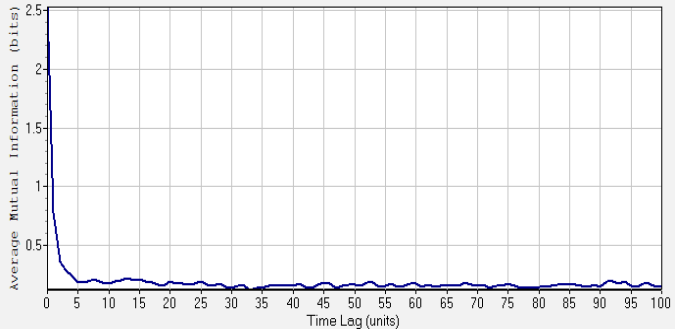


Fig. 1. Graph of the Mutual information function versus the delay

The 2D Poincaré plot is constructed with the independent coordinates $(x(t),x(t+\tau))$ and the 3D Poincaré plot is plotted with the independent coordinates $(x(t),x(t+\tau),x(t+2\tau))$.

### C. Auto-correlation in frequency domain

For the auto-correlation process [26], let $\left\{x\left(k\right)\right\}_{k=1}^{N}$ be the sample of a discrete time signal and $\left\{X(j)=a_j+ib_j\equiv\left(a_j,b_j\right)\right\}_{j=1}^{N}$ be its Fourier spectrum. The time series $\{X(j)\}_{j=1}^{N}$ is subdivide into two groups $U=\left\{X\left(j\right)\right\}_{j=1}^{N-\mu}=\left\{\left(a_j,b_j\right)\right\}_{j=1}^{N-\mu}$ and $V=\left\{X\left(j\right)\right\}_{j=1+\mu}^{N}=\left\{\left(a_j,b_j\right)\right\}_{j=1+\mu}^{N}$ for $\mu=1,2,3,4,5,.....$

The autocorrelation of $\{X(j)\}_{j=1}^{N}$ in frequency domain corresponding to lag variable $\mu$ is defined by:

$$(\mu)=\frac{\sum_{j=1}^{N}\left|\left\{\left(a_j,b_j\right)-\left(\bar{a}_j,\bar{b}_j\right)\right\}\cdot\left\{\left(a_{j+\mu},b_{j+\mu}\right)-\left(\bar{a}_{j+\mu},\bar{b}_{j+\mu}\right)\right\}\right|}{\sqrt{\sum_{j=1}^{N}\left|\left\{\left(a_j,b_j\right)-\left(\bar{a}_j,\bar{b}_j\right)\right\}\right|^2}\cdot\sqrt{\sum_{j=1}^{N}\left|\left\{\left(a_{j+\mu},b_{j+\mu}\right)-\left(\bar{a}_{j+\mu},\bar{b}_{j+\mu}\right)\right\}\right|}} \quad (2)$$

Where, $\left(\bar{a}_j,\bar{b}_j\right),\left(\bar{a}_{j+\mu},\bar{b}_{j+\mu}\right)$ are the mean values of $\{(a_j,b_j)\}_{j=1}^{N-\mu}$ and $\{(a_j,b_j)\}_{j=1+\mu}^{N}$; respectively. In addition, $(a_r,b_r)\cdot(a_s,b_s)=(a_ra_s-b_rb_s,a_rb_s+b_ra_s)$ for $r,s=1,2,3,4,5,.....N$, which called auto-correlation in the frequency domain amongst two stages. In order to define the auto-correlation in the frequency domain amongst three stages, the time series $\{X(j)\}_{j=1}^{N}$ is subdivided into three groups $U=\{X(j)\}_{j=1}^{N-2\mu}=\{(a_j,b_j)\}_{j=1}^{N-2\mu}$, $V=\{X(j)\}_{j=1+\mu}^{N-\mu}=\{(a_j,b_j)\}_{j=1+\mu}^{N-\mu}$, $W=\{X(j)\}_{j=1+2\mu}^{N}=\{(a_j,b_j)\}_{j=1+2\mu}^{N}$. Thus, the auto-correlation of $\{X(j)\}_{j=1}^{N}$ in frequency domain amongst three stages corresponding to the frequency delay $\mu$ repeated is defined by:

$$R_X(\mu)=\frac{\sum_{j=1}^{N}\left|\zeta_j\cdot\zeta_{j+\mu}\cdot\zeta_{j+2\mu}\right|}{\sqrt{\sum_{j=1}^{N}|\zeta_j|^2}\cdot\sqrt{\sum_{j=1}^{N}|\zeta_{j+\mu}|^2}\cdot\sqrt{\sum_{j=1}^{N}|\zeta_{j+2\mu}|^2}} \quad (3)$$

Where, $\mu=1,2,.....,(N-1)$, $\zeta_j=\left\{\left(a_j,b_j\right)-\left(\overline{a_j},\overline{b_j}\right)\right\},\zeta_{j+\mu}=\left\{\left(a_{j+\mu},b_{j+\mu}\right)-\left(\overline{a_{j+\mu}},\overline{b_{j+\mu}}\right)\right\}$, $\zeta_{j+2\mu}=\left\{\left(a_{j+2\mu},b_{j+2\mu}\right)-\left(\overline{a_{j+2\mu}},\overline{b_{j+2\mu}}\right)\right\}$ and $\left(\bar{a}_j,\bar{b}_j\right)$ is the mean of $\left(a_j,b_j\right)$. Moreover, $\left(a_r,b_r\right)\cdot\left(a_s,b_s\right)=\left(a_ra_s-b_rb_s,a_rb_s+b_ra_s\right)$ for $r,s=1,2,3,4,5,.....N$ and $\mu=1,2,3,4,5,.....$

In most cases, the signal interpretation in the frequency domain is based on the periodogram (Periodogram analysis), which is framed from the Fourier spectra. Since, a considerable amount of the spectra has to be overlooked or removed during the interpretation of the signals from the corresponding periodogram. Thus, the generality of the frequency domain analysis is lost. To solve this context, Poincaré plot can be used to compare the behaviour of the signal at a given frequency with that at a different frequency in the whole spectrum using analysis similar to what is done in time domain.

### *D. The 3D Frequency delay plot and its Quantification*

The 3D frequency delay plot [26] is a plot in 3D space constructed with the independent coordinates $|X(j)|,|X(j+\mu)|,|X(j+2\mu)|$, where $X(j)$ is the frequency spectrum of the discrete time-signal $X(k)$ obtained by FFT [32] of $X(k)$. The idea is quite similar to that of the 3D Poincaré plot, but as this plot is constructed in the frequency domain with a proper frequency-delay, it is called frequency-delay plot. The proper frequency-delay $(\mu)$ is obtained from the graph of $R_{X(j)}(\mu)$ versus $\mu$ using Eq. (3). In fact, the optimal frequency-delay ( $\mu$ ) is one for which $R_{X(j)}(\mu)$ comes nearer to zero for the first time. Since, $|X(j)|$ denotes the signal energy, thus the frequency-delay plot gives an insight to the changing energy dynamics of the signal.

Quantification of 3D frequency-delay plot is generally done by ellipsoid method [26]. Since, for most of the signals, the 3D frequency-delay plots are found to be almost dense and well-shaped. Therefore, an ellipsoid having its major axis along the line of identity is fitted to the dense region of the 3D frequency-delay plot. Axes of the ellipsoid stand as a strong indicator of the changing energy dynamics of HRV. Fig. 2 shows the ellipsoid fit to the dense region of the phase space.

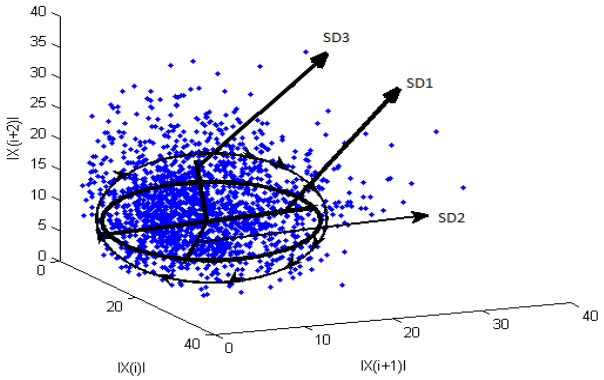


Fig. 2. Ellipsoid fitted on the dense region

Where, SD1, SD2 and SD3 are the axes of the ellipsoid. Let $\{X(j)\}_{j=1}^{N}$ be a discrete signal obtained by applying FFT [35] of the HRV signal. The 3D frequency-delay plot can be constructed by sub-dividing this signal into three groups as $x^+,x^-,x^{--}$ with the same frequency delay $\mu$, where:

$$x^+=\{|X(j)|\}_{j=1}^{N-2\mu},\ x^-=\{|X(j)|\}_{k=1+\mu}^{N-\mu},\ x^{--}=\{|X(j)|\}_{j=1+2\mu}^{N} \quad (4)$$

Where, $\mu=1,2,...,(N-1)$. The co-ordinate system is transformed by a 3D rotation with same angle $\frac{\pi}{4}$ with respect to $X$, $Y$ and $Z$ axis. The transform is given by:

$$\begin{pmatrix}x_m\\x_n\\x_p\end{pmatrix}=\begin{pmatrix}\cos\frac{\pi}{4}\cos\frac{\pi}{4} & \cos\frac{\pi}{4}\sin\frac{\pi}{4}\sin\frac{\pi}{4}-\cos\frac{\pi}{4}\sin\frac{\pi}{4} & \cos\frac{\pi}{4}\cos\frac{\pi}{4}\sin\frac{\pi}{4}+\sin\frac{\pi}{4}\sin\frac{\pi}{4}\\ \cos\frac{\pi}{4}\sin\frac{\pi}{4} & \cos\frac{\pi}{4}\cos\frac{\pi}{4}+\sin\frac{\pi}{4}\sin\frac{\pi}{4}\sin\frac{\pi}{4} & -\cos\frac{\pi}{4}\sin\frac{\pi}{4}+\cos\frac{\pi}{4}\sin\frac{\pi}{4}\sin\frac{\pi}{4}\\ -\sin\frac{\pi}{4} & \cos\frac{\pi}{4}\sin\frac{\pi}{4} & \cos\frac{\pi}{4}\cos\frac{\pi}{4}\end{pmatrix}\begin{pmatrix}x^+\\x^-\\x^{--}\end{pmatrix}$$

$$= \frac{1}{2\sqrt{2}} \begin{pmatrix} 2\sqrt{2} & -(\sqrt{2}-1) & (\sqrt{2}+1) \\ 2\sqrt{2} & (\sqrt{2}+1) & -(\sqrt{2}-1) \\ -2 & \sqrt{2} & \sqrt{2} \end{pmatrix} \begin{pmatrix} x^{+} \\ x^{-} \\ x^{--} \end{pmatrix} \tag{5}$$

Hence,

$$\begin{aligned} x_m &= \frac{1}{2}\cdot x^{+} + (\frac{1}{2\sqrt{2}} - \frac{1}{2})\cdot x^{-} + \left(\frac{1}{2\sqrt{2}} + \frac{1}{2}\right)\cdot x^{--} = \frac{2\sqrt{2}\cdot x^{+} - (\sqrt{2}-1)\cdot x^{-} + (\sqrt{2}+1)\cdot x^{--}}{2\sqrt{2}} \\ x_n &= \frac{1}{2}\cdot x^{+} + \left(\frac{1}{2\sqrt{2}} + \frac{1}{2}\right)\cdot x^{-} + \left(\frac{1}{2\sqrt{2}} - \frac{1}{2}\right)\cdot x^{--} = \frac{2\sqrt{2}\cdot x^{+} + (\sqrt{2}+1)\cdot x^{-} - (\sqrt{2}-1)\cdot x^{--}}{2\sqrt{2}} \\ x_p &= \left(-\frac{1}{\sqrt{2}}\right)\cdot x^{+} + \frac{1}{2}\cdot x^{-} + \frac{1}{2}\cdot x^{--} = \frac{-2\cdot x^{+} + \sqrt{2}\cdot x^{-} + \sqrt{2}\cdot x^{--}}{2\sqrt{2}} \end{aligned} \tag{6}$$

Thus, a new co-ordinate system $(x_m, x_n, x_p)$ is formed.

Let $\overline{x_m} = Mean(x_m), \overline{x_n} = Mean(x_n), \overline{x_p} = Mean(x_p)$ and $SD_1 = \sqrt{Var(x_m)}$, $SD_2 = \sqrt{Var(x_n)}$, $SD_3 = \sqrt{Var(x_p)}$. Lastly, an ellipsoid centred at $(\overline{x_m}, \overline{x_n}, \overline{x_p})$ with three axes of length $SD_1$, $SD_2$ and $SD_3$ is taken for quantification of the existing 3D frequency-delay plot.

### *E. Statistical Hypothesis Test*

Comparison of two populations mean is normally performed by hypothesis testing using Student's t–test [36]. However, the test stands on the assumptions: (i) the populations are normally distributed, and (ii) their variances are homogeneous. Usually the populations are taken to be normally distributed, but the homogeneity of population variances is always to be verified.

*Test for equality of the two variances*

Consider the null hypothesis $H_o : \sigma_1^2 = \sigma_2^2$ and the alternative hypothesis $H_A : \sigma_1^2 \neq \sigma_2^2$, where $\sigma_1^2$ and $\sigma_2^2$ are the variances.

The test statistic is given by $F = \frac{s_1^2}{s_2^2}$, where $s_i^2$ are the sample variances. If this calculated value of F is less than $F_{0.05(2),\nu_1,\nu_2}$; where $\nu_1$ and $\nu_2$ are the degrees of freedom, then $H_0$ holds, otherwise $H_A$ holds.

*Test for equality of two means* $\mu_1, \mu_2$ *with equal population variances* $\sigma_1^2 = \sigma_2^2$

Let the null hypothesis be $H_0 : \mu_1 = \mu_2$ and the alternate hypothesis is $H_A : \mu_1 \neq \mu_2$. The samples $X_1$ and $X_2$ with sizes $n_1$ and $n_2$ are used, where $\overline{X}_1$ and $\overline{X}_2$ are the corresponding sample means. The standard error $s_{\overline{X}_1 - \overline{X}_2}$ is given by:

$$s_{\overline{X}_1 - \overline{X}_2} = s_p \sqrt{\left(\frac{1}{n_1} + \frac{1}{n_2}\right)} \tag{7}$$

Where, $s_p$ ariance given by $s_p = \frac{\sum_i SS_i}{\sum_i \nu_i} = \frac{\sum_i \nu_i s_i^2}{\sum_i \nu_i}$ and $\nu_i$ represents the $i^{th}$ sample degrees of freedom. The test statistic 't' with degrees of freedom $\nu_1 + \nu_2$ is given by:

$$t = \frac{\overline{X} - \overline{Y}}{s_p \sqrt{\left(\frac{1}{n_1} + \frac{1}{n_2}\right)}} \tag{8}$$

If this calculated value of t is less than $t_{0.05(2),\nu_1,\nu_2}$, then $H_0$ holds, i.e., $\mu_1 = \mu_2$, otherwise $H_A$ holds, i.e., $\mu_1 \neq \mu_2$.

From the preceding methodology the Poincaré plots with proper delay of HRV signal in pre-meditation and post-meditation states in time domain are employed. Moreover, 3D Frequency-delay plot of HRV signals in pre-meditative and meditative states is represented.

## III. Results and Discussions

The current work is concerned with the HRV analysis to study the effect of the pre-meditation and post-meditation of the Chinese-chi and Kundalini yoga Meditations using time and frequency domain representations.

### *A. The 2D Poincaré plot with proper delay of HRV signal*

A 2D Poincaré plots with proper delay for the HRV signals of pre-meditative and meditative states are constructed in the time domain. The proper delay is obtained by the AMI method. Fig. 3 illustrates one such pair of 2D Poincaré plots in pre-meditative and meditative states under Chinese chi meditation.

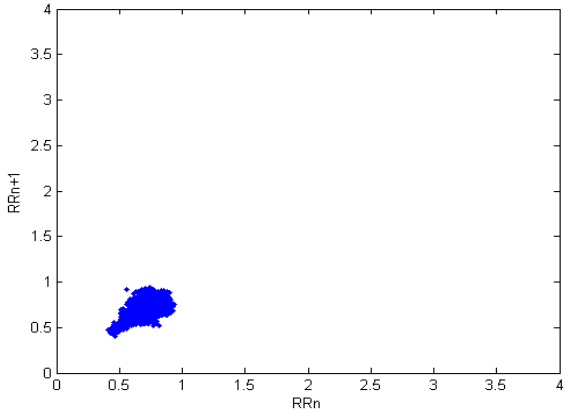


(i)

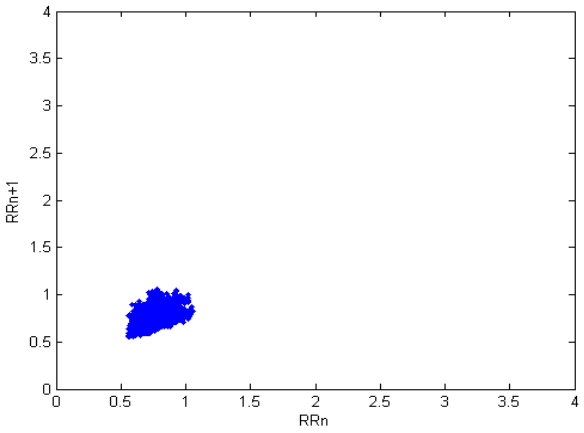


(ii)

Fig.3. The 2D Poincaré Plot with proper delay of HRV signals in (i) pre-meditative and (ii) meditative state

Fig. 3 illustrates that both the Poincaré plots are almost dense with very few outliers. Essentially, there is no approach to eliminate these outliers of the plots except with manual supervision and visual inspection. Additionally, it is necessary to focus on the main cluster because the important, relevant and necessary information in this context is hidden within the orientation of the main cluster. Thus, these plots are quantified by fitting an ellipse to their main cluster; and compute the lengths of the major and minor axis in each case. Finally, the ratio of two axes is considered as a quantifying parameter. The results of quantification of 2D Poincaré plot of HRV signals in pre-meditative and meditative states under Chinese-chi meditation and Kundalini yoga are summarized in Table I.

TABLE I
QUANTIFICATION TABLE OF 2D POINCARÉ PLOT OF HRV SIGNALS IN PRE-MEDITATIVE AND MEDITATIVE STATES

| Subjects | Pre-meditative States | | | Meditative States | | |
|---|---|---|---|---|---|---|
| | SD1 | SD2 | SD2/SD1 | SD1 | SD2 | SD2/SD1 |
| CHINESE – CHI MEDITATION | | | | | | |
| c1 | 0.217168 | 0.248071 | 1.142297 | 0.096461 | 0.092843 | 0.9625 |
| c2 | 0.08111 | 0.17088 | 2.106766 | 0.092317 | 0.091992 | 0.996483 |
| c3 | 0.065666 | 0.168197 | 2.561396 | 0.072398 | 0.085996 | 1.187816 |
| c4 | 0.067267 | 0.177687 | 2.641518 | 0.098595 | 0.10242 | 1.038795 |
| c5 | 0.035275 | 0.085689 | 2.429142 | 0.054112 | 0.066373 | 1.226589 |
| c6 | 0.051249 | 0.095185 | 1.857299 | 0.078813 | 0.103829 | 1.317402 |
| c7 | 0.201171 | 0.224579 | 1.116359 | 0.100892 | 0.123328 | 1.222379 |
| c8 | 0.048568 | 0.106893 | 2.200897 | 0.081619 | 0.09105 | 1.115541 |
| KUNDALINI YOGA | | | | | | |
| y1 | 0.034221 | 0.050117 | 1.464478 | 0.056986 | 0.067504 | 1.184563 |
| y2 | 0.050891 | 0.087036 | 1.710252 | 0.078341 | 0.065093 | 0.830892 |
| y3 | 0.062703 | 0.078124 | 1.245926 | 0.099425 | 0.079435 | 0.798945 |
| y4 | 0.163102 | 0.235673 | 1.444941 | 0.166584 | 0.15217 | 0.91347 |

Table I depicts that the ratio of the axis length $SD_2/SD_1$ decreases in meditative states for all subjects except c7 under Chinese-chi meditation, where the ratio value increases in the meditative states. However, the ratio decreases in meditative state for all subjects under Kundalini yoga. Thus, the 2D Poincaré plot with proper delay is improper tool for distinguishing the two different techniques of meditations. Therefore, the 3D Poincaré plot with proper delay is used instead of the 2D Poincaré plot with proper delay.

### *B. The 3D Poincaré Plot with proper delay of HRV signal*

The 3D Poincaré plots with proper delay for the HRV signals of pre-meditative and meditative states are constructed. The proper delay is obtained by the AMI method as obtained in case of 2D Poincaré plots. Fig.4 shows a pair of 3D Poincaré plots in pre-meditative and meditative states under Chinese-chi meditation.

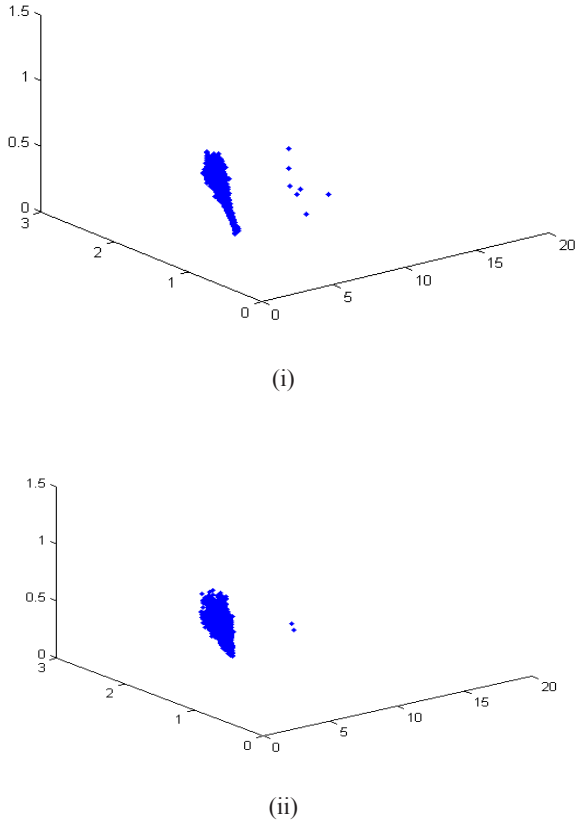

(i)

(ii)

Fig. 4. The 3D Poincaré plot with proper delay of HRV signals in (i) pre-meditative and (ii) meditative state

Fig. 4 establishes that both the plots are well-formed and dense compared to the previously obtained 2D Poincaré plots in pre-meditative and meditative states. So, these plots are quantified by fitting an ellipsoid to their main clusters. For this purpose, the lengths of three axes SD1, SD2, and SD3 are computed. In addition, R21= SD2/SD1 and R23= SD2/SD3 are calculated. Finally, the quantifying parameter (R) is identified as the average of the two aforesaid ratios, which given by:

$$R = \frac{1}{2}\left(\frac{SD_2}{SD_1} + \frac{SD_2}{SD_3}\right) \tag{9}$$

Table II depicts the quantification Table of the 3D Poincaré plot of HRV signals in pre-meditative and meditative states under Chinese-chi meditation and Kundalini yoga.

TABLE II
QUANTIFICATION TABLE OF THE 3D POINCARÉ PLOT OF HRV SIGNALS IN PRE-MEDITATIVE AND MEDITATIVE STATES

| Subject | Pre-meditative States | | | | Meditative States | | | |
|---|---|---|---|---|---|---|---|---|
| | SD1 | SD2 | SD3 | R | SD1 | SD2 | SD3 | R |

| | | | | | | | | |
|---|---|---|---|---|---|---|---|---|
| CHINESE – CHI MEDITATION | | | | | | | | |
| c1 | 0.319503 | 0.322197 | 0.220053 | 1.236306 | 0.107617 | 0.1262 | 0.103898 | 1.193662 |
| c2 | 0.210006 | 0.214627 | 0.090175 | 1.701052 | 0.131799 | 0.119873 | 0.086545 | 1.147309 |
| c3 | 0.201802 | 0.20643 | 0.078011 | 1.834554 | 0.11065 | 0.11111 | 0.073301 | 1.259989 |
| c4 | 0.211601 | 0.218672 | 0.082219 | 1.846527 | 0.136911 | 0.134332 | 0.09753 | 1.179251 |
| c5 | 0.102699 | 0.105205 | 0.041458 | 1.781009 | 0.088842 | 0.084218 | 0.052217 | 1.280406 |
| c6 | 0.114162 | 0.118252 | 0.057124 | 1.552955 | 0.139055 | 0.130878 | 0.075301 | 1.339627 |
| c7 | 0.290027 | 0.292599 | 0.203594 | 1.223019 | 0.156848 | 0.158954 | 0.10314 | 1.27729 |
| c8 | 0.128552 | 0.132456 | 0.055714 | 1.703893 | 0.121789 | 0.117936 | 0.080072 | 1.22062 |
| KUNDALINI YOGA | | | | | | | | |
| y1 | 0.064352 | 0.063299 | 0.03404 | 1.421586 | 0.071748 | 0.089372 | 0.065443 | 1.305651 |
| y2 | 0.108028 | 0.1092 | 0.053639 | 1.523349 | 0.096473 | 0.08805 | 0.073817 | 1.052757 |
| y3 | 0.091121 | 0.10185 | 0.069268 | 1.294063 | 0.098497 | 0.111917 | 0.103686 | 1.107814 |
| y4 | 0.301835 | 0.297696 | 0.163431 | 1.403916 | 0.239872 | 0.198262 | 0.145926 | 1.092589 |

Table II illustrates that the values of $R$ in meditative states are less than that of the pre-meditative states in all the subjects except c7 under Chinese-chi meditation. However, $R$ decreases in meditative states for all the subjects under Kundalini yoga. Thus, the 3D Poincaré plot with proper delay is improper tool for distinguishing these two different meditation techniques, even it is better than the 2D Poincaré plot. Therefore, frequency domain analysis is to be employed instead of the time domain analysis.

### *C. 3D Frequency-delay plot of HRV signals in pre-meditative and meditative states*

Each of the HRV signals of pre-meditative and meditative states are transformed into the frequency domain by applying FFT [35] and 3D frequency-delay plots as described in section 2.4. Fig. 5 shows a pair of 3D frequency-delay plots in pre-meditative and meditative states under Chinese-chi meditation.

Fig. 5 illustrates that all the plots are well-formed and dense compared to the previously obtained 3D Poincaré plots in pre-meditative and meditative states in time domain. So, these plots are quantified by fitting an ellipsoid to their main clusters. For this purpose, the lengths of three axes $SD_1$, $SD_2$ and $SD_3$ are used to calculate the ratios: $R_{21} = SD_2/SD_1$ and $R_{23} = SD_2/SD_3$. Finally, the quantifying parameter (R) is taken as the average of the two aforesaid ratios. Table III summarizes quantification of the 3D frequency-delay plot of HRV signals in pre-meditative and meditative states under Chinese-chi meditation and Kundalini yoga.

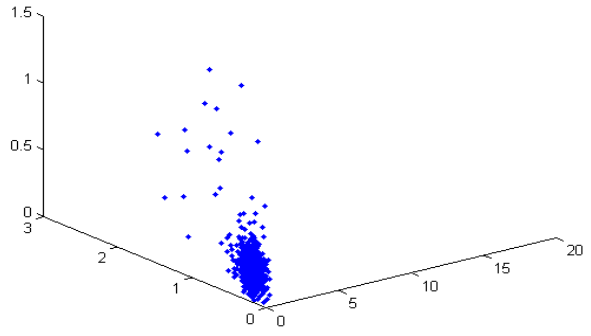


(i)

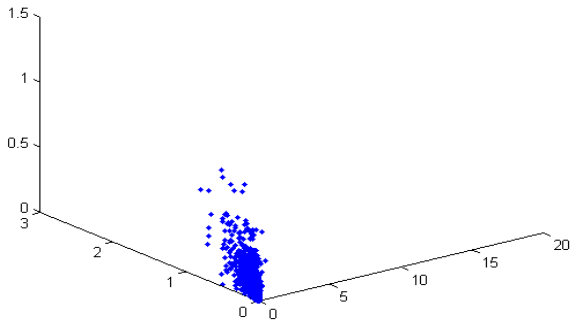


(ii)

Fig. 5. 3D frequency-delay Plot of HRV signals in (i) pre-meditative and (ii) meditative states under Chinese-chi meditation

Table III demonstrates that the value of the quantifying parameter R decreases during meditation in all cases under Chinese-chi meditation, while it increases in all cases under Kundalini yoga. In fact, the values of R in pre-meditative states are always greater than that of the meditative states under Chinese-chi meditation; whereas the values of R in pre-meditative states are always smaller than that of the meditative states under Kundalini yoga. So, for the purpose of distinction of these two different meditation techniques, 3D frequency-delay plot with proper frequency delay is most suitable and R may be taken as good quantifying parameters.

TABLE III
QUANTIFICATION TABLE OF 3D FREQUENCY-DELAY PLOT OF HRV SIGNALS IN PRE-MEDITATIVE AND MEDITATIVE STATES

| Subjects | Pre-meditative States | | | | Meditative States | | | |
|---|---|---|---|---|---|---|---|---|
| | SD1 | SD2 | SD3 | R | SD1 | SD2 | SD3 | R |
| CHINESE - CHI MEDITATION | | | | | | | | |
| c1 | 0.87494 | 0.87358 | 0.59789 | 1.22979 | 0.839484 | 0.83856 | 0.5782 | 1.22459 |
| c2 | 0.74884 | 0.76308 | 0.50651 | 1.26279 | 0.73776 | 0.73375 | 0.51748 | 1.20624 |
| c3 | 0.76789 | 0.759589 | 0.50276 | 1.25002 | 0.823847 | 0.81703 | 0.56742 | 1.21581 |
| c4 | 0.75385 | 0.765949 | 0.51233 | 1.25554 | 0.831385 | 0.82855 | 0.55787 | 1.24089 |
| c5 | 0.80417 | 0.790928 | 0.53416 | 1.23212 | 0.897689 | 0.89759 | 0.62104 | 1.22261 |
| c6 | 0.80117 | 0.800267 | 0.55362 | 1.22219 | 0.890694 | 0.88643 | 0.61745 | 1.21542 |
| c7 | 0.75701 | 0.741045 | 0.49878 | 1.23232 | 0.751869 | 0.74948 | 0.52927 | 1.20644 |
| c8 | 0.71789 | 0.711774 | 0.47106 | 1.25126 | 0.611144 | 0.61674 | 0.42316 | 1.23330 |
| KUNDALINI YOGA | | | | | | | | |
| y1 | 0.937103 | 0.934930 | 0.65878 | 1.20843 | 0.622553 | 0.62178 | 0.43369 | 1.21619 |
| y2 | 0.914141 | 0.900827 | 0.62502 | 1.21336 | 0.619447 | 0.61809 | 0.42854 | 1.22006 |
| y3 | 0.912866 | 0.914739 | 0.64064 | 1.21495 | 0.759536 | 0.75743 | 0.52769 | 1.21630 |
| y4 | 1.385892 | 1.3731806 | 0.95659 | 1.21317 | 0.723196 | 0.72271 | 0.50644 | 1.21318 |

### *D. Limitations and Remedy for the proposed method*

As the effect of meditation is studied under a few numbers of cases, thus the resultant effect is limited and cannot be generalized. However, the data set cannot be enlarged due to non-availability of such data in the Physionet database, which is the only source in these cases. So, this problem is resolved in the current work by statistical hypothesis testing as stated in section 2.5. For this purpose, eight values of the quantifying parameter $R$ for each of the eight different subjects in pre-meditative and meditative states are considered as two samples denoted by $R_1$ and $R_2$, then arranged in two columns. Therefore, it is established that the means of the corresponding populations consisting of all such

elements of $R_1$ and $R_2$ coming out of a large number of subjects do differ significantly. The existence of any significant difference ensures that at certain level of confidence, it is enough to consider small samples of the form $R_1$ and $R_2$ in order to differentiate between meditative and pre-meditative states for large set of subjects.

Towards this goal, the population variances equality is tested in pre-meditative and meditative states using the test statistic, which given by:

$$F = \frac{s_1^2}{s_2^2} \tag{10}$$

Where, $s_1^2$ and $s_2^2$ are the sample variances. In case of Chinese-chi meditation, $s_1^2 = 0.000187268$ and $s_2^2 = 0.000131178$. Therefore, F= 1.427595 < $F_{0.05(1),7,7}$ =3.79. Consequently, $H_0$ holds and hence $\sigma_1^2 = \sigma_2^2$. So, it is justified to apply student's t-test.

Meanwhile, the Student's *t*-test is performed to test the equality of population means in pre-meditative and meditative states as described in section 2.5.2, where $n_1 = n_2 = 8$ and $\nu_1 = 7, \nu_2 = 7$, thus:

$$s_p = \frac{\sum_i SS_i}{\sum_i \nu_i} = \frac{\sum_i \nu_i s_i^2}{\sum_i \nu_i} = 0.017845056 \tag{11}$$

Where, $\overline{R_1} = 1.242003657$ and $\overline{R_2} = 1.220663651$, hence the test statistics is given by:

$$t = \frac{\overline{R}_1 - \overline{R}_2}{s_p \sqrt{\left(\frac{1}{n_1} + \frac{1}{n_2}\right)}} = \frac{0.02134}{0.008923}$$

$$= 2.39169955 > t_{0.05(2),14} = 1.76 \tag{12}$$

Therefore, the alternative hypothesis $H_A$ holds as well as a significant difference between the population means of pre-meditative and meditative states under Chinese-chi meditation is exist.

Similarly, for Kundalini yoga, $s_1^2 = 0.000005933$ and $s_2^2 = 0.00000595738$. Therefore, F=0.99593949 is less than F (0.05(2), 3, 3) =15.4; Hence $H_0$ holds. So, $\sigma_1^2 = \sigma_2^2$ to perform the Student's t-test as follows:

$n_1 = n_2 = 4, \overline{X} = 1.21247765$, $\overline{Y} = 1.216435246$, thus $S_p = 0.0028155$ and the t-test value will be:

$t = 4.82765986 > t(0.05(2),6) = 2.447$. Therefore, the alternative hypothesis $H_A$ holds and there is significant difference between the population means of pre-meditative and meditative states under Kundalini yoga.

From the preceding results, it is confirmed that the same trend in the results is observed even if the present work was carried out for larger sample size in both cases of Chinese-chi meditation and Kundalini yoga. The decrease of the quantifying parameter (R) for each of the subjects in meditative states under Chinese-chi meditation, and the increase in each cases of Kundalini yoga indicates the impact effect of the chi meditation over the Kundalini yoga on the HRV. This establishes that the type of change is depending on the two different meditation techniques.

## IV. Conclusion

Meditation has a very strong effect on ANS and the type of effect is different for different mediation techniques. However, a very few attempts have been performed to mathematically differentiate the different meditation techniques. In the present study, the effect of Chinese-chi meditation and Kundalini yoga on the ANS has been studied towards distinguishing these two meditation techniques through the notion of 3D frequency-delay plots [26]. For this purpose, HRV signals in pre-meditative and meditative states of the persons practising Chinese-chi meditation and Kundalini yoga are obtained.

Since, time domain analysis fails to distinguish the aforesaid meditation techniques, the notion of 3D frequency-delay plot is applied. It has been observed that the value of the quantifying parameter (R) decreases for each of the subjects in meditative states under Chinese-chi meditation, while it increases in each cases of Kundalini yoga. This not only establishes that the change in energy dynamics has taken place during meditation under both of Chinese-chi meditation and Kundalini yoga, but also it shows that the type of change is different for the two different meditation techniques.

Since, the samples are of small sizes, the results are substantiated by the statistical t-test. Thus, it may be concluded that the Chinese-chi meditation and Kundalini yoga produce different types of changes in ANS. This changing pattern clearly distinguishes the aforesaid meditation techniques.

## References


[1] R.A. Baer, "Mindfulness training as a clinical intervention: A conceptual and empirical review," *Clin. Psychol. Sci. Pract.*, vol. 10, pp. 125-143, 2003.

[2] M. B. Ospina, T. K. Bond, M. Karkhaneh, L. Tjosvold, B. Vandermeer, Y. Liang, L. Bialy, N. Hooton, N. Buscemi, D.M. Dryden, T. P. Klassen, "Meditation practices for health: state of the research," *Evid. Rep. Technol. Assess (Full Rep)*, vol. 115, pp. 1-263, 2007.

[3] H.C. Lou, T.W. Kjaer, L. Friberg, G. Wildschiodtz, S. A Holm, "15O-H2OPET study of meditation and the resting state of normal consciousness," *Hum. Brain Mapp.*, vol. 7, no.2, pp. 98-105, 1999.

[4] A. Newberg, A. Alavi, M. Baime, M. Pourdehnad, J Santanna, E. D. Aquili, "The measurement of regional cerebral blood flow during the complex cognitive task of meditation: A preliminary SPECT study," *Psychiatr. Res.*, vol. 106, no. 2, pp. 113-122, 2001.

[5] M. M. S. Ahuja, M. G. Karmarkar, S. Reddy, TSH, LH, "Cortisol response to TRH and LH-RH and insulin hypoglycaemia in subjects practising transcendental meditation," *Ind. J. Med. Res*., 74, pp. 715, 1981.

[6] T. K. Akers, D. M. Tucker, R. S. Roth, J. S. VIDILOFF, "Personality correlates of EEG change during meditation," *Psychological Reports*, vol. 40, 1977.

[7] Y. Akishige, "Psychological studies on Zen," *Bull. Fac. Lit. Kyushu Univ. (Japan)*, 5, 1968.

[8] I. B. Albert, B. McNeece, "The reported sleep characteristics of meditators and non-meditators," *Bull. Psychon. Soc*., vol. 3, 1974.

[9] C. Y. Liu, C. C. Wei, P. C. Lo, "Variation analysis of the sphygmogram to assess the cardiovascular system under meditation," *Evid. Based Complement Alternat. Med*., vol. 6, 2009.

[10] P. Lehrer, Y. Sasaki, Y. Saito, "Zazen and cardiac variability," *Psychosom. Med*. Vol. 61,1999.

[11] C. K. Peng, I. C. Henry, J. E. Mietus, J. M. Hausdorff, G. Khalsa, H. Benson, A. L. Goldberger, "Heart rate dynamics during three forms of meditations," *Int. J. Cardiol*., vol. 95, 2004.

[12] C. K. Peng, J. E. Mietus, Y. Lie, G. Khalsa, P. S. Douglas, H. Benson, A. L. Goldberger, "Exaggerated heart rate oscillations during two meditation techniques," *Int. J. Cardiol*., vol. 70, 1999.

[13] D.P. Goswami, D.N. Tibarewala, D.K. Bhattacharya, "Analysis of heart rate variability signal in meditation using second-order difference plot," *J. Appl. Phys*., vol. 109, 2011.

[14] Y.H. Shiau, "Detecting Well-Harmonized Homeostasis in Heart Rate Fluctuations," *BMEI*, vol. 2, pp.399-403, 2008.

[15] A. Dey, S. Mukherjee, S. K. Palit, D. K. *Bhattacharya, D. N. Tibarewala, "A new technique for the classification of pre-meditative and meditative states," Proc. of the International Conf. ICCIA, Kolkata, India*, pp. 26 – 28, 2010.

[16] M. Toichi, T. Sugiura, T. Murai, A. Sengoku, "A new method of assessing cardiac autonomic function and its comparison with spectral analysis and coefficient of variation of r-r interval," *J. Auton. Nerv. Syst*., vol. 62, pp. 79-82, 1997.

[17] M. P. Tulppo, T. H. Makikallio, T. E. S. Takala, T. Seppanen, H. V. Huikuri , "Quantitative beat-to-beat analysis of heart rate dynamics during exercise," *Am. J. Physiol*., vol. 271, pp. 244–252, 1996.

[18] M. P. Tulppo, T. H. Makikallio, T. Seppanen, J. K. E. Airaksinen, H. V. Huikuri, "Heart rate dynamics during accentuated sympathovagal interaction," *Am. J. Physiol*., vol. 247, pp.810–816, 1998.

[19] J. Hayano, H. Takahash, T. Toriyama, S. Mukai, A. Okada, S. Sakata, A, Yamada, N. Ohte, H. Kawahara, "Prognostic value of heart rate variability during long term follow-up in chronic haemodialysis patients with end-stage renal disease," *Nephrol. Dial. Transplant*., vol.14, pp. 1480–1488, 1999.

[20] Heart Rate Variability: An Indicator of Autonomic Function and Physiological Coherence, Institute of Heart Math, 2003. Available http://www.heartmath.org/research/ science-of-the-heart/soh_13.html.

[21] B. Irfan, A. E. Metin, K. Dayimi, T. Muhsin, K. Osman, M. Mehmet, B. E.Ozlem, B. Yelda, "Cigarette smoking and heart rate variability: dynamic influence of parasympathetic and sympathetic maneuvers*," Ann. Noninv. Electrocardiol*., vol. 10, pp. 324-329, 2005.

[22] U. R. Acharya, K. P. Joseph, N. Kannathal, L. C. Min, J. S. Suri, "Advances in Cardiac Signal Processing: Heart Rate Variability," Springer, New York, pp. 121–165, 2007.

[23] C. K. Peng, J. E. Mietus, Y. Liu, G. Khalsa, P. S. Douglas, H. Benson, A. L. Goldberger, "Exaggerated heart rate oscillations during two meditation techniques," *International journal of cardiology*, vol. 70, no. 2, pp. 101-107, 1999.

[24] G. Kheder, A. Kachouri, R. Taleb, M. Ben Messaoud, M. Samet, "Feature extraction by wavelet transforms to analyze the heart rate variability during two meditation techniques," *Advances in Numerical Methods*, pp. 379-387, Springer US, 2009.

[25] G. Kheder, A. Kachouri, M. B. Massoued, M. Samet, "Heart rate variability analysis using threshold of wavelet package coefficients," *International Journal on Computer Science and Engineering*, Vol. 1, no. 3, pp. 131-136, 2009.

[26] S. Mukherjee, S. K. Palit, "A New Scientific Study towards Distinction of ECG Signals of a Normal healthy person and of a Congestive Heart Failure Patient," *J. Inter. Acad. Phys. Sci,*. vol.15, no. 4, pp. 413-433, 2011.

[27] J. Piskorski, "Filtering Poincaré plots," *Comp. Methods in Sci. & Tech*., vol. 11, 2005.

[28] M. Brennan, M. Palaniswami, P. Kamen, "Do existing measures of Poincaré plot geometry reflect nonlinear features of heart rate variability?," *IEEE Trans. Biomed. Eng*., vol 48, 2001.

[29] A. Voss, S. Schulz, R. Schroeder, M. Baumert, P. Caminal, "Methods derived from nonlinear dynamics for analysing heart rate variability," *Phil. Trans. R Soc*., pp. 277-296, 2009.

[30] C. Lerma, O. Infante, H. P. Grovas, M. V. Jose´," Poincare´ plot indexes of heart rate variability capture dynamic adaptations after haemodialysis in chronic renal failure patients," *Clin. Physiol. & Func. Im*., vol.23, pp. 72–80, 2003.

[31] M. Brennan, M. Palaniswami, P. Kamen, "Poincare´ plot interpretation using a physiological model of HRV based on a network of oscillators," *Am. J. Physiol. Heart Circ. Physiol*., vol. 283, pp. H1873–H1886, 2002.

[32] J. Haaksma, J. Brouwer, W.A. Dijk, W.R.M. Dassen, D.J.V. Veldhuisen, "The dimension of 2D and 3D Poincaré plots obtained from 24 hours ECG registrations," *IEEE Comp. in Cardiol*., vol. 29, pp. 453−456,2002.

[33] A. S. Khaled, I. O. Mohamed, A. S. A. Mohamed, "Employing Time-Domain Methods and Poincaré Plot of Heart Rate Variability Signals to Detect Congestive Heart Failure," *BIME J*., vol. 6, no.1, 2006.

[34] S. Mensing, J. Limberis, G. Gintant, A. Safer, "A Novel Method for Poincaré Plot Shape Quantification Demonstrates Cardiac Tissue Repolarization Inhomogeneities Induced by Drugs," IEEE Comp. in Cardiol., vol. 35, 2008.

[35] M. Weeks, "Digital Signal Processing," *Infinity Science Press LLC*, Massachusetts, 2007.

[36] J. H. Zar, "Biostatistical Analysis," *Pearson Education*, 2006.

[37] A. L. Goldberger, L. A. N. Amaral, L. Glass, J. M. Hausdorff, P. Ch. Ivanov, R. G. Mark, J. E. Mietus, G. B. Moody, C. K. Peng, H. E. Stanley, "Physiobank, physiotoolkit, and physionet components of a new research resource for complex physiologic signals," *Circul.,* vol. 101, no.23, 2000.

[38] G. P. Williams, "Chaos Theory Tamed," *Joseph Henry Press*, Washington, D.C.,1997.

**Dr.Anilesh Dey** was born in West Bengal, India in 1977. He received the B.E in Electronics from Nagpur University and M.Tech.(Gold-Medallist) in Instrumentation and Control Engineering from Calcutta university and received PhD. from Jadavpur University. He is working as Associate Professor and H.O.D of Electronics and Communication Engineering at The Assam Kaziranga University, Assam. He is author or co-author of more than 40 scientific papers in international/national journals and proceedings of the conferences with reviewing committee. His research topics nonlinear time series analysis, time and frequency domain analysis of bio- medical and music signals, effect of music in autonomic and central nervous system.

**Prof.(Dr.)D. K. Bhattacharya** was born in West Bengal, India in 1943. He is a retired Professor and Head in the department of Pure Mathematics University of Calcutta, India. He is presently an UGC Emeritus Fellow; prior to this he was an AICTE Emeritus Fellow of Govt. of India. He had his undergraduate, postgraduate and doctoral duty from the University of Calcutta. He has a long teaching experience of forty six years; he has supervised many Ph.D. students in Pure and Applied Mathematics. He is author or co-author of about 100 scientific papers in international /national journals and proceedings of the conferences with reviewing committee. His expertise is in Mathematical modeling and optimal control. His present interest is in application of Mathematics in Biology and Medicine including Bio-informatics.

**Prof.(Dr.)D.N. Tibarewala** was born in Kolkata, December 1951. He is presently a Professor of Biomedical Engineering and formerly was Director in the School of Bioscience & Engineering at Jadavpur University, Kolkata, India, he did his BSc (Honours) in 1971, and B. Tech (Applied Physics) in 1974 from the Calcutta University, India. He was admitted to the Ph.D. (Tech) degree of the same University in 1980. Having professional, academic and research experience of more than 30 years, Dr. Tibarewala has contributed about 200 research papers in the areas of Rehabilitation Technology, Biomedical Instrumentation and, related branches of Biomedical Engineering.

**Amira S. Ashour, PhD**., is an Assistant Professor and Vice Chair of Computers Engineering Department, Computers and Information Technology College, Taif University, KSA. She has been the vice chair of CS department, CIT college, Taif University, KSA for 5 years. She is in the Electronics and Electrical Communications Engineering, Faculty of Engineering, Tanta University, Egypt. She received her PhD in the Smart Antenna (2005) from the Electronics and Electrical Communications Engineering, Tanta University, Egypt. Her research interests include: image processing, Medical imaging, Machine learning, Biomedical Systems, Pattern recognition, Signal/image/video processing, Image analysis, Computer vision, and Optimization. She has 3 books and about 50 published journal papers. She is the Editor-in-Chief for the International Journal of Synthetic Emotions (IJSE), IGI Global, US. She is an Associate Editor for the IJRSDA, IGI Global, US as well as the IJACI, IGI Global, US. She is an Editorial Board Memberof the International Journal of Image Mining (IJIM), Inderscience.

**Nilanjan Dey, PhD.,** is an Asst. Professor in the Department of Information Technology in Techno India College of Technology, Rajarhat, Kolkata, India. He holds an honorary position of Visiting Scientist at Global Biomedical Technologies Inc., CA, USA and Research Scientist of Laboratory of Applied Mathematical Modeling in Human Physiology, Territorial Organization Of-Sgientifig and Engineering Unions, BULGARIA, Associate Researcher of Laboratoire RIADI, University of Manouba, TUNISIA. He is the Editor-in-Chief of International Journal of Ambient Computing and Intelligence (IGI Global), US, International Journal of Rough Sets and Data Analysis (IGI Global), US, and the International Journal of Synthetic Emotions (IJSE), IGI Global, US. He is Series Editor of Advances in Geospatial Technologies (AGT) Book Series, (IGI Global), US, Executive Editor of International Journal of Image Mining (IJIM), Inderscience, Regional Editor-Asia of International Journal of Intelligent Engineering Informatics (IJIEI), Inderscience and Associated Editor of International Journal of Service Science, Management, Engineering, and Technology, IGI Global. His research interests include: Medical Imaging, Soft computing, Data mining, Machine learning, Rough set, Mathematical Modeling and Computer Simulation, Modeling of Biomedical Systems, Robotics and Systems, Information Hiding, Security, Computer Aided Diagnosis, Atherosclerosis. He has 8 books and 170 international conferences and journal papers. He is a life member of IE, UACEE, ISOC etc. https://sites.google.com/site/nilanjandeyprofile/

**Dac-Nhuong Le** has a MSc and Ph.D. in computer science from Vietnam National University, Vietnam in 2009 and 2015, respectively. He is Deputy-Head of Faculty of Information Technology, Haiphong University, Vietnam. Presently, he is also the Deputy-Cheif of Department of Educational Testing and Quality Assurance, Vice-Director of Information Technology Apply Center in the same university. He is a research scientist of R&D Center of Visualization & Simulation in, Duytan University, Danang, Vietnam. He has published numerous research articles in reputed international conferences, journals and online book chapters contributions. Currently his research interests are evaluation computing and approximate algorithms, network communication, security and vulnerability, network performance analysis and simulation, cloud computing, medical imaging.

**Evgeniya Gospodinova** is an Assistant Professor of computer systems engineering at Institute of Systems Engineering and Robotics of Bulgarian Academy of Sciences. She received a M.Sc. degree in Microelectronics from the Department of Electronics at the Technical University of Gabrovo, Bulgaria and Ph.D. degree from the Central Laboratory of Mechatronics and Instrumentation of Bulgarian Academy of Sciences in 2009. The major fields of professional and scientific research interests include digital image processing, computer networks and communications, special instruments for information exchange, fractal modeling and analysis in traffic engineering and investigation of Heart Rate Variability of digital ECG signals. She is a member of the National Union of Automatics and Informatics.

**Mitko Gospodinova** is an Assosiate Professor of computer systems engineering at Institute of Systems Engineering and Robotics of Bulgarian Academy of Sciences. He received a M.Sc. degree in Microelectronics from the Department of Electronics at the Technical University of Gabrovo, Bulgaria and Ph.D. degree from the Department of Computer Sciences at the Saint-Petersburg State Electrotechnical University, Russia in 1985. The major fields of professional and scientific research interests include digital image processing, computer networks and communications, analysis and design of electronic systems, automation of biomedical research, special instruments for information exchange, fractal modeling and analysis of self-similarity in traffic processes and biomedical systems. He is a member of the National Union of Automatics and Informatics.

# Improved Shape Parameter Estimation in K Clutter with Neural Networks and Deep Learning

José Raúl Machado Fernández, Jesús de la Concepción Bacallao Vidal

*Instituto Superior Politécnico José Antonio Echeverría, Cuba*

***Abstract* — The discrimination of the clutter interfering signal is a current problem in modern radars' design, especially in coastal or offshore environments where the histogram of the background signal often displays heavy tails. The statistical characterization of this signal is very important for the cancellation of sea clutter, whose behavior obeys a K distribution according to the commonly accepted criterion. By using neural networks, the authors propose a new method for estimating the K shape parameter, demonstrating its superiority over the classic alternative based on the Method of Moments. Whereas both solutions have a similar performance when the entire range of possible values of the shape parameter is evaluated, the neuronal alternative achieves a much more accurate estimation for the lower Fig.s of the parameter. This is exactly the desired behavior because the best estimate occurs for the most aggressive states of sea clutter. The final design, reached by processing three different sets of computer generated K samples, used a total of nine neural networks whose contribution is synthesized in the final estimate, thus the solution can be interpreted as a deep learning approximation. The results are to be applied in the improvement of radar detectors, particularly for maintaining the operational false alarm probability close to the one conceived in the design.**

***Keywords* — Sea Clutter, K Distribution, Shape Parameter Estimation, Artificial Neural Networks, Deep Learning**

## I. Introduction

Radars are responsible for detecting nearby targets using electromagnetic waves [1]. The echo amplitude received by the radar, besides carrying the target's information, contains a distortion introduced by surrounding objects. In the particular case of the operation in sea environments, the distortion signal is originated in the sea surface and it's therefore called sea clutter [2].

Among the various ways of improving radars' performance, clutter discrimination is frequently addressed in the literature [3]. Although other models can be used [4-6], the K distribution is widely recognized as the best choice for sea clutter representation [7]. Consequently, several solutions have been proposed taking as a priori condition the assumption of K clutter [8-10].

Radar classic detectors, such as the CA-CFAR (Cell Averaging - Constant False Alarm Rate), use, as a general rule, a fixed adjustment factor to define a desired value of false alarms probability [11]. However, when a variation appears in the clutter's statistics, a correction of the adjustment factor is necessary to ensure the operating false alarm probability remains close to the one conceived in the design [12].

The statistical variation of the background signal translates mathematically into a modification of the shape parameter of the assumed model. The problem can be then reduced to a search of the shape parameter using a finite set of samples.

The more popular technique for estimating the K shape parameter is the Method of Moments (MoM) which uses the 2nd and 4th order algebraic moments [13]. The MoM is also used in the estimation under Weibull clutter, through the computing of the first two moments. A previous research related to the Weibull model has shown that Artificial Neural Networks (ANN) are able to replace the MoM in some cases, achieving a more accurate estimate without incurring into a high computational cost [14, 15].

In view of the presented analysis, the authors established as the goal of the investigation the design and training of a neural network capable of estimating the K shape parameter from a finite set of samples. Initially they expected to find the proper solution by modifying multiple internal variables or conditions of the neural network and using groups of 3000 samples, according to what was done in [15]. However, this approach was insufficient to achieve good results.

Then, considering the recommendations given in [16] and adopting an strategy similar to [17], they decided to divide the region of possible values of the shape parameter in five reduced estimation intervals. The new solution, which includes nine neural networks, achieved significantly better results than those exhibited by the MoM and constitutes, therefore, the contribution of this paper. The design can be interpreted as a deep learning approach to the K parameter shape estimation given the high degree of integration of the nine networks.

## II. Materials and Methods

This paper's results were achieved by performing simulations in MATLAB 2011software. The current section is devoted to facilitate the replication of the experiment by third parties. Therefore, it describes (A) the way in which clutter samples were generated and (B) the methods considered for obtaining K shape parameter estimates.

### *A. Samples used in the Simulations*

The following PDF was employed for the K distribution [18]:

$$f_x(x) = \frac{4c}{\Gamma(v)}(cx)^v K_{v-1}(2cx) \tag{1}$$

Where $c$ is the scale parameter, $v$ is the shape parameter, $\Gamma(.)$ is the Gamma function and $\Gamma(.)$ is the Bessel function of second kind and order $v-1$. A complete definition of the functions related to the K distribution can be found in [19]. Actually, the MATLAB functions implemented and validated in [19] were used in this study.

As a design principle, it was decided that the neural network should use histograms as a distinctive feature of the data. Replicating what was done in [15], a quantity of 3000 samples was selected to assemble each histogram.

By observing multiple sets of histograms, the authors concluded



DOI: 10.9781/ijimai.2016.3714

that the greatest amount of information was concentrated below the amplitude equal to five. Consequently, samples with magnitude greater than five were ignored when histograms were prepared.

Three sets of samples, in which the shape parameter ($v$) was varied from 0.1 to 30 according to the investigations found in [20-22], were created. Moreover, the scale parameter ($c$) was maintained as $c = \sqrt{v}$ to fix the average of the samples to one [18].

The generated data sets have the structure shown in Fig. 1. Each of the sets covered the range of values of $v$ between 0.1 and 30 in different ways.

Set A started with a group of 3000 samples corresponding to $v = 0.1$. The next ten groups maintained the same $v$ value, representing different outcomes of the same configuration of parameters. Then, group number 11 resulted from adding 0,01 to the shape parameter before generating the samples. Again, the next ten groups maintained the parameter configuration. Next, the mechanism was repeated until 30 000 samples sets were created, with a change in $v$ every ten groups. The total number of samples of Set A was 90 million.

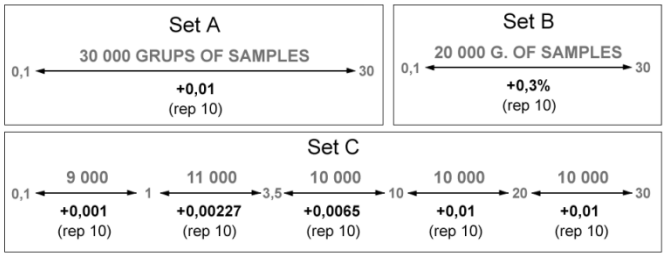


Fig. 1. Data Sets Prepared for the Training and test of Neural Networks in the Estimation of the K Shape Parameter.

Set B and Set C also changed the $v$ value every ten groups but they followed different rules. Set B increased $v$ a 0,3% every ten groups, ensuring thus that the lower $v$ Fig.s were covered with a smaller step. According to recommendations given in [16], the high magnitudes of the shape parameter have a reduced influence in the heavy property of the K distribution tails. Therefore, there is no great interest in providing a reliable estimate for such values. In fact, the purpose of the Set B is to indicate the neural network to pay less attention to the estimation of high $v$ magnitudes.

Set C achieves a similar effect by applying different variation steps into five incremental length intervals. For the interval $0.1 < v < 1$ a variation step of 0,001 was used; for $1 < v < 3{,}5$ the step was of 0,00227; for $3{,}5 < v < 10$ of 0,0065; and for $10 < v < 20$ and $20 < v < 30$ of 0,01. Finally, Set C included 150 million samples distributed in 50000 groups of 3000 samples each, and was the one more intensively used in the neuronal training.

Sets A, B and C were created in that order in response to observed outcomes in the performed trials. The objective was to positively influence the performance of the neuronal solution. The reasons for the creation of each set are explained in the section "Results and Discussion".

### *B. Methods for Obtaining K Shape Parameter Estimates*

Several methods for estimating the K distribution parameters have been proposed in the literature [23-30]. In [31], a comparison of four different methods was performed, concluding that the MoM based on second and fourth moments [32] displays the best results. Additionally, the same method was used in [13] for obtaining estimates from samples taken at the coast of Taiwan.

For the above reasons, the authors selected the MoM that uses the second and fourth moments like the classical estimator of K parameters. According to this method, expression (2) is to be applied:

$$\hat{v} \approx \frac{1}{\left(\frac{m_4}{2m_2^2}-1\right)} \qquad \hat{c} \approx 2\sqrt{\frac{v}{m_2}} \tag{2}$$

Therefore, the objective of this research is to build a neural network based scheme that will exceed the performance of the previously described MoM.

For the design of the neural scheme, the authors took as a start point the solutions given in [15, 33-37] for different situations. Consequently, the initial configuration of the neural network internal variables was arranged according to Table I.

The first trained neural network was a classic three layers Perceptron. It had 50 inputs for reading 50 values resulting of samplings made on the histograms obtained from each 3000 samples group extracted from sets A, B and C. This network failed to outperform the MoM; so the authors, after trying several alternatives, decided to use a nine neural networks scheme, in which each net would read the same data and reach to an independent conclusion. The synthesis of these conclusions would produce the final estimate.

TABLE I
CONFIGURATION OF THE INTERNAL NEURAL NETWORK VARIABLES

| Network Variables | Choice |
|---|---|
| Network Type | Feed Forward Network (Multilayer Perceptron) |
| Training Function | BackPropagation (Levenberg-Marquardt) |
| Number of Layers | 3 (Input Layer – Hidden Layer – Output Layer) |
| Transference or Activation Function | Hyperbolic Tangent Sigmoid (Hidden Layer), Lineal Transference Function (Output Layer) |
| Activation Order | Topological (Asynchronous Activation) |
| Error Measurement | Mean Square Error |
| Training Set Division | 70% Training - 15% Validation - 15% Test |
| Samples' Presentation | Batch Training |

The logical process that led to the design of the neural networks based solution is described in the next section. Five of the nine networks use a configuration very similar to the one presented in Table I; whereas the other four change the transfer function of the output layer to *Hyperbolic Tangent Sigmoid*. As a result, their output turns to be restricted to the range between 0 and 1. For a detailed understanding of the meaning of each of the parameters in Table I, the reader is referred to specialized literature [38].

## III. Results and Discussion

The current section shows evidence of the new neuronal solution's proper functioning and demonstrates its superiority after performing a comparison with the MoM. First, efforts are presented regarding the training of a single network for obtaining K shape parameter estimates. Then, the final scheme, obtained after trying different alternatives, is described. This scheme is based on the interaction of nine neural networks trained in an independent way to solve fractions of the problem at hand.

### *A. Design of a Single Network*

Multiple trainings were executed with a neural network that used the configuration shown in Table I and processed the data from Set A. The size of the hidden layer was changed between 5 and 50 neurons,

without obtaining a significant improvement. Finally, it was found that the biggest success rate was achieved by using 30 neurons.

Aiming to improve the network's performance, the authors made several modifications on the training process. First, they proceeded to omit some of the 50 inputs. So, they repeated the essays omitting the last 3, 5, 10, 15, 20 and 25 values from the tail of the input histograms. The results showed a reduction in the effectiveness. Then, values from the beginning of the input histograms were skipped from the training procedure. The experiments showed that the first 20 inputs could be omitted without significantly affecting the estimator's performance. However, almost no improvement was achieved.

Two main problems prevented the performance's improvement. The first one was the rapid convergence of the training. The process often concluded between iterations 15 and 20 because the network began to lose generalization and the validation made with a percentage of data stopped the training. The reader should note that this effect is common in *Early Stopping* based trainings. The authors chose a high limit on validation failures but the performance did not improve. It was noted that once the network begins to particularize its performance, it fails to generalize the behavior even after 30 iterations.

Searching for a slower convergence, *Scaled Conjugate Gradient* and *Bayesian Regularization* training algorithms were tested. They both succeeded in offering a slower convergence, and there was a slightly enhancement in the results. It was also decided to create a training set with more samples to see if a wider variety of presentation helped the network to generalize the results. To this end, trainings were repeated with a Set very similar to Set A but having 20 repetitions of $v$ instead of ten. Again, the results improved slightly.

The second problem was the poor performance in the $0.1 < v < 1$ region. Recommendations given in [16] clearly indicate the need for a very accurate estimate in this area, which is responsible for the heavy property of the K histograms tails. Heavy tails have a marked influence on the selection of the adjustment factor in detectors such as the CA-CFAR, and therefore, in the performance of radar detection schemes.

Accordingly, the authors created Set B, which includes more groups of samples in the region of reduced $v$ magnitudes. Trainings conducted with this group achieved a greater precision in the $0.1 < v < 1$ interval, maintaining the previously achieved overall performance.

Set C was also created as a way to expand the number of samples and place a larger amount of them in the regions of interest. Trainings conducted with this group positively contributed to improve the network performance.

Once the above described modifications were considered, together with others that were omitted to simplify the explanation, the authors arrived to the conclusion that follows. After using a set of 150 million samples (Set C), varying the size of the hidden layer from 5 to 50 neurons, altering training variables and placing more groups of samples in the region of interest, it was found that a single neural network is unable to outperform the MoM in the estimation of the K distribution shape parameter. Fig. 2 shows a detailed comparison of both estimators by displaying error histograms.

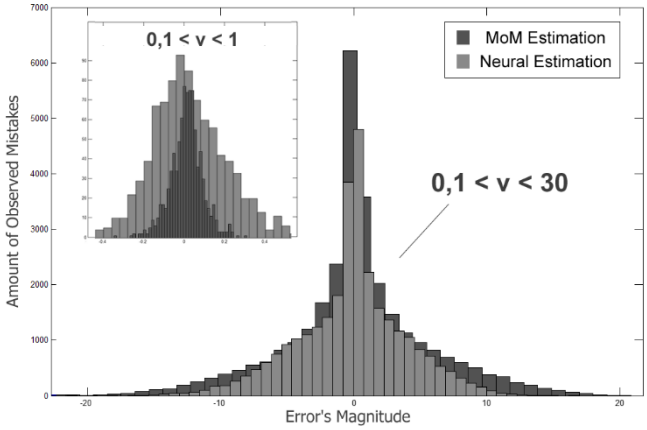


Fig. 2. Histograms of Errors Committed by the Neural and MoM Estimators.

If Fig. 2 is examined, it can be seen that even though the overall performance of the neural network is better than the MoM, this cannot be considered an advantage because the improvement is detrimental of the quality of the estimates in the region of interest ($0.1 < v < 1$). Inevitably, the neural network's learning mechanism compels it to maintain a uniform performance through the entire search region. Such behavior is desirable in many situations but causes unwanted results in the estimation of the K shape parameter. In conclusion, it can be stated with certainty that the variations applied in [15] for training a single network to find the Weibull shape parameter, are not sufficient to achieved the same for the K case.

### A. Two Stage Neural Solution

Given the difficulties encountered training a single network, the authors resolved to assess the estimation problem using multiple neural networks that would provide fractions of the solution. A similar principle was followed in [17] leading to suitable results.

However, unlike [17], two stages were used in the design, each one including several neural networks; being the response of the second stage determined by the output of the first one. The first stage was responsible for dividing the region into smaller sub-regions. Then, the second stage was in charge of producing an accurate estimate within each sub-region. Thus, the problem was divided in easier to process portions which would present a simplified problem to specialized networks.

Networks from the first stage were designed using the *Hyperbolic Tangent Sigmoid* function in the output layer. Note that this configuration differs from the one presented in Table I. The intention was to force the output values to be 0 or 1. So, each network from the first stage had a single output whose task was to decide which of two $v$ regions contained a given group of samples. Therefore, each network divided the search region in a portion that it classified as 0 and another that it classified as 1. This solution can be interpreted as form of pattern recognition.

In contrast, internal variables from second stage networks remained

TABLE II
ERROR INTERVAL FOR EACH TESTED BOUNDARY VALUE.

| $X$ | 20 | 18 | 16 | 15 | 14 | 13 | 12 | 11 | 10 | 9 | 8 |
|---|---|---|---|---|---|---|---|---|---|---|---|
| $X_2 - X_1$ | 22,12 | 22,46 | 23,36 | 24,03 | 23,89 | 24,88 | 24,52 | 24,18 | 24,42 | 18,98 | 18,80 |

| $X$ | 7 | 6 | 5 | 4 | 3 | 2 | 1 | 0,95 | 0,90 | 0,85 | 0,80 |
|---|---|---|---|---|---|---|---|---|---|---|---|
| $X_2 - X_1$ | 10,94 | 8,7 | 5,07 | 3,48 | 1,72 | 0.91 | 0.22 | 0.24 | 0.29 | 0.16 | 0.20 |

very similar to what was shown in Table I, and only suffered minor changes according to the comments made on section 3.1. These networks had no restrictions on the output values.

Next, the following section will explain how the first stage networks were designed. Understanding the results obtained at the output of the first stage is a key element in the justification of the search intervals intersection conceived for stage two nets.

### B. B.1. First Stage Networks

The first stage of the neural solution sustains a complexity that has not been yet discussed. In order to divide two regions, it's necessary to place a boundary between them. Given the variability of the histograms that were assembled with a finite amount of samples, the continuity of the search region, and complexities associated with the training of artificial intelligence systems, it is virtually impossible to establish an absolute border without incurring in a certain degree of error. Consequently, the expected behavior after establishing a boundary is the one shown in Fig. 3.

After conducting a training for establishing a border ($X$) between Regions 0 and 1, an area of uncertainty (between $X_1$ and $X_2$ ) will always appear. This area will contain network mistakes on the election of the proper region. In the interval between $X$ and $X_1$ , the network will make mistakes classifying groups of samples belonging to the Region 0 as Region 1 (errors $1/0$). The opposite can be expected between $X$ and $X_2$, where groups of samples belonging to Region 1 will be classified as Region 0 (errors $0/1$). This behavior is impossible to avoid, and the designer can only seek to reduce the interval between $X_1$ and $X_2$ as much as possible.

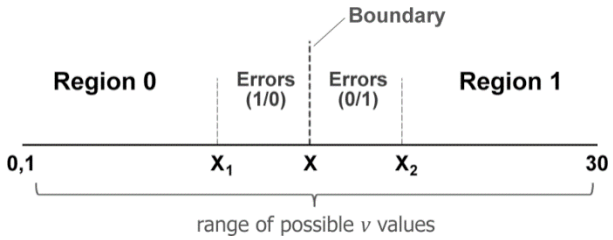


Fig. 3. Expected Neural Behavior after Conducting a Training for Dividing the Search Region in two sub-Regions.

Table II shows a measurement of the length of the error interval ($|X_2 - X_1|$) incurred by a neural network in relation to the selected $X$. Note that $X$ may vary through the whole range of possible $v$ values (from 0.1 to 30). The experiments correspond to the best network of ten neurons in the hidden layer after executing 20 trainings for each $X$.

Even though values in Table II are only an approximation, they allow appreciating the effect of $X$ variation on the magnitude of the error. As it can be seen, as $X$ gets reduced, the interval of mistakes gets smaller. The first value that is worth considering is $X = 7$ which provides an error of 10,94. Any value above $X = 7$ is completely unacceptable.

For the design of the first network for dividing the search region into two smaller sub-regions, the authors chose $X = 0.90$ and executed multiple trainings to find an improved error interval. A neural network, capable of operating with $X_1 = 0.8040$ and $X_2 = 0.983$, and having only five neurons in the hidden layer, was found. The results were achieved using the Set C, and were subsequently validated with Set A.

This first network, called $net\ 1$, it's able to clearly distinguish between the $0.1 < v < 0.8$ and $0.8 < v < 30$ regions, but it makes some mistakes in the $0.8 < v < 1$ portion. If $net\ 1$ is placed in the stage one, the next stage must have at least two networks operating with an interception on its operating regions: the first must operate in $0.1 < v < 1$ and the second in $0.8 < v < 30$. Thus, they will both perform the estimation in the $0.8 < v < 1$ interval, which is where the first stage makes mistakes.

Three additional networks for the first stage were later designed. Following a similar logic, each one divided the search region into two smaller sub-regions. So, $net\ 2$ attempted to place a boundary close to $X = 1{,}5$, $net\ 3$ close to 2,7 and $net\ 4$ close to 5,7. The reader should note that, as it was pointed out in [16], the influence of the K shape parameter on the heavy property of the distribution becomes rapidly saturated with $v$ increase. This means that the difference will be much greater between histograms with $v = 1$ and $v = 2$ than between histograms with $v = 11$ and $v = 12$.

### C. B.2. Connecting both Stages

Fig. 4 summarizes the interconnection structure of the nine neural networks that were finally included the scheme. The four networks from the first stage make decisions on the region in which the data is located and choose which network from the second stage should be used to acquire the final result.

For example, $net\ 1$ decides whether to use $net\ 1E$ to get the result. If it concludes that it's not appropriate to use $net\ 1E$, the decision passes to *net* 2. Then, $net\ 2$ decides if the data belong to the region for which $net\ 2E$ was trained. Otherwise, the decision is passed to $net\ 3$ which performs a similar operation. The $net\ 4$ is the last one from the first stage and makes the final decision by choosing between $net\ 4E$ and $net\ 5E$. Note that in many cases it won't be necessary to use $net\ 4$.

The error interval of each network from the first stage and the training region for each network from the second stage are revealed in Fig. 5. All networks use five neurons in the hidden layer, except $net\ 5E$ which uses 20.

The network $net\ 1$ seeks to find groups of samples with a $v$ lower than 0,9 and send them to $net\ 1E$. It has an error interval of $0.8 < v < 1$. Therefore, the network $net\ 1E$ must be able to process samples up to $v = 1$ and $net\ 2E$ must be able to perform the estimation from $v = 0.8$.

The network $net\ 2$ searches for groups of samples with $v < 1{,}5$ for sending them to $net\ 2E$. It has an error interval of $1{,}3 < v < 1{,}73$. Therefore, $net\ 2E$ must be able to process samples up to $v = 1{,}73$ and $net\ 3E$ must be able to perform the estimation from $v = 1{,}3$.

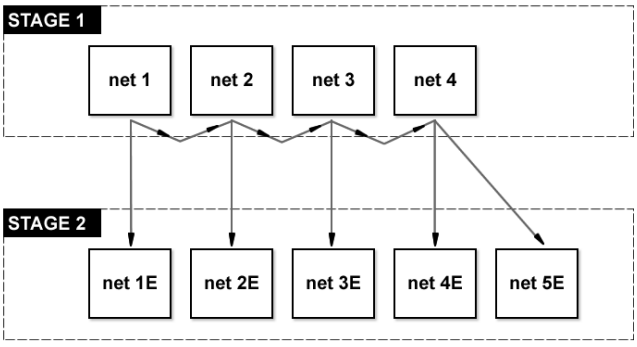


Fig. 4. Interconnection of Internal Networks from both Stages.

The network $net\ 3$ searches for groups of samples with $v < 2{,}7$ for sending them to $net\ 3E$. It has an error interval of $1{,}92 < v < 3{,}6$. Therefore, $net\ 3E$ must be able to process samples up to $v = 3{,}6$

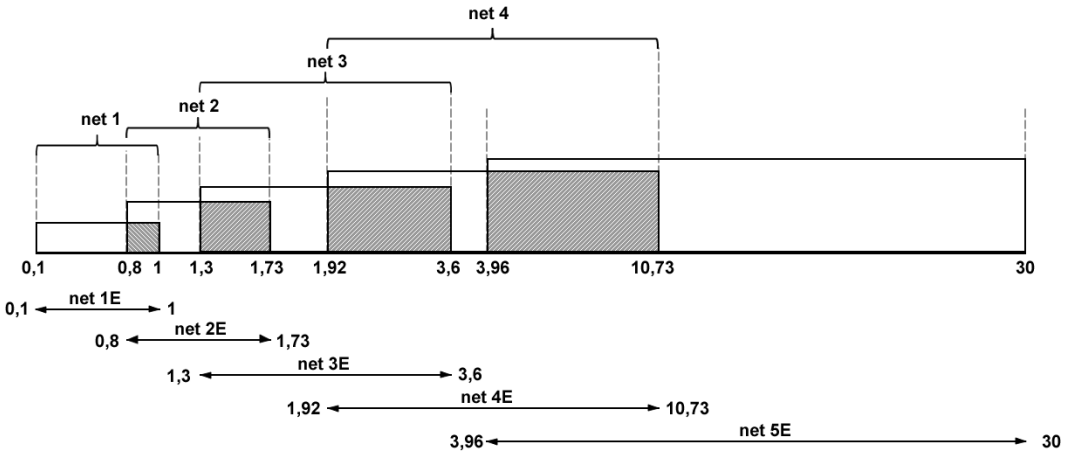


Fig. 5. Error Intervals for Stage One Networks and the Resulting Search Regions for Stage Two Networks.

and $net\ 4E$ must be able to perform the estimation from $v = 1{,}92$.

The network $net\ 3$ searches for groups of samples with $v < 2{,}7$ for sending them to $net\ 3E$. It has an error interval of $1{,}92 < v < 3{,}6$. Therefore, $net\ 3E$ must be able to process samples up to $v = 3{,}6$ and $net\ 4E$ must be able to perform the estimation from $v = 1{,}92$.

The network $net\ 4$ searches for groups of samples with $v < 5{,}7$ for sending them to $net\ 4E$. It has an error interval of $3{,}96 < v < 10{,}73$. Therefore, $net\ 4E$ must be able to process samples up to $v = 10{,}73$ and $net\ 5E$ must be able to perform the estimation from $v = 3{,}96$. The network $net\ 5E$ perfoms the estimation up to $v = 30$ which is the end of the search region.

### *D. B.3. Stage Two Networks*

A double procedure was followed for training stage two networks. A subset was taken from Set C in the desired range, for example $0.1 < v < 1$ for $net\ 1E$, and multiple trainings were conducted to find the best network called $Best - C$. Afterwards, trainings were executed with a new network and a subset from Set A, calling $Best - A$ to the best obtained network. Then the $Best - C$ net was tested with Set A and the $Best - A$ net was tested with Set C. The network with better performance facing the set for which it was not trained was chosen as the best.

The previously described process led to the selection of $Best - C$ networks for $net\ 1E$, $net\ 2E$ and $net\ 3E$. On the other hand, $Best - A$ networks displayed the best outcomes for $net\ 4E$ and $net\ 5E$.

### *E. Comparison of the Three Estimators*

Once finished the design, the authors resolved to test the Two Stages Neuronal Solution with Set B, whose data were not used in the training of any of the nine networks included in the scheme. For comparing the results, they also tested the other two addressed estimators: the Method of Moments and the Single Neural Network.

As an intermediate test, the performance of the first stage was verified. For this purpose, the 20000 groups of samples from Set B were processed with the neuronal solution to check if the first stage was able to correctly choose the proper net from the second stage. The result was almost perfect: errors occurred only in four groups of samples corresponding to $v = 1.8310$, $v = 3.1599$, $v = 3.6774$ and $v = 3.8947$. This represents a success percentage of 99.98%. The same experiment was repeated with the MoM and it was found that only in the 41% of the cases the estimator could choose the correct network from the second stage.

Regarding the performance test of the three estimators, Fig. 6 exhibits the mistakes made by each one in the search of the K shape parameter. After evaluating set B, it was found that the MoM has a mean error of 1,3249 and a maximum error equal to the maximum length of the search interval. Moreover, the Single Neural Network achieves an average error of 1,1399 and a maximum error of 19,9390. Finally, the Two Stages Neural Solution has an average error of 1,0716 and a maximum error of 19,77.

The above Fig.s reflect only a slight improvement in the accuracy achieved with the Two Stages Neural Solution. However, the true gain is visible in the graph for the $0.1 < v < 1$ region, also included in Fig. 6. Mistakes made in this region by the Two Stage Solution have very small magnitude. This is exactly the desired behavior, because the best estimate occurs in the region of greatest influence on the heavy property of the histogram tails and, therefore, in the region that requires a greater adjustment of the radar detector parameters.

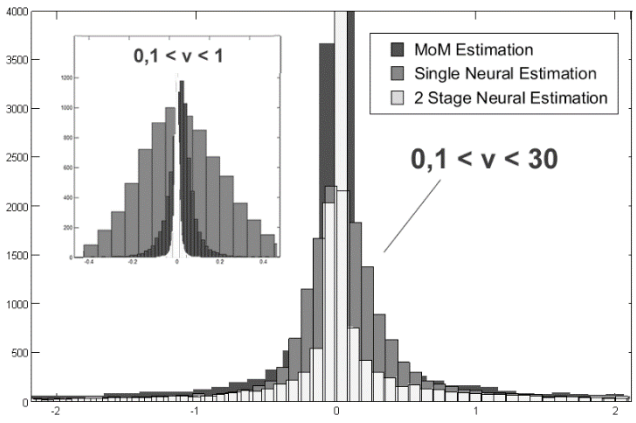


Fig. 6. Histogram of the Errors Made by the Three Estimators.

The exact Fig.s that characterize the estimators are given in Table III, where the results obtained by the Two Stages Solution are compared with the other two addressed estimators. For each region, the average error is offered first and the maximum error second. In addition, the last row contains the gain achieved by using the Two Stage Neural Solution in relation to the precision of the MoM estimates.

For example, the network $net\ 1E$, which operates in the $0.1 < v < 1$ region, sustains a mean error of 0,0095 and a maximum

TABLE III
MAGNITUDE OF MISTAKES MADE BY EACH ESTIMATOR IN FIVE DIFFERENT REGIONS.

| Estimators/**Estimation Region** | **0,1-1** | **0,8-1,73** | **1,3-3,6** | **1,92-10,73** | **3,96-30** |
|---|---|---|---|---|---|
| MoM | 0,0455-0,424 | 0,13-0,7 | 0,23-1,29 | 0,55-3,85 | 5,01-30 |
| Single Neural Network | 0,165-1,991 | 0,14-0,77 | 0,21-1,05 | 0,46-3,84 | 3,27-19,9 |
| Two Stages Neural Net | 0,0095-0,1076 | 0,04-0.23 | 0.11-0,7 | 0,4-3,03 | 3,33-19,7 |
| Gain | 4,79-3,94 | 3,25-3,04 | 2,1-1,84 | 1,37-1,27 | 1,5-1,52 |

error of 0,1076. That represents a 4,79 times better estimate than the one achieved by the MoM regarding the average, and a 3,94 times better estimate regarding the maximum error.

As it's shown in Table III, the gain of applying the Two Stage Solution is significant in the first three intervals; whereas the performance in the last two intervals is close to the one exhibited by the Single Neural Network. This means that the new solution is able to improve the performance in the region of interest, without affecting the quality of the overall estimate. Therefore, the superiority of the Two Stage Neuronal proposed Solution is demonstrated.

Moreover, Fig. 7 is presented as a complement of the information provided in Table III. The Fig. shows the error histograms for the last four regions.

### *F. About Speed of Execution*

The execution speed of the algorithms is a critical issue in developments related to radar devices where a quick response is required. Indeed, the MoM using the second and fourth moments is very popular because it gets reduced to a closed mathematical expression that provides direct results, preventing the need for an iterative process. Then, the delay in the method's implementation lays only in the constant re-calculation of moments.

The Two Stages Neuronal Solution, despite containing nine neural networks, can be implemented without introducing significant delays. Although the response of each of the networks depends on the results of the others, all networks can evaluate information from the start. This can be done in parallel if implemented in FPGA (Field Programmable Gate Array) kits.

The evaluation will provide a result that can be manipulated using combinational logic, once the decision on which network must provide the estimation will become available. So, the neuronal solution does not require of any iterative process to produce and output. The only delay is introduced in the building of histograms, which will not take a longer time than the one required by the MoM for calculating the second and fourth order moments.

### *B. Significance of Results*

Presented results support the neural networks capacity to solve statistical [39] and parameter estimation [40] problems. The current proposal applied a novel feature extraction method by using histograms of groups of K samples, which was combined with deep learning and classifier fusion approaches to produce an improved K parameter estimator. Recent investigations have also applied these principles to produce outstanding results in various fields [41-44]. So, the authors encourage new researchers to apply artificial intelligence methods for solving current problems.

## IV. Conclusions and Future Work

A new method for estimating the K shape parameter, based on a combination of nine independently trained neural networks, was created. The new method is as fast as the classic alternative based on the method of moments and achieves a much more accurate estimate in the region of small magnitudes of the K shape parameter. This is precisely the desired behavior for an estimator under K clutter, as the best performance is achieved in the region with the greater influence on the correction of the CFAR adjustment factor.

The new neural solution provides an important progress in in radar related solutions, as it allows the creation of a new improved CA-CFAR detector, able to adapt itself to changing sea conditions. The authors will focus next on the building of this new scheme which will improve the quality of detection by keeping the operational false alarm probability very close to the one conceived in the design. The authors will also focus on the development of a similar multi-stage neural solution for estimating the shape parameter under Log-Normal and Pareto clutter models.

To improve the presented scheme, the authors recommend adding an additional stage for further reducing the search regions before executing the final estimation. Additionally, the design could be improved by optimizing several simulation variables, such as the number of neurons in each hidden layer, the number of samples included in the histograms and the upper limit of the amplitude samples.

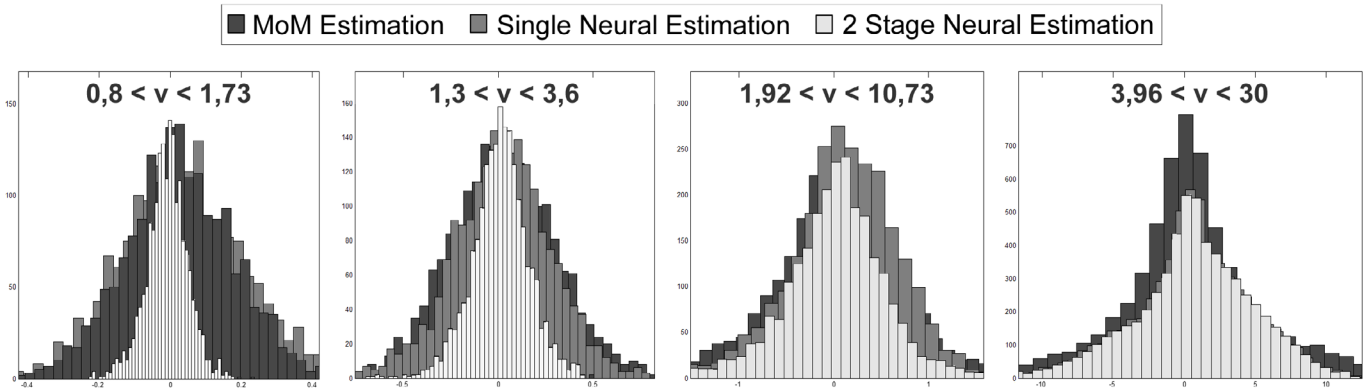


Fig. 7. Mistakes Made by each Estimator in Four Different Regions.

## References


[1] D. K. Barton and S. A. Leonov, Radar Technology Encyclopedia (Electronic Edition) ed.: Artech House, 1998.

[2] H. Meikle, Modern Radar Systems, 2nd Edition ed.: Artech House 2008.

[3] M. I. Skolnik, Radar Handbook, 3er ed.: McGraw-Hill, 2008.

[4] X. Shang and H. Song, "Radar Detection Based on Compound-Gaussian Model with Inverse Gamma Texture", IET Radar, Sonar and Navigation, vol. 5, pp. 315-321, 2010.

[5] S. Ishii, S. Sayama, and K. Mizutani, "Effect of Changes in Sea-Surface State on Statistical Characteristics of Sea Clutter with X-band Radar", Wireless Engineering and Technology, vol. 2, pp. 175-183, 2011.

[6] S. Sayama and S. Ishii, "Suppression of Log-Normal Distributed Weather Clutter Observed by an S-Band Radar", Wireless Engineering and Technology vol. 4 pp. 125-133, 2013.

[7] K. Ward, R. Tough, and S. Watts, Sea Clutter Scattering, the K Distribution and Radar Performance, 2nd ed. London, United Kingdom: The Institution of Engineering and Technology, 2013.

[8] Z. Zhijian, X. Ruilai, H. Yong, and G. Jian, "New Nonparametric Detectors under K-Distributed Sea Clutter in Radar Applications", in IEEE 2011 CIE International Conference on Radar, 2011, pp. 1752-1755.

[9] X. Meng, G. Feng, H. Xue, and Z. He, "Wideband Radar Target Detection Theory in Coherent K Distributed Clutter", Research Journal of Applied Sciences, Engineering and Technology, vol. 5, pp. 1528-1532, 2013.

[10] G. Tanriverdi, "Arma Model Based Clutter Estimation and its Effect on Clutter Supression Algorithms", Master of Science in Electrical and Electronics Engineering, The graduate School of Natural and Applied Sciences 2012.

[11] R. C. Sánchez Rams, "Implementación del detector CA-CFAR en VHDL para crear un PC-Radar Cubano usando FPGA", Ing. en Telecomunicaciones y Electrónica, Departamento de Telecomunicaciones y Telemática, Facultad de Ingeniería Eléctrica, Instituto Superior Politécnico José Antonio Echeverría (ISPJAE), La Habana, Cuba, 2014.

[12] J. R. Machado Fernández and J. C. Bacallao Vidal, "MATE-CFAR: Ambiente de Pruebas para Detectores CFAR en MATLAB", Telem@tica, vol. 13, pp. 86-98, 2014.

[13] J. Z. Yim, C.-R. Chou, and W.-K. Wong, "A Study of the Statistics of Sea Clutter in the Northern Coast of Taiwan", in Proceedings of the Seventeenth International Offshore and Polar Engineering Conference, Lisbon, Portugal, 2007, pp. 1-6.

[14] J. R. Machado Fernández, "Weibull Clutter Assumption Neural Adaptive Threshold Estimation Cell Averaging Constant False Alarm Rate (W-NATE-CA-CFAR) Detector (under revision)", Ingeniare, 2015.

[15] J. R. Machado Fernández, J. C. Bacallao Vidal, and N. Chávez Ferry, "A Neural Network Approach to Weibull Distributed Sea Clutter Parameter's Estimation", Inteligencia Artificial vol. 18, pp. 3-13, 2015.

[16] J. R. Machado Fernández and J. C. Bacallao Vidal, "Optimal Selection of the CA-CFAR Adjustment Factor for K Distributed Amplitude Samples with a Fluctuating Shape Parameter (Under Review)", Nova Scientia, 2016.

[17] A. Machado Gil and B. García Delgado, "Reconocimiento de Parámetros Asociados a distribuciones del Clutter Marino con Redes Neuronales Artificiales", Ingeniero en Telecomunicaciones y Electrónica, Grupo de Radares, Departamento de Telecomunicaciones y Telemática, Instituto Superior Politécnico José Antonio Echeverría (ISPJAE), La Habana, Cuba, 2014.

[18] A. Cetin, "CFAR Detection in K-Distributed Sea Clutter", Master of Science in Electrical and Electronics Engineering, The Graduate School of Natural and Applied Sciences of Middle East Technical University, 2008.

[19] J. R. Machado Fernández and J. C. Bacallao Vidal, "Modelación de la Distribución K en MATLAB para Aplicaciones de Radar (bajo revisión)", Revista de Ingeniería Electrónica, Automática y Comunicaciones (RIELAC), 2016.

[20] M. Greco, F. Bordoni, and F. Gini, "X-Band Sea-Clutter nonstationarity: Influence of Long Waves", IEEE Journal of Oceanic Engineering, vol. 29, 2004.

[21] T. J. Nohara and S. Haykin, "Canadian East Coast Radar Trials and the K-Distribution", in IEE Proceedings on Radar and Signal Processing, 1991, pp. 80-88.

[22] Y. Dong, "Distribution of X-Band High Resolution and High Grazing Angle Sea Clutter, Technical Report DSTO-RR-0316", Electronic Warfare and Radar Division, Defence Science and Technology Organization, Edinburgh, South Australia2006.

[23] R. S. Raghavan, "A Method for Estimating Parameters of K-Distributed Clutter", IEEE Transactions on Aerospace and Electronic Systems, vol. 27, pp. 238-246, 1991.

[24] I. R. Joughin, D. B. Percival, and D. P. Winebrenner, "Maximum Likelihood Estimation of K distribution Parameters for SAR Data", IEEE Transactions on Geoscience and Remote Sensing, vol. 31, pp. 989-999, 1993.

[25] D. Blacknell, "Comparison of Parameter Estimators for K-Distribution", IEE Proceedings on Radar, Sonar and Navigation, vol. 141, pp. 45-52, 1994.

[26] P. Lombardo and C. J. Oliver, "Estimation of texture parameters in K-distributed clutter", IEE Proceedings on Radar, Sonar and Navigation, vol. 141, pp. 196-204, 1994.

[27] D. R. Iskander and A. M. Zoubir, "Estimating the parameters of the K-distribution using the ML/MOM approach", Proceedings 1996 IEEE TENCON Digital Signal Processing Applications, TENCON'96, vol. 2, pp. 769-774, 1996.

[28] D. R. Iskander and A. M. Zoubir, "Estimation of the parameters of the K-distribution using higher order and fractional moments [radar clutter]", IEEE Transactions on Aerospace and Electronic Systems,, vol. 35 pp. 1453-1457, 1999.

[29] W. J. J. Roberts and S. Furui, "Maximum likelihood estimation of K-distribution parameters via the expectation-maximization algorithm", IEEE Transactions on Signal Processing, vol. 48, pp. 3303-3306, 2000.

[30] P. J. Chung, W. J. J. Roberts, and J. F. Bohme, "Recursive K distribution parameter estimation", IEEE Transactions on Signal Processing, vol. 53, pp. 397-402, 2005.

[31] I. Antipov, "Analysis of sea clutter data, DSTO-TR-0647", Defence Science Technology Organisation, Australia1998.

[32] S. Watts, "Radar Detection Prediction in Sea Clutter using the Coumpound K-Distribution Model", in IEE Proceedings in Communications, Radar and Signal Processing, 1985, pp. 613-620.

[33] D. Ling and W. Pingjun, "A Method for Determining Scale Factor of CFAR Detector Based on BP Neural Networks", presented at the The 2nd International Conference on Computer Application and System Modeling, 2012.

[34] J. A. Garzón Guerrero, "Clasificación de blancos de radar en ambientes de ruido arbitrario mediante resonancias naturales y técnicas de componentes principales", Doctor en Ciencias, Universidad de Granada, 2012.

[35] N. B. Gálvez and J. E. Cousseau, "Improved Neural Network Based CFAR Detection for non Homogeneous Background and Multiple Target Situations", Latin American Applied Research, vol. 42, pp. 343-350, 2012.

[36] K. Mezzoug and B. Djebbar, "Étude Comparative d'un Détecteur CFAR Neuronal de Plusieurs Cibles Radar dans un Fouillis de type K-Distribution", 2008.

[37] A. Mezache and M. Sahed, "Parameter Estimation in K-Distributed Clutter with Noise using Nonlinear Networks", Université de Constantine, Faculté des Sciences de l'Ingénieur, 2010.

[38] H. Demuth, M. Beale, and M. Hagan, Neural Network Toolbox 5: MathWorks, 2007.

[39] N. Settouti, M. E. A. Bechar, and M. A. Chikh, "Statistical Comparisons of the Top 10 Algorithms in Data Mining for Classi cation Task", International Journal of Interactive Multimedia and Artificial Inteligence, Special Issue on Artificial Intelligence Underpinning, vol. 4, pp. 46-51, 2016.

[40] C. K. Chong, M. S. Mohamad, S. Deris, M. S. Shamsir, Y. W. Choon, and L. En-Chai, "Improved Differential Evolution Algorithm for Parameter Estimation to Improve the Production of Biochemical Pathway", International Journal of Interactive Multimedia and Artificial Intelligence, Special Issue on Distributed Computing and Artificial Intelligence, vol. 1, pp. 22-29, 2012.

[41] J. Singha and R. Hussain Laskar, "Recognition of global hand gestures using self co-articulation information and classifier fusion", Journal on Multimodal User Interfaces, vol. 10, pp. 77-93, 2016.

[42] J. Singha and R. Hussain Laskar, "Self co-articulation detection and trajectory guided recognition for dynamic hand gestures", IET Computer Vision, 2015.

[43] J. Singha and R. Hussain Laskar, "Hand gesture recognition using two-

level speed normalization, feature selection and classifier fusion", Multimedia Systems, 2015.

[44] V. B. Semwal, M. Kaushik, and G. C. Nandi, "Robust and accurate feature selection for humanoid push recovery and classification: deep learning approach", Neural Computing and Applications, vol. 26, pp. 1-10, 2015.

**José Raúl Machado Fernández** received his Telecommunications and Electronics Engineering Degree from the Instituto Superior José Antonio Echeverría (ISPJAE-CUJAE) in 2012. He is currently a Ph.D. student at the same institution. His research topics include teledetection, digital signal processing, sea clutter modeling and the application of artificial intelligence for solving diverse engineering problems.

**Jesús de la Concepción Bacallao Vidal** received his engineering Telecommunications and Electronics Engineering Degree and Master Degrees from the Instituto Superior Politécnico José Antonio Echeverría (ISPJAE-CUJAE), and the Ph.D. Degree from the Instituto Técnico Militar José Martí in 2003. Since 2013, he has been co-directing the CUJAE radar research team. His research topics include teledetection, CFAR detectors performance evaluation and the creation of alternative detection schemes based on processing signal in the moment's domain (DRACEC).